The Preparation And Characterization Of Multinuclear Catalysts Based On Novel Dendrimers:

Application In The Oligomerization And Polymerization Of Unsaturated Hydrocarbons.

By

Rehana Malgas-Enus

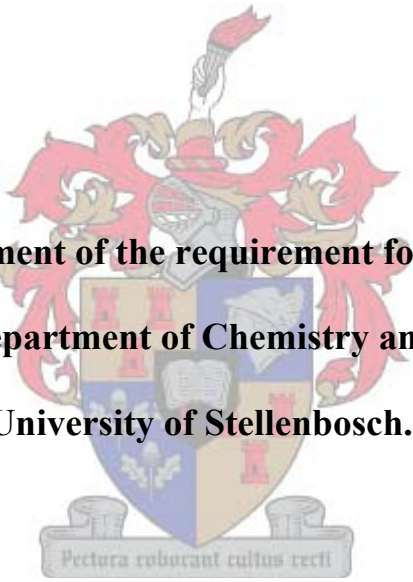

A dissertation in fulfilment of the requirement for the degree of PhD in Chemistry in the Department of Chemistry and Polymer Science, University of Stellenbosch.

Supervisor: Prof. S. F. Mapolie

March 2011

Declaration

By submitting this thesis/dissertation electronically, I declare that the entirety of the work contained therein is my own, original work, that I am the sole author thereof (save to the extent explicitly otherwise stated), that reproduction and publication thereof by Stellenbosch University will not infringe any third party rights and that I have not previously in its entirety or in part submitted it for obtaining any qualification.

March 2011

Abstract

In this thesis we describe the application of novel salicylaldimine and iminopyridyl nickel metallodendrimer complexes as catalysts in the transformation of á-olefins as well as in the polymerization of norbornene.

New cyclic dendrimers based on cyclam as a core (**L1-L8**) were synthesized and characterized via FTIR and NMR spectroscopy, mass spectrometry and microanalysis. Subsequently the generation 1 cyclam-based dendrimers as well as the commercial generation 1 to generation 3 DAB-PPI dendrimers were functionalized with salicylaldimine and iminopyridyl moieties on the periphery to produce new ligands, **DL1-DL10**. These modified dendritic ligands were subsequently complexed to Ni salts to obtain the metallodendrimer complexes, **C1-C8**. The metallodendrimers were characterized by FTIR spectroscopy, mass spectrometry, microanalysis, magnetic susceptibility measurements, UV-Vis spectroscopy and thermal gravimetrical analysis (TGA).

The DAB G1-G3 salicylaldimine ligands (**DL1-DL3**) were subjected to computational studies and the optimized structures were obtained by density functional theory (DFT) calculations. The effect of the increase in dendrimer generation on the structural arrangement of the dendrimer was also investigated. The following aspects were probed using molecular modeling: a) the possible coordination site for the Ni to the first generation dendrimer ligand, **DL1**, and b) the optimized structure of the first generation salicylaldimine nickel complex, **C1**.

We subsequently evaluated catalysts, **C1-C7**, in the vinyl polymerization of norbornene, using methylaluminoxane (MAO) as a co-catalyst. All the catalysts were found to be active for norbornene polymerization with the weight of the polymers obtained ranging

from 5.12×10^5 - 11.17×10^6 g/mol. The DAB-based iminopyridyl catalysts (**C4-C6**) exhibited higher activities than its analogous salicylaldimine catalysts (**C1-C3**) under the same reaction conditions. Also, the cyclam-based salicylaldimine nickel catalyst (**C7**) exhibited higher activities than the DAB-based salicylaldimine nickel catalyst, **C1**. A negative dendritic effect was observed for the G1-G3 DAB salicylaldimine catalysts since the optimum activity for the G3 catalyst, **C3**, was lower than that for the G2 catalyst, **C2**.

These nickel complexes were also evaluated as ethylene oligomerization catalysts and were found to produce a range of ethylene oligomers (C_4-C_{18}) as well as some longer chained oligomers, when employing $EtAlCl_2$ as a co-catalyst. We observed however that the free $EtAlCl_2$ mediates the Friedel-Crafts alkylation of the solvent, toluene, in the presence of the obtained ethylene oligomers to give uneven carbon number products, which are mixtures of alkylated benzenes.

Our metallodendrimer catalysts also isomerized and in some cases dimerized 1-pentene. In both ethylene oligomerization and 1-pentene isomerization processes, the salicylaldimine catalysts exhibited higher activity towards olefin transformation than the iminopyridyl catalysts. The cyclam-cored dendrimer catalyst again showed the highest activity. From the results obtained thus far it can be concluded that these nickel metallodendrimers exhibit great potential as catalysts in the transformation of unsaturated hydrocarbons.

Acknowledgements

I would like to express my sincere gratitude to the following persons, who's kind assistance have enabled me to complete my PhD studies:

My Supervisor, Prof Selwyn F. Mapolie, thank you for the valuable advice and guidance throughout the pursuit of my degree.

Mrs Sylette May, for your kindness and assistance with anything I needed throughout the last three years. Thank you for making my studies as pleasant as possible.

Dr Cornie van Sittert, for the DFT calculations, as well as your valuable suggestions and advice. It is greatly appreciated.

The Inorganic/Organometallic research group at Stellenbosch university, Nomvano Mketo, Yolanda Tancu, Jane Mugo, Andrew Swarts, Hennie Kotze, Wallace Manning, Danie van Niekerk, Dr Gangadhar Bagihalli and Dr Douglas Onyancha. Being part of a research group that gets along well with each other, advises each other when the research becomes a bit tricky, supports each other during presentations, and of course drives each other a bit crazy sometimes, must be every post graduate researcher's dream. I have lived it, and I am really grateful for the friendship, the guidance and even the disagreements. Thanks everyone.

Thanks to my good friend Andrew Swarts, for your extraordinary linguistic skills which helped me out tremendously during the writing of this thesis.

Jane Mugo, for your friendship throughout the years as well as the valuable discussions. Ursula Wanza, for your friendship and motivation throughout the course of my studies.

Mr Phillip Allen, for assisting us with everything we could possible require in our laboratory and Mr Johnny Smit, our technical officer, your hard work and assistance is greatly valued.

Dr Marietjie Stander, for the MS analysis; Dr Nyambeni Luruli and Sasoltech R&D, for the GPC analysis; and Ms Elsa Malherbe, for NMR analysis.

The *c change Centre of Excellence in Catalysis, the Department of Science and Technology (DST) and the National Research Foundation (NRF) for financial assistance.

My family, in particular my mother Jasmiena Malgas, for their support and encouragement throughout the course of obtaining all my degrees.

Finally, I would like to thank my husband, Shammiem Enus, for his constant support and patience during my PhD studies, especially for lifting my spirit when I felt a bit (very) down and encouraging me to keep going through numerous setbacks. Shukran.

Publications

Journal articles:

1. **Norbornene polymerization using multinuclear nickel catalysts based on a polypropylene imine dendrimer scaffold.**

   Rehana Malgas-Enus, Selwyn F. Mapolie, Gregory S. Smith, *Journal of Organometallic Chemistry* 693 (2008) 2279–2286.

2. **The application of novel dendritic nickel catalysts in the oligomerization of ethylene.**

   R. Malgas, S.F. Mapolie, S.O. Ojwach, G.S. Smith, J. Darkwa, *Catalysis Communications* 9 (2008) 1612–1617.

3. **An electrochemical DNA biosensor developed on novel multinuclear Nickel (II) salicylaldimine metallodendrimer platform.**

   Omotayo A. Arotiba, Anna Ignaszak, Rehana Malgas, Amir Al-Ahmed, Priscilla G.L. Baker, Selwyn F. Mapolie, Emmanuel I. Iwuoha, *Electrochimica Acta* 53 (2007) 1689–1696.

Conference Presentations:

1 Poster titled, "**Synthesis of Schiff base metallodendrimers for application as catalysts in the oligomerization of olefins.**", R. Malgas, S. F. Mapolie, presented at CATSA 2009, Rawsonville, Western Cape, South Africa, November 2009.

2 Poster titled, "**Synthesis of novel metallodendrimers based on cyclam cores.**", R. Malgas, S. F. Mapolie, presented at CATSA 2008, Parys, South Africa, November 2008.

3 International conference: Poster titled, "**The application of novel multinuclear nickel catalysts derived from dendrimeric ligands for the oligomerization of 1-pentene.**", R. Malgas, S. F. Mapolie, presented at ISHC_XVI, Florence, Italy, July 2008.

4 Poster titled, "**The application of novel multinuclear nickel catalysts derived from dendrimeric ligands for the oligomerization of 1-pentene.**", R. Malgas, S. F. Mapolie, presented at CATSA 2007, Richard's Bay, South Africa, November 2007.

Table Of Contents

List of Figures

Chapter 1 Figures

Chapter 2 Figures

Chapter 3 Figures

Chapter 4 Figures

Chapter 5 Figures

Chapter 6 Figures

List of Schemes

Chapter 1 Schemes

Chapter 2 Schemes

Chapter 3 Schemes

Chapter 4 Schemes

Chapter 6 Schemes

List of Tables

Chapter 2 Tables

Chapter 3 Tables

Chapter 4 Tables

Chapter 5 Tables

Chapter 6 Tables

List of Abbreviations

º	degrees
ºC	degrees Celsius
á	alpha
â	beta
ä	chemical shift
ð	pi
μ_{eff}	μ effective
μmol	micromole
Å	Ångstrom
AIBN	azoisobutyronitrile
atm	atmosphere
ATP	adenosine triphosphate
ATRP	atom transfer radical polymerization
BM	Bohr magnetons
br	broad
calc	calculated
cm^{-1}	wavenumber
COD	cyclooctadiene

d	doublet
DAB	diaminobutane
DCM	dichloromethane
DFT	density functional theory
DHBA	3,5 dihydroxy benzyl alcohol
DME	dimethoxy ethane
DMF	dimethyl formamide
DNA	deoxyribonucleic acid
DNP	double numeric polarized
DSC	differential scanning calorimetry
ESI-MS	electronspray ionization mass spectrometry
Fig	figure
FT-IR	Fourier Transform infrared spectroscopy
g	grams
G1	generation 1
G2	generation 2
G3	generation 3
GC	gas chromatography
GCE	glassy carbon electrode

GC-MS	gas chromatography mass spectrometry
GGA	generalized gradient approximation
GPC	gel permeation chromatography
h	hours
Ha	Hectare
HOMO	highest occupied molecular orbital
Hz	Hertz
i-Pr	isopropyl
K	Kelvin
kg	kilogram
kJ/mol	kilojoule per mole
kV	kilovolt
LUMO	lowest unoccupied molecular orbital
m	multiplet
m/z	mass to charge ratio
MALDI-TOF	Matrix-assisted laser desorption ionization – Time of Flight
MAO	methylaluminoxane
MHz	Megahertz
min	minute(s)

ml	milliliters
MLCT	metal-to-ligand charge transfer
mmol	millimole
M_n	number average molecular weight
mp	melting point
MRI	magnetic resonance imaging
M_w	molecular weight
nm	nanometer
NMR	nuclear magnetic resonance
PAMAM	poly (amido amide)
PAMAM-SA	poly (amido amide) salicylaldimine
PDI	polydispersity index
PNB	polynorbornene
POPAM	poly (propylene amine)
POSS	polyhedral oligomeric silsesquioxane
PPI	poly (propylene imine)
ppm	parts per million
Pyr	iminopyridyl
RBF	round bottom flask

ROMP	ring opening metathesis polymerization
RVP	Reid vapor pressure
s	singlet
Sal	salicylaldimine
SCF	self consisted field
SHOP	Shell higher olefins process
SPA	solid phosphoric acid
t	triplet
TGA	thermogravimetric analysis
TLC	thin layer chromatography
TMSD	trimethylsilyl diazomethane
TOF	turn-over frequency
TON	turn-over number
UV/Vis	ultraviolet/visible

Chapter 1:

An introduction to dendrimers and their applications.

1.1 The Discovery of Dendrimers.

Dendrimers are described as hyperbranched macromolecules that are monodisperse in nature and are characterized by a high density of peripheral groups. They possess three distinguishing architectural components, mainly (a) an initiator core, (b) an interior layer (generations), composed of repeating units, radially attached to the initiator core and (c) exterior (terminal functionality) attached to the outermost interior generation (Fig 1.1).[1]

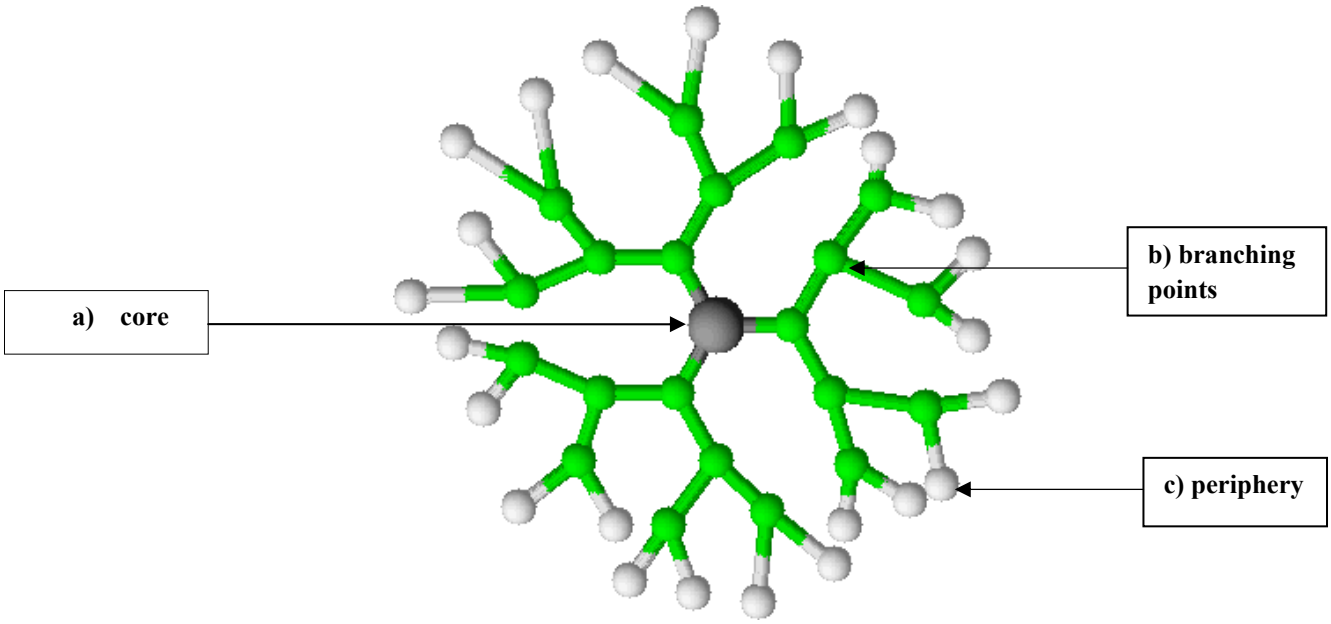

Figure 1.1: Schematic representation of a 3rd Generation Dendrimer.

The very first synthesis of dendrimers was described by Vögtle *et al* in 1978 who used the term "cascade macromolecules".[2] This was followed closely by the parallel and independent development of the divergent, macromolecular synthesis of "true dendrimers" by Tomalia *et al* in 1985, first using the term "dendrimer" and describing in great detail the preparation of poly(amidoamine) (PAMAM) dendrimers.[1] In the same year a communication by Newkome *et al* reported the synthesis of arborols (a synonym for dendrimers).[3]

Dendrimers are generally produced in an iterative sequence of reaction steps, in that each additional iteration leads to a higher generation dendrimer. Each of the new layers

creates a new 'generation' along with doubling the number of end groups (or active sites) and with approximately double the molecular weight of the previous generation.[4]

1.2 Synthesis of Dendrimers.

Dendrimers can be constructed via two synthetic strategies, namely the divergent method and the convergent method.

The divergent route to dendrimer synthesis, introduced by Tomalia *et al*, involves starting with a focal point or core that possesses a specific number of active sites and then progressing outward to the periphery by attaching successive branches to the core structure.[1] The number of active sites on the core determines their *n*-directionality and limits the number of building blocks that can be added to form the next generation. This trend is repeated (iterative synthesis) as the reactive sites on the periphery of the previous generation are exposed for the assembly of the next generational growth layer.[5]

The convergent method that was pioneered by Fréchet *et al* proceeds from what will become the dendron molecular surface (i.e. from the "leaves" of the molecular tree) inward to a reactive focal point at the "root". This leads to the formation of a single reactive dendron, after which several of these dendrons are then reacted with a multi-functional core to obtain the dendrimer molecule (Fig 1.2).[6]

The divergent approach is successful for the production of large quantities of dendrimers since, in each generation-forming step, the molar mass of the dendrimer is almost doubled. Very large dendrimers have been prepared in this way, but incomplete growth steps and side reactions often lead to the isolation of slightly imperfect samples. Divergently grown dendrimers are often impossible to isolate completely from their side products. The advantages of convergent dendrimer growth over the divergent method stems from the fact

that only two simultaneous reactions are required for any generation adding step, making the purification of perfect dendrimers simpler.

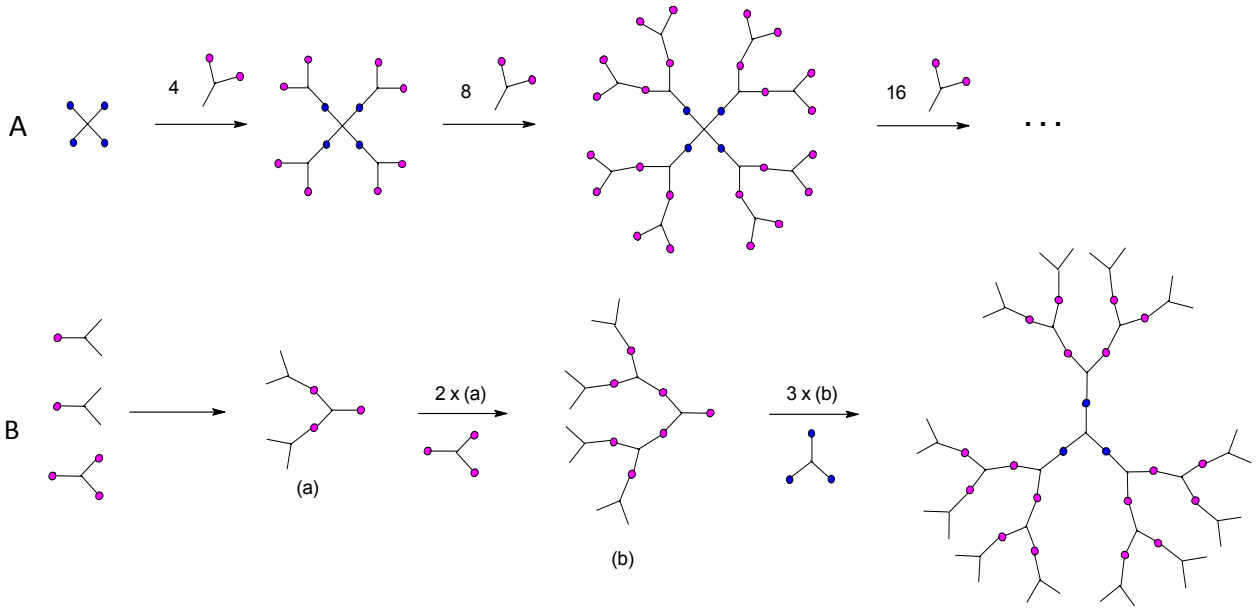

Figure 1.2: Representation of dendrimer growth by A) divergent and B) convergent methods.

However, the number of steps required to construct a large dendrimer is not reduced when compared to using the divergent method, but a much larger amount of starting material is required. The convergent method also suffers from low yields when attempting to synthesize large dendritic structures, due to dendritic wedges of higher generations encountering steric problems.

1.2.1 Divergent Dendrimer Synthesis.

Since the pioneering work done by Vögtle and Tomalia, thousands of dendrimer syntheses have been reported in the literature. Below are a few examples of divergent dendrimer construction.

Vassilieff *et al* [7] reported the synthesis of dumbbell-shaped dendrimers (Fig 1.3) by developing hyperbranched structures using symmetric growth on either side of a bifunctional

linear core. 2-Butyne-1,4-diol was used as the linear core and the dendron arms were based on 3,5-dihydroxybenzyl alcohol (DHBA). The synthetic procedure was based on the controlled addition of bis(dimethylamino)dimethylsilane to the bifunctional core, followed by the addition of DHBA. They observed that these dendrimers evolved from a very open structure in lower generations to a more globular architecture in higher generations.

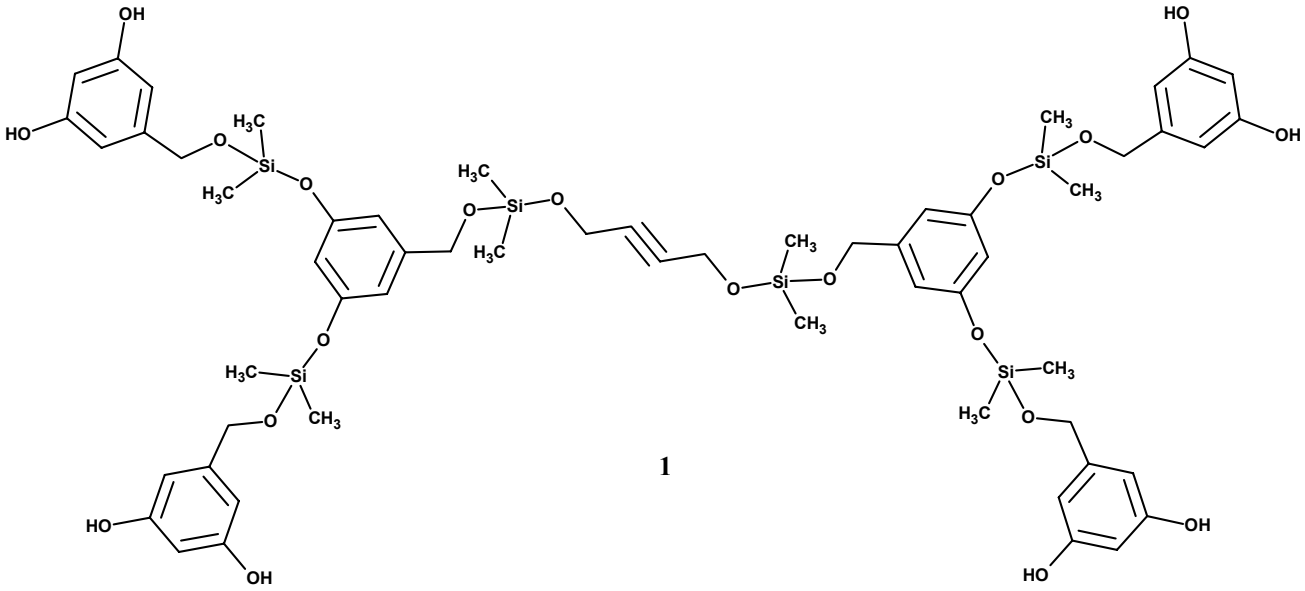

1

Figure 1.3: Dumbbell-Shaped dendrimers reported by Vassilieff [7] et al.

Molecular self-assembly of these dendrimers is influenced by their backbone structure, as indicated by a much higher critical aggregation concentration for generations 1-3, compared to that for globular dendrimer counterparts, such as generation 4.

Another example of dumbbell-shaped dendrimers is the diaminobutane polypropylene imine (DAB-PPI) dendrimer range first synthesized by Vögtle *et al* [2] and then later modified by de Brabander-van den Berg and Meijer [8] from the polymer company DSM. They were able to develop a vastly enhanced synthetic route of the Vogtle approach to prepare these polypropylene imine dendrimers (Scheme 1.1).

With these dumbbell-shaped dendrimers, the higher generations result in more spherical structures.

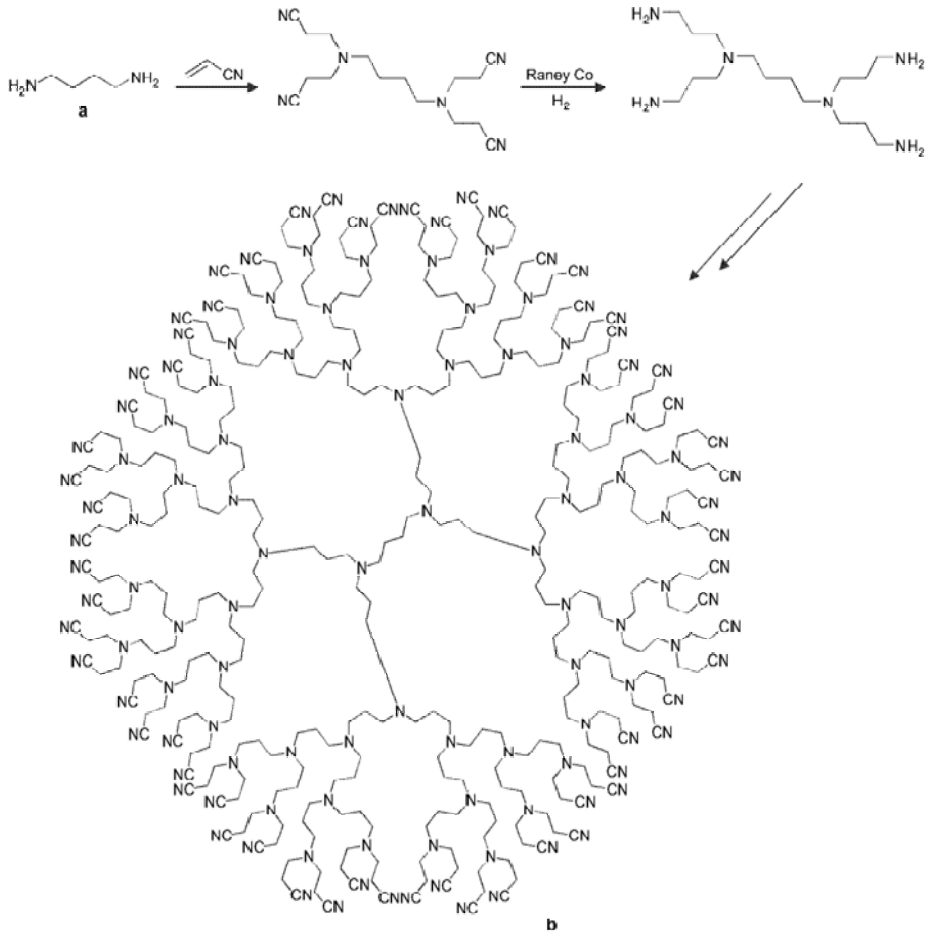

Scheme 1.1: The commercial synthesis of DAB-PPI dendrimer range by DSM.[8]

In 1999, Vögtle *et al* reported the synthesis of poly(propyleneamine) (POPAM) dendrimers with peripheral dansyl units (Fig 1.4).[9] They noted that the presence of charged guests inside the dendrimer affected the reactivity of the peripheral units. This could impact on the type of functionalization employed on the dendrimer periphery. They also concluded that protonated dendrimers could be biologically relevant since they can efficiently interact with DNA which could potentially be transported into the nucleus of eukaryotic cells.

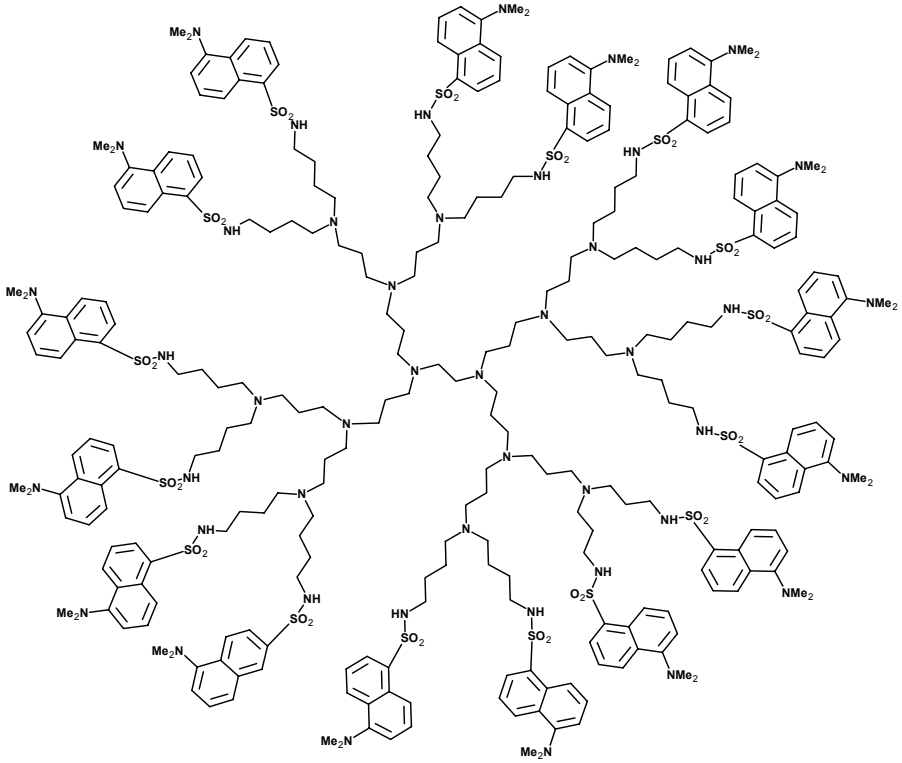

2

Figure 1.4: Generation 3 dansyl modified POPAM dendrimer synthesized by Vögtle *et al.* [9]

In 2008, Figueira-Duarte *et al* published the synthesis of a new type of stiff multichromophoric system, based on polypyrene dendrimers (Fig 1.5), incorporating a well-defined number of pyrene units in a confined volume.[10] The rigid and strongly twisted 3D structure allows for a precise spatial arrangement in which each unit is a chromophore. The large extinction coefficient and fluorescence quantum yield make these dendrimers attractive candidates for use as fluorescence labels. Studies of excited-state processes in these types of multichromophoric systems are continuing.

Majoros *et al* synthesized novel hybrid dendrimers which they coined as POMAM hybrid dendrimers, constructed from poly(propylenimine) (PPI or POPAM) core and poly(amidoamine) PAMAM shells (Scheme 1.2).[11]

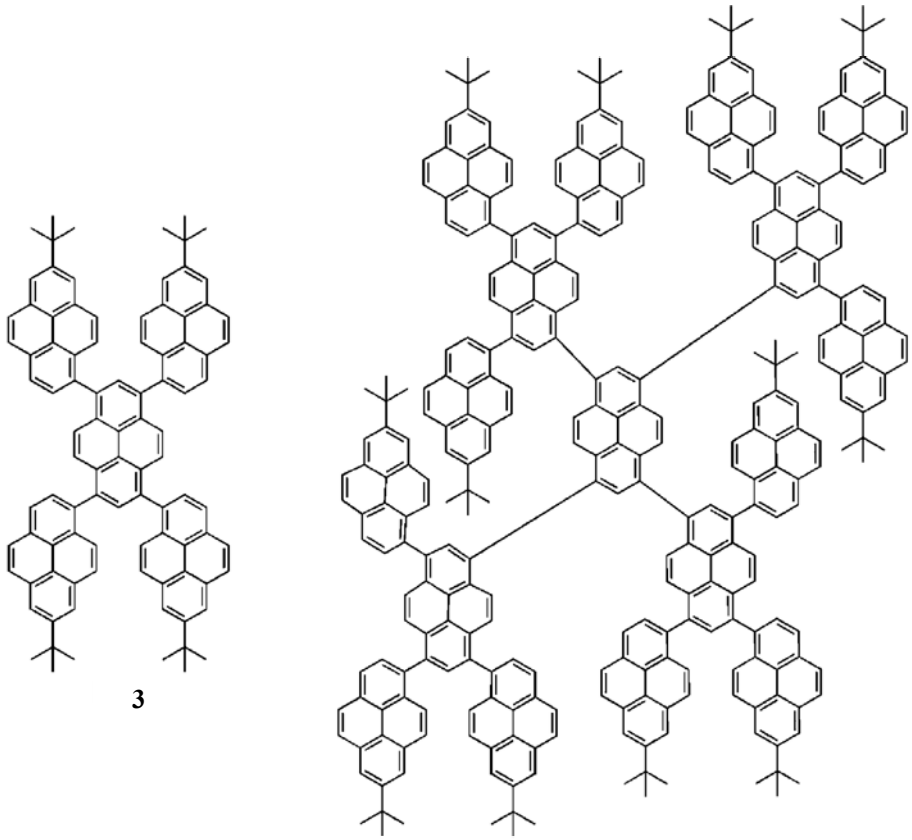

Figure 1.5: First-generation pyrene dendrimer (5 pyrene units) and second-generation pyrene dendrimer (17 pyrene units).[10]

The synthesis was accomplished by a divergent reiterating method which involved repeating subsequent Michael addition and amidation reactions. Their objective was to combine poly(propyleneimine) and poly(amidoamine) synthesis to improve the production of a multifunctional generation 5 poly(amidoamine) (PAMAM) dendrimer which was employed as a nano drug carrier in cancer therapy. Scale-up synthesis of this PAMAM nanodevice was limited because of the long reaction sequence (12 reaction steps) and time consuming and difficult work-up of the products after each reaction step. The new POMAM hybrid dendrimer has also shown gene transfer activity and is also non-toxic as compared to POPAM dendrimers.

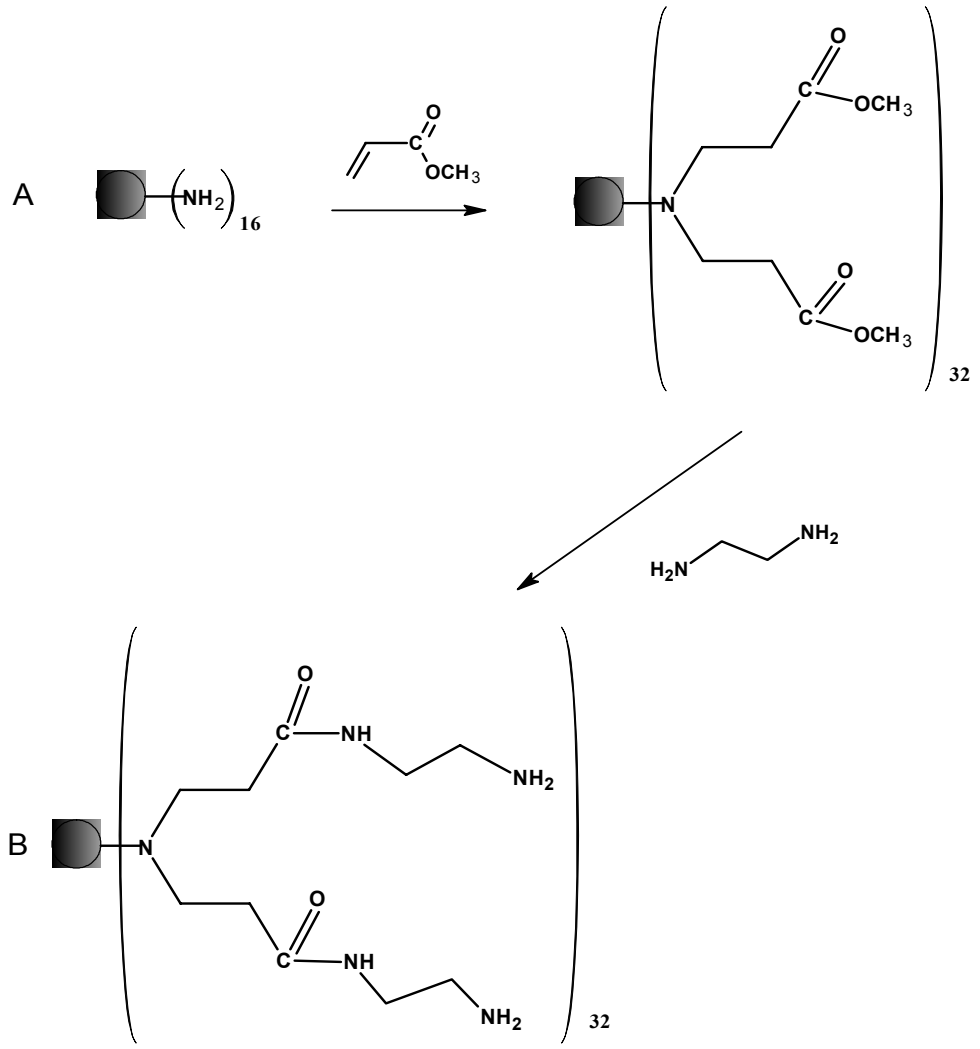

Scheme 1.2: (A) Synthesis of half-generations of POMAM hybrid dendrimers (step growth process).

(B) Synthesis of full generations of POMAM hybrid dendrimers (chain growth process).[11]

1.2.2 Convergent Dendrimer Synthesis.

Convergent synthesis of dendrimers includes the synthesis of "dendrons", followed by subsequent attachment of these dendrons to a functionalised core. Dendrons are the basic building blocks of dendrimers, and are also referred to as "dendritic wedges". Here we discuss selected examples of convergently synthesized dendrimers.

In 1999, van Heerbeek *et al* reported the divergent synthesis of carbosilane dendrons as versatile building blocks for the convergent synthesis of core functionalised carbosilane dendrimers with a 1,3,5-benzene triamide as the core molecule. [12] A bromide functional

group was selected to serve as a focal point of the carbosilane wedges because it was inert under the required reaction conditions and could readily be modified by substitution reactions (Scheme 1.3). Amine functionalised wedges were prepared by stirring the different generation bromine functionalised wedges in a large excess of liquid ammonia. Condensation of these amine functionalised wedges with 1,3,5-benzene tricarbonyl trichloride yielded carbosilane dendrimers containing a 1,3,5-benzene triamide core up to the third generation.

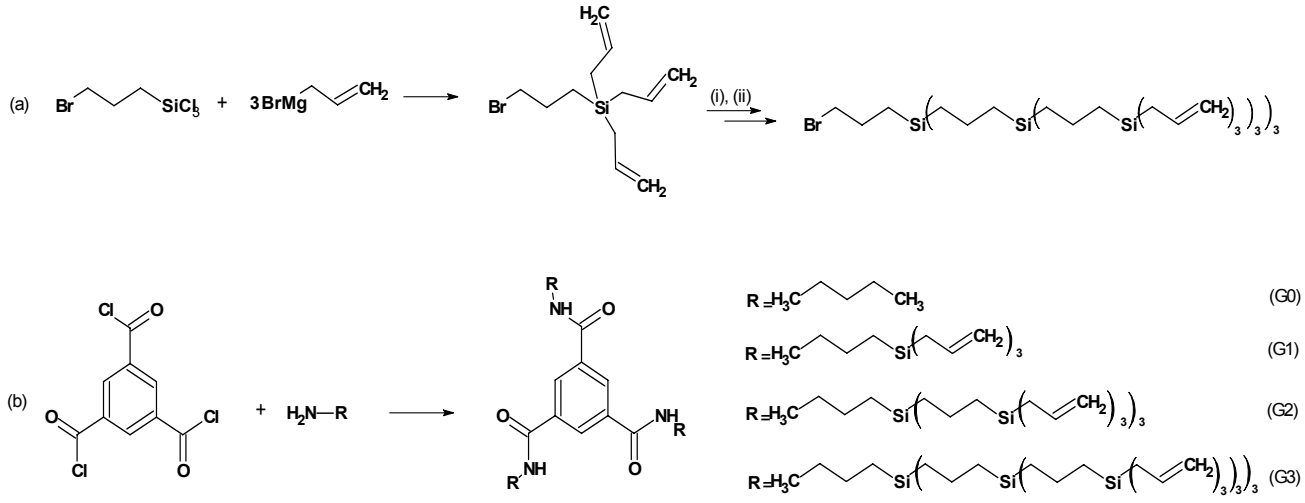

Scheme 1.3: (a) Synthesis of higher generation carbosilane wedges using a bromide function. **(b)** Synthesis of different generation carbosilane dendrimers containing a 1,3,5-benzene triamide core.[12] *Reaction conditions:* (i) $HSiCl_3$, $(Bu_4N)_2PtCl_6$, r.t.; (ii) (allyl)MgBr, Et_2O, reflux 4-6 hrs.

Binding studies of these G0-G3 dendrimers to guest molecules such as FMOC-glycine, Z-glutamic acid 1-methylester and propionic acid were performed in dry $CDCl_3$. Results showed that binding of the guest molecules to the dendrimers occurs via hydrogen bonding.

Maes *et al* synthesized novel dendrimers containing pyrimidine units, in which 4,6-dichloro-2-(4-methoxyphenyl)-pyrimidine was used as the building block.[13] A porphyrin molecule, 5,15-bis(pyrimidyl)porphyrin, was used as a dendrimer core (Fig 1.6).

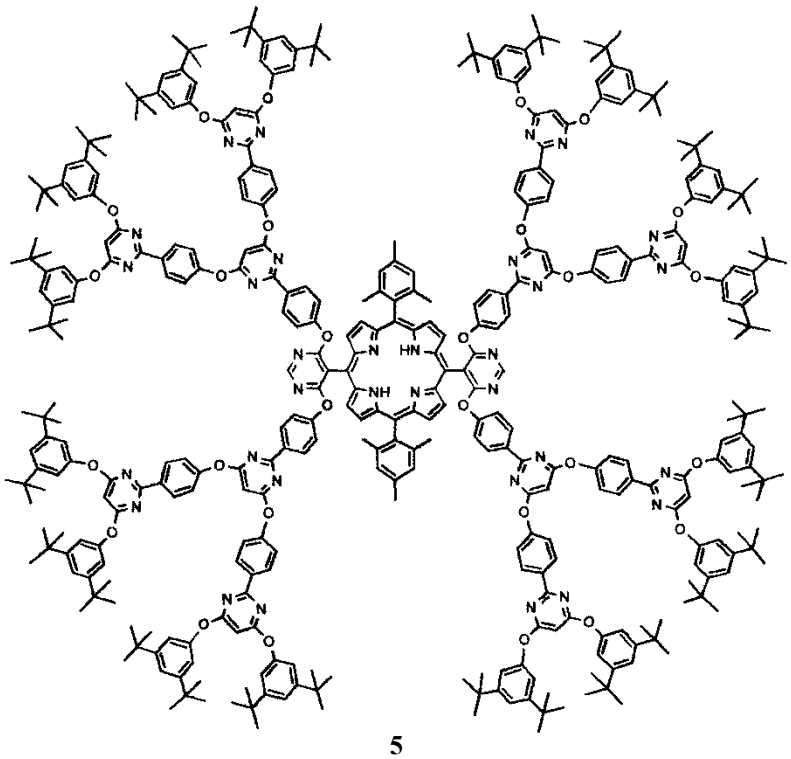

5

Figure 1.6: The second generation porphyrin dendrimer synthesized by Maes *et al.* [13]

Porphyrins represent attractive cores for the design of dendrimers because of their large size and the possibility of host–guest interactions. The presented dendrimer system provided a new, promising, rigid dendrimer backbone for various applications. It therefore presents an alternative to commonly used dendrimers, containing aliphatic amides or amines, or benzyl ether linkages.

In 2007 Lee *et al* published their results on the efficient synthesis of immolative carbamate dendrimers with an olefinic periphery. 4-Nitrophenyl (PNP) chloroformate was used as the carbamate-forming reagent and 1,3-diamino-2-propanol as the branching unit (Fig 1.7).[14] The olefinic periphery was designed to permit easy modification of surface

properties. The tertiary alkyl allyl end groups of the dendrons and dendrimer could be functionalized to generate surface functional groups or be subjected to metathesis or hydrosilylation with alkoxysilanes or chlorosilanes for shell cross-linking if desired.

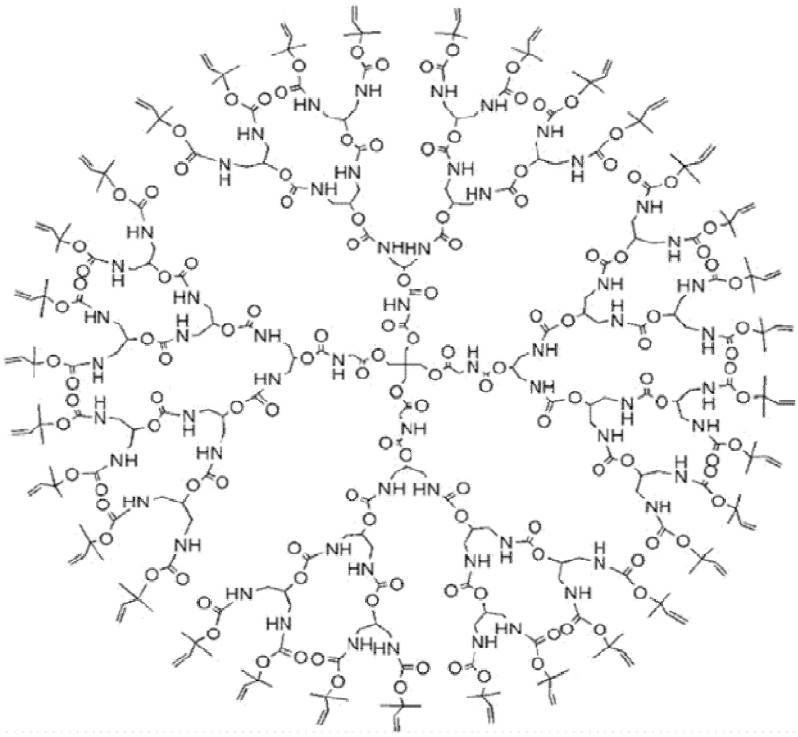

6

Figure 1.7: Structure of the G4-carbamate dendrimer synthesized by Lee *et al.* [14]

Recently, Endo *et al* reported the synthesis of a novel water-soluble polyamide dendrimer based on a facile convergent method. This third generation polyamide dendrimer bears 32 trifluoroacetamide moieties at its periphery (Fig 1.8). [15] The formation of the amino terminated dendrimer prompted these researchers to further synthesize a new water-soluble polyamide dendrimer with oligo(ethylene glycol) chains via its reaction with the amino groups on the dendrimer surface. This was motivated by the interest in water-soluble dendrimers which have unique and specific properties; for example, unimolecular micellation

behaviour. In addition, potential applications of dendrimer-inorganic hybrid materials (solution-phase catalysis, additives for polymer blends) could benefit from the versatile solubility of the dendrimer. This dendrimer was prepared based on a novel, very simple, inexpensive, and highly efficient convergent approach using thionyl chloride.

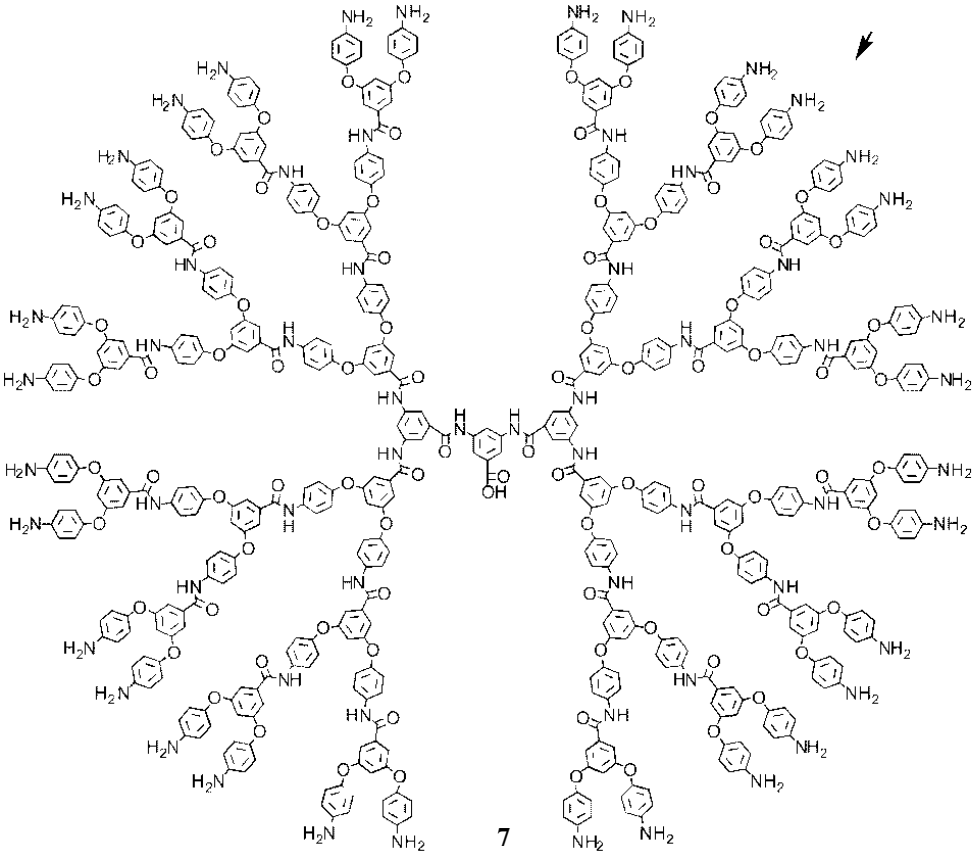

Figure 1.8: Structure of the G3 amine-terminated dendrimer synthesized by Endo *et al.*[15]

1.3 Properties of Dendrimers.

Dendrimer properties are determined by the size, shape and multiplicity of the construction components that are used for the core, interior and surface of the dendrimer. However, dendrimers in general have a few common properties.

Unlike linear polymers, dendrimers are spherical, monodisperse macromolecules. The classical polymerization process which results in linear polymers is usually random in nature and produce molecules of different sizes, whereas the size and molecular mass of dendrimers can be specifically controlled during synthesis.[16]

Dendrimers have some unique properties because of their globular shape and the presence of internal cavities. These internal cavities permit the encapsulation of molecules/ions, essentially allowing the dendrimer to perform as a nanoscopic container with the possibility of encapsulating guest molecules in the macromolecule interior.

At higher generations, dendrimers have a densely packed surface area that is composed of a large number of surface functionalities. Thus, in large dendrimers, the focal core is completely encapsulated by the dendrimer framework and is isolated from the outer environment, leading to specific site-isolation effects on their properties. [17] The solubility of dendrimers is predominately controlled by their peripheral functionalities.

Another intriguing aspect is that functional units can be placed at specific sites in dendrimers (interior and/or surface) allowing for a different functionality of materials.[18]

1.4 Applications of Dendrimers.

1.4.1 Dendrimers as Organocatalysts.

Organic dendrimer compounds have been shown to have promise in many applications in the literature, such as sulfonated PAMAM dendrimers employed as a novel dendritic HIV/ AIDS drug [19] while the same PAMAM scaffolds with hydrophilic oligo(ethylene glycol) end groups have been used as pore generating agents for the development of dielectric layers for advanced microelectronic devices.[20]

A more recent application is the use of dendrimers as organocatalysts. Organocatalysis brings about the prospect of a complementary mode of catalysis, with the potential for savings in cost, time and energy, an easier experimental procedure and reductions in chemical waste. This is due to the fact that organic molecules are generally insensitive to oxygen and moisture in the atmosphere, so there is no need for special reaction vessels, storage containers and experimental techniques, or for ultra-dry reagents and solvents.[21] On the other hand, the main disadvantage of organocatalysts is that the final separation of catalysts from products is difficult and time consuming. This can be potentially overcome by employing dendrimers as organocatalysts. In this case the large dendritic catalyst can be separated from products via ultrafiltration. Other separation techniques will be discussed later in this chapter. Here we discuss a few examples of dendrimers as organocatalysts.

Gitsov *et al* used a poly(aryl ether) dendron, with an alkoxide group at the focal point (Fig 1.9), to initiate anionic ring opening polymerizations.[22] The products obtained from these dendrimer assisted reactions were much better than those obtained using a standard alkali metal-alkoxide initiator. When the poly(aryl ether) dendrimer was used as the initiator, high molecular weight polymers with very narrow polydispersities were obtained.

In 2008, Krishnan *et al* published their results on the use of polystyrene-supported PAMAM dendrimers as highly efficient and reusable catalysts for Knoevenagel condensations between carbonyl compounds and molecules containing active methylene groups. [23] They reported that the catalysis could be performed even in water and the catalyst (Fig 1.10) could also be recycled many times without loss of activity, offering a greener route to conventional Knoevenagel condensation products.

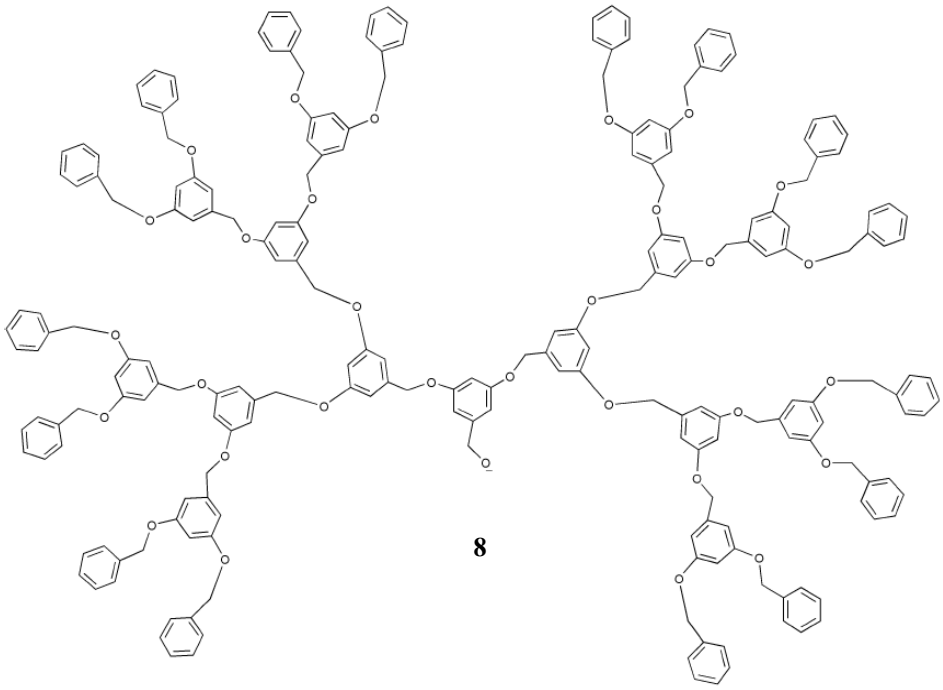

8

Figure 1.9: Dendron with an alkoxide focal point used to initiate ring opening anionic polymerisation.[22]

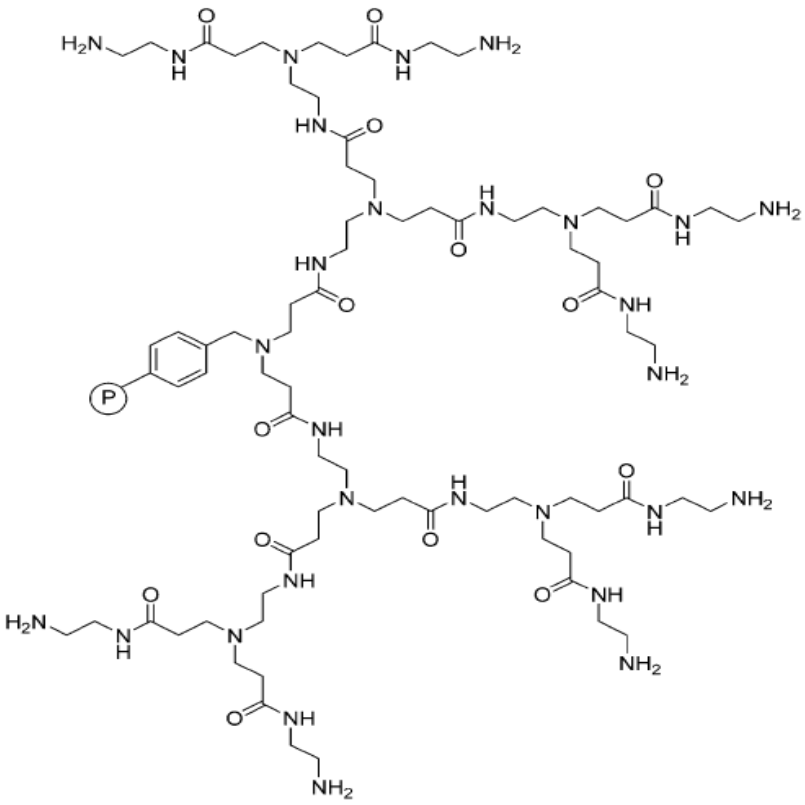

9

Figure 1.10: Third-generation PAMAM dendrimer supported on polystyrene (P).[23]

When comparing the G0-G3 dendrimer catalysts, they found that the third-generation catalyst gave better results under identical reaction conditions. From these experiments it is possible to assume that the catalytic species situated at the periphery of a dendrimer exhibits cooperative interaction that can play a decisive role in catalysis.

The catalytic efficiency of the immobilized third-generation dendrimer was compared to that of the unsupported first-generation PAMAM dendrimer (both compounds have the same number of peripheral units), and it was found that the unsupported dendrimer required only half the time as compared to the supported dendrimer for completion of the reaction between benzaldehyde and malononitrile under similar conditions. However, removal and recycling of the unsupported catalyst was difficult and required chromatographic separation.

In 2009, Kapoor *et al* described the divergent synthesis, characterization and catalytic properties of different generations of triazine based aromatic amine dendrimers supported on mesoporous silicas.[24] This was derived via a stepwise functionalization of mesoporous silica substrates of different pore sizes with 2,4,6 trichlorotriazine and ethylene diamine (Fig 1.11). These mesoporous supported dendrimers were also applied as catalysts in Knoevenagel condensation reactions. By changing the chemical nature of the dendritic networks (aliphatic or aromatic), it is possible to have predominantly base catalysts within a large range of well-defined and controlled basicities. The hydrophobic nature of the dendritic mesostructures was advantageous in increasing reaction rates by altering local water concentration in Knoevenagel condensation reaction.

Although the dendrimer supported mesoporous silicas with aromatic networks were not recyclable for multiple uses, it could however be valid for many catalyzed reactions which involved alkylation, dehydrogenation of alkyl-amines to nitriles, double bond

isomerization and transesterification reactions etc. Thus the potential applications of basic dendritic mesostructures are quite promising and merits further consideration.

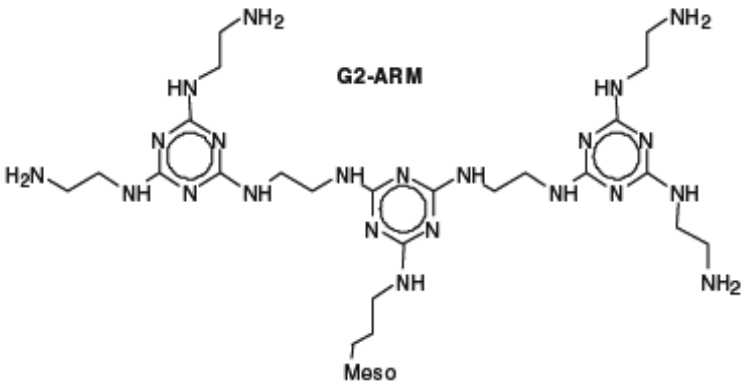

10

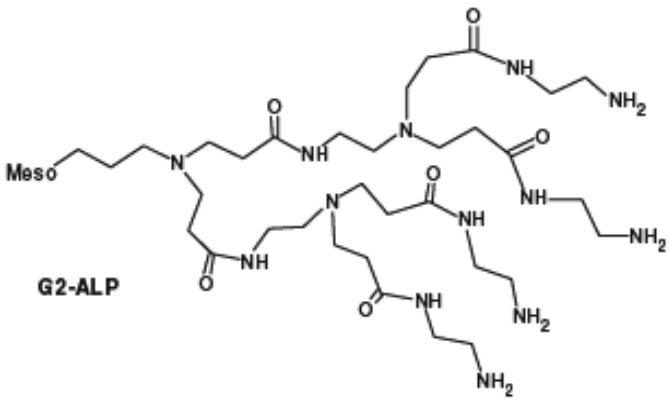

11

Meso = Mesoporous Silica

Figure 1.11: The triazine based aromatic (**10**), and the polyamidoamine based aliphatic dendrimer supported mesoporous silica composites (**11**). [24]

1.4.2 Metallodendrimers and its Applications.

Metallodendrimers are dendrimer molecules that incorporate metal ions into their infrastructure (Fig 1.12) either as cores, branching centres, arm connectors, termini or by metal incorporation at specific loci within the preassembled dendritic framework.[25]

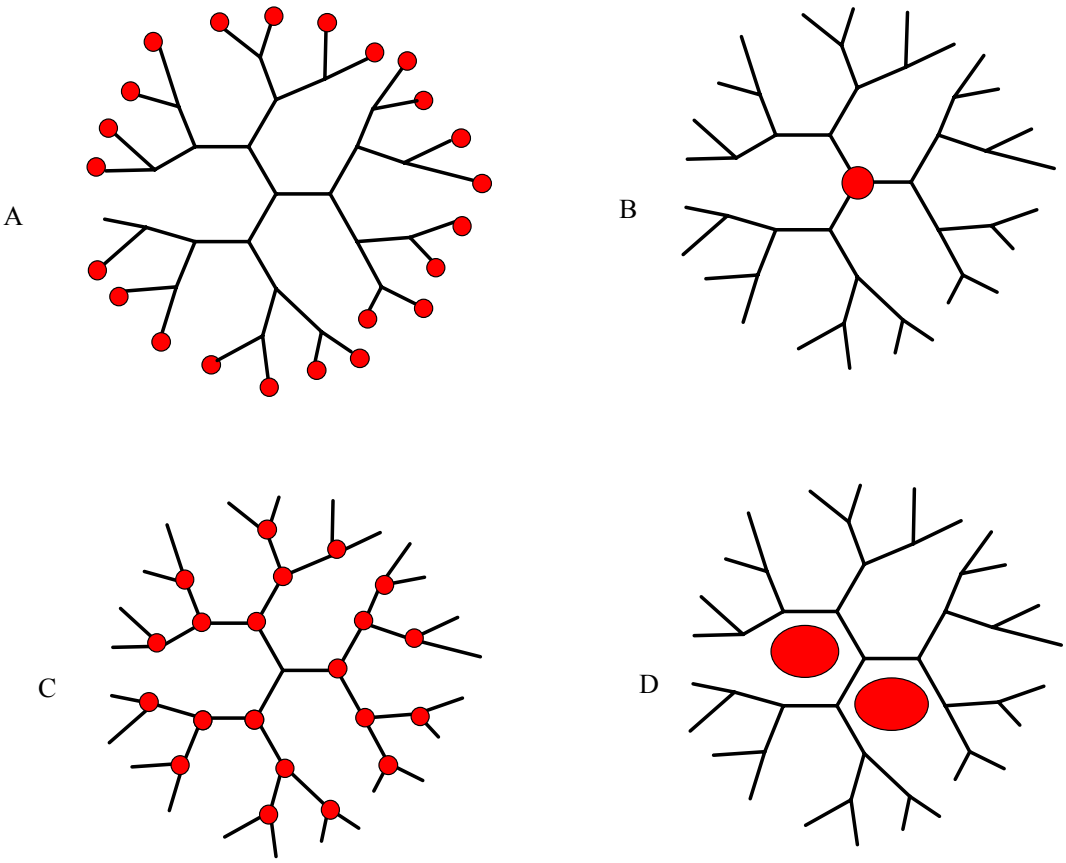

Figure 1.12: Dendrimers can have metal containing end groups (A), metal containing cores (B) or metal containing branches (C). Dendrimers can also encapsulate metal nanoparticles (D).[26]

Due to their repetitive branching, dendrimers tend to have a higher density on the outside (periphery) than in their interior. Thus dendrimers also have voids in their interiors

that can be used to encapsulate other molecules and/or nanoparticles. Nanoparticles are shielded from their surrounding environment and are stabilized in solution by the dendritic shell. [26] The dendritic branches and termini can serve as gates to control the access of small substrates into the dendrimer and thus to the encapsulated nanoparticles. Gold nanoparticles represent one of the most widely studied of these nanoparticle systems.[27, 28]

Metallodendrimers are an important class of materials with valuable properties and applications in a large number of areas. Some of these applications are briefly discussed.

1.4.2.1 Metallodendrimers as drug delivery agents and other biological applications.

Dendrimers have a nanometer size range and low polydispersity, which allows for easy passage across biological barriers. Because of this dendrimers have been applied as nanomedicines. Dendrimers also have the ability to host guest molecules such as drugs either in its interior cavities or on its periphery. In order to be used as biological agents, dendrimers have to fulfill certain biological demands. The dendrimer should be non-toxic, non-immunogenic (except for vaccines), able to stay in circulation for the time needed to have a clinical effect and able to target specific structures. Dendrimers have the capacity to do all this by modification with the appropriate functional groups to obtain a particular property. There are many reports in the literature on the study of biological applications of dendrimers which include dendrimers as artificial enzymes,[29] dendrimers for drug delivery,[30-32] dendrimers as anti-microbial agents,[33] as MRI and X-ray contrast agents,[17] as anti-HIV agents [34] and dendrimer applications in cancer diagnosis and therapy.[35]

1.4.2.2 Metallodendrimers in molecular electronics.

It has been reported that when the branches of a dendrimer are sufficiently long, the redox events at the many termini of the metallodendrimer are independent, appearing as a single wave in the cyclic voltammogram, because of very weak electrostatic effects. As a result, these metallodendrimers have applications in molecular recognition and sensing.

In a review by Astruc *et al,* they conclude that redox-robust metallocenyl-terminated dendrimers have useful molecular electronic properties including very fast electron transfer, independence of the redox centers, and increased adsorption ability as their size increases.[36] Applications are as: (i) anion exoreceptors with dendritic effects whose selectivity vary with the metallocenyl dendrimer structure, size and terminal groups; and (ii) catalysts whereby recognition and titration of transition-metal ions allow preparation of precise nanoparticles of various sizes for optimization and mechanistic determination.

1.4.2.3 Metallodendrimers as sensors.

Metallodendrimers have also been applied as immunosensors, [37] as electrochemical adenosine triphosphate (ATP) sensors, [38] as dendritic glucose sensors, [39] as functionalized antibody and antigen biosensors [40] and as DNA biosensors, where a nickel metallodendrimer was found to be electroactive with two reversible redox couples, as well as being conducting and electrocatalytic in the presence of $[Fe(CN)_6]^{3-/4-}$ when immobilized on a glassy carbon electrode (GCE) surface. The GCE metallodendrimer also adsorbed DNA strongly because the biosensor retained its activity after a series of electrochemical measurements except after denaturation.[41]

1.4.2.4 The advantages of using metallodendrimers as catalysts.

In general, heterogeneous catalysts are most commonly used in industry because they can be easily separated from the products formed. These heterogeneous catalysts are very stable materials, but often show limited selectivity due to their non-uniform nature. Transition-metal based homogeneous catalysis, on the other hand, has progressed significantly in recent years and involves the use of well-defined and highly active and selective catalysts. However, the separation of catalysts from the products is difficult and very costly which limit the use of homogeneous catalysts in industrial applications. The ability to recycle and reuse these catalysts should increase their overall productivity and subsequently make them economically more viable. [42]

By immobilizing homogeneous catalysts on insoluble supports, the advantages of both homogeneous as well as heterogeneous catalysis are achieved. The immobilized catalyst will have the high activity and selectivity of a homogeneous system as well as the ability to be separated from the product mixture as in the case of a heterogeneous system.

There are three types of supports that catalysts can be immobilized on, namely polymer supports, inorganic supports and dendrimers. One of the effects of having a dendritic support instead of an inorganic support, is that it gives the reaction a degree of homogeneous character as the dendrimer is normally highly soluble in a suitable solvent system. The dendrimer supported catalyst's efficiency can thus be equal to that of unsupported mononuclear homogeneous catalysts and they can then easily be recovered via ultra-filtration and then re-used in many ensuing reactions.

One method of separation of the dendrimer supported catalyst from its products is via nanofiltration/ultrafiltration.

This approach is based on size-exclusion filtration of dendrimer-supported catalysts using suitable membranes.[43]

Another method is via precipitation of the catalyst, where the precipitation ability of the metallodendrimer exceeds that of the reference monomeric catalyst or in those cases where dendritic effects on the stability of the active sites result in more efficient recovery. This is achieved by modifying the periphery of the metallodendrimer, which relates to the solubility of the catalyst, since it is the most exposed part of the molecule.[44]

A different concept for overcoming the problem of catalyst separation is to use multiphase systems where the catalyst and products are dissolved in different phases that can easily be separated. Again this can be accomplished by altering the dendritic end-groups to affect the solubility of the catalysts anchored to dendrimers.[45]

As discussed earlier, metallodendrimers are very good catalysts for a number of catalytic processes. In the rest of this chapter the application of metallodendrimers as catalysts are briefly reviewed.

1.4.2.4.1 *Metallodendritic catalysts in Diels-Alder reactions*

Fujita *et al* used a series of dendritic ligands with 2,2-bipyridine functionalities to prepare their corresponding copper(II) trifluoromethanesulfonate (triflate) metallodendrimer complexes as catalysts in the Diels-Alder reaction (Fig 1.13).[46] They found that the chemical yield of an adduct was enhanced by increasing the generation of the dendritic $Cu(OTf)_2$ catalyst, hence a positive dendritic effect was observed. It was assumed that this profound dendritic effect was probably derived from the increase of the Lewis acidity due to the

distorted bipyridine skeleton of the dendrimeric copper triflate complexes, by the steric repulsion of the dendritic wedges.

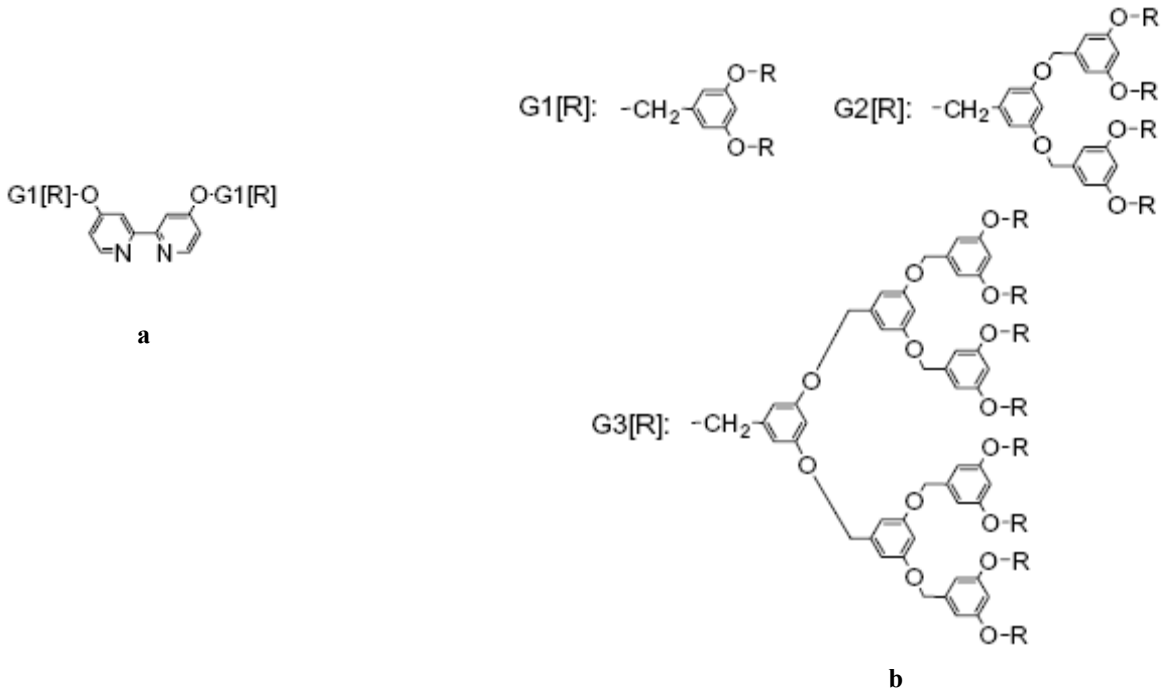

Figure 1.13: Dendritic 2,2 bipyridine dendrimers synthesised by Fujita *et al* [46]; (a) Bipyridine core, (b) G1-G3 dendritic wedges.

1.4.2.4.2 *Metallodendritic catalysts in Heck Coupling reactions*

In 2004, Krishna *et al* reported the synthesis of new alkyldiphenyl phosphine modified poly(ether-imine) dendrimers up to the third generation.[47] These dendritic ligands were reacted with $Pd(COD)Cl_2$ to give dendritic phosphine–Pd(II) complexes (Fig 1.14) which were evaluated in a prototypical C–C bond forming reaction, namely the Heck reaction, using various olefin substrates. The catalytic reactions involving these new dendritic catalysts in the Heck coupling reaction, showed good conversion in the reaction of an aromatic halide with a variety of alkene substrates.

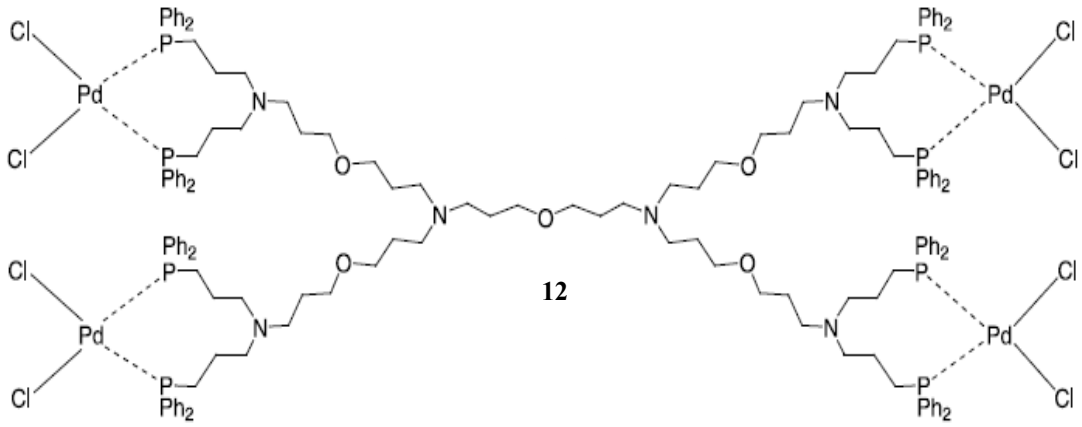

Figure 1.14: Synthesis of G2 Pd-metallodendrimer with 4 catalytic sites. [47]

It was observed that the turn over number (TON) generally increased using higher generation dendrimers. Thus the second and third generation dendritic catalysts were more active than the first generation dendritic catalyst, indicating a positive dendritic effect. In addition the dendritic catalysts were more efficient than the model mononuclear catalyst.

1.4.2.4.3 *Metallodendritic catalysts in Hydroformylation reactions*

The hydroformylation reaction is an important chemical transformation in which alkenes are converted into aldehydes and/or alcohols. This process is typically catalyzed by group 9 metals such as cobalt and rhodium.

The Cole-Hamilton group reported the evaluation of dendrimer-based phosphines having polyhedral oligomeric silsesquioxane (POSS) cores (Fig 1.15) as alkene

hydroformylation catalysts.[48] They concluded that dendrimer-based phosphines with 8, 24 or 72 phosphine groups attached to them are good ligands for rhodium and that they offer the potential for increasing the selectivity to the desired linear alcohols in hydroformylation reactions whilst retaining high activity.

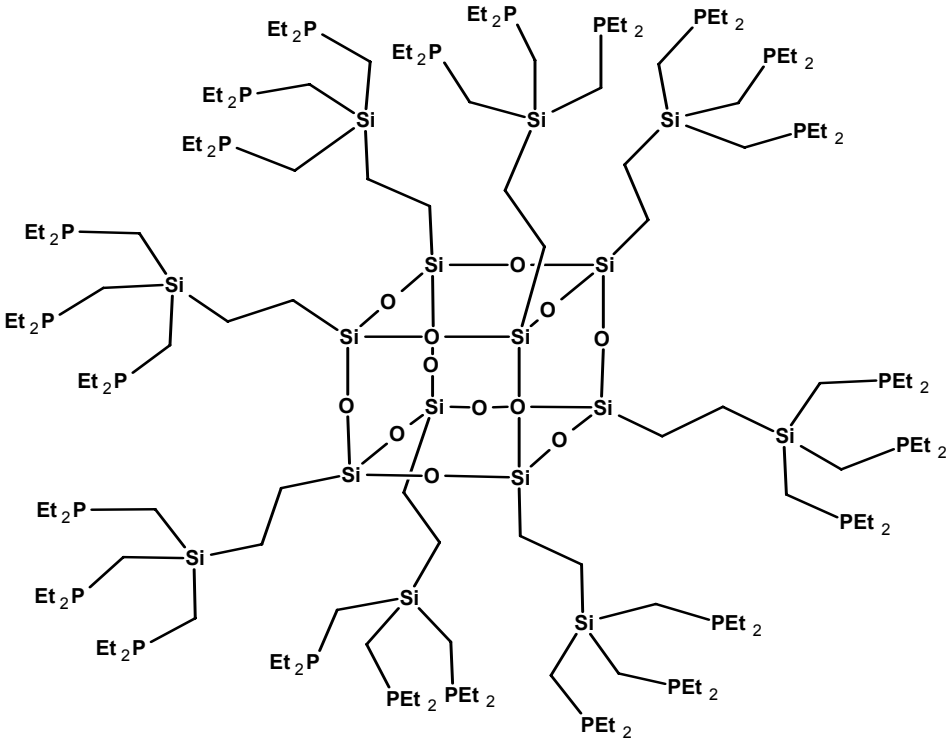

13

Figure 1.15: An example of one of the dendrimer-bound phosphines synthesized by Cole-Hamilton *et al*.[48]

Reek and van Leeuwen have studied both periphery- and core functionalized dendrimers in the hydroformylation reaction.[49] The position of the catalytic sites and their spatial separation was determined by the geometry of the dendrimer and this was ultimately very important for the performance of the catalyst (Fig 1.16). In the peripherally functionalized systems the high local concentration of phosphine ligands led to slower catalysis, but on the

other hand higher selectivity. In the core functionalized systems, the selectivity and activity was largely determined by the ligand backbone located at the core.

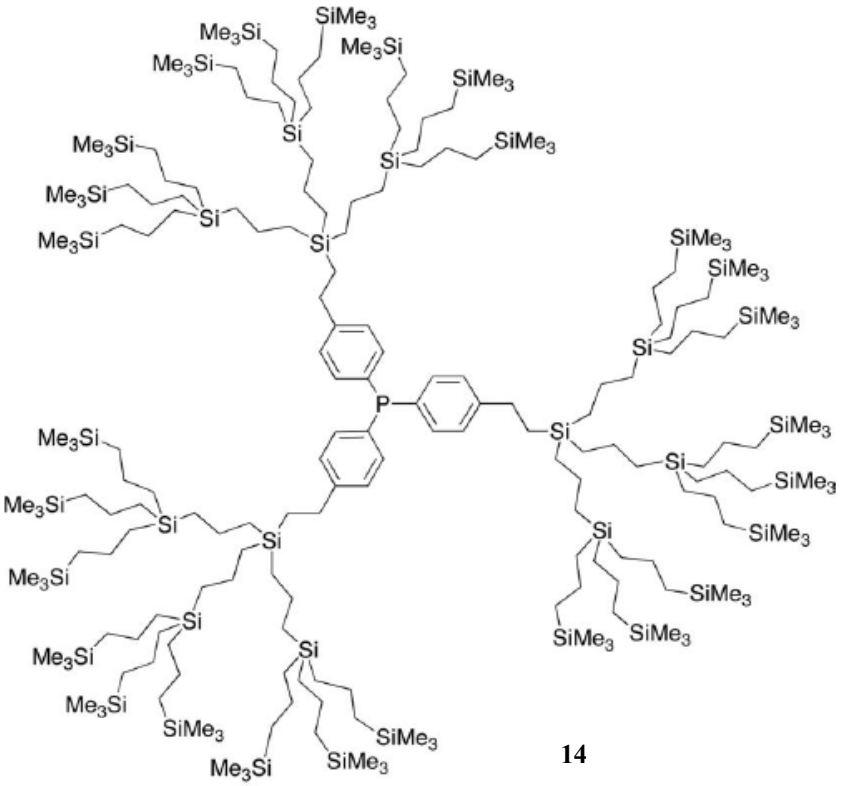

Figure 1.16: An example of one of the carbosilane dendrimers synthesised by Reek and van Leeuwen *et al.*[49]

1.4.2.4.4 *Metallodendritic catalysts in Hydrogenation reactions*

Dendrimer cores based on benzene 1,3,5-tricarboxylic acid and 1,3,5,7-adamantanetetracarboxylic acid with 5-substituted isophthalic acid derivatives constituting the branching units (Fig 1.17), were described by Köllner *et al.*[50] These dendrimers have been used in Rh-catalyzed hydrogenation of dimethylitaconate. There was a small, but significant and reproducible difference in the enantioselectivities between the G0 dendrimers and their first- and second-generation counterparts.

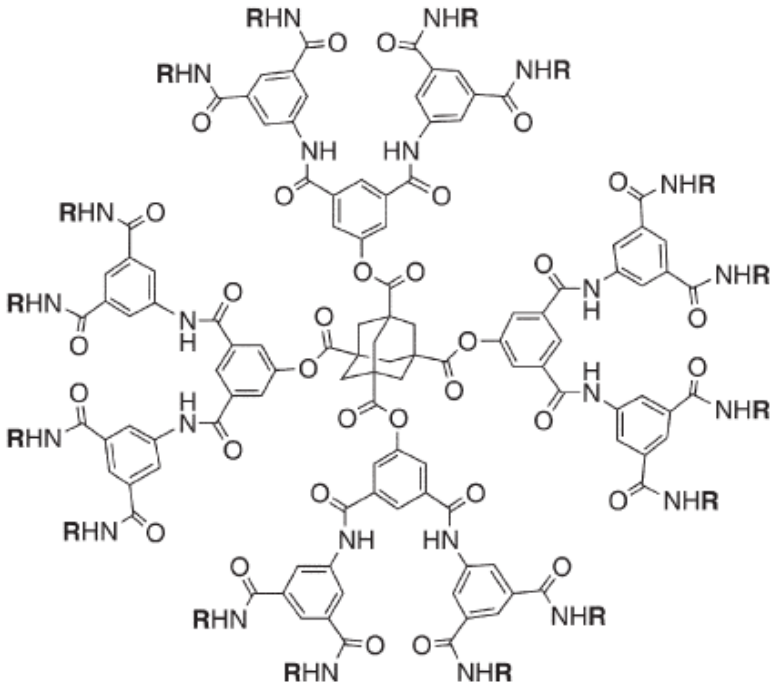

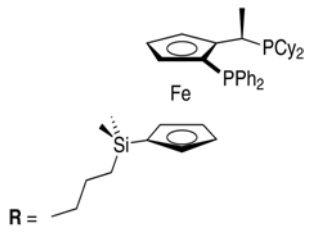

15

Figure 1.17: Dendrimers containing chiral ferrocenyl diphosphines synthesised by Köllner *et al*.[50]

The loss of stereoselectivity was relatively minimal and the fact that the dendrimers still gave excellent catalysis in this reaction indicates that the modified molecular environment of the single catalyst units show practically negligible effects.

1.4.2.4.5 *Metallodendritic catalysts in Oxidation reactions*

Lei *et al* reported the oxidation of cyclohexene by dendritic poly(amido-amide) salicylaldimine manganese (PAMAMSA-Mn(II)) complexes (Fig 1.18).[51]

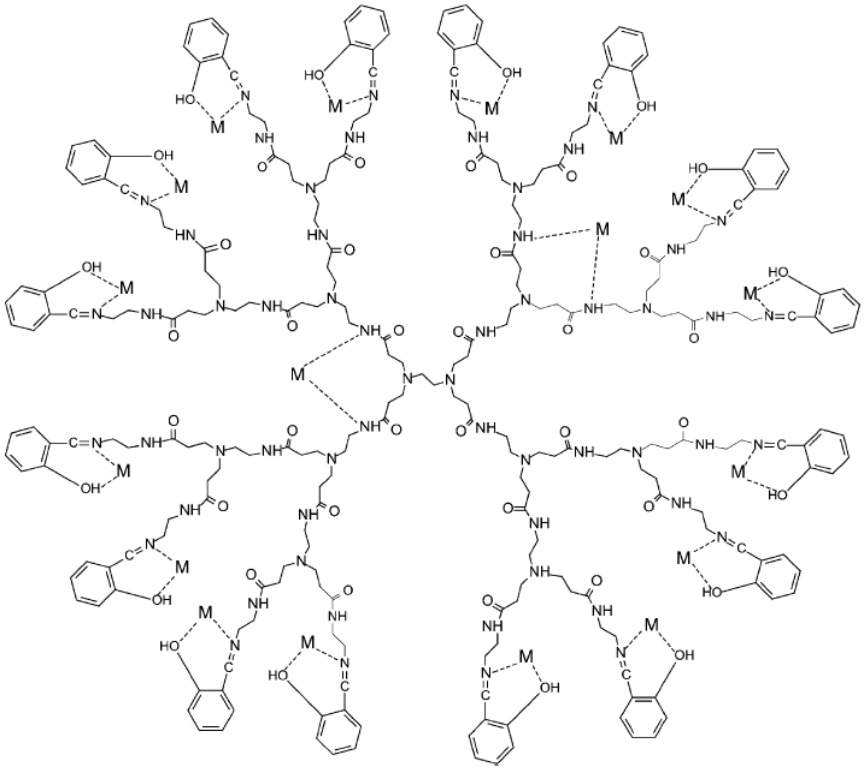

16

Figure 1.18: The structure of the dendritic G3 PAMAMSA-Mn(II) complex synthesized by Lei *et al*. [51]

They synthesised the G1-G6 manganese metallodendrimer complexes and found that the G3 catalyst gave the highest activity towards cyclohexene oxidation. The observed products of the oxidation was 7-oxabicyclo[4.1.0]heptane, 2-cyclohexen-2-ol, 2-cyclohex-2-one and 7-oxabicyclo[4.1.0]heptan- 2-one. The same research group described the synthesis of dendritic Sn(II) complexes incorporated into chloromethyl polystyrene through a solid phase

synthetic methodology and their performance as catalysts for the Baeyer–Villiger oxidation of ketones with hydrogen peroxide.[52] The complexes showed high catalytic activities for the Baeyer–Villiger oxidation of ketones using environmentally friendly 30 % hydrogen peroxide as oxidant in a shorter time. Since these complexes did not dissolve in ordinary organic solvents, the catalysts could be easily separated from reaction mixture, recycled and stored.

1.4.2.4.6 *Metallodendritic catalysts in Oligomerization and Polymerization of olefins.*

New peripherally bound G1 and G2 iron metallodendrimers, with four and eight bis(imino)pyridyl units situated on the dendritic surface were synthesized via hydrosilylation and complexation reactions by Zheng *et al*.[53] These multinuclear iron complexes (Fig 1.19) displayed much higher catalytic activity for ethylene polymerization and produced much higher molecular weight polymers than the corresponding mononuclear complex in reactions performed at low Al/Fe molar ratios.

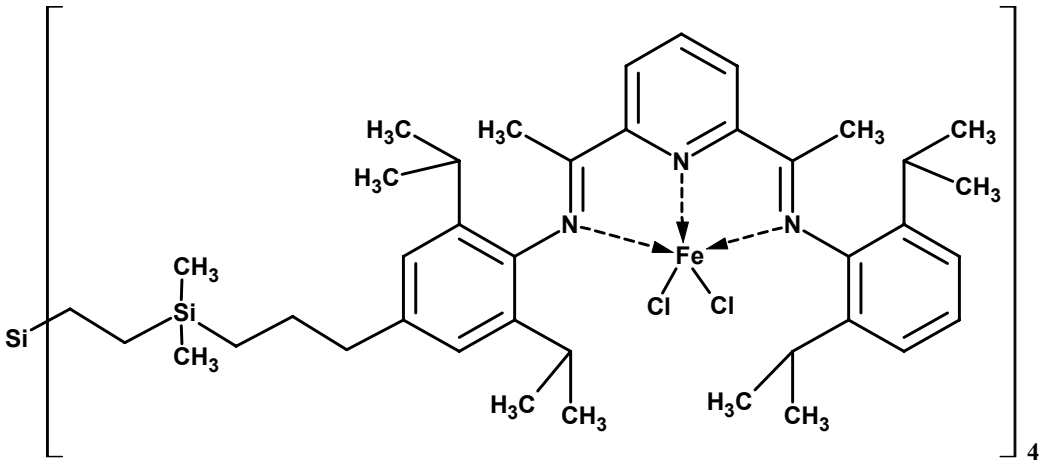

17

Figure 1.19: Structure of the G1 Iron metallodendrimer synthesized by Zheng *et al.*[53]

At higher Al/Fe ratios however, all three catalysts had similar activity although the dendrimeric catalysts produced higher molecular weight polymers than the mononuclear catalyst. These results indicate that steric crowding in the dendritic iron catalysts controls chain transfer during ethylene polymerization to some extent.

Arevalo *et al* reported a study of the ethylene polymerization behaviour of a G2 metallodendrimer based on cyclopentadienyl-aryloxy titanium units (Fig 1.20).[54] Results showed that catalyst performance depended on the aging of the precatalyst solution. The aging of the precatalyst varied from 0 to 7 weeks and it was observed that up to week 6, the activity of the dendrimer catalyst as well as the molecular weight of the products increased. At week 7 the activity and molecular weight decreased. The polydispersity index (PDI)

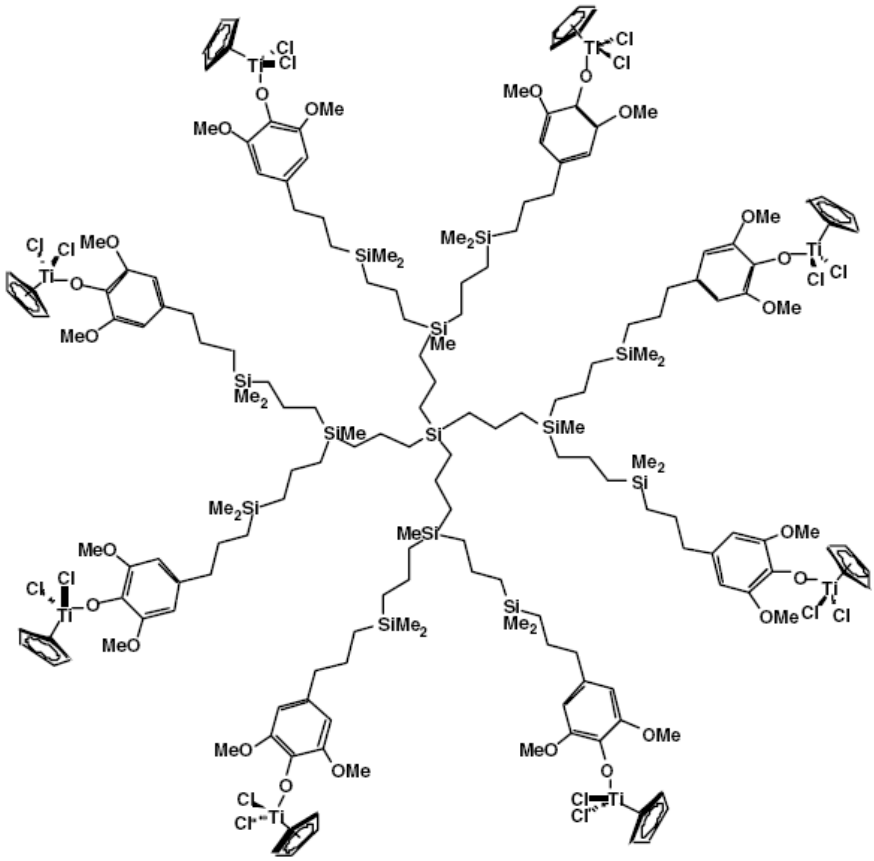

18

Figure 1.20: Molecular representation of the second generation organotitanium-containing dendrimer.[54]

values ranged from 1.51-1.61, and the molecular weights from 6.63 x 10^5 - 10.04 x 10^5 g/mol. The values obtained are of the same order or even higher than those found for the monometallic complex evaluated. Hence, these values suggest that the aging process was not responsible for the high molecular weights and low polydispersities. Instead, the environment around the metal centres may be responsible for such effects.

Andres *et al* described the synthesis of dendritic β-diketiminato titanium and zirconium complexes (Fig 1.21) and their application as ethylene polymerization catalysts. [55] The location of the dendritic wedges in the complexes was chosen in such a way that little steric hindrance should be expected in the environment close to the metal centre.

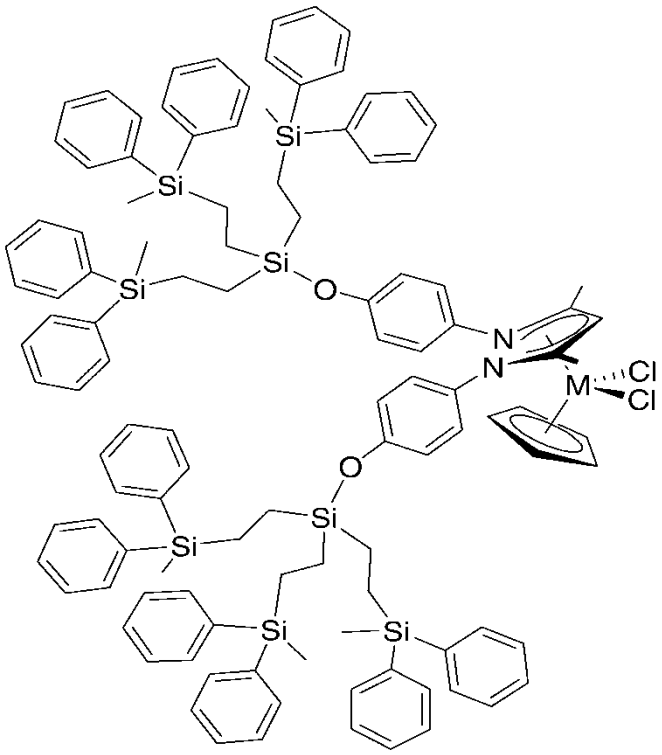

19: M = Ti

20: M = Zr

Figure 1.21: Structures of Ti (**19**) and Zr (**20**) complexes synthesized by Andres *et al*. [55]

When compared to their non-dendritic analogues, the dendritic catalysts showed an increased activity. Also the titanium metallodendrimer catalyst was 7 times more active than the zirconium metallodendrimer catalyst for the polymerization of ethylene.

Benito *et al* described the synthesis of dendritic nickel(II) complexes containing *N*,*N*-iminopyridine chelating ligands (Fig 1.22), and the generation effects on the catalytic oligomerization and polymerization of ethylene .[56] Upon activation with MAO under mild conditions, the nickel derivatives are active for ethylene oligomerization and polymerization, and their catalytic properties are definitely sensitive to the ligand structure and the dendrimer generation.

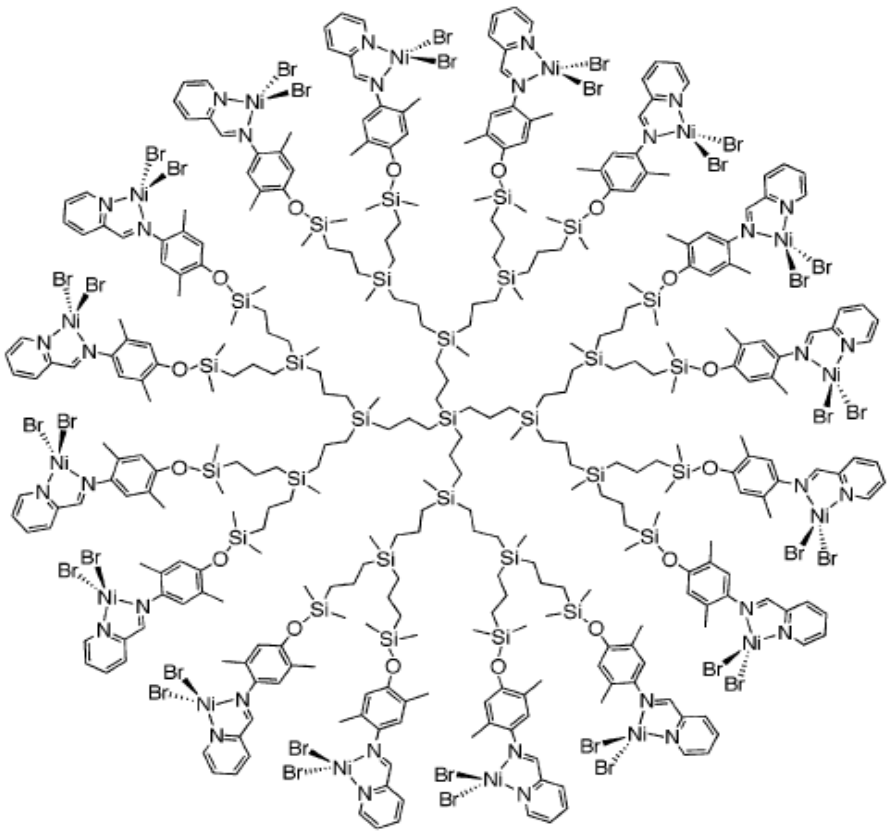

21

Figure 1.22: Generation 3 Nickel Iminopyridine metallodendrimer structure. [56]

Steric protection of axial coordination sites by methyl substituents on the aryl ring increases the activities for both oligomer and polyethylene production. However, the presence of a methyl group on the 6-position of the pyridine moiety, hinders the equatorial coordination sites and causes the reverse effect. The size of the dendrimer regulates the production of ethylene insertion products (oligomer vs polymer), the oligomer chain-length distribution, and the branching density, molecular weight and polydispersity of the polymers. These findings may be useful for controlling the structure or properties of ethylene insertion products.

Although catalyst recycling plays an important role with metallodendrimer catalysts in other catalytic processes, oligomerization and polymerization of olefins using dendrimer catalysts can benefit from improvements in the stability of the active species or in the control of the microstructure, molecular weight or stereochemistry of the polymers.

1.5 Conclusion and Project Objectives.

1.5.1 Conclusion

Dendrimers are versatile three-dimensional macromolecules with appealing properties which can be functional for a multitude of applications. An advantage of dendrimer construction is that functional groups can be added to produce a compound with a specific property. A major aspect of dendrimer chemistry involves the synthesis of metallodendrimers. Dendrimers enrich all fields of chemistry including organic, inorganic, analytical and physical polymer chemistry. The applications of dendrimers are also found in physics, biology, and medicine.

Although metallodendrimer applications are vast, one of its most economically attractive uses is its application as catalysts for various processes. This is due to the ability of metallodendrimer catalysts to bridge the fields of homogeneous and heterogeneous catalysis by not only having the same activity and selectivity as homogeneous catalysts, but also having the ability to be separated from the products and to be recycled like heterogeneous catalysts. Thus metallodendrimers offer lots of potential in the field of catalytic research.

1.5.2 Project objectives.

The main objective of this study was therefore to synthesize new metallodendrimer catalysts based on linear- and cyclic-cored dendrimer frameworks. The linear-cored framework is based on the commercial diaminobutane poly(propylene imine) (DAB-PPI) range (Fig 1.23A). The cyclic-cored dendrimers on the other hand is based on cyclam as a core molecule with the amine groups on the periphery suitable for further modification (Fig 1.23B).

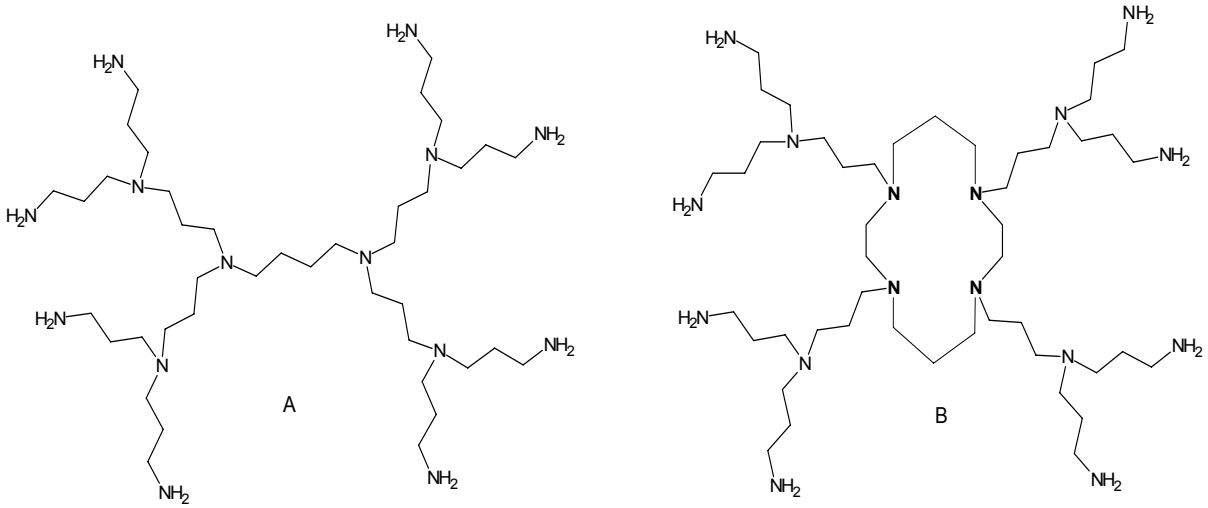

Figure 1.23: (A) Structure of commercially available G2 DAB-PPI dendrimer and (B) Structure of proposed G2 Cyclam-cored propyl chained dendrimer.

It's thought that the cyclic-cored dendrimer framework could lead to more spherical and globular architectures rather than the dumbbell shapes of the DAB dendrimer framework. This could have an impact on the metallodendrimer's properties and hence its catalytic ability.

A further aim was to modify both types of dendrimers via Schiff base condensation reactions and then to complex the functionalised dendrimers to metal salts to form metallodendrimers. The new dendrimers and metallodendrimers were characterized via several analytical techniques such as Infrared (IR) spectroscopy, nuclear magnetic resonance (NMR) spectroscopy, mass spectrometry (MS), elemental analysis, magnetic moment measurements, UV-Vis spectroscopy, thermal gravimetrical analysis (TGA) and differential scanning calorimetry (DSC).

The final aim was to evaluate the synthesized metallodendrimer complexes as catalysts in olefin oligomerization/polymerization as well as norbornene polymerization. The catalytic performance of the linear-cored metallodendrimers is compared to that of the cyclic-cored metallodendrimers. In addition, the effect of dendrimer generation on catalyst activity and selectivity is also investigated.

1.6 References.

[1] D. A. Tomalia, H. Baker, J. Dewald, M. Hall, G. Kallos, S. Martin, J. Roeck, J. Ryder, P. Smith, *Polym. J.,* 17, **1985**, 117.

[2] E. Buhleier, W. Wehner, F. Vogtle, *Synthesis*, **1978**, 155.

[3] G. R. Newkome, Z-Q. Yao, G. R. Baker, V. K. Gupta, *J. Org. Chem.,* **1985**, 50, 2003.

[4] B. K. Nanjwadea, H. M. Bechraa, G. K. Derkara, F.V. Manvia, V. K. Nanjwade, *Eur. J. Pharm. Sci.,* 38, **2009**, 185.

[5] G. R. Newkome, C. D. Shreiner, *Polymer,* 49, **2008**, 1.

[6] C. J. Hawker, J. M. J. Fréchet, *J. Am. Chem. Soc*., 112, **1990**, 7638.

[7] T. Vassilieff, A. Kakkar, *Can. J. Chem.,* 86, **2008**, 540.

[8] E. M. M. de Brabander-van den Berg, E. W. Meijer, *Angew. Chem. Int. Ed*., 32, **1993**, 1308.

[9] F. Vogtle, S. Gestermann, C. Kauffmann, P. Ceroni, V. Vicinelli, L. De Cola, V. Balzani, *J. Am. Chem. Soc.,* 121,**1999**, 12161.

[10] T. M. Figueira-Duarte, S. C. Simon, M. Wagner, S. I. Druzhinin, K. A. Zachariasse, K. Mullen, *Angew. Chem. Int. Ed.,* 47, **2008**, 10175.

[11] I. J. Majoros, C. R. Williams, D. A. Tomalia, J. R. Baker, Jr., *Macromolecules,* 41 **2008**, 8372.

[12] R. van Heerbeek, J. N. H. Reek, P. C. J, Kamer and P. W. N. M. van Leeuwen, *Tetrahedron Lett.,* 40, **1999**, 7127.

[13] W. Maes, D. B. Amabilino, W. Dehaen, *Tetrahedron,* 59, **2003**, 3937.

[14] J. Lee, Y. Suh, M. C. Kung, C. M. Downing, H. H. Kung, *Tetrahedron Lett.,* 48, **2007**, 4919.

[15] K. Endo, Y. Ito, T. Higashihara, M. Ueda, *Eur. Pol. J.,* 45, **2009**, 1994.

[16] B. Klajnert, M. Bryszewska, *Acta Biochim. Pol.,* 48, **2001**, 199.

[17] W. Janga, K. M. K. Selim, C. Lee, I. Kang, *Prog. Polym. Sci.,* 34, **2009**, 1.

[18] A. Trinchi, T. H. Muster, *Supramol. Chem.,* 19, **2007**, 431.

[19] B. R. Matthews, G. Holan, *US Patent 6*, 190, 650, **2001**.

[20] C. J. Hawker, J. L. Hedrick, R. D. Miller and W. Volksen, *MRS Bull*., 25, **2000**, 54.

[21] D. W. C. MacMillan, *Nature*, 455, **2008**, 304.

[22] L. Gitsov, P. T. Ivanova and J. M. J. Fréchet, *Macromol. Rapid Commun.,*15, **1994**, 387.

[23] G. R. Krishnan, K. Sreekumar, *Eur. J. Org. Chem.,* **2008**, 4763.

[24] M. P. Kapoor, H. Kuroda, M. Yanagi, H. Nanbu, L. R. Juneja, *Top. Catal.,* 52, **2009**, 634.

[25] G. R. Newkome, H. J. Kim, K. H. Choi, C. N. Moorefield, *Macromolecules,* 37, **2004**, 6268.

[26] B. J. Ravoo, *Dalton Trans.*, **2008**, 1533.

[27] X. Luo, *Colloid. J.,* 71, 2, **2009**, 281.

[28] E. C. Cutler, E. Lundin, B. D. Garabato, D. Choi, Y. Shon, *MRS Bull.,* 42, **2007**, 1178.

[29] J. Kofoed, J. Reymond, *Curr. Opin. Chem. Biol.,* 9, **2005**, 656.

[30] M. Liu, J. M. J. Fréchet, *PSTT*, 2, 10, **1999**, 393.

[31] S. Svenson, *Eur. J. Pharm. Biopharm.,* 71, **2009**, 445.

[32] A. E. Beezer, A. S. H. King, I. K. Martin, J. C. Mitchel, L. J. Twyman, C. F. Wain, *Tetrahedron,* 59, **2003**, 3873.

[33] L. Balogh, D. R. Swanson, D. A. Tomalia, G. L. Hagnauer, A. T. McManus, *Nano. Lett.,* 1, 1, **2001**, 18.

[34] T. Dutta, N. K. Jain, *Biochim. Biophys. Acta,* 1770, **2007**, 681.

[35] I. J. Majoros, C. R. Williams, J. R. Baker Jr., *Curr. Med. Chem.,* 8, **2008**, 1165.

[36] D. Astruc, C. Ornelas, J. Ruiz, *Acc. Chem. Res.*, 41, **2008**, 841.

[37] K. K. Onga, A. L. Jenkins, R. Cheng, D. A. Tomalia, H. D. Durst, J. L. Jensen, P. A. Emanuel, C. R. Swim, R. Yin, *Anal. Chim. Acta,* 444, **2001**, 143.

[38] E. Alonso, C. Vale´rio, J. Ruiz, D. Astruc, *New J. Chem.,* 21,**1997**, 1139.

[39] J. Losada, I. Cuadrado, M. Moran, C. M. Casado, B. Alonso, M. Barranco, *Anal. Chim. Acta,* 338, **1997**, 191.

[40] H. C. Yoon, D. Lee, H-S. Kim, *Anal. Chim. Acta*, 456, **2002**, 209.

[41] O. A. Arotiba, A. Ignaszak, R. Malgas, A. Al-Ahmed, P. G.L. Baker, S. F. Mapolie, E. I. Iwuoha, *Electrochim. Acta,* 53, **2007**, 1689.

[42] E. de Jesus, J. C. Flores, *Ind. Eng. Chem. Res.,* 47, **2008,** 7968.

[43] N. Brinkmann, D. Giebel, G. Lohmer, M. T. Reetz, U. Kragl, *J. Catal.,* 183, **1999**, 163.

[44] M. T. Reetz, G. Lohmer, R. Schwickardi, *Angew. Chem., Int. Ed.,* 36, **1997**, 1526.

[45] R. W. J. Scott, O.M. Wilson, R. M. Crooks, *J. Phys. Chem. B, 109*, **2005**, 692.

[46] K. Fujita, T. Muraki, H. Hattori, T. Sakakura, *Tetrahedron Lett.,* 47, **2006**, 4831.

[47] T. R. Krishna, N. Jayaraman, *Tetrahedron,* 60, **2004**, 10325.

[48] L. Ropartz, R. E. Morris, G. P. Schwarz, D. F. Foster, D. J. Cole-Hamilton, *Inorg. Chem. Commun.,* 3, **2000**, 714.

[49] J. N. H. Reek, D. de Groot, G. E. Oosterom, P. C. J. Kamer, P. W. N. M. van Leeuwen, *C. R. Chimie,* 6, 2003, 1061.

[50] C. Köllner, A. Togni, *Can. J. Chem.,* 79, **2002**, 1762.

[51] Z. Yang, Q. Kang, H. Ma, C. Li, Z. Lei, *J. Mol. Cat. A: Chem.,* 213, **2004**, 169.

[52] C. Li, Z. Yang, S. Wu, Z. Lei, *React. Funct. Polym.,* 67, **2007**, 53.

[53] Z. Zheng, J. Chen, Y. Li, *J. Organomet. Chem.,* 689, **2004**, 3040.

[54] S. Arevalo, E. de Jesus, F. de la Mata, J. C. Flores, R. Gomez, M. Rodrigo, S. Vigo, *J. Organomet. Chem.,* 690, **2005**, 4620.

[55] R. Andres, E. de Jesus, F. J. de la Mata, J. C. Flores, R. Gomez , *J. Organomet. Chem.,* 690, **2005**, 939.

[56] J. M. Benito, E. de Jesus, F. J. de la Mata, J. C. Flores, R. Gomez, P. Gomez-Sal, *Organometallics, 25,* **2006,** 3876.

Chapter 2:

Synthesis and Characterization of Cyclam-cored dendrimer compounds.

2.1 Introduction to cyclam-based dendrimers.

In this chapter we discuss the synthesis and characterization of new cyclam-cored dendrimers. As an introduction, a brief overview of cyclam-based dendrimers is given below.

2.1.1 Why use Cyclam as a dendritic core?

1,4,8,11-Tetraazacyclotetradecane (cyclam) is one of the most extensively investigated ligands in coordination chemistry. Both cyclam and its 1,4,8,11-tetramethyl derivative can be protonated in aqueous solution and can coordinate a range of metal ions such as Co(II), Ni(II), Cu(II), Zn(II), Cd(II), and Hg(II) with very large stability constants. Furthermore, cyclam and its derivatives have been studied as carriers of metal ions in antitumor and imaging applications and most recently, as anti-HIV agents.[1-5]

Enoki *et al* [6] synthesized novel dendrimers that have a cyclam core. The dendrimer selectively coordinated a $ZnCl_2$ unit in the cyclam ring, and not via the dendron imines. It formed a stable 1:1 complex that was soluble in organic solvents (Fig 2.1). The structure of the dendrimer was investigated by NMR spectroscopy and it showed that the steric characteristics of the core were affected by the generation of the dendrimer and the nature of the coordinated metal.

Saudan *et al* [7] reported the synthesis of novel naphthyl cyclam dendrimers and studied their absorbance, luminescence and effect of protonation (Fig 2.2). They concluded that cyclam is a very interesting core for constructing dendrimers for the following reasons: (i) it can be easily functionalised with dendrons at each of its four nitrogen atoms; (ii) it is 'silent' from the viewpoint of absorption and emission spectra, but it can interact with

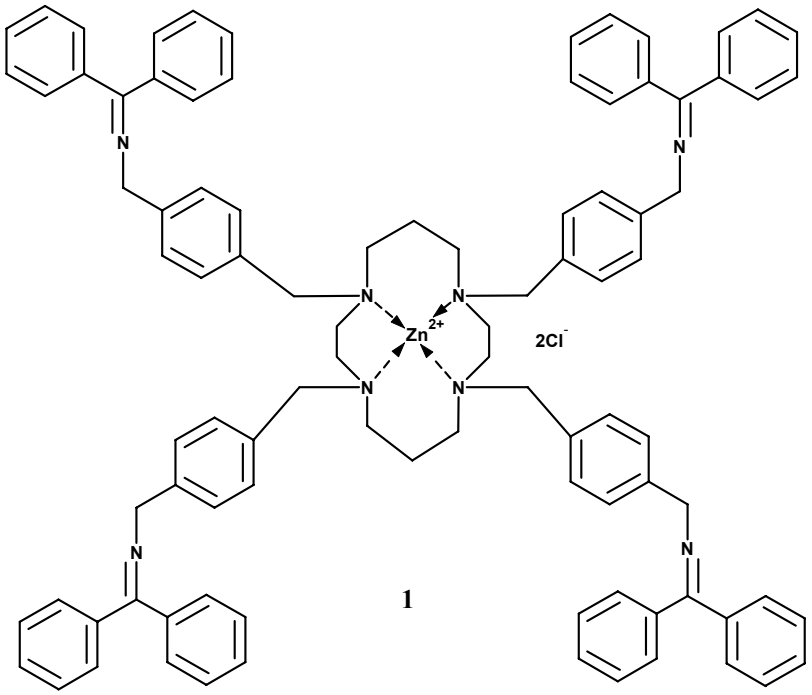

Figure 2.1: Structure of G1 Phenylazomethine Cyclam Dendrimer Zinc Complex.[6]

photoactive groups contained in the dendrimer branches; such interactions can modify the emission properties of the chromophoric dendron units and can cause the appearance of new emission bands; (iii) it can undergo protonation reactions which induce electronic as well as structural rearrangements, with dramatic effects on the emission spectra of the whole dendrimer; (iv) it is an excellent ligand for a variety of transition metal ions.

Saudan *et al* also reported the coordination of zinc to the core of their cyclam based dendrimers[8,9] and later performed experiments on the effect of the simple and dendritic cyclam derivatives on the inhibition of cell growth in the human neuroblastoma TS12 cell line (since cyclam is used as an antitumor agent).[10]

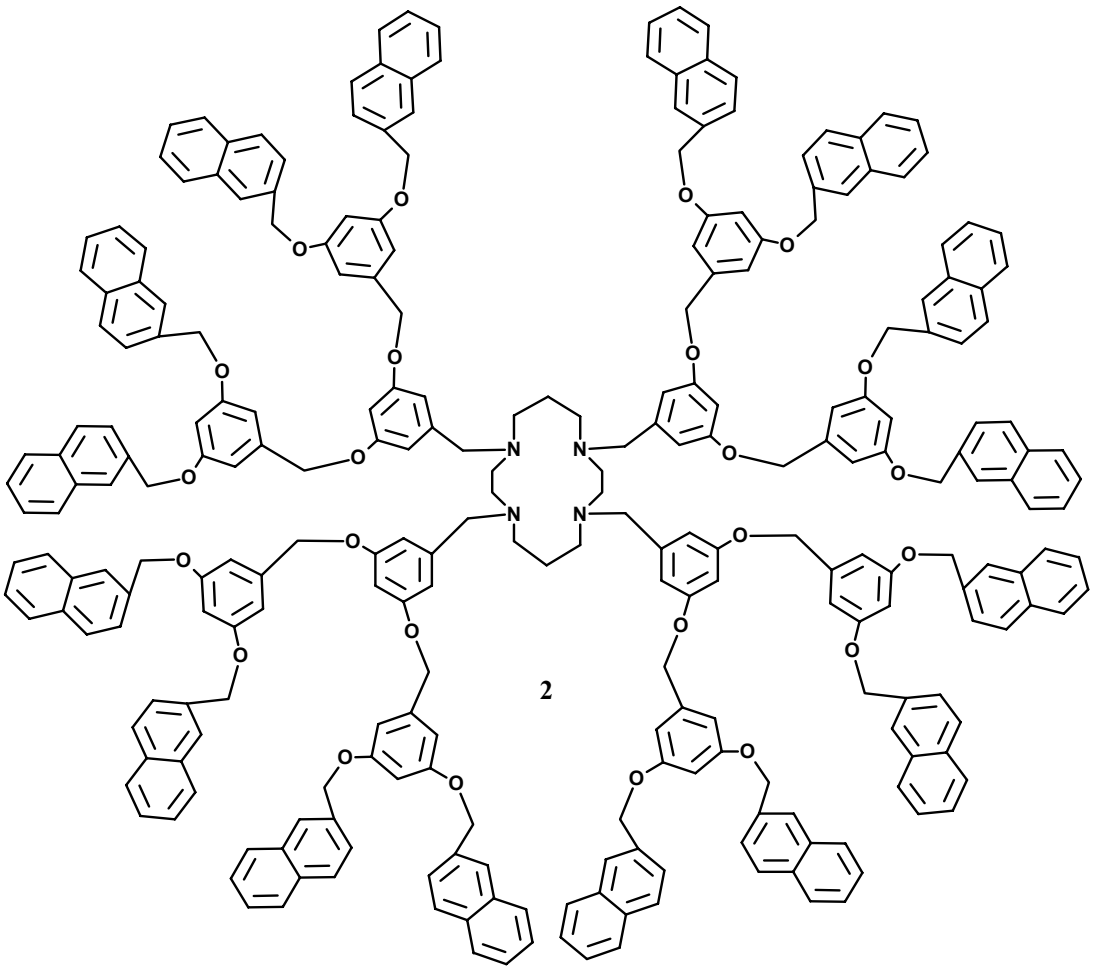

Figure 2.2: Cyclam naphthyl dendrimer synthesized by Saudan *et al.*[7-9]

The results showed that the inhibition effect was practically absent in the case of the generation 1 and generation 2 benzyl and naphthyl dendrimers, moderate for tetranaphthyl substituted cyclam and strong for tetrabenzyl substituted cyclam. Thus in this instance, the simple cyclam complexes showed a higher inhibition effect than their dendrimeric analogues.

Bergamini *et al* [11] prepared for the first time a dendrimer with a biscyclam core appended with dimethoxybenzene and naphthyl units (Fig 2.3). It was thought that the presence of a well-defined metal coordinating unit in the dendritic structure could be useful to

develop opportunities for signal amplification offered by luminescent dendrimers. It was found that the spectral changes caused by these compounds were too weak and too complex to be used for sensory purposes when complexed with $Zn(CF_3SO_3)_2$ and $Cu(CF_3SO_3)_2$ to form the corresponding complexes. It was concluded that while the availability of dendrimers possessing a well-defined ligand unit like cyclam, opens the way for the construction of mixed dendritic-ligand complexes, dendrimers containing two cyclam units can be used, in principle, to construct dendrimers containing two different types of metal ions.

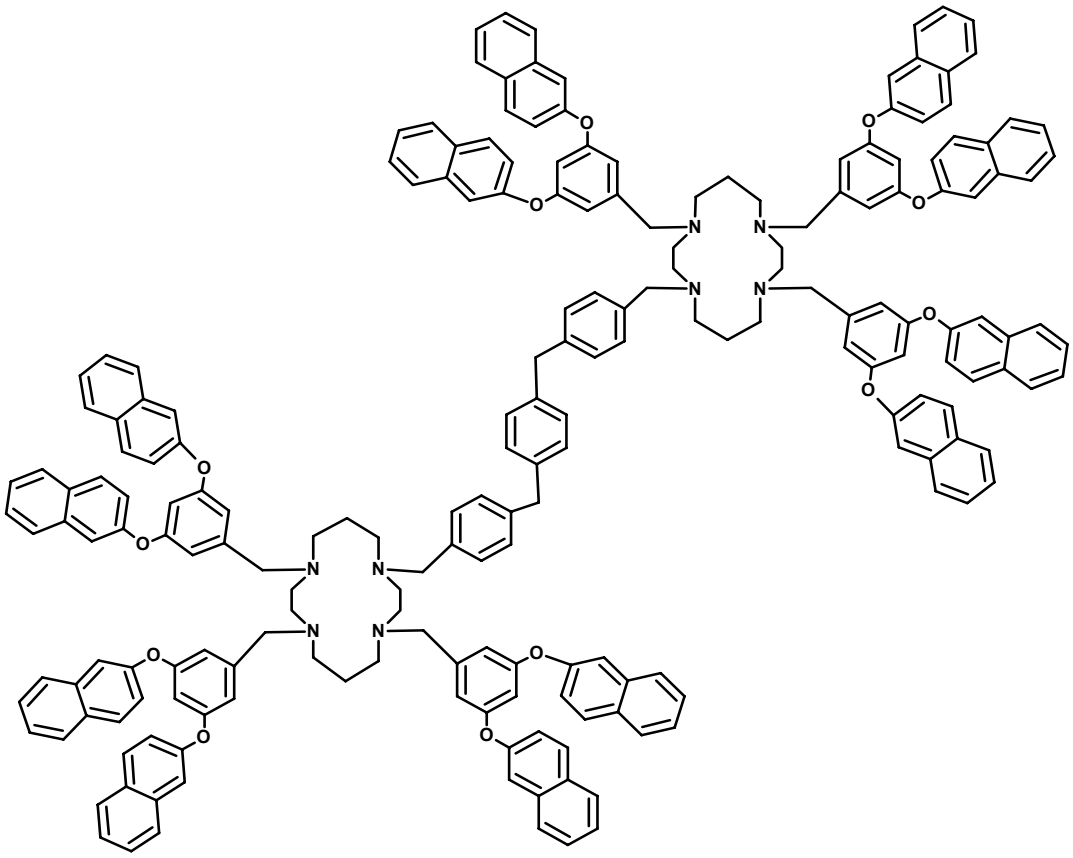

3

Figure 2.3: Bis-cyclam cored dendrimer prepared by Bergamini et al.[11]

Branchi *et al* [12] synthesized a dendrimer (Fig 2.4) consisting of a cyclam core appended with four benzyl substituents that carry, in the 3- and 5-positions, a dansyl amide derivative in which the amide hydrogen is replaced by a benzyl unit that carries an oligoethylene glycol chain in the 3- and 5-positions. It was thought that this dendrimer could be soluble in water because of the oligoethylene glycol chains, but this was not the case. They studied the absorption and luminescence properties of these dendrimers and the changes taking place upon titration with acid and a variety of divalent (Co^{2+}, Ni^{2+}, Cu^{2+}, Zn^{2+}), and trivalent (Nd^{3+}, Eu^{3+}, Gd^{3+}) metal ions as triflate and/or nitrate salts.

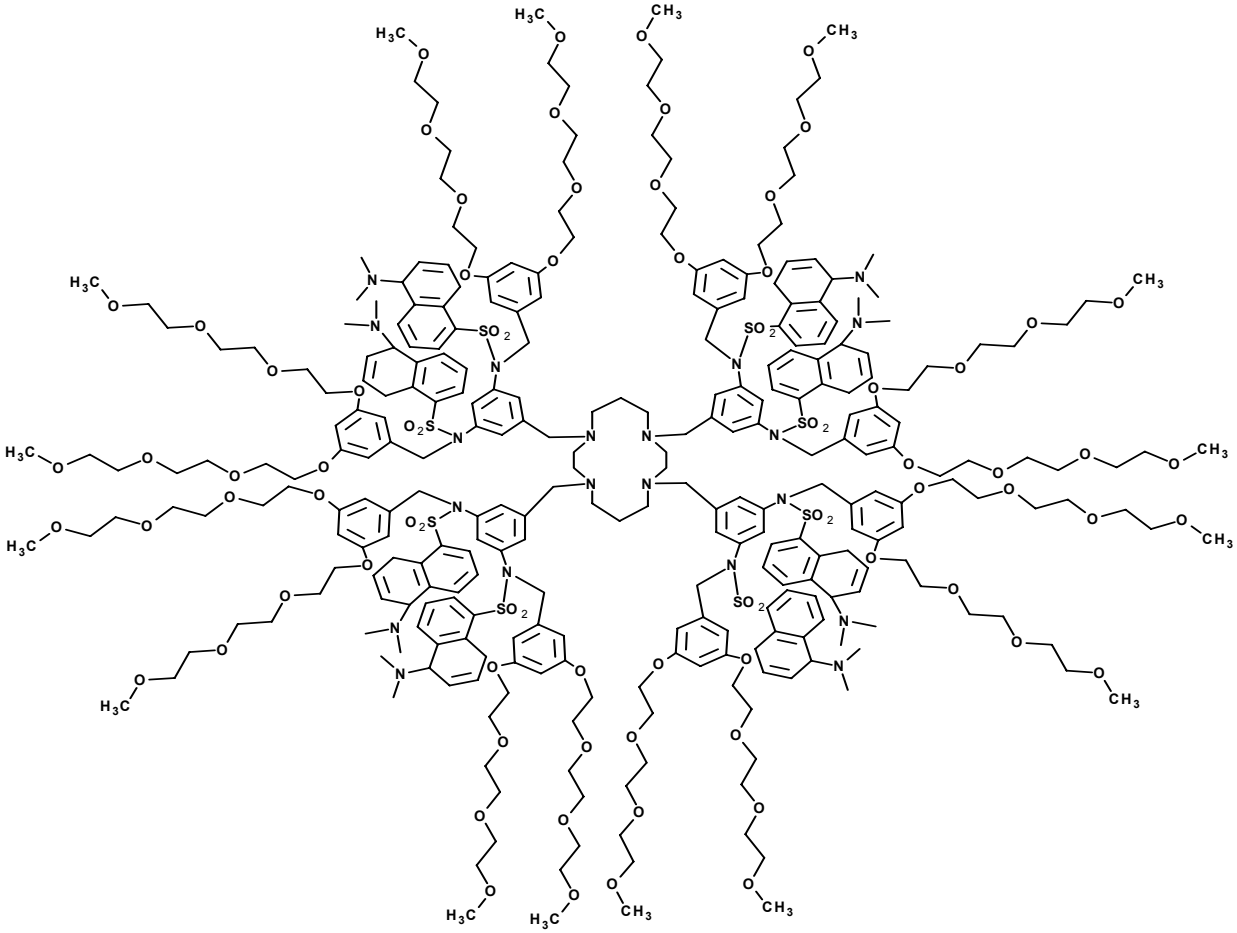

4

Figure 2.4: Structure of cyclam dansyl amide dendrimer synthesised by Branchi *et al.*[12]

The first site to be involved in the metal coordination (one equivalent of metal ion) is the cyclam core, followed by the dansyl units. It was concluded that cyclam was an ideal core for obtaining dendrimers capable of associating protons and metal ions and that the dansyl chromophoric group was a useful unit to construct dendrimers sensitive to environmental perturbations.

Cyclam-based dendrimers is a relatively new concept, with not many examples reported in literature. However, those reported show favourable properties especially since the cyclam core is able to coordinate to metal centres.

Wainwright[13] described the synthesis of N,N',N'',N'''-tetrakis(2-cyanoethyl)-1,4,8,11-tetra-azacyclotetradecane which is referred to as a tetracyanoethylcyclam ligand, **L1** (Fig 2.5). He later published the results of the reduction of this ligand with sodium and toluene as a reducing agent, to afford the modified amine ligand, **L2**.[14]

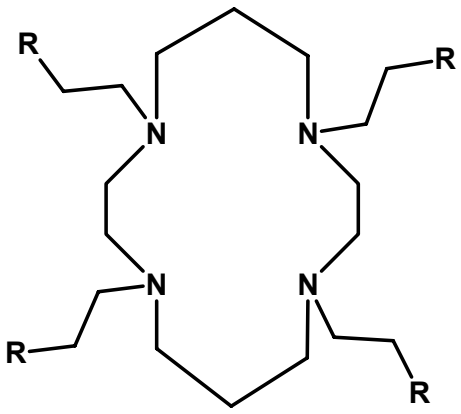

L1: R = CN

L2: R = CH_2NH_2

Figure 2.5: Tetracyanoethylcyclam ligands **L1** and its reduced analogue **L2** reported by Wainwright.[13,14]

To our knowledge, there have been no other reports on attempts to elaborate this ligand to higher generations. This can be done via sequential stepwise Michael addition reactions followed by nitrile reduction in order to obtain cyclic-cored amine terminated dendrimers (Chapter 1, Fig 23B). Hence, in this chapter we describe the synthesis and characterization of **L1** and **L2** (which will be regarded as a generation 1 cyclam propyl dendrimer ligand) and further attempts to expand this ligand to generation 2 dendrimers, **L3** and **L4**. We also describe the synthesis of cyclam cored dendrimers with 4-amino benzyl units, **L5**-**L8**.

2.2 Results and Discussion.

2.2.1 *Synthesis and characterization of ligand, **L1**.*

The ligand, **L1**, was first synthesized by Wainwright[13] by reacting cyclam with excess acrylonitrile under reflux in the absence of solvent via a Michael addition reaction and then subsequent recrystallization of the oily residue to obtain a white crystalline solid. In our hands, this synthetic method was found to be not as efficient as claimed by Wainwright, with only low yields being obtained. A possible reason for the low yield could either be the short reaction time which is insufficient for complete Michael addition or the work-up process which might require successive recrystallization steps.

Consequently this reaction was attempted under various reaction conditions, varying temperature, time and also employing several different solvents. It was determined that the optimum conditions were simply the addition of the reagents employed, at room temperature, using methanol as a solvent. The two starting materials are completely soluble in the solvent,

and results in a colourless reaction mixture. The mixture was stirred for 24 hours, during which time gradual formation of a white precipitate is observed. Isolation of this white precipitate via filtration followed by drying under vacuum, gave the desired product in approximately 95 % yield. Recrystallization of the white solid from dichloromethane and methanol yielded colourless crystals. The method reported here is more efficient than that reported by Wainwright in that it results in an improved yield, does not require excess reagents and involves a relatively simple work-up procedure.

The FTIR spectrum of **L1**, shows an intense band at 2244 cm^{-1} which is indicative of the í(C≡N) stretching frequency, of which the appearance and disappearance will be monitored when this ligand is reduced to obtain the amine terminated ligand, **L2**. Also as the í(C≡N) band disappears, the N-H (amine) band appears. The ^{1}H NMR spectrum of **L1** shows two peaks at 1.67 ppm and 2.48 ppm, which is due to the cyclam protons and another two peaks at 2.63 ppm and 2.79 ppm for the cyanoethyl protons. **L1** was further characterized by ^{13}C NMR, ESI-MS and elemental analysis. All the spectral data corresponds well to that published by Wainwright.[13] In our hands, acceptable elemental analysis was obtained for this compound. All characterization data are reported in the experimental section at the end of this chapter.

2.2.2 *Synthesis and characterization of ligand, **L2**.*

L2 is synthesized by reducing the peripheral nitrile groups of **L1** to obtain the amine terminated G1 ligand, N,N',N'',N'''- tetrakis(aminopropyl) cyclam dendrimer. There are several ways to reduce a nitrile to an amine; either by catalytic hydrogenation or by using

reducing agents such as lithium aluminium hydride ($LiAlH_4$), sodium borohydride ($NaBH_4$) and potassium borohydride (KBH_4).

Several different approaches were employed in an attempt to reduce **L1** to **L2**. When using $LiAlH_4$ it was found that only partial reduction occurred to yield a mixture of nitrile, imine and amine terminated compounds, with the unreduced nitrile being the major fraction of the product mixture. Varying reaction conditions had no significant impact on the nature of products obtained; thus this method was not pursued any further.

Using $NaBH_4$ as a reducing agent afforded no reduction of **L1** even after several attempts and employing varying reaction conditions. Wu *et al* [15] published an efficient and mild system for the reduction of nitriles to amines using Raney Ni and KBH_4. However in our case, when employing this method, only partial reduction of the nitrile was obtained.

Catalytic hydrogenation of **L1** was attempted, using 5 % Pt/C as a catalyst in methanol at 70 ºC and 20 bar H_2 pressure. Characterization of products with IR and ^1H NMR revealed a mixture of the unreduced starting material, **L1**, the partially reduced imines and the expected amine, **L2**. Thin Layer Chromatography (TLC) of the oily residue confirmed three different fragments. However, the conversion to the expected amine was very low (10 %) and separating the imine from the amine proved difficult.

Using 5 % Pd/C as a catalyst instead of the Pt/C, did not show much difference in yield or selectivity. Even extending the reaction time to 24 hours proved futile. Catalytic hydrogenation of nitriles to amines usually involves high pressure (50-100 bar) reactions, which we were not equipped to perform.

Jebasingh *et al* [16] reported the efficient reduction of cyanoethyl cyclen, an analogue of the cyclam compound, by using a sodium-toluene reduction system. Wainwright [14] also used

this type of sodium-toluene reduction system to reduce the cyanoethyl cyclam dendrimer to the tetrakis (aminopropyl) cyclam dendrimer. This method entails refluxing the cyclam in a suspension of sodium metal in toluene over a specified time, after which an appropriate amount of ethanol is added dropwise to the mixture until all the sodium metal is dissolved. The source of H_2 for the reduction comes from the reaction of ethanol with sodium metal, to produce sodium ethoxide and hydrogen gas. The mixture is then further refluxed for a set time. It is then allowed to cool, during which time sodium ethoxide settles out of solution. The sodium ethoxide is then filtered off, washed with toluene and the filtrate is then concentrated to give the reduced product as a pale yellow oily residue. Both reduction processes are essentially the same, except for the purification steps. Wainwright extracted the product with boiling benzene which resulted in a pale yellow oil. In the Wainwright reduction, the ligand, **L2**, was purified by first preparing the complex $[Ni(H_4\mathbf{L2})(ClO_4)][ClO_4]_5$, and then removing pure **L2** from it. Jebasingh extracted the pale yellow residue with chloroform and obtained an off white solid as product.

Using Jebasingh's method we obtained the desired product as an oil, however in very low yield (20 %). The reaction time was extended but there was no significant improvement in the yield. It was thought that the product is possibly lost during the filtration process, and that thorough washing of the sodium ethoxide could increase the amount of product obtained. The extensive washing made little difference. The procedure was then adapted where instead of filtering off the sodium ethoxide, a specified amount of water was added to the vessel containing the product mixture. The sodium ethoxide dissolved in the water and the mixture separated into two layers. The organic layer was separated from the aqueous layer using a separating funnel. The organic layer was dried over potassium carbonate and after the filtration of the drying agent, the filtrate was concentrated via rotary evaporation. The

resulting light brown residue was extracted by adding chloroform to the product, and allowing the solution to stand for 72 hours. The resulting impurities are filtered off and the solution concentrated to give a pale yellow oil as product. The exhaustive extraction is needed as all the impurities do not precipitate out over shorter times as monitored by FTIR. The yield increased significantly from 20 % to between 70-75%.

The FTIR spectrum of **L2**, shows the absence of the band at 2244 cm^{-1} which is due to the í(C≡N) stretching frequency of the starting nitrile, and the appearance of the í(N-H) stretching frequency at 3352 cm^{-1}. This shows that reduction of the nitrile had occurred. The ^{1}H NMR spectrum of **L2** shows the appearance of the peak at 3.59 ppm, due to the methylene protons of the carbon attached to the amino group. This is further confirmation that the reduction of the CN to CH_2NH_2 had taken place. Additional characterization of this compound was previously published by Wainwright.[14]

2.2.3 *Synthesis and characterization of ligand, **L3**.*

L3 is the generation 1.5 octakis(cyanoethyl) cyclam dendrimer which is synthesized by a Michael addition reaction of the G1 tetrakis(aminopropyl) cyclam dendrimer with an excess of acrylonitrile as shown in Scheme 2.1. The same synthetic procedure was followed as that used for the synthesis of the G1 compound, **L1**. Ligand **L3**, which is a novel compound, was isolated as a light beige oil. The FTIR spectrum of **L3** shows the appearance of a nitrile band at 2246 cm^{-1} which is expected, and also the disappearance of the N-H band around 3300-3500 cm^{-1}. This indicates that Michael addition had taken place to afford the G1.5 octakis(cyanoethyl) cyclam dendrimer.

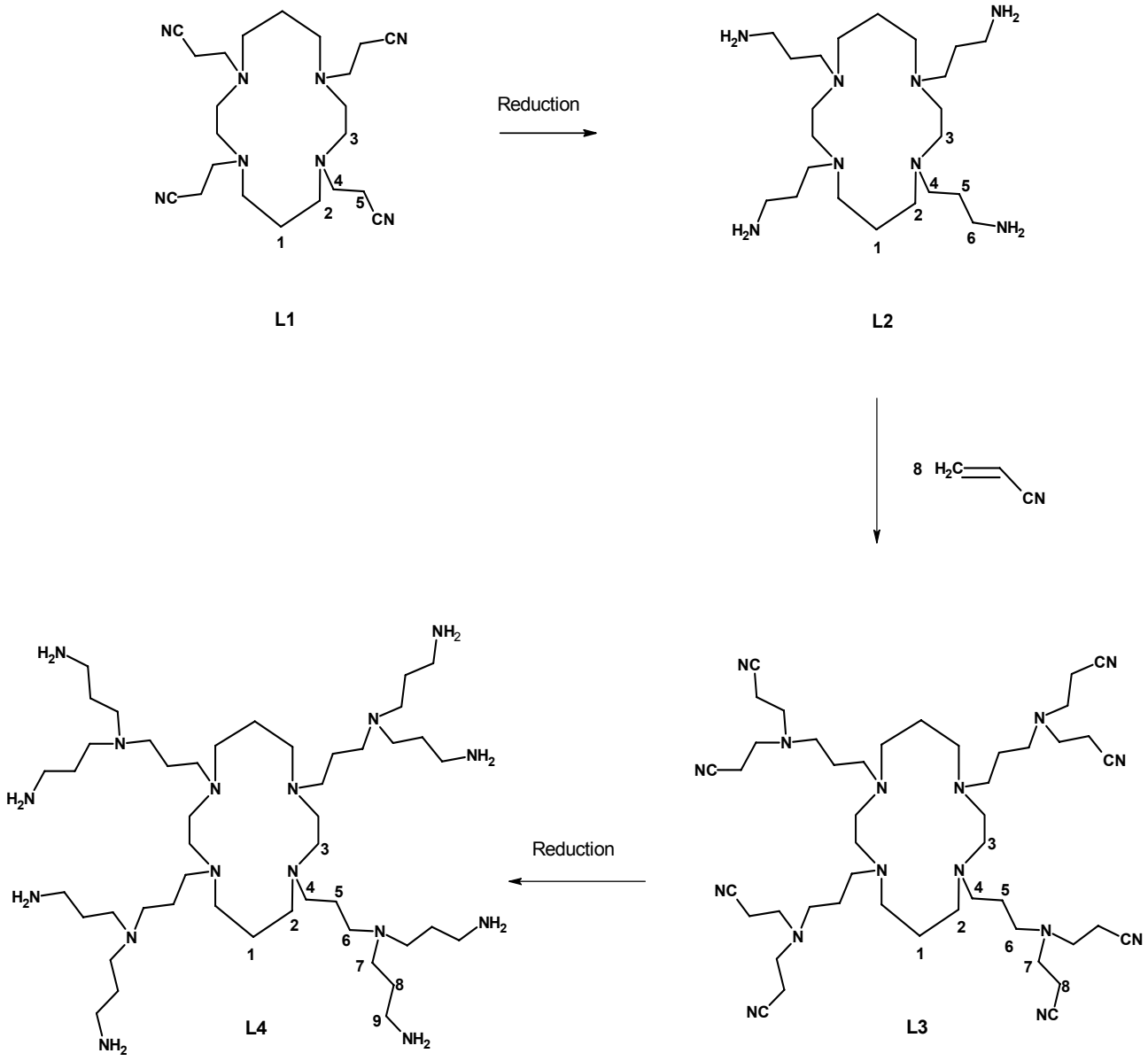

Scheme 2.1: Reaction scheme for synthesis of **L3** and **L4**, numbered protons for reference to ^{1}H NMR spectra.

The ^{1}H NMR spectrum of **L3** also shows the absence of a peak at 3.59 ppm which was present in the ^{1}H NMR spectrum of **L2** and which is due to the CH_2 group adjacent to the amino functionality. This is expected since the amino group will react with the vinyl group of acrylonitrile in the Michael addition step. The ^{13}C NMR spectrum shows the nitrile carbon at

119 ppm as expected as well as the carbons surrounding the tertiary amine (aliphatic branches) at 50.13 ppm; 50.46 ppm and 51.09 ppm, indicating that Michael addition to generate the G1.5 dendrimer was successful.

The ESI-MS fragmentation pattern for **L3** is shown in Scheme 2.2.

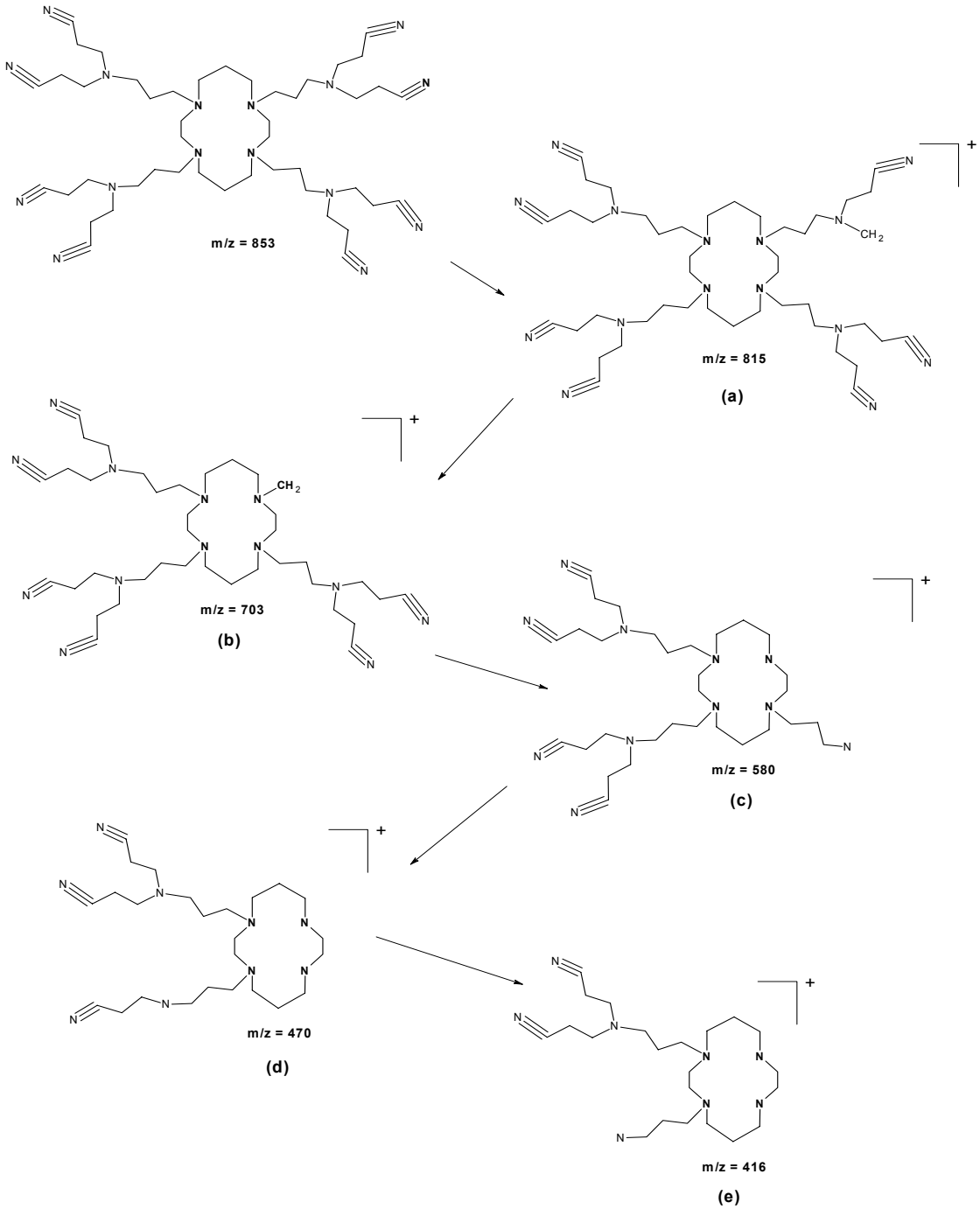

Scheme 2.2: ESI-MS fragmentation pattern for ligand, **L3**.

The spectrum shows a molecular ion peak at m/z = 815, which corresponds to a loss of a methylene cyano group as shown by fragment **(a)** in the scheme. This is followed by the loss of an alkyl branch resulting in fragment **(b)** at m/z = 703. A sequential loss of the alkyl branches occurs to give fragments **(c)** at m/z = 580, **(d)** at m/z = 470 and **(e)** at m/z = 416. It is not unusual for dendrimers to undergo this type of fragmentation.[17]

The elemental analysis data corresponds well to the calculated data, with the inclusion of 0.75 mol of dichloromethane. The dendrimer products are usually oils and are subsequently transferred by dissolving in dichloromethane and then evaporating the solvent. These solvent molecules are often trapped within the dendrimer framework and attempts to remove these encapsulated solvent molecules under vacuum are unsuccessful. The entrapment of CH_2Cl_2 was confirmed by proton NMR analysis. A clear signal at 5.30 ppm shows the presence of the CH_2Cl_2 protons. **L3** is obtained in good yield, 85 %. Full characterization data is recorded in the experimental section.

2.2.4 *Synthesis and characterization of ligand, **L4**.*

L3 was reduced in the same manner as **L1**, in order to obtain the amino terminated G2 dendrimer **L4**. The initial product obtained was a light brown oil but was found to be impure. Attempts to purify this compound were not successful since separation via column chromatography resulted in the products being immobilized on the silica, thus it was established that the best solution was to ensure complete reduction by increasing the reaction time as deemed necessary, which we have subsequently done.

The FTIR spectrum of **L4** shows the disappearance of the í(C≡N) band of the starting material with the concomitant appearance of a í(N-H) band at 3396 cm^{-1} as illustrated in

Fig 2.6. Going from **L1** to **L4**, the presence and absence of the nitrile band was monitored by FTIR spectroscopy during each synthetic step. The concurrent absence and presence of the N-H band (from reduction of the CN group) is also depicted in column 3 of Table 2.1 which represents a summary of the spectral data for ligands, **L1-L4**.

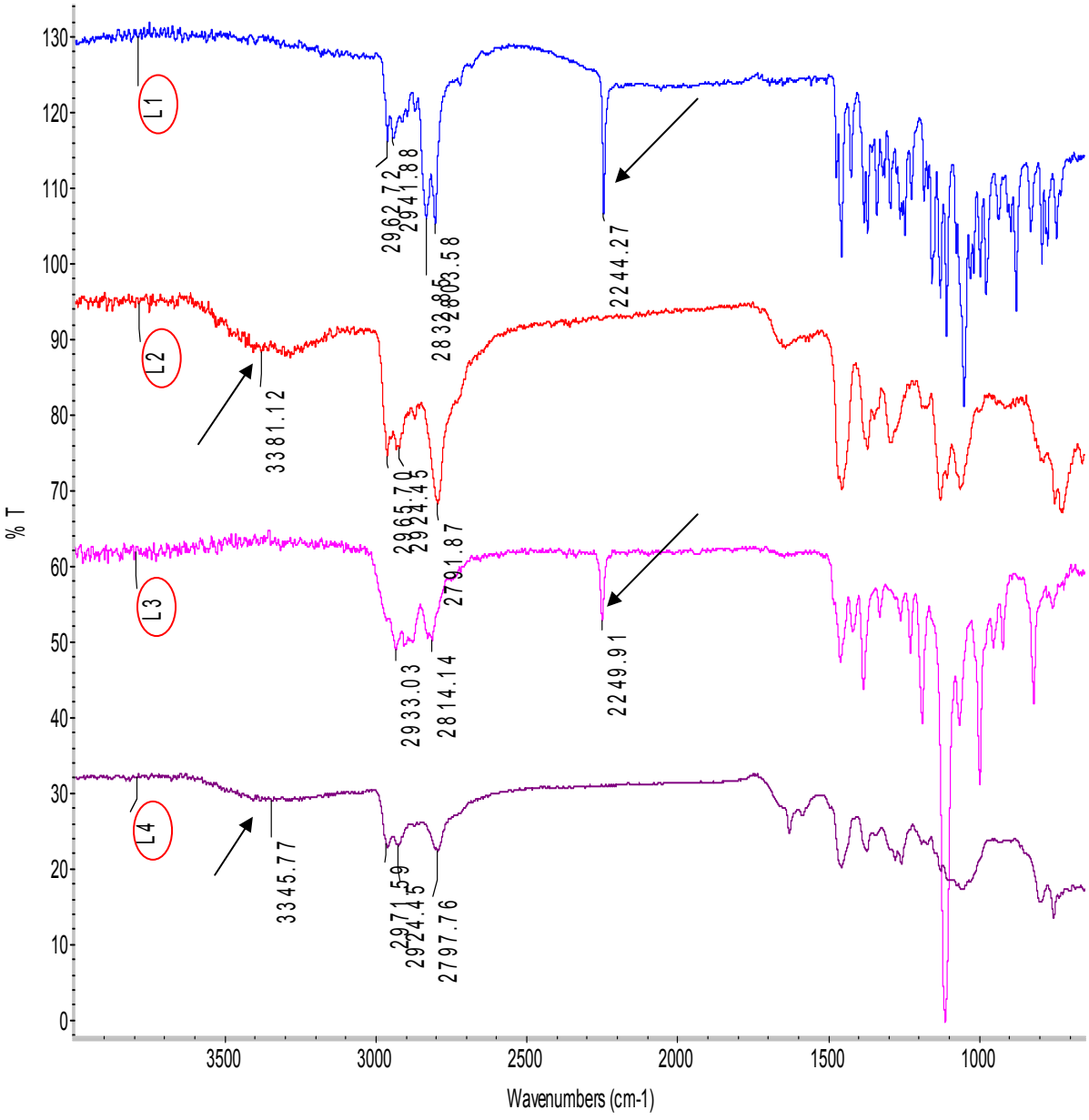

Figure 2.6: FTIR spectra with the arrows depicting the appearance and disappearance of the ί(C≡N) with the concomitant disappearance and appearance of the ί(N-H) band going from **L1-L4**.

Table 2.1: Spectral data for ligands **L1-L4**.

Ligand	FTIR[a] (cm^{-1})		^{1}H NMR[b] (ppm)	[ESI$^+$] [c] (m/z)
	í(C≡N)	í(N-H)	$C\underline{H}_2NH_2$	$[M]^+$
L1	2244	-	-	413
L2	-	3269	3.59	428[d]
L3	2264	-	-	840[e]
L4	-	3396	3.68	953[f]

[a]Recorded in solid state on ZnSe crystal using ATR accessory. [b]Recorded as a $CDCl_3$ solution. [c]Recorded in solution using an acetonitrile and water mixture. [d]Published results [14]. [e]$[M-N]^+$ at m/z = 840. [f]$[M+3Na]^+$ at m/z = 953.

The ESI-MS spectrum of **L4**, shows a molecular ion peak at m/z = 953, which can be assigned to an adduct of the parent ion with three sodium ions.

The appearance of terminal amino groups in the reduced ligands, **L2** and **L4**, were also monitored by ^{1}H NMR spectroscopy, shown in Table 2.2 with the proton labels corresponding to those in Scheme 2.1. The ^{1}H NMR spectrum shows all the relevant peaks, most importantly the peak at 3.68 ppm, which is indicative of the protons attached to the carbon atom adjacent to the amino groups of the product, **L4**. The microanalysis results for **L1-L4** are shown in Table 2.3. From the characterization summary, we can confirm that the desired dendrimers were synthesized.

Table 2.2: ^{1}H NMR spectral data for ligands, **L1-L4**.

Atom label	L1		L2		L3		L4	
	ä/ppm	Integration/ Multiplicity	ä/ppm	Integration/ Multiplicity	ä/ppm	Integration/ Multiplicity	ä/ppm	Integration/ Multiplicity
1	1.67	4H, m, br	1.56	4H, m, br	1.04	4H, m	1.11	4H, m
2	2.48	8H, t	2.26	8H, t	2.58	32H, m	2.05	8H, t, br
3	2.63	8H, t	2.67	8H, t	2.58	32H, m	2.34	8H, t, br
4	2.79	8H, t	2.46	8H, t	2.58	32H, m	2.22	8H, t, br
5	2.59	8H, t	1.67	8H, m	1.65	8H, m	1.34	8H, m
6	-	-	3.59	8H, t	2.58	32H, m	2.64	32H, m, br
7	-	-	-	-	2.77	16H, t	2.64	32H, m, br
8	-	-	-	-	2.45	16H, t	1.69	16H, m
9	-	-	-	-	-	-	3.66	16H, t

Table 2.3: Microanalysis data for ligands **L1-L4**.

Ligand	% Calculated			% Found		
	C	H	N	C	H	N
L1	64.05	8.80	27.16	64.08	8.65	27.60[a]
L2	31.90	8.0	13.80	31.80	8.0	13.80[a,b]
L3	61.30	8.45	24.5	61.10	8.82	25.06[c]
L4	62.40	12.29	25.31	62.41	12.52	25.40

[a]Published results.[13,14] [b]Inclusion of 2 mol HCl. [c]Inclusion of 0.75 mol CH_2Cl_2.

2.2.5 *Synthesis and characterization of ligand, **L5**.*

In an attempt to synthesize more rigid dendrimer structures than the cyclam-cored propyl branched compounds, we embarked on the synthesis of G1 and G2 cyclam-cored dendrimers with benzyl branches (**L5-L8**) instead of the more linear propyl branches (**L1-L4**). **L5** (Fig 2.7) is the benzyl branched analogue of **L1**. The synthesis of **L5** was first published by Comba *et al* [18] in 2001. They studied the copper(II) compounds of these cyclam benzonitrile derivatives. To our knowledge there have been no reports on the use of **L5** as a dendrimer scaffold. Our aim was thus to reduce the nitrile bond to an amine, and then subsequently apply a divergent growth protocol to afford a cyclam-aminobenzyl dendrimer framework.

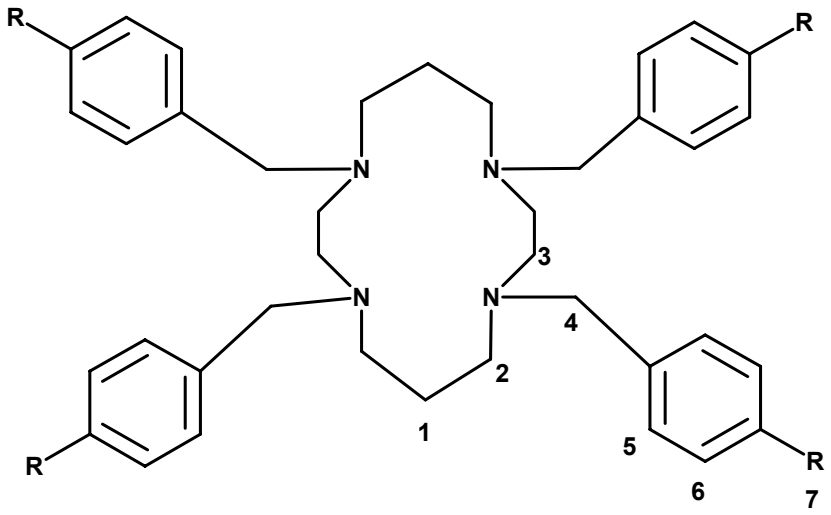

L5: R = CN

L6: R = CH_2NH_2

Figure 2.7: Tetracyanobenzylcyclam ligands **L5** reported by Comba[18] and **L6**.

A similar synthetic procedure was followed as that published by Comba *et al*. Cyclam and NaOH was dissolved in water and 4-bromomethyl benzonitrile was dissolved in chloroform. The organic solution was added dropwise to the aqueous solution, and the mixture was stirred at room temperature for 8 hours. The organic phase was separated from the aqueous phase and then dried over Na_2SO_4. After solvent evaporation a white solid was produced. The product was recrystallized from chloroform and methanol to yield colourless crystals. Product yield is 90 %. The FTIR spectrum shows a strong sharp band at 2225 cm^{-1} assigned as the í(C≡N) stretching frequency. A medium intensity band at 1608 cm^{-1} is also observed and this is due to the benzene ring's í(C=C) stretching frequency. The ^1H NMR spectrum show peaks (assignment of atom labels in Fig 2.7) at 1.64 ppm **(1)**, 2.47 ppm **(2)** and 2.58 ppm **(3)** that are due to the methylene protons on the cyclam ring. A peak at

3.42 ppm **(4)** is due to the protons of the methylene group linking the cyclam and the benzonitrile rings, and the peaks at 7.41 ppm **(5)** and 7.53 ppm **(6)** are due to the aromatic protons. The ^{13}C NMR spectrum shows a peak at 119.58 ppm which is assigned to the nitrile carbon atom and the peak at 59.43 ppm is due to the protons of the methylene group linking the cyclam and the benzonitrile rings.

L5 was further characterized by ESI-MS and elemental analysis. All the spectral data corresponds well to that published by Comba.[17] In our hands, acceptable elemental analysis was obtained for this compound. All other characterization data are reported in the experimental section at the end of this chapter.

2.2.6 *Synthesis and characterization of ligand, **L6**.*

Reduction of **L5** afforded the amino terminated dendrimer, **L6**. The same reduction method was used as that employed for **L2**, i.e. the sodium/toluene reduction process. The tetrakis(cyanobenzyl) cyclam compound was refluxed with sodium in toluene for 15 hours, after which ethanol was added dropwise. The solution appears light pink until all the sodium is destroyed, after which the solution became grey. The solution was allowed to cool to ensure that all the sodium ethoxide precipitated out. The same aqueous work-up used previously was employed, and after extraction with chloroform, a light yellow oily residue was obtained.

The appearance and disappearance of the nitrile band was followed by FTIR spectroscopy. The nitrile band at 2225 cm^{-1} disappeared and the presence of a í(N-H) band was observed at 3369 cm^{-1}, indicating that the compound was successfully reduced. The ^{1}H NMR spectrum shows the benzene ring protons at 7.17 ppm and 7.30 ppm, as well as a

peak at 3.86 ppm due to the protons of the methylene group adjacent to the amino functionality in **L6**. This proves that reduction of the benzonitrile G1 dendrimer compound **L5** had indeed occurred. The ^{13}C NMR spectrum shows the carbon atom adjacent to the amino group has shifted from 119.58 ppm (for the nitrile carbon) to 52.10 ppm (for the reduced nitrile).

The ESI-Mass spectrum of **L6** shows a high mass peak at m/z = 659. This corresponds to the fragment [M-NH_2]. Elemental analysis results are shown in Table 2.6. All characterization data confirm the structure of **L6**.

2.2.7 *Synthesis and characterization of ligand, **L7**.*

L7 and **L8** (Fig 2.8) are the G2 cyclam-benzyl dendrimer compounds. A similar synthetic procedure was followed as that for **L5**, however, the G1 aminobenzyl cyclam dendrimer was dissolved in chloroform instead of water as in the previous method. This is because the starting G1 benzyl dendrimer is an oil and is more soluble in chloroform than in water. After dissolving NaOH in water and 4-bromomethyl benzonitrile in chloroform, all three solutions were added together. The biphasic mixture was stirred at room temperature for 72 hours. The organic phase was separated from the aqueous phase, and then dried over Na_2SO_4. The organic layer was then evaporated via rotary evaporation to produce an oily yellow product.

Attempts to solidify the product by precipitation from chloroform and methanol proved futile. From TLC of the isolated product, we observe 2 fragments, one of which corresponds to bromomethyl benzonitrile. To separate the product from unreacted bromomethyl benzonitrile, the residue was dissolved in DCM (5 ml). Hexane (15 ml) was

then added to the solution. The mixture was swirled and an oil was observed to form at the bottom of the round bottom flask. The excess bromomethyl benzonitrile is left in solution. The solution was then decanted, and the oil was dried. DCM (1 ml) was added to the dried oil, and the pentane (5ml) was layered on top of the solution. Slow evaporation of the mixed solvents gave the product as a light yellow solid material with an 80 % yield.

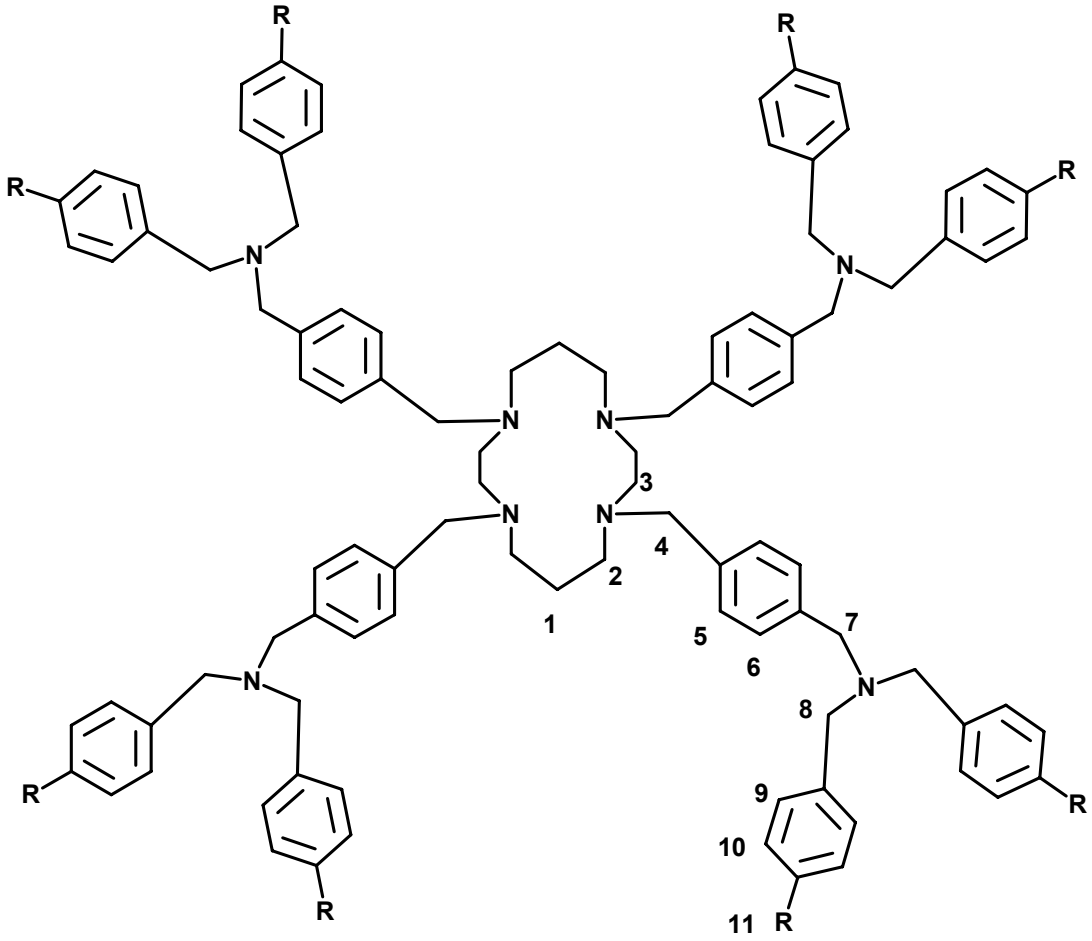

L7: R = CN

L8: R = CH_2NH_2

Figure 2.8: Structure of Generation 2 octakis(cyanobenzyl)cyclam ligand, **L7** and octakis(aminobenzyl)cyclam ligand **L8**.

The FTIR spectrum shows the appearance of a nitrile band at 2226 cm^{-1}. Aliphatic C-H bands are also visible at 2923 cm^{-1} and 2812 cm^{-1} which is absent in the IR spectrum of bromomethyl-benzonitrile. When compared to the spectrum of bromomethyl benzonitrile, it is clear that no excess starting material is present in the product. A strong band at 1607 cm^{-1} is also observed and this is due to the benzene ring's í(C=C) stretching frequency.

The ^{1}H NMR spectrum displays the four 1^{st} generation phenyl ring protons at 7.52 ppm and the eight 2^{nd} generation proton peaks at 7.62 ppm as determined by the intensity of the proton signals. The peak at 3.60 ppm is due to the methylene protons surrounding the tertiary amine units of **L7**. The ^{13}C NMR shows the nitrile carbon signal at 118.98 ppm and the carbon signal at 58.17 ppm is due to the three carbon atoms adjacent to the internal tertiary amine N-atoms of **L7** indicating the extension of the G1 dendrimer to the G2 dendrimer. The ESI-Mass spectrum shows a high mass peak at m/z = 1621 which can be assigned to a sodium adduct of the parent ion. Microanalysis results are shown in Table 2.6.

2.2.8 *Synthesis and characterization of ligand, **L8**.*

Reduction of **L7** afforded the generation 2 octakis(aminobenzyl)cyclam dendrimer, **L8**. The same reduction method was used as that employed for **L6**. The octakis(cyanobenzyl) cyclam compound was refluxed with sodium in toluene for 15 hours, after which ethanol was added dropwise. The solution appears light yellow until all the sodium is destroyed, after which the solution became grey. The solution was allowed to cool to ensure that all the sodium ethoxide precipitated out. The same aqueous work-up used previously was employed, and after extraction with chloroform, a light yellow oily residue was obtained. The spectral data for **L5-L8** are shown in Table 2.4.

From the IR spectrum of **L8** it was observed that the nitrile band at 2226 cm^{-1} (present in **L7**) has disappeared and it shows the presence of a N-H band observed at 3360 cm^{-1}, indicating that the compound was successfully reduced. Column 2 in Table 2.4 shows the successive appearance and disappearance of the nitrile group as the dendrimer is alkylated and then reduced. The ^{13}C NMR spectrum shows the carbon atom adjacent to the amino group has shifted from 118.98 ppm (for the nitrile carbon) to 57.17 ppm (for the reduced nitrile group).

Table 2.4: Spectral data for ligands **L5-L8**.

Ligand	**FTIR[a] (cm^{-1})**		**^{1}H NMR[b] (ppm)**	**[ESI$^+$] [c] (m/z)**
	í(C≡N)	í(N-H)	$C\underline{\mathbf{H}}_2NH_2$	$[M]^+$
L5	2225	-	-	661
L6	-	3369	3.86	659[d]
L7	2226	-	-	1621[e]
L8	-	3360	3.84	782[f]

[a]Recorded in solid state on ZnSe crystal using ATR accessory. [b]Recorded as a $CDCl_3$ solution. [c]Recorded in solution using an acetonitrile and water mixture. [d] $[M\text{-}NH_2]^+$ at m/z = 659. [e] $[M+Na]^+$ at m/z = 1621. [f] $[M\text{-}(4NH_2)]^{2+}$ at m/z = 782.

The appearance of terminal amino groups in the reduced ligands **L6** and **L8** were also monitored by ^1H NMR spectroscopy, shown in Table 2.5 with the proton labels

corresponding to those in Figures 2.7 and 2.8. Microanalysis data of **L5-L8** is shown in Table 2.6. All the spectral data confirms the successful synthesis of ligands, **L5-L8**.

Table 2.5: ^{1}H NMR spectral data for ligands **L5-L8**.

Atom label	L5		L6		L7		L8	
	ä/ppm	Integration/ Multiplicity	ä/ppm	Integration/ Multiplicity	ä/ppm	Integration/ Multiplicity	ä/ppm	Integration/ Multiplicity
1	1.74	4H, m	1.64	4H, m	1.27	4H, m	1.28	4H, m
2	2.47	8H, t	1.95	8H, t	1.78	8H, t	1.74	8H, t
3	2.58	8H, t	2.57	8H, t	2.28	8H, t	2.38	8H, t
4	3.42	8H, s	3.53	8H, s	2.59	8H, s	2.86	8H, s
5	7.41	8H, d	7.17	8H, d	7.48	8H, d	7.23	8H, d
6	7.53	8H, d	7.30	8H, d	7.48	8H, d	7.23	8H, d
7	-	-	3.86	8H, s	3.60	8H, s	3.64	8H, s
8	-	-	-	-	3.60	16H, s	3.64	16H, s
9	-	-	-	-	7.62	16H, d	7.38	16H, d
10	-	-	-	-	7.62	16H, d	7.38	16H, d
11	-	-	-	-	-	-	3.84	16H, s

Table 2.6: Microanalysis data for ligands **L5-L8**.

Ligand	% Calculated			% Found		
	C	H	N	C	H	N
L5	76.33	6.71	16.96	76.29	6.35	17.91
L6	70.75	9.05	15.72	70.71	9.94	12.97[a]
L7	72.01	5.80	12.38	72.38	6.97	12.37[b]
L8	78.09	8.16	13.75	78.11	8.37	13.21

[a]Inclusion of 2 mol H_2O. [b]Inclusion of 2.5 mol CH_2Cl_2.

2.3 Conclusion

In this chapter we discussed the synthesis of cyclic-cored dendrimers, specifically cyclam-cored dendrimers, in order to achieve a more spherical and possibly less flexible structure than the dumbbell-shaped DAB-PPI dendrimers. It is thought that this type of structure might have an influence on the behaviour of complexes of these dendrimer systems when employed in catalysis. This will be investigated in subsequent chapters. Cyclam dendrimers with propyl branches (up to generation 2), were synthesized and fully characterized. The higher the generation, the more complex the synthesis, due to an increasing number of purification steps as well as an increase in reaction time. The first and second generation aminobenzyl cyclam dendrimers were also successfully synthesized and characterized. These cyclic cored dendrimers as well as the DAB dendrimer range will be used as scaffolds for the immobilization of catalysts. A comparison between the two dendrimeric structures (spherical and dumbbell shaped) will be drawn.

2.4 Experimental

Toluene was dried by refluxing over sodium/benzophenone. Methanol was dried by refluxing over magnesium turnings and iodine. Dichloromethane was dried by refluxing over phosphorus pentoxide. Cyclam, acrylonitrile, 4-bromomethyl benzonitrile, Na_2SO_4, NaOH, chloroform and sodium metal was purchased from Sigma Aldrich and was used without any further purification. Silica gel used for chromatography was purchased from Merck Chemicals. Infrared spectra were recorded on a Nicolet Avatar 330 FT-IR spectrophotometer, using an ATR accessory with a ZnSe crystal. ^{1}H NMR (300 MHz and 400 MHz) or ^{13}C NMR (75 MHz) spectra were recorded on a Varian VNMRS 300 MHz and a Varian Unity Inova 400 MHz spectrometer, using tetramethylsilane as an internal standard. ESI Mass spectra were done using a Waters API Q-TOF Ultima instrument in V-mode. The source temperature was 100 ºC and the desolvation temperature was 350 ºC. The capillary voltage used was 3.5 kV. Microanalyses were done at the University of Cape Town.

2.3.1 Synthesis of L1, Generation 0.5 N,N',N'',N'''-tetrakis(2-cyanoethyl) cyclam dendrimer.

Cyclam (1.0 g, 4.8 mmol) was added to methanol (30 ml) in a Schlenk tube under nitrogen whilst stirring. Excess acrylonitrile (1.8 ml, 29.8 mmol) was then added to the solution dropwise. The reagents dissolved and a colourless solution is observed. The mixture was stirred at room temperature for 24 hours after which a white precipitate formed. The precipitate was filtered off via gravity filtration and a white solid was obtained. The solid was dried in the oven at 100 ºC. Yield: 96 %. m.p. 128-130 ºC. IR (cm^{-1}): aliphatic ν(C-H) 2833; 2805 (s); ν(C≡N) 2244 (s); ^{13}C NMR in $CDCl_3$ (δ ppm): 16.42; 24.75; 50.23; 51.31; 119.23. ESI-MS: $[M+H]^+$ at m/z = 413.

2.3.2 Synthesis of L2, Generation 1 N,N',N'',N'''- tetrakis (aminopropyl) cyclam dendrimer.

Tetrakis(cyanoethyl)cyclam (***L1***) (2.2 g, 5.4 mmol) was added to dry toluene (150 ml) in a round bottom flask under nitrogen. Na pieces (10.0 g, 435 mmol) were added and the reaction mixture was refluxed for 20 hours. Dry ethanol (50 ml) was then added gradually over 3 hours after which the mixture was refluxed for 16 hours. A clear brown solution is observed. The solution was cooled to room temperature until the sodium ethoxide precipitated out. Water (50 ml) was added carefully to the reaction mixture. The sodium ethoxide dissolved in the aqueous phase while the expected product is soluble in the organic layer. The two layers were separated and the organic layer was dried over potassium carbonate, and evaporated to give a light brown oil. The oil was dissolved in chloroform (20 ml), and allowed to stand for 72 hours, after which the resulting precipitate was filtered off and the filtrate was evaporated to give a light beige oil. Yield: 75 %. IR (cm^{-1}): ν(N-H) 3269 (s); aliphatic ν(C-H) 2926; 2800 (s). ^{13}C NMR in $CDCl_3$ (δ ppm): 10.95; 22.43; 29.66; 46.22; 49.92; 50.99. No additional characterization was carried out since the compound has previously been reported.[14]

2.3.3 Synthesis of L3, Generation 1.5 N,N',N'',N'''-octakis(2-cyanoethyl) cyclam dendrimer.

Tetrakis(aminopropyl) cyclam (**L2**) (0.55 g, 5.5 mmol) was added to dry methanol (10 ml) in a Schlenk tube under nitrogen while stirring. Acrylonitrile (0.8 ml, 12.0 mmol) was then added to the solution dropwise. The mixture was stirred at room temperature for 96 hours after which the colour of the solution changed to light beige. The solvent (and acrylonitrile) was evaporated using a rotavapor and a light brown oil was obtained. Yield: 90 %. IR (cm^{-1}): aliphatic ν(C-H) 2931; 2804 (s); ν(C≡N) 2246 (s). ^{13}C NMR in $CDCl_3$

(δ ppm): 16.64; 23.25; 24.15; 24.95; 48.78; 50.13; 50.46; 51.09; 51.54; 51.75; 53.66; 119.48. ESI-MS: $[M-N]^+$ at m/z = 840.

2.3.4 Synthesis of L4, Generation 2 N,N',N'',N'''- octakis (aminopropyl) cyclam dendrimer.

Octakis(cyanoethyl)cyclam (0.2 g, 0.2 mmol) was added to dry toluene (100 ml) in a round-bottom flask under nitrogen. Na pieces (1g, 43 mmol) were added and the reaction mixture was refluxed for 20 hours. Dry ethanol (20 ml) was added gradually over 3 hours after which the mixture was refluxed for a further 16 hours. The solution was cooled to room temperature and left to stand for 7 hours to allow for precipitate formation. Water (100 ml) was added to the reaction mixture. The sodium ethoxide dissolved in the water, while the expected product is soluble in the organic layer. The two layers were separated and the organic layer was dried with potassium carbonate, and evaporated to give a light brown oil. The oil was dissolved in chloroform (20 ml), and left to stand for 24 hours. The resulting precipitate was filtered off and the filtrate was evaporated to give a light brown oil. Yield: 67 %. IR (cm^{-1}): ν(N-H) 3396 (s); aliphatic ν(C-H) 2966; 2810 (s). ^{13}C NMR in $CDCl_3$ (δ ppm): 22.70; 26.40; 30.36; 38.73; 49.81; 50.79; 62.49. ESI-MS: $[M+3Na]^+$ at m/z = 953.

2.3.5 Synthesis of L5, Generation 0.5 N,N',N'',N'''-tetrakis(cyanobenzyl) cyclam dendrimer.

4-Bromomethyl benzonitrile (2.0 g, 10 mmol) dissolved in $CHCl_3$ (10 ml) was added to Cyclam (0.5 g, 2.5 mmol) and NaOH (0.75 g, 18 mmol) in H_2O (80 ml), in a round-bottom flask. The mixture was stirred for 7 hours. The two-phase mixture was separated using a separating funnel and the organic solution was dried with Na_2SO_4. After filtration, the organic solvent was evaporated to yield a white solid. For recrystallization purposes, the

solid was dissolved in 10 ml DCM after which 15 ml methanol was layered on top of the solution. Within seconds crystal formation was completed to yield a white crystalline solid which was filtered off and dried. Yield: 90 %. m.p. 201-203 ºC. IR (cm^{-1}): aliphatic ν(C-H) 2933; 2804 (s); ν(C≡N) 2225 (s). ^{13}C NMR in $CDCl_3$ (δ ppm): 25.09; 51.28; 52.15; 59.43; 119.58; 129.97; 132.67; 146.53. ESI-MS: $[M-N]^+$ at m/z = 661.

2.3.6 Synthesis of L6, Generation 1 N,N',N'',N'''-tetrakis(aminobenzyl) cyclam dendrimer.

Tetrakis(cyanobenzyl) cyclam (**L5**) (0.2 g, 0.3 mmol) was added to dry toluene (60 ml) in a round-bottom flask under nitrogen. Na-metal (2.0 g, 86.9 mmol) was added and the reaction vessel was refluxed for 15 hours. Dry ethanol (20 ml) was then added gradually over 3 hours after which the mixture was refluxed for 16 hours. The solution was cooled to room temperature until sodium ethoxide precipitates out. Water (100 ml) was added to the reaction mixture. The two layers were separated and the organic layer was dried over potassium carbonate, and evaporated to give a light brown oil. The oil was then redissolved in chloroform (20 ml) and allowed to stand for 72 hours, after which the resulting precipitate was filtered off and the filtrate was evaporated to give the product, an off-white oil. Yield: 80 %. IR (cm^{-1}): ν(N-H) 3369 (s); aliphatic ν(C-H) 2921; 2792 (s). ^{13}C NMR in $CDCl_3$ (δ ppm): 27.31; 46.91; 52.10; 60.23; 124.86; 127.77; 129.06; 139.14. ESI-MS: $[M-NH_2]$ at m/z = 659.

2.3.7 Synthesis of L7, Generation 1.5 N,N',N'',N'''-octakis(cyanobenzyl) cyclam dendrimer.

4-Bromomethyl-benzonitrile (0.6 g, 2.88 mmol) dissolved in $CHCl_3$ (8 ml) was added to tetrakis(aminobenzyl) cyclam (0.26 g, 0.4 mmol) dissolved in $CHCl_3$ (2 ml) and NaOH (0.26 g, 6 mmol) in H_2O (50 ml), in a round-bottom flask under nitrogen. The mixture was

stirred for 72 hours. The two-phase mixture was separated using a separating funnel and the organic solution was dried with potassium carbonate. After filtration of the drying agent, the organic solvent was evaporated to yield a light yellow oil. The product was dissolved in DCM (5 ml). Hexane (15ml) was then added to the solution. The solution was then decanted, and the oil was dried. DCM (1 ml) was added to the dried oil, and then pentane (5 ml) was layered on top of the solution. Slow evaporation of the mixed solvents gave the product as a light cream solid material. Yield: 80 %. m.p. 108-112 ºC. IR (cm^{-1}): aliphatic ν(C-H) 2925; 2814 (s); ν(C≡N) 2226 (s). ^{13}C NMR in $CDCl_3$ (δ ppm): 26.70; 51.64; 58.17; 58.97; 111.10; 118.98; 129.39; 132.47, 144.93. ESI-MS: [M+Na] at m/z = 1621.

*2.3.8 Synthesis of **L8**, Generation 2 N,N',N'',N'''-octakis(aminobenzyl) cyclam dendrimer.*

Octakis(cyanobenzyl) cyclam (0.11 g) was added to dry toluene (100 ml) in a round-bottom flask under nitrogen. Na-metal (2.0 g) was added and the reaction vessel was refluxed for 6 hours. Dry ethanol (30 ml) was added gradually over 2 hours after which the mixture was refluxed for 16 hours. The solution was cooled for 2 hours. Water (100 ml) was added to the reaction mixture. The sodium ethoxide dissolved in the water and the resulting two layers were separated. The organic layer (light yellow solution) was dried over potassium carbonate, and evaporated to give a light yellow oil. The oil was dissolved in chloroform (50 ml), and left to stand for 72 hours. The resulting precipitate was filtered off and the filtrate was evaporated to give a light yellow oil. Yield: 65 %. IR (cm^{-1}): ν(N-H) 3360 (s); aliphatic ν(C-H) 2921; 2797 (s). ^{13}C NMR in $CDCl_3$ (δ ppm): 27.01; 31.88; 43.95; 49.32; 57.12; 121.75; 125.87; 126.68; 133.73; 136.36. ESI-MS: $[M-(4NH_2)]^{2+}$ at m/z = 1630.

2.5 References

[1] (a) A. Branchi, M. Micheloni, P. Paoletti, *Coord. Chem. Rev*., 110, **1991**, 17. (b) E. Kimura, *Prog. Inorg. Chem.,* 41, **1994**, 443. (c) L. Fabbrizzi, M. Licchelli, P. Pallavicini, D. Sacchi, *Supramol. Chem.,* 13, **2001**, 569.

[2] M. Meyer, V. Dahaoui-Gindrey, C. Lecomte, R. Guilard, *Coord. Chem. Rev.,* 178, **1998**, 1313.

[3] J. W. Sibert, A. H. Cory, J. G. Cory, *Chem. Commun*., **2002**,154.

[4] (a) E. Brucher, A. D. Sherry, *In The Chemistry of Contrast Agents in Medical Magnetic Resonance Imaging*; A. E., Toth, E., Eds.; Wiley: New York, 2001; *Chapter 6*. (b) P. Caravan, J. J. Ellison, T. J. McMurry, W. H. Lauffer, *Chem. Rev*., 99, **1999**, 2293.

[5] (a) E. Kimura, T. Koike, Y. Inouye, *Perspective on Bioinorganic Chemistry*; R. W. Hay, J. R. Dilworth, K. B. Nolan, Eds.; JAI: Stamford, CT, 14, **1999**; 145. (b) X. Liang, J. Parkinson, M. Weishaupl, R. O. Gould, S. J. Paisey, H-S. Park, T. M.Hunter, C. A. Blindauer, S. A. Parson, P. J. J. Sadler, *J. Am. Chem. Soc*., 124, **2002**, 9105.

[6] O. Enoki, T. Imaoka, K. Yamamoto, *Org. Lett.,* 5, **2003**, 2547.

[7] C. Saudan, V. Balzani, P. Ceroni, M. Gorka, M. Maestri, V. Vicinellia, F. Vogtle, *Tetrahedron,* 59, **2003**, 3845.

[8] C. Saudan, V. Balzani, M. Gorka, S. Lee, M. Maestri, V. Vicinelli, F. Vogtle, *J. Am. Chem. Soc.*, 125, **2003**, 4424.

[9] C. Saudan, V. Balzani, M. Gorka, S. Lee, J. van Heyst, M. Maestri, P. Ceroni, V. Vicinelli, F. Vogtle, *Chem. Eur. J*., 10, **2004**, 899.

[10] C. Saudan, P. Ceroni, V. Vicinelli, V. Balzani, M. Gorka, S. Lee, F. Vogtle, M. Orlandi, G. Bartolini, S. Tavolari, P. Rocchi, A. M. Ferreri, *Supramol. Chem.,* 16, **2004**, 541.

[11] G. Bergamini, P. Ceroni, V. Balzani, L. Cornelissen, J. van Heyst, S. Leeb, F. Vogtle, *J. Mater. Chem.,* 15, **2005**, 2959.

[12] B. Branchi, P. Ceroni, G. Bergamini, V. Balzani, M. Maestri, J. van Heyst, S. Lee, F. Luppertz, F. Vogtle, *Chem. Eur. J.,* 12, **2006**, 8926.

[13] K. P. Wainwright, *J. Chem. Soc.,* **1980**, 2117.

[14] K. P. Wainwright, *J. Chem. Soc.,* **1983**, 1149.

[15] B. Wu, J. Zhang, M. Yang, L. Ma, X. Yu*, Arkivoc,* 7, **2008**, 95.

[16] B. Jebasingh, V. Alexander, *Syn. Commun.,* 34, **2004**, 2843.

[17] C. L. Mazzitelli, J. S. Brodbelt, *J. Am. Soc. Mass. Spectrom*., 17, **2006**, 676.

[18] P. Comba, P. Jurisic, Y. D. Lampeka, A. Peters, A. I. Prikhodko, H. Pritzkow, *Inorg. Chim. Acta,* 324, **2001**, 99.

Chapter 3:

Surface modification of Diaminobutane (DAB)- and Cyclam-cored dendrimers.

3.1 Introduction to the surface modification of dendrimers.

3.1.1 What is dendrimer surface modification?

Dendrimers have attracted great interest because of their well-defined structure and the ease with which surface functionality can be controlled. By modifying the periphery of the dendrimer with a specific functional group, the properties of the dendrimer can be changed to suit specific applications. Figure 3.1 shows the reactions of an amine terminated dendrimer molecule with various functional groups.[1]

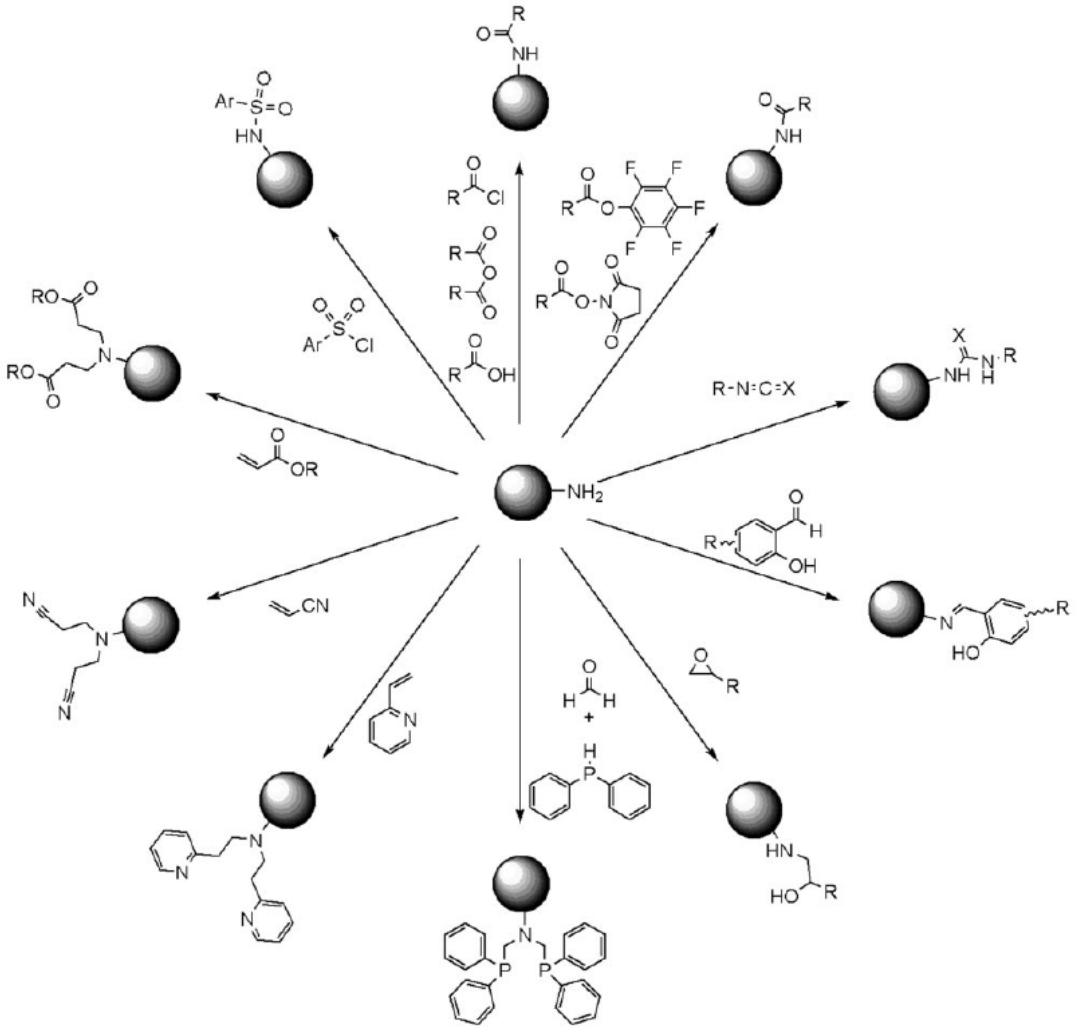

Figure 3.1: Surface modification of an amine terminated dendrimer with several functional groups.[1]

3.1.2 Applications of modified dendrimer compounds.

There is extensive interest in the pharmaceutical applications of dendrimers however, conflicting evidence regarding their biological safety exists. [2] Conversely, by modifying the dendrimer surface, the toxicity of the compound can be changed as reported by Jevprasesphant *et al.*[3] A marked decrease in the cytotoxicity of cationic PAMAM dendrimers was noted when the surface was modified, with the addition of six lauroyl or four polyethylene glycol (PEG) chains being particularly effective in decreasing cytotoxicity. This decrease in cytotoxicity is thought to be due to a reduction/shielding of the positive charge on the dendrimer surface by the attached chains.

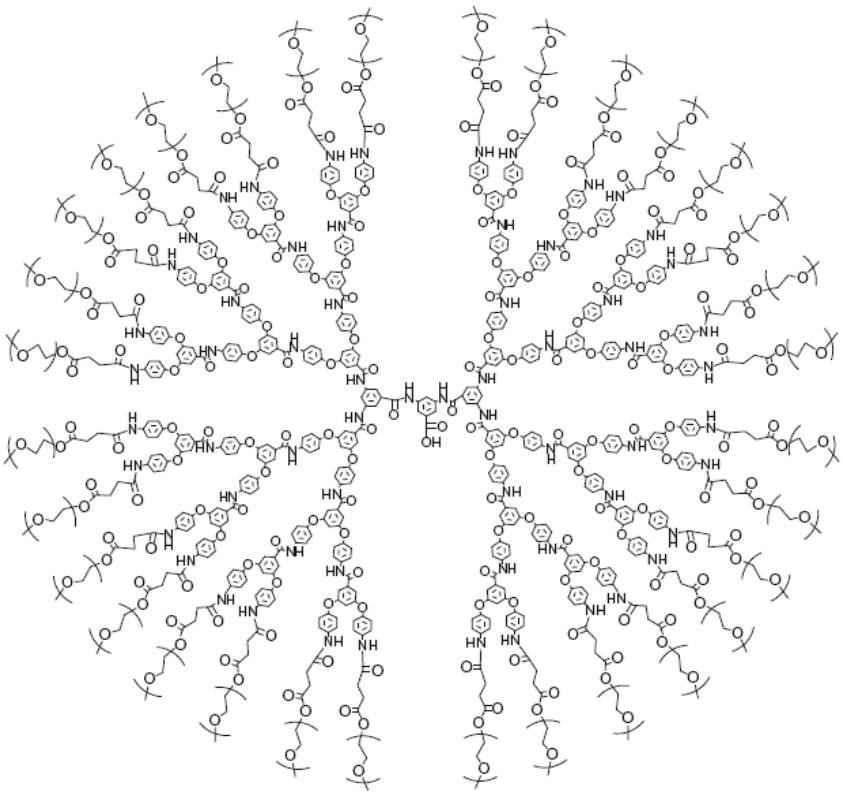

1

Figure 3.2: Water-soluble G3 Dendrimer synthesised by Endo *et al.*[4]

Another effect of dendrimer surface modification is the tweaking of the compound's solubility. Endo *et al* synthesized a third generation polyamide dendrimer which bears 32 trifluoroacetamide moieties at its periphery.[4] Similarly the reaction of the amino groups with oligo(ethylene glycol) chains at the surface resulted in the formation of a new water-soluble polyamide dendrimer (Fig 3.2). Thus by altering the surface of the dendrimer, the water solubility was enhanced.

By altering the surface of amine terminated dendrimers via reaction with aldehydes, Schiff base dendrimer ligands are produced. These types of compounds have numerous beneficial properties and applications as discussed later in this chapter.

3.1.3 Schiff base ligands.

A functional group containing a carbon-nitrogen double bond with the nitrogen atom connected to an aryl or alkyl group, is known as a Schiff base. These types of ligands are synthesized via Schiff Base condensation, where an aldehyde, or ketone is reacted with a primary amine, to produce an imine. A general structure of a Schiff base is shown in Figure 3.3.

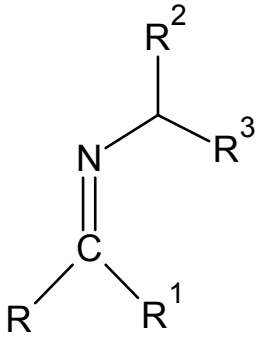

Figure 3.3: General structure of a Schiff base ligand.

Schiff base ligands are easily synthesized and form complexes with almost all metal ions. Thus in order to form metallodendrimer catalysts (metal containing dendrimer complexes) which will be discussed in Chapter 4, the amine terminated dendrimer surfaces first need to be modified with Schiff bases. A review on Schiff base catalysis by Gupta *et al* [5] states that the convenient route of synthesis and thermal stability of Schiff base ligands have contributed significantly to the application of metal complexes of these ligands in catalysis. Schiff base complexes of transition metals are versatile and efficient catalysts and are suitable to catalyze various reactions under mild experimental conditions. Some of the catalytic reactions discussed include polymerization, oxidation, carbonylation, Heck coupling and Diels-Alder reactions.

A few examples of salicylaldimine and iminopyridyl based Schiff Base catalysts are described below. Salicylaldimine ligands contain an N,O chelating system, while the iminopyridyl systems contain an N,N chelating system. Both these systems are routinely prepared in our laboratory.

3.1.3.1 Salicylaldimine based catalysts.

Cui *et al* reported the preparation of a series of amino-salicylaldimine–palladium(II) complexes bearing 5-methyl-3-(R-1-ylmethyl)-salicylaldimine ligands (R = morpholine, piperidine, pyrrolidine, 4-methylpiperazine, diisopropylamine).[6] These palladium complexes (Fig 3.4) are active catalysts for Suzuki cross-coupling of activated aryl chlorides with phenylboronic acid when using DMF as solvent with yields reaching up to 98 %. The catalysts also exhibit good activities in the Heck coupling reaction of aryl bromides with

styrene or *n*-butyl acrylate. Another advantage of these catalysts is the fact that they are air, moisture and temperature stable, as well as reasonably inexpensive to produce.

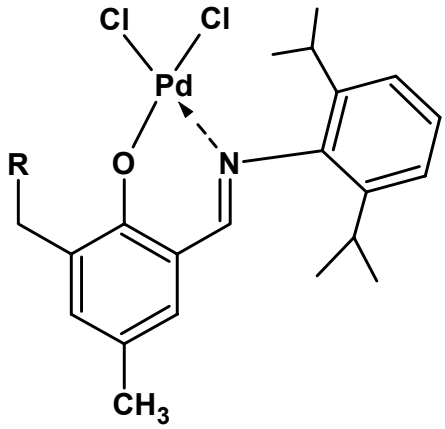

2 **R = morpholine**

3 **R=piperidine**

4 **R=pyrrolidine**

5 **R=4-methylpiperazine**

6 **R=diisopropylamine**

Figure 3.4: Amino-salicylaldimine Pd(II) complexes synthesised by Cui *et al*.[6]

De Clercq *et al* reported a new class of ruthenium complexes containing Schiff base ligands (Fig 3.5) as promising catalysts for atom transfer radical polymerization (ATRP) and ring opening metathesis polymerization (ROMP) of norbornene.[7] The ruthenium-based catalysts exhibited good activity in ATRP reactions. On the other hand, the ROMP activity of the catalytic systems for norbornene was poor. However, upon addition of trimethylsilyl diazomethane (TMSD) as a co-catalyst the activity for the ring opening metathesis polymerization of norbornene increased significantly. With the TMSD-activated catalysts, even the less strained cyclooctene could be reacted smoothly. The results show that the

control over polymerization is very dependent on the electronic and steric properties of the Schiff base ligands.

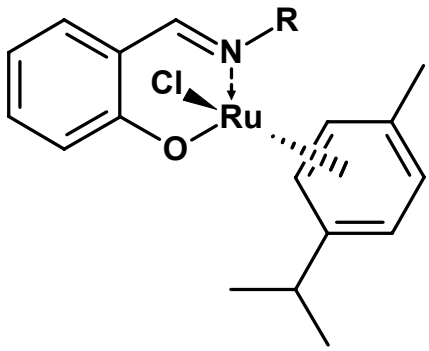

7 **R = Me**

8 **R = t-Bu**

9 **R =** 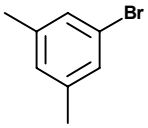

Figure 3.5: Ruthenium Schiff base complexes synthesised by De Clercq *et al*.[7]

The molecular weight of polynorbornene produced using these catalysts ranged from 4.62 x 10^5-6.82 x 10^5 g/mol and the molecular weight of the polycyclooctene ranged from 1.81 x 10^5- 2.62 x 10^5 g/mol. These results prove that by further fine-tuning of the Schiff base ligands, the potential of these catalytic systems in the field of ROMP and ATRP can be much improved.

Wang *et al* reported a series of zirconium salen-type complexes that were prepared by using $ZrCl_4$ and sodium salts of tetradentate Schiff base ligands (Fig 3.6).[8] These complexes showed good activity when evaluated as catalysts in the oligomerization of ethylene. With Et_2AlCl as a co-catalyst at 150 ºC, the effect of different salen-type ligands on the catalytic activity and oligomer distribution using the precatalysts, **10-13**, was explored. Complex **10**

gave the highest activity towards the production of ethylene oligomers whereas complex **13** gave the lowest. The main products were C_4–C_{10} olefins with good selectivity to linear *á*-olefins. The experimental results showed that N_2O_2-tetradentate zirconium complexes, which were conveniently prepared and easily handled, was promising homogeneous catalysts for ethylene oligomerization to low-carbon number linear *á*-olefins when activated by a proper co-catalyst.

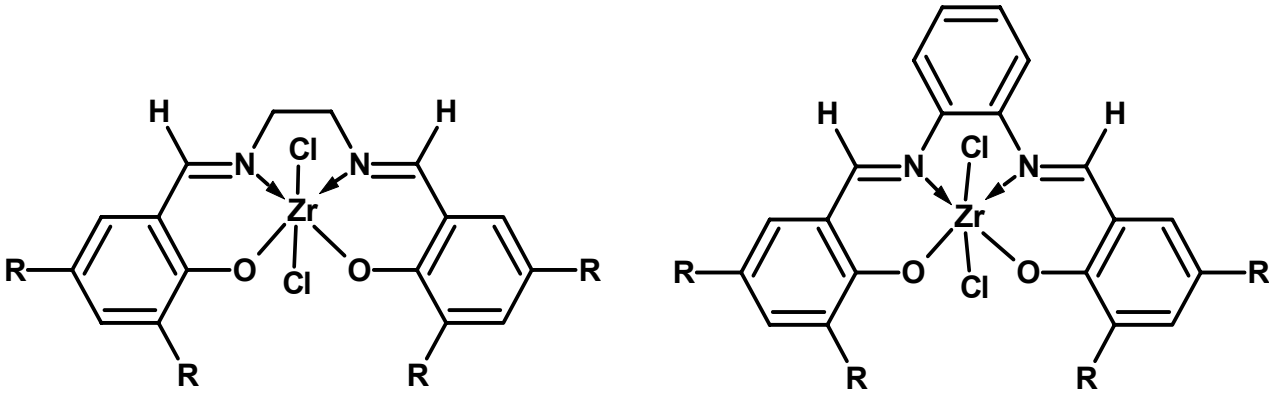

10 R=H

11 R=tBu

12 R=H

13 R=tBu

Figure 3.6: Zirconium Schiff base complexes synthesised by Wang *et al*.[8]

3.1.3.2 Imino pyridyl based catalysts.

Iminopyridyl based complexes are commonly used as catalysts for oligomerization and polymerization processes, of which a few examples were published in a review by Bianchini *et al.* [9]

Berchtold *et al* reported the synthesis of Pd(II) complexes with á-dioxime ligands.[10] The complexes (Fig 3.7) were activated with different co-catalysts such as MAO, $B(C_6F_5)_3/AlEt_3$ and $B(C_6F_5)_3$ for the polymerization of norbornene. Activities ranged from

1.2 x 10^4 - 3.2 x 10^7 g polymer/mol Pd.h^{-1}. MAO and $B(C_6F_5)_3/AlEt_3$ proved to be the best co-catalysts.

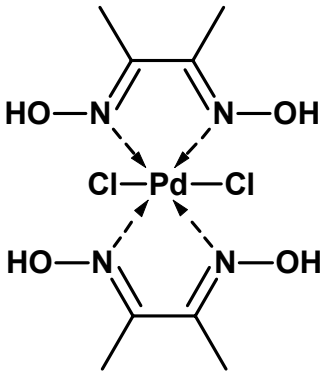

14

Figure 3.7: One of the Pd catalysts synthesised by Berchtold *et al.*[10]

Iron(II)- and cobalt(II)-based complexes bearing 2,6-bis(imino)pyridyl ligands that contain bulky aromatic substituents such as pyrenyl, 2-benzylphenyl and naphthyl were reported by Abu-Surrah *et al.*[11] These iron catalysts (Fig 3.8) were very active towards polymerization of ethylene with activity reaching up to 40.86 x 10^3 kg PE/mol cat.h^{-1}. It was concluded that by varying the steric bulkiness of the aryl groups in the tridentate ligands, both the molecular weight and the microstructure of the resulting polyethylene can be controlled.

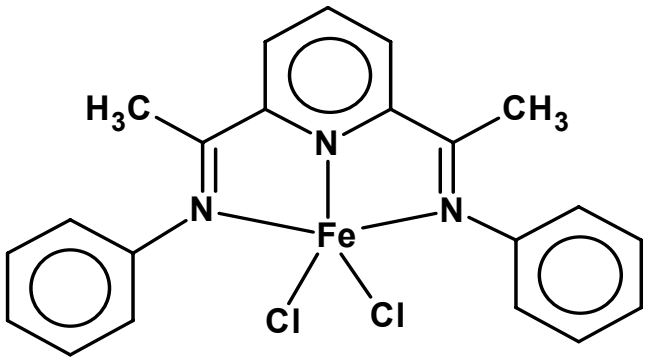

15

Figure 3.8: Iron catalyst synthesised by Abu-Surrah *et al.*[11]

3.1.4 Objectives.

The literature examples described show that Schiff base complexes are efficient catalysts for a variety of catalytic processes. Our aim was thus to modify the periphery of the commercial G1-G3 diaminobutane polypropylene imine (DAB-PPI) dendrimers as well as the synthesized cyclam based dendrimers (discussed in Chapter 2) via Schiff base condensation of the dendritic terminal amines with appropriate aldehydes. This resulted in salicylaldimine and iminopyridine functionalized dendrimers, which are able to coordinate metal precursors on its periphery to form metallodendrimers. In this chapter we discuss the dendrimer modification process, as well as the characterization of the resulting ligands.

3.2 Results and Discussion.

*3.2.1 Modification and characterization of the Generation 1-3 DAB salicylaldimine ligands **DL1-DL3**.*

We have recently reported the synthesis of ligands **DL1** and **DL2** (Fig 3.9) via Schiff base condensation of the G1 and G2 DAB-PPI dendrimers respectively with salicylaldehyde.[12]

The same synthetic approach was used to prepare the generation 3 DAB salicylaldimine analogue **DL3**. The reaction scheme for ligand, **DL3**, is shown in Scheme 3.1. Due to its higher number of surface groups, the G3 ligand **DL3** needed longer reaction time than its lower generation analogues, **DL1** and **DL2**, to ensure complete reaction of all the peripheral amino groups with the aldehydes. Thus the reaction was carried out over 96 hours instead of 72 hours for the lower generation ligands.

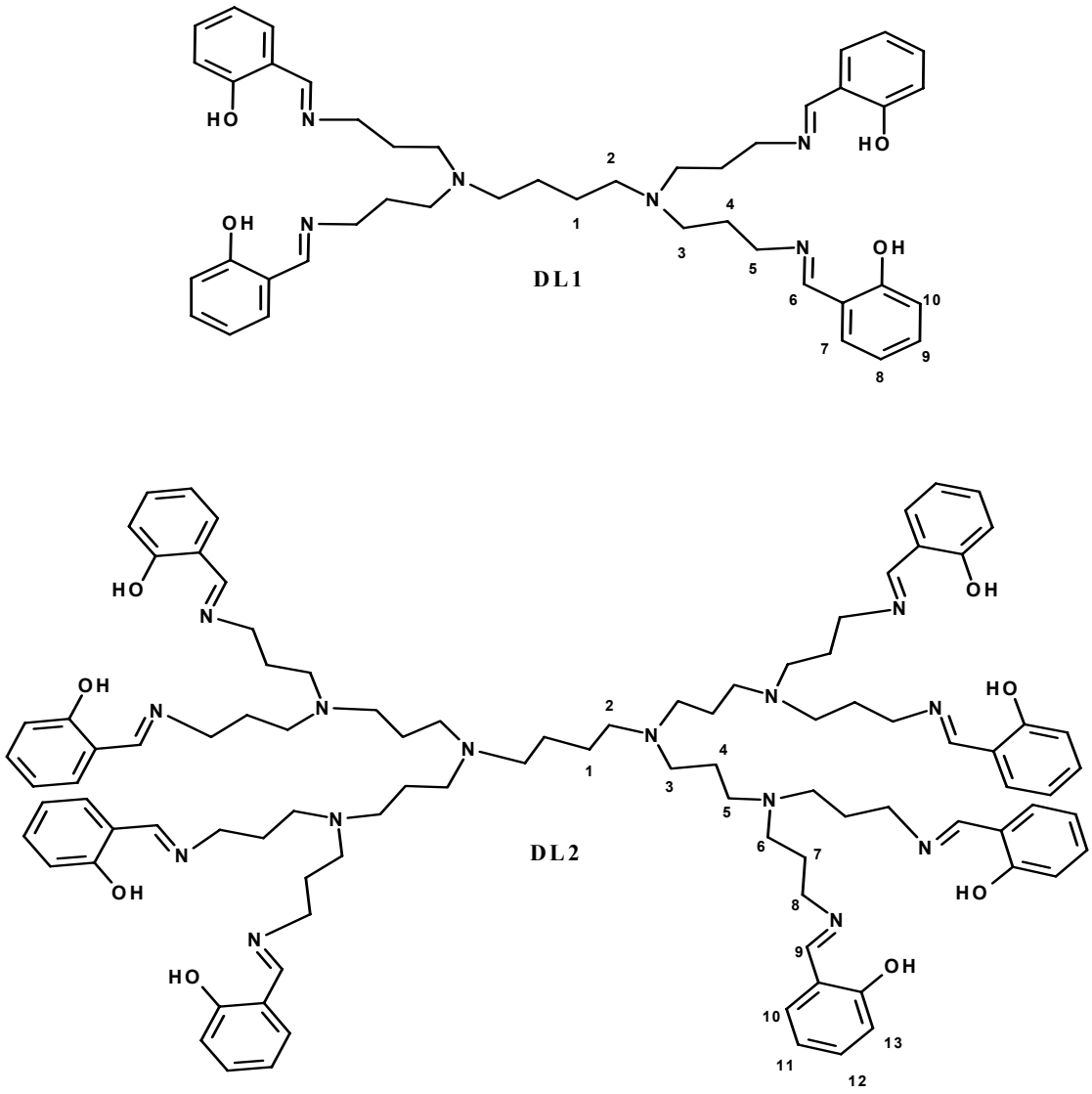

Figure 3.9: DAB G1 and G2 salicylaldimine modified dendrimers, **DL1** and **DL2**.[12] Numbered for ^{1}H NMR assignments.

In all cases the crude product is initially isolated as a yellow oil. Only in the case of ligand **DLI**, is the final product isolated from the oily residue as a yellow solid by recrystallization from dichloromethane:hexane mixtures. Thin layer chromatography on **DL3** confirms the presence of excess salicylaldehyde.

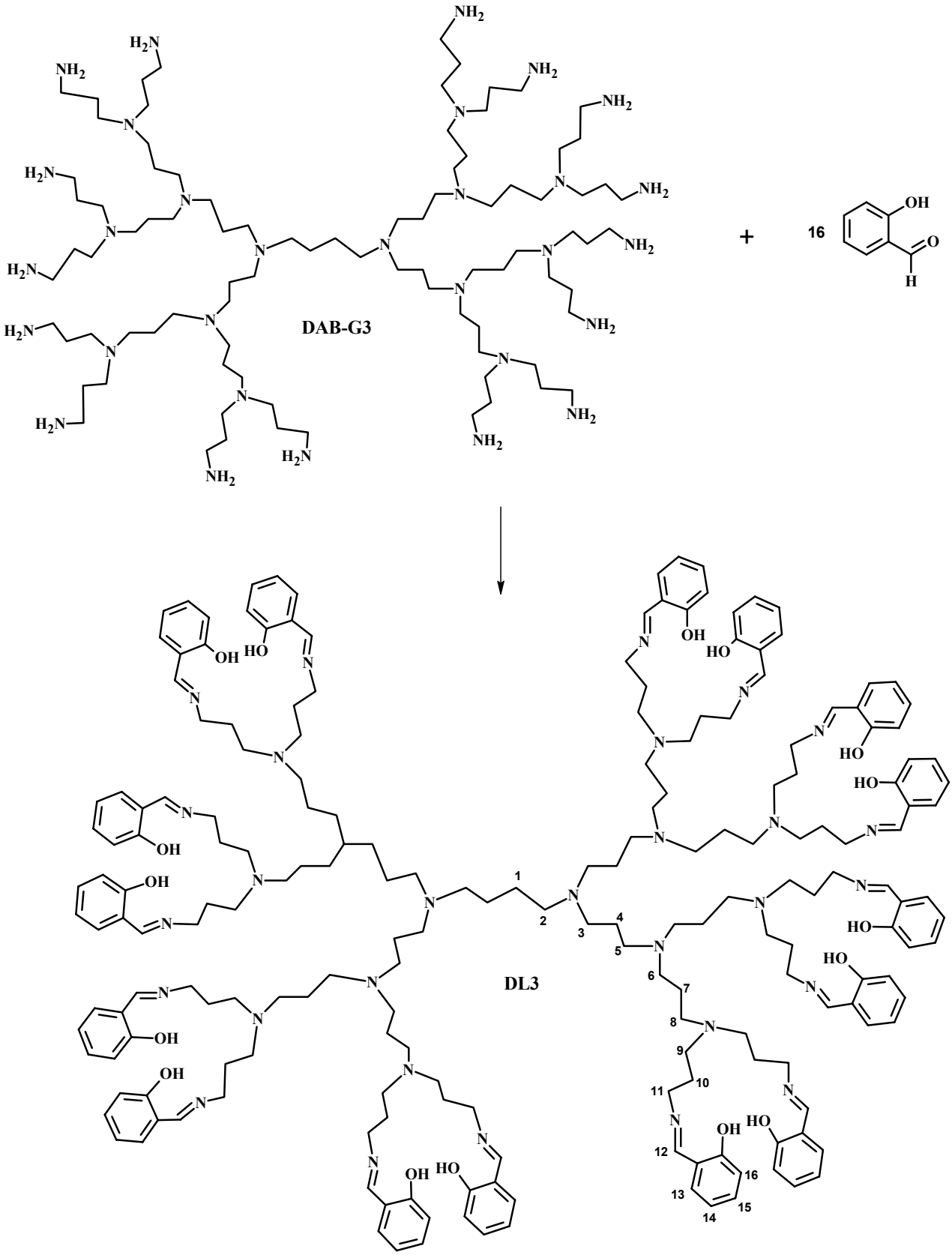

Scheme 3.1: Synthesis of the DAB G3 salicylaldimine modified dendrimer, **DL3**.

The higher the generation of the dendrimer, the more spherical the molecules appear. Thus the G3 dendrimer ligand **DL3** has several empty cavities that can potentially trap unreacted salicylaldehyde molecules. Several attempts to remove the excess aldehyde from the products seemed to be unsuccessful. Solvent extraction did not work since the salicylaldehyde and the dendrimer ligand have the same solubility. This is because the modified dendrimer usually takes on the properties of its surface functionality, which in this case is salicylaldimine. Column chromatography was also attempted and the salicylaldehyde could be separated from the dendrimer ligand. However the dendrimer ligand remained immobilized on the silica gel and could not be eluted from the column. Thus the G3 salicylaldimine dendrimer ligand was obtained with excess salicylaldehyde encapsulated within the dendrimer voids. Dendrimers are known to encapsulate organic molecules inside their cavities.[13,14]

We proceeded to characterize the three salicylaldimine ligands with FTIR and NMR spectroscopy, mass spectrometry and microanalysis. Table 3.1 shows the spectral data of ligands **DL1-DL3**.

Table 3.1: Spectral data for ligands **DL1-DL3**.

Ligand	FTIR[a] (cm^{-1})		^{13}C NMR[b] (ppm)	MALDI-TOF[c] (m/z)
	í(C=N)	í(C-O)	**C**=N	$[M]^+$
DL1	1632	1284	161.3	733
DL2	1630	1279	161.2	1606
DL3	1629	1277	161.4	3352

[a] Recorded in solid state on ZnSe crystal using ATR accessory.[b] Recorded as a $CDCl_3$ solution. [c] Recorded in solid state after mixing with NaTFA as a salt and using Dithranol as a matrix.

The most important band monitored by FTIR is the í(C=N) band, which indicates that condensation between the amine and the aldehyde had occurred. This band is clearly visible in the FTIR spectra of all three ligands in the region of 1629-1632 cm^{-1}. In the ^{13}C NMR spectra, the imine carbon was also monitored. This peak is observed at 161 ppm for all three generations of dendrimer ligands. This also confirms the successful surface modification of the DAB-PPI dendrimer with salicylaldimine units.

MALDI-TOF mass spectrometry was done on the ligands, and the observed molecular ion peaks match very well to the calculated mass of the ligands. **DL3** was also analyzed by ESI-MS (Fig 3.10) and the spectrum shows a doubly charged ion peak $[M]^{2+}$ at m/z = 1676.5. The high mass peaks at m/z = 1696 and m/z = 1705 is possibly due to water entrapment and accounts for 3 moles of water per ligand. The source of water is possibly due to the fact that sample preparation for the mass spectral analysis involves dissolving the compound in a mixture of water and acetonitrile.

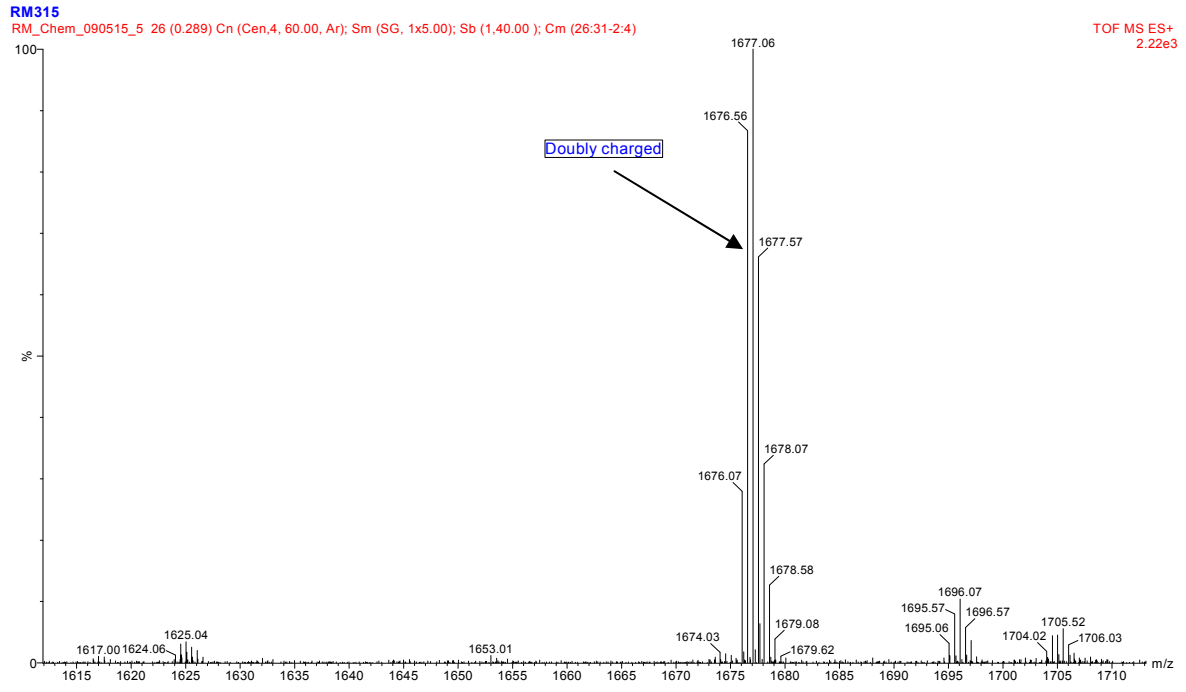

Figure 3.10: ESI-MS spectrum of the DAB G3 salicylaldimine modified dendrimer, **DL3**.

In the ^{1}H NMR spectra, the proton attached to the imine group was monitored. This peak is observed from 8.43-8.27 ppm going from the first generation to the third generation dendrimer ligand. The rest of the ^{1}H NMR data is shown in Table 3.2, with the proton labels corresponding to those in Fig 3.9 for **DL1** and **DL2**, and Scheme 3.1 for **DL3**.

Table 3.2: H NMR spectral data for ligands **DL1-DL3**.

Atom label	DL1		DL2		DL3	
	ä/ppm	Integration/ Multiplicity	ä/ppm	Integration/ Multiplicity	ä/ppm	Integration/ Multiplicity
1	1.42	4H, m	1.31	4H, m, br	1.37	4H, m
2	2.42	4H, t	2.35	4H, t	2.36	4H, t
3	2.57	8H, t	2.38	8H, t	2.36	8H, t
4	1.87	8H, m	1.54	8H, m, br	1.54	8H, m
5	3.55	8H, t	2.48	8H, t, br	2.40	8H, t
6	**8.32**[a]	**4H, s**	2.48	16H, t, br	2.40	16H, t
7	7.35	4H, d	1.78	16H, m	1.54	16H, m
8	6.88	4H, t	3.57	16H, t	2.48	16H, t
9	7.25	4H, t	**8.29**[a]	**8H, s**	2.48	32H, t
10	7.19	4H, d	7.55	8H, d	1.78	32H, m
11	-	-	6.82	8H, t	3.56	32H, t
12	-	-	7.17	8H, t	**8.27**[a]	**16H, s**
13	-	-	6.91	8H, d	7.56	16H, d
14	-	-	-	-	6.82	16H, t
15	-	-	-	-	7.17	16H, t
16	-	-	-	-	6.91	16H, d

[a] The proton attached to the imine group.

The microanalysis results are shown in Table 3.3. In the case of **DL3**, excess salicylaldehyde is included in the calculated percentage, and this accounts for what we observe in the found results. A peak at 9.91 ppm in the ^{1}H NMR spectrum of ligand, **DL3,** confirms the presence of excess salicylaldehyde.

Table 3.3: Microanalysis data for ligands **DL1-DL3**.

Ligand	% Calculated			% Found		
	C	H	N	C	H	N
DL1	72.10	7.70	11.47	71.90	7.90	11.49
DL2	71.09	8.03	12.21	71.87	8.28	11.86
DL3	71.38	7.86	11.30	71.19	7.85	11.13[a]

[a]Inclusion of 3 mol salicylaldehyde.

*3.2.2 Modification and characterization of the Generation 1-3 DAB Iminopyridyl ligands **DL4-DL6**.*

The synthesis of the imino pyridyl modified dendrimer ligands **DL4** and **DL5** (Fig 3.11) have previously been reported by Smith *et al* [15] and Mketo *et al.*[16] The generation 3 iminopyridyl analogue, **DL3**, was synthesised in a similar manner as its lower generation analogues i.e. via the Schiff base condensation of the DAB-G3 dendrimer with 2-pyridine carboxyaldehyde. The reaction pathway for **DL3** is shown in Scheme 3.2. The lower generation ligands need only 48 hours for complete reaction, whereas the generation 3 iminopyridyl ligand needs at least 72 hours of reaction time due to its high number of surface

groups. All three ligands were isolated as dark brown oils. Because the 2-pyridine carboxyaldehyde is soluble in water, separation of the unreacted starting reagents from the product is relatively easy. This is done by washing a dichloromethane solution of the product mixture with water several times. After this extensive washing, no excess aldehyde band is observed in the FTIR and ^{1}H NMR spectra of the product.

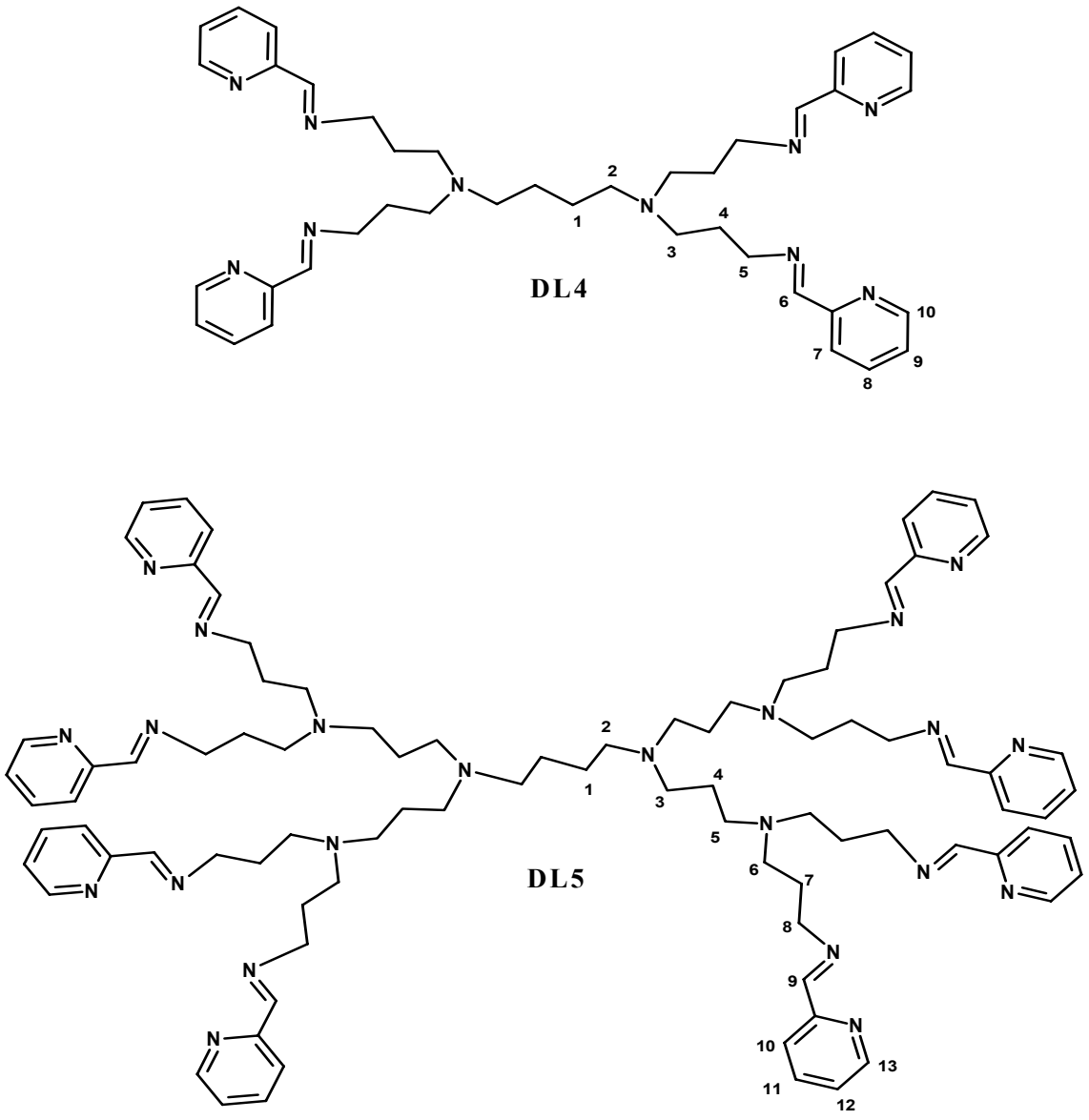

Figure 3.11: DAB G1-G2 iminopyridyl modified dendrimers, **DL4** [13] and **DL5**. [14]

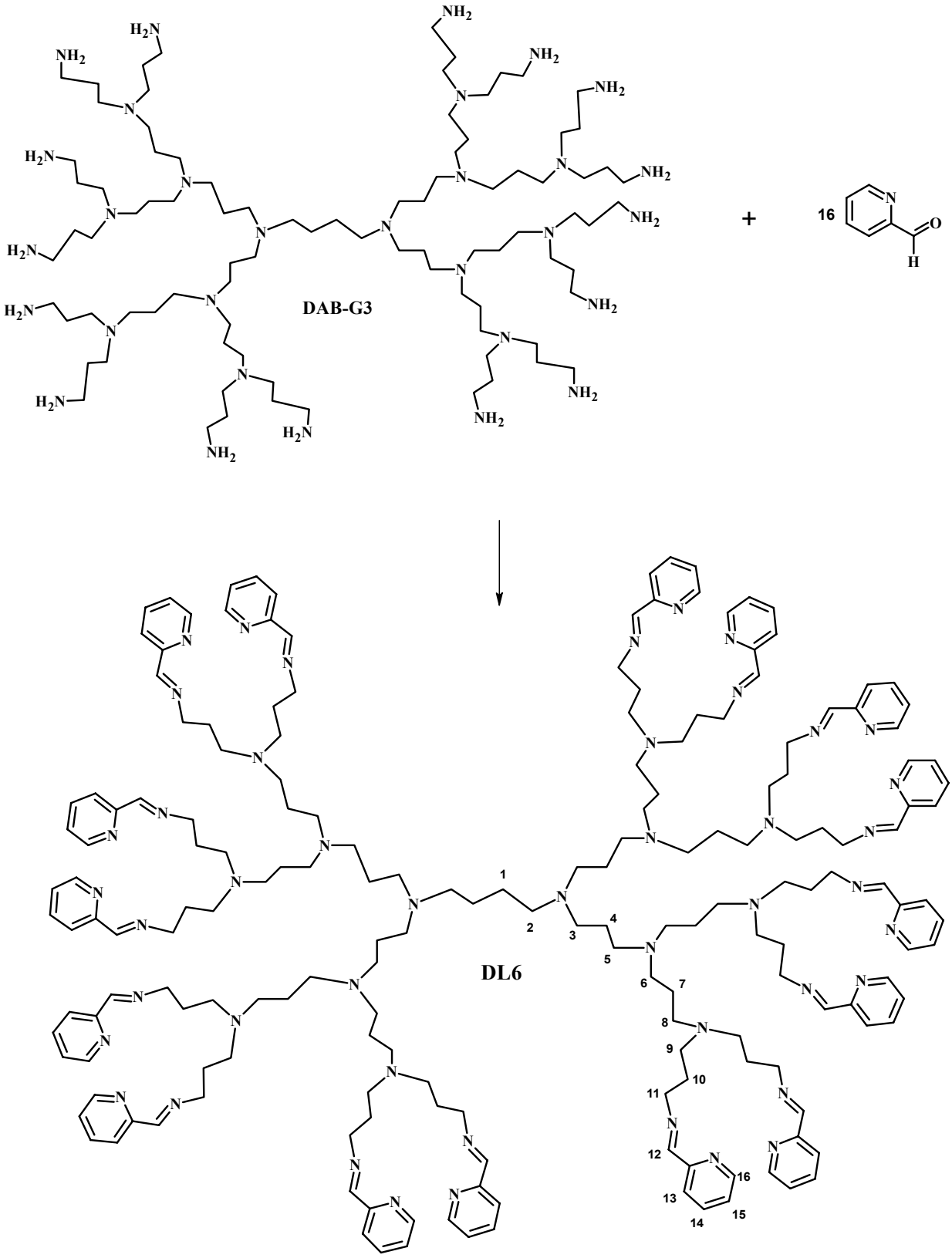

Scheme 3.2: Synthesis of the DAB G3 iminopyridyl modified dendrimer, **DL6**.

DL4-DL6 was further analyzed via ESI-MS and a summary of the spectral data is shown in Table 3.4. The most important bands monitored by FTIR spectroscopy is the í(C=N) band which confirms the reaction of the aldehyde with the dendrimer periphery. This band is observed around 1647 cm^{-1}. The í(C=N) bands from the pyridine ring are also observed in the product spectrum around 1586 cm^{-1}. In the ^{13}C NMR spectra, a peak assigned to the carbon atom of the imine of **DL4-DL6** is observed in the range 161.4 - 161.8 ppm for the G1-G3 iminopyridyl ligands.

Table 3.4: Spectral data for ligands, **DL4-DL6**.

Ligand	**FTIR[a] (cm^{-1})**			**^{13}C NMR[b] (ppm)**	**[ESI$^+$] [c] (m/z)**
	í(C=N)	í(C=N) (*pyr*)	í(C=C) (*pyr*)	**C**=N	$[M]^+$
DL4	1647	1586	1562	161.4	672.80
DL5	1647	1586	1562	161.8	1487.0
DL6	1648	1587	1567	161.7	622.12[d]

[a] Recorded in solid state on ZnSe crystal using ATR accessory. [b] Recorded as a $CDCl_3$ solution. [c] Recorded in solution in an acetonitrile and water mixture. [d] $[M]^{5+}$ at m/z = 622.12.

Mass spectrometry analysis for **DL4** and **DL5** show a molecular ion peak at m/z = 672.80 and m/z = 1487.0 which correspond to the respective molar masses of the ligands. **DL6** shows a multiply charged ion $[M]^{5+}$ at m/z = 622.12 also confirming the expected molar mass of the ligand.

In the ^1H NMR spectra (Table 3.5), the proton attached to the carbon of the imine of **DL4-DL6** is observed in the range 8.37 - 8.36 ppm for the G1-G3 iminopyridyl ligands. The

iminopyridyl imine proton peaks are slightly more upfield compared to that of the salicylaldimine ligands. The pyridine ring protons are observed in the range 8.63-8.61 ppm for **DL4-DL6**.

Table 3.5: H NMR spectral data for ligands **DL4-DL6**.

Atom label	DL4		DL5		DL6	
	ä/ppm	Integration/ Multiplicity	ä/ppm	Integration/ Multiplicity	ä/ppm	Integration/ Multiplicity
1	1.42	4H, m	1.36	4H, m, br	1.38	4H, m
2	2.42	4H, t	2.41	4H, t	2.14	4H, mt, br
3	2.53	8H, t	2.41	8H, t	2.14	8H, m, br
4	1.85	8H, m	1.57	8H, m	1.59	8H, m, br
5	3.68	8H, t	2.52	8H, t,br	2.42	8H, t
6	**8.37**[a]	**4H, s**	2.52	16H, t,br	2.42	16H, t
7	7.95	4H, d	1.84	16H, m	1.59	16H, m, br
8	7.71	4H, t	3.58	16H, t	2.52	16H, t
9	7.31	4H, t	**8.36**[a]	**8H, s**	2.52	32H, t
10	8.63	4H, d	7.96	8H, d	1.85	32H, m, br
11	-	-	7.70	8H, t	3.67	32H, t
12	-	-	7.28	8H, t	**8.37**[a]	**16H, s**
13	-	-	8.61	8H, d	7.97	16H, d
14	-	-	-	-	7.70	16H, t, br
15	-	-	-	-	7.29	16H, t
16	-	-	-	-	8.62	16H, d

[a] The proton attached to the imine group.

Table 3.6: Microanalysis data for ligands, **DL4-DL6**.

Ligand	% Calculated			% Found		
	C	H	N	C	H	N
DL4	70.40	7.79	20.82	70.44	8.16	20.55
DL5	69.62	7.93	20.13	69.61	8.13	20.58[a]
DL6	67.41	7.86	19.39	67.02	7.28	20.60[b]

[a]Inclusion of 0.5 mol CH_2Cl_2. [b]Inclusion of 2.5 mol CH_2Cl_2.

The microanalysis results are shown in Table 3.6. In the case of **DL5** and **DL6**, dichloromethane is included in the calculated percentage, and the found results can be accounted for by the encapsulation of dichloromethane in the cavities of the dendrimer products. This was confirmed by ^{1}H NMR spectroscopy where the spectra of the dendrimers show a peak at 5.32 ppm, which are due to the dichloromethane protons (Fig 3.12).

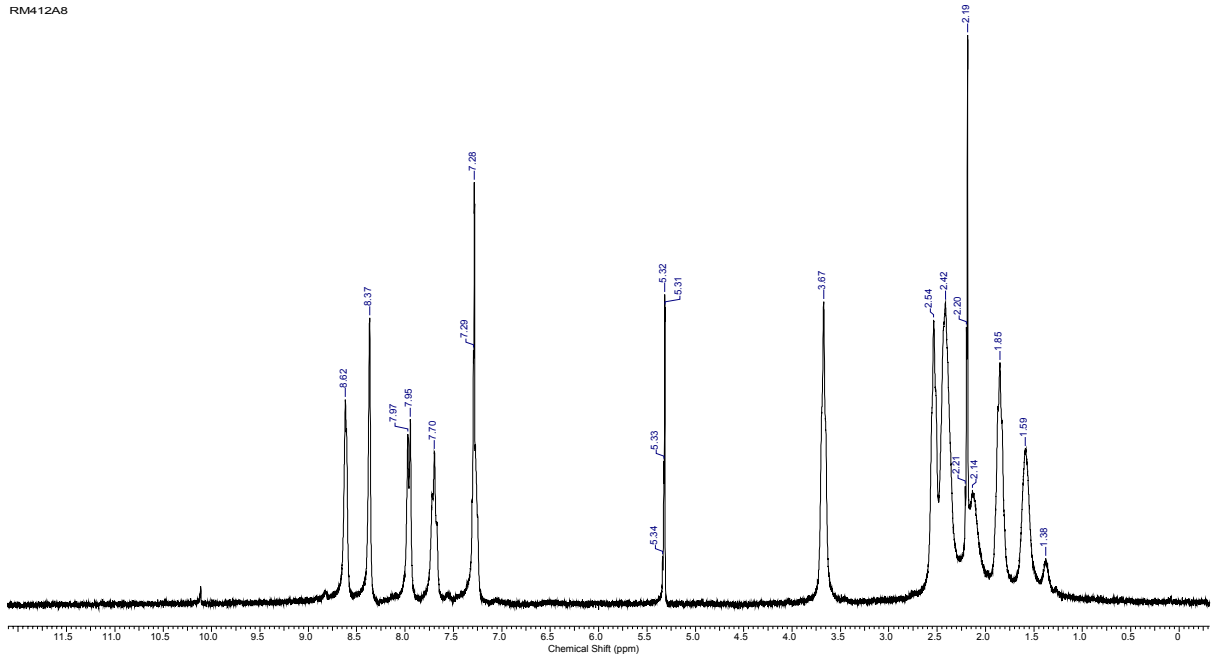

Figure 3.12: ^{1}H NMR spectrum of **DL6**.

*3.2.3 Modification and characterization of the Generation 1 cyclam-propyl and cyclam-benzyl Schiff base ligands **DL7-DL10**.*

The G1 cyclam-propyl dendrimer, **L1**, and the G1 cyclam-benzyl dendrimer, **L2**, were modified with salicylaldimine and iminopyridyl functional groups to obtain the modified dendrimer ligands **DL7-DL10** as shown in Fig 3.13.

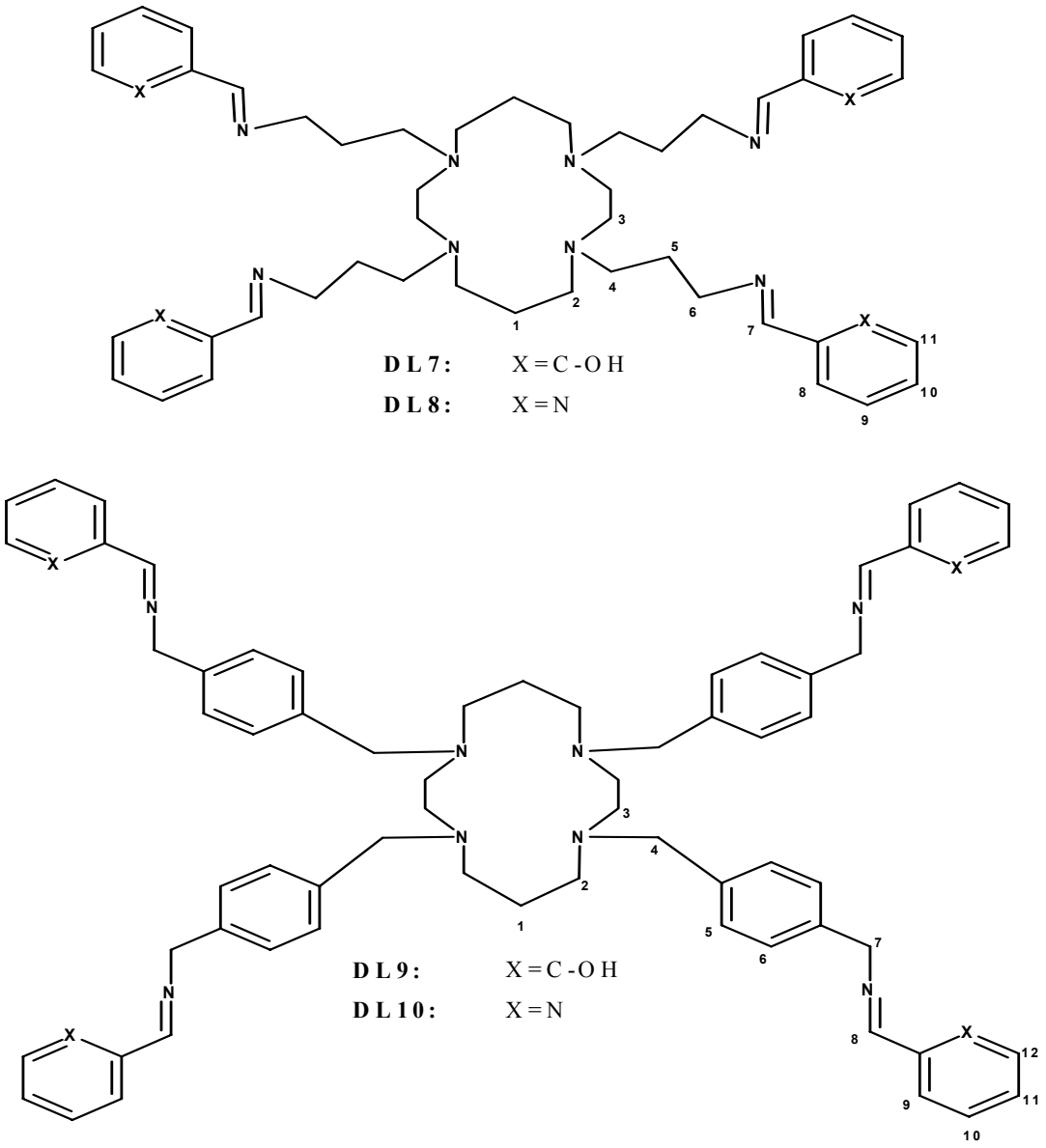

Figure 3.13: The G1 cyclam-propyl Schiff base modified dendrimers, **DL7** and **DL8**, and G1 cyclam-benzyl Schiff base modified dendrimers, **DL9** and **DL10**.

The cyclam based dendrimers were modified similarly to the DAB based dendrimers by a Schiff base reaction with the appropriate aldehyde. All dendrimer ligands were isolated as oils. The salicylaldimine ligands **DL7** and **DL9** are red in colour, and the iminopyridyl ligands **DL8** and **DL10** are dark brown in colour. The reaction time was 72 hours for all four ligands, and the isolated products were characterised by FT-IR and NMR spectroscopy, ESI-MS and microanalysis.

The characterization data for the salicylaldimine ligands **DL7** and **DL9** are shown in Table 3.7. As in the case of the DAB based ligands, the most significant band monitored by FTIR is the í(C=N) band, which indicates that the condensation between the amine and the aldehyde had occurred.

Table 3.7: Spectral data for the G1 cyclam based dendrimer salicylaldimine ligands **DL7** and **DL9**.

Ligand	**FTIR[a] (cm^{-1})**		**^{13}C NMR[b] (ppm)**	**[ESI$^+$] [c] (m/z)**
	í(C=N)	í(C-O)	**C**=N	$[M+H]^+$
DL7	1662	1276	161.85	846.0
DL9	1663	1277	161.88	1111.3

[a] Recorded in solid state on ZnSe crystal using ATR accessory. [b] Recorded as a $CDCl_3$ solution. [c] Recorded in solution in an acetonitrile and water mixture.

The ν(C=N) band for **DL7** and **DL9** is observed at 1662 and 1663 cm^{-1} respectively and the ν(C-O) stretching frequency at 1276 and 1277 cm^{-1}. In the ^{13}C NMR spectra, the imine carbon of **DL7** and **DL9** is observed at 161.85 ppm and 161.88 ppm respectively.

The spectral data for the cyclam-based salicylaldimine ligands, **DL8** and **DL10**, are shown in Table 3.8. The most important bands monitored by FTIR spectroscopy was the í(C=N) band, which confirm the reaction between the aldehyde and the dendrimer, as well as the í(C=N) and the í(C=C) bands from the pyridine rings. The aliphatic imine signal is observed at 1648 cm^{-1} and 1630 cm^{-1} for the respective ligands and the í(C=N) bands of pyridine is observed at 1586 and 1574 cm^{-1} for **DL8** and **DL10**. In the ^{13}C NMR spectra, the imine carbon of **DL8** and **DL10** is observed at 150.43 ppm and 150.93 ppm respectively.

Table 3.8: Spectral data for the G1 cyclam based dendrimer iminopyridyl ligands **DL8** and **DL10**.

Ligand	FTIR[a] (cm^{-1})			^{13}C NMR[b] (ppm)	[ESI$^+$] [c] (m/z)
	í(C=N)	í(C=N) (*pyr*)	í(C=C) (*pyr*)	**C**=N	$[M]^+$
DL8	1648	1586	1567	150.43	825
DL10	1630	1574	1510	150.93	516[d]

[a] Recorded in solid state on ZnSe crystal using ATR accessory. [b] Recorded as a $CDCl_3$ solution. [c] Recorded in solution with acetonitrile and water mixture. [d] $[M]^{2+}$ at m/z = 516.

In the ^1H NMR spectra, the proton attached to the imine carbon of **DL7** and **DL9** is observed at 8.33 ppm and 8.31 ppm respectively. The same proton for **DL8** and **DL10** observed at 8.36 ppm and 8.63 ppm respectively, again confirms the reaction between the aldehyde and the dendrimer. Full spectral data of the ^1H NMR analysis is shown in Table 3.9, with the proton numbers corresponding to that of the ligand protons in Fig 3.13 for **DL7-DL10**.

Table 3.9: H NMR spectral data for ligands **DL7-DL10**.

Atom label	DL7		DL8		DL9		DL10	
	ä/ppm	Integration/ Multiplicity	ä/ppm	Integration/ Multiplicity	ä/ppm	Integration/ Multiplicity	ä/ppm	Integration/ Multiplicity
1	1.59	4H, m	1.61	4H, m	1.70	4H, m	1.26	4H, m
2	2.48	8H, t	2.50	8H, t	2.34	8H, t	2.52	8H, t
3	2.52	8H, t	2.55	8H, t	2.59	8H, t	2.64	8H, t
4	2.48	8H, t	2.50	8H, t	3.48	8H, s	3.53	8H, s
5	1.80	8H, m	1.83	8H, m	7.04	2H, d	7.28	2H, d
6	3.58	8H, t	3.65	8H, t	7.00	2H, d	7.26	2H, d
7	**8.33**[a]	**4H, s**	**8.36**[a]	**4H, s**	4.79	8H, s	4.85	8H, s
8	7.56	4H, d	7.94	4H, d	**8.31**[a]	**4H, s**	**8.64**[a]	**4H, s**
9	6.93	4H, t	7.70	4H, t	7.52	4H, d	7.89	4H, d
10	7.21	4H, t	7.52	4H, t	6.96	4H, t	7.74	4H, t
11	7.02	4H, d	8.60	4H, d	7.57	4H, t	7.52	4H, t
12	-	-	-	-	6.89	4H, d	8.82	4H, d

[a] The proton attached to the imine group.

The microanalysis results for ligands **DL7-DL10** is shown in Table 3.10. In many cases we experienced a common error with the % N throughout our microanalysis characterization. This seems to be an inherent systems problem at the micro-analytical unit at the University of

Cape Town. The combined spectral data for ligands **DL1-DL10** confirm the synthesis of Schiff base modified DAB-PPI and cyclam-cored dendrimers.

Table 3.10: Microanalysis data for ligands **DL7-DL10**.

Ligand	% Calculated			% Found		
	C	H	N	C	H	N
DL7	63.63	7.30	11.53	64.46	7.35	11.27[a]
DL8	64.88	7.65	19.32	64.84	7.43	20.85[b]
DL9	74.53	6.85	9.86	74.89	7.40	8.36[c]
DL10	74.22	6.86	15.60	74.45	7.41	13.49[c]

[a]Inclusion of 1.5 mol CH_2Cl2. [b]Inclusion of 1 mol CH_2Cl_2. [c]Inclusion of 0.5 mol CH_2Cl_2.

3.3 Molecular modeling: Structural optimization of Ligands *DL1-DL3*.

All computational studies were conducted using the DMol^3 DFT (Density Functional Theory) code[17-19] as implemented in Accelrys Materials Studio® 5.0.[20] DFT was used since it usually gives realistic geometries, relative energies and vibrational frequencies for transition metal compounds. The aim was to combine the dendrimer with a transition metal, and using the DFT calculations to ascertain valuable information regarding this. The non-local generalized gradient approximation (GGA) functional by Perdew and Wang (PW91) [21] with the spin-restricted approximations was used for all geometry optimizations. The convergence criteria for these optimizations consisted of threshold values of 2 x 10^{-5} Ha, 0.004 Ha/Å and

0.005 Å for energy, gradient and displacement convergence, respectively, while a self consisted field (SCF) density convergence threshold value of 1×10^{-5} Ha was specified. DMol^3 utilizes a basis set of numeric atomic functions, which are exact solutions to the Kohn-Sham equations for the atom. These basis sets are generally more complete than a comparable set of linearly independent Gaussian functions and have been demonstrated to have small basis set superposition errors.[22] In this study a polarized split valence basis set, termed double numeric polarized (DNP) basis set has been used. All geometry optimizations employed highly efficient delocalized internal coordinates. [23] The use of delocalized coordinates significantly reduces the number of geometry optimization iterations needed to optimize larger molecules, compared to the use of traditional Cartesian coordinates. All results were mass balanced for the isolated system in the gas phase.

The optimized structures of the DAB G1-G3 salicylaldimine ligands (**DL1-DL3**) were obtained and the effect of the increase in generation of the dendrimer on the geometry of the dendrimer was investigated.

3.3.1 Structural optimization of the generation 1 salicylaldimine dendrimer ligand, ***DL1.***

The molecule was drawn "flat" in plane, with all the HO-C_6H_4-CHN-groups at ideal orientation. After optimization there was a clear rearrangement in the structure (Fig 3.14). One side of the dendrimer molecule stays close to the starting orientation, while on the other side one of the groups twist out of the plane. This gives an indication of the flexibility of the DAB- cored dendrimer ligands. The bite angles between the OH groups were calculated as 57.2º and 45.2º as shown in Fig 3.15. The dihedral angles between the OH groups were calculated as 26.4º and 16.9º as shown in Fig 3.16.

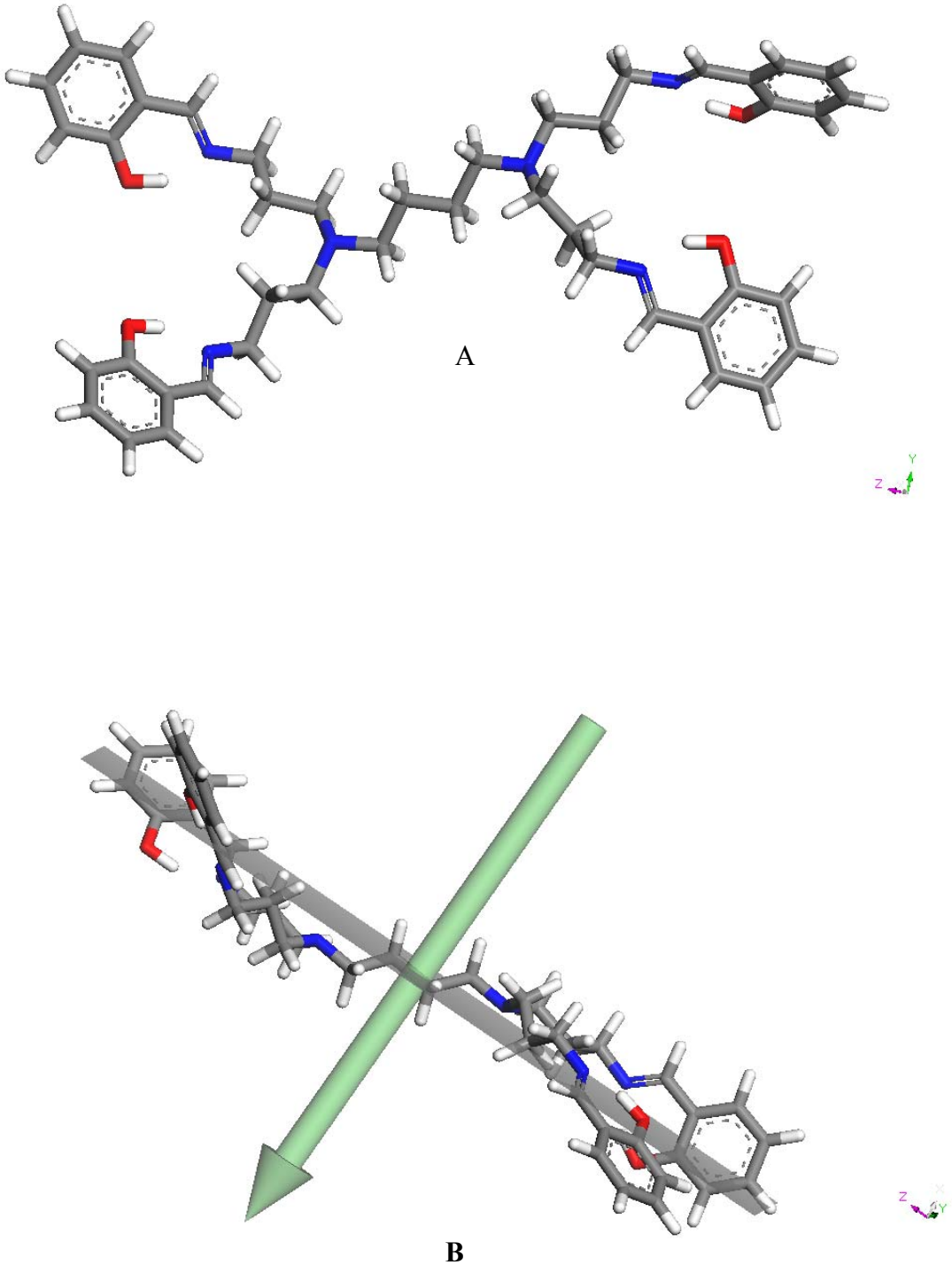

Figure 3.14: DAB G1 salicylaldimine modified dendrimer, **DL1**, optimized (A) and the best fit plane (B).

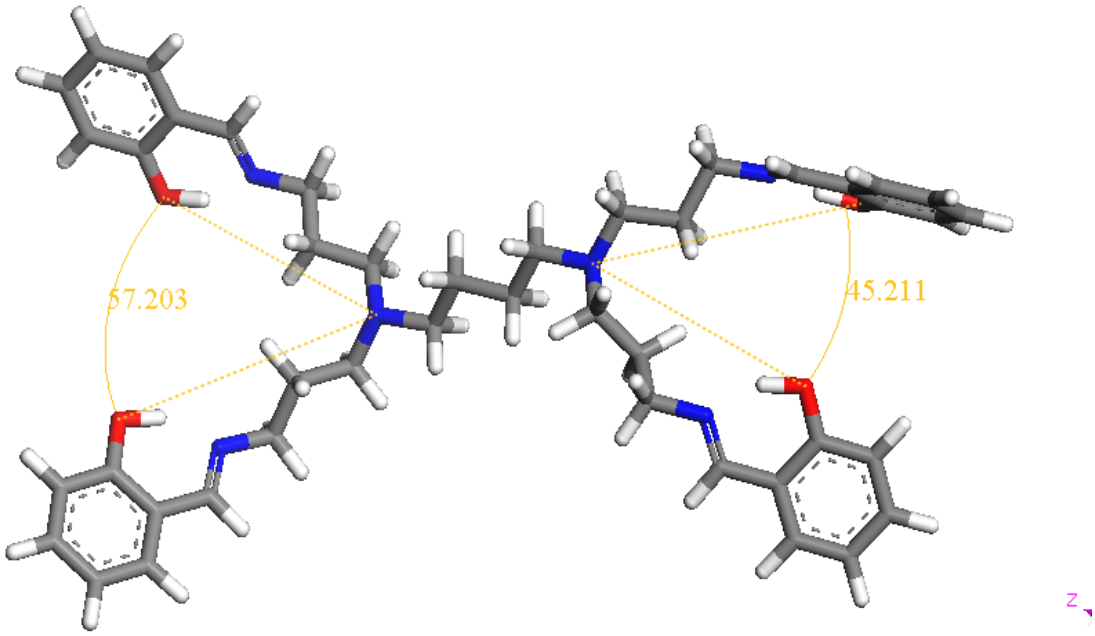

Figure 3.15: Bite angles between the OH groups of **DL1**.

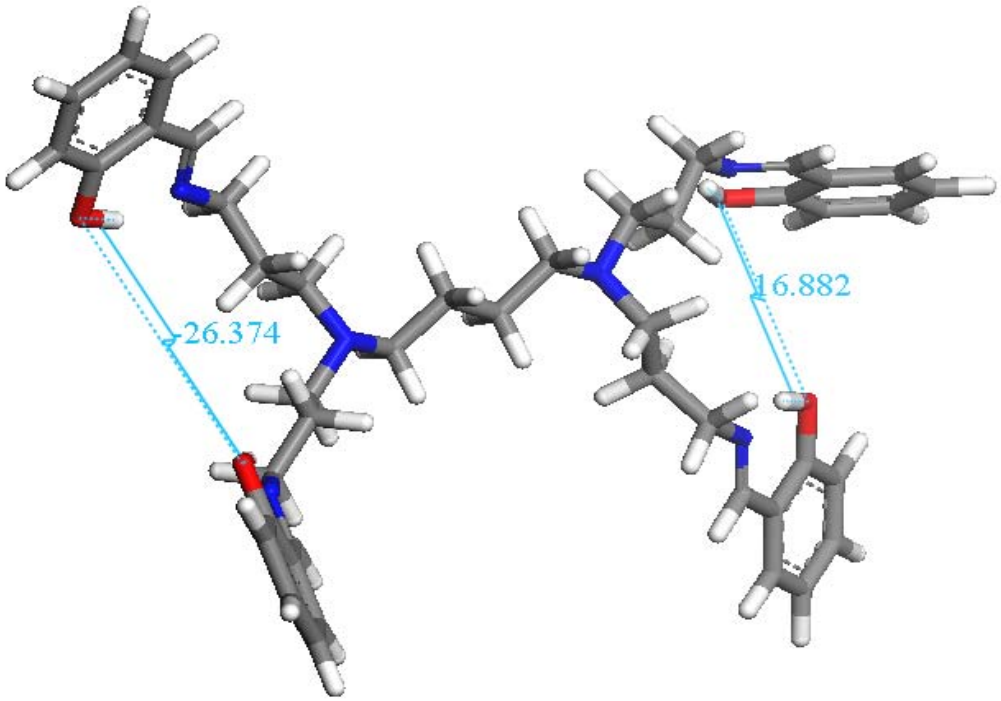

Figure 3.16: Dihedral angles between the OH groups of **DL1**.

Fig 3.17 shows the f(-)-Fukui function mapped on the total electron density of **DL1**, where the red colour shows high electron density. The Fukui function is one of the most important concepts in the theory of chemical reactivity. For the fixed positions of nuclei, it describes reorganization in electron density of a given molecule due to overall chemical oxidation/reduction. Therefore, it is able to give us information about site reactivity, information about what region of a molecule is better prepared to accept or donate charge.

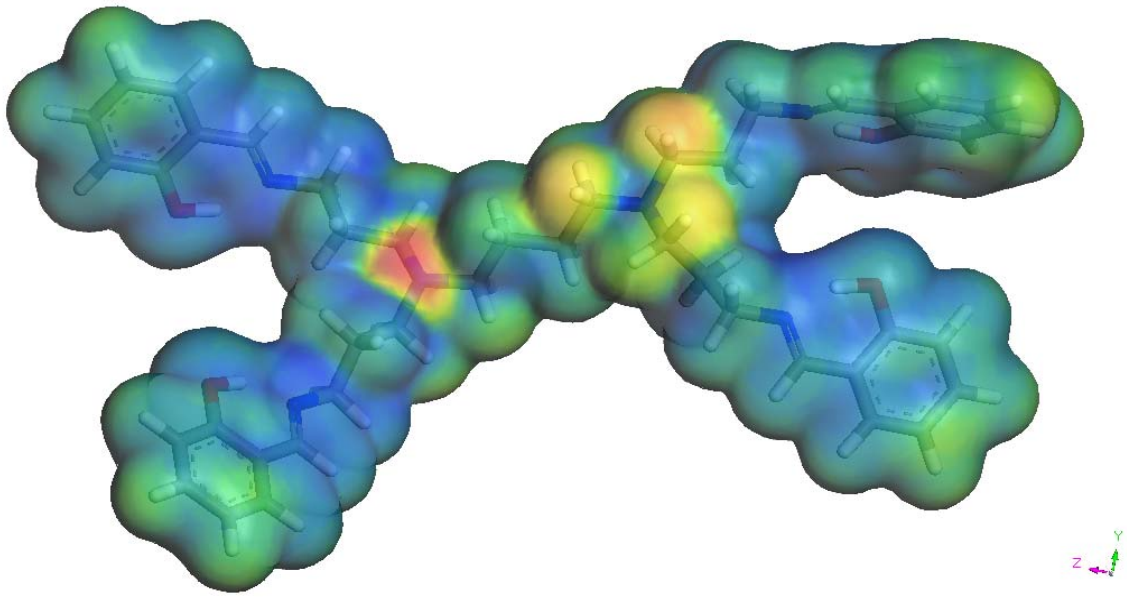

Figure 3.17: f(-)-Fukui function of **DL1**.

The f(-)-Fukui function of **DL1** shows that the area around the tertiary nitrogen atoms has the most electron density as indicated by the red and orange colours. This could potentially attract electron deficient species in subsequent reactions. The OH groups are less electron dense than the imine groups as shown by the blue region. From these calculations we can deduce that although both N and O atoms will coordinate to an appropriate metal precursor, the N-atom from the imine will coordinate more readily than the O-atom from the OH group

of the ligand. The highest occupied molecular orbitals (HOMO) is the tertiary N-atoms as shown in Fig 3.18. The lowest unoccupied molecular orbitals are the salicylaldimine functional groups as shown in Fig 3.19.

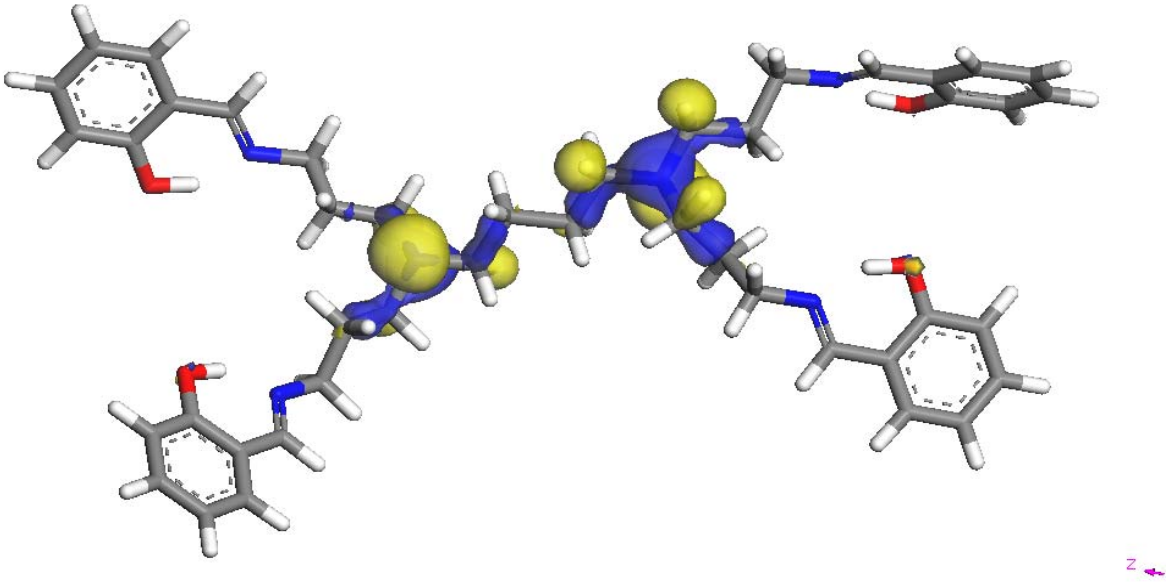

Figure 3.18: Highest occupied molecular orbitals (HOMO) of **DL1**.

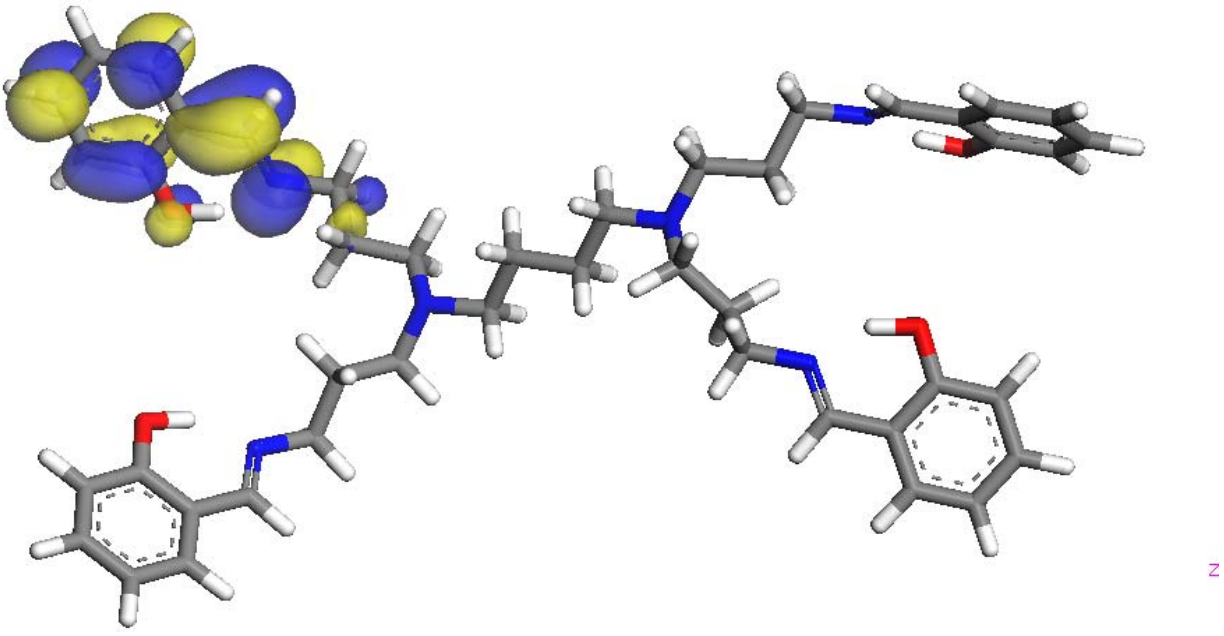

Figure 3.19: Lowest unoccupied molecular orbitals (LUMO) of **DL1**.

The LUMO of **DL1** confirms that coordination of any metals will occur at the dendrimer periphery i.e. the O-atom from the OH-groups and the N-atom from the imines of the ligand. The LUMO of **DL1**, shows that the metal will first coordinate on one side of the dendrimer ligand, and once this is complete, coordination of the metal on the other side will occur.

3.3.2 Structural optimization of the generation 2 salicylaldimine dendrimer ligand, ***DL2.***

The molecule was initially drawn "flat" in plane, with all the HO-C_6H_4-CHN-groups at ideal orientation. After optimization there was a clear rearrangement in the structure (Fig 3.20). The best fit plane of the G2 salicylaldimine dendrimer ligand is shown Fig 3.21.

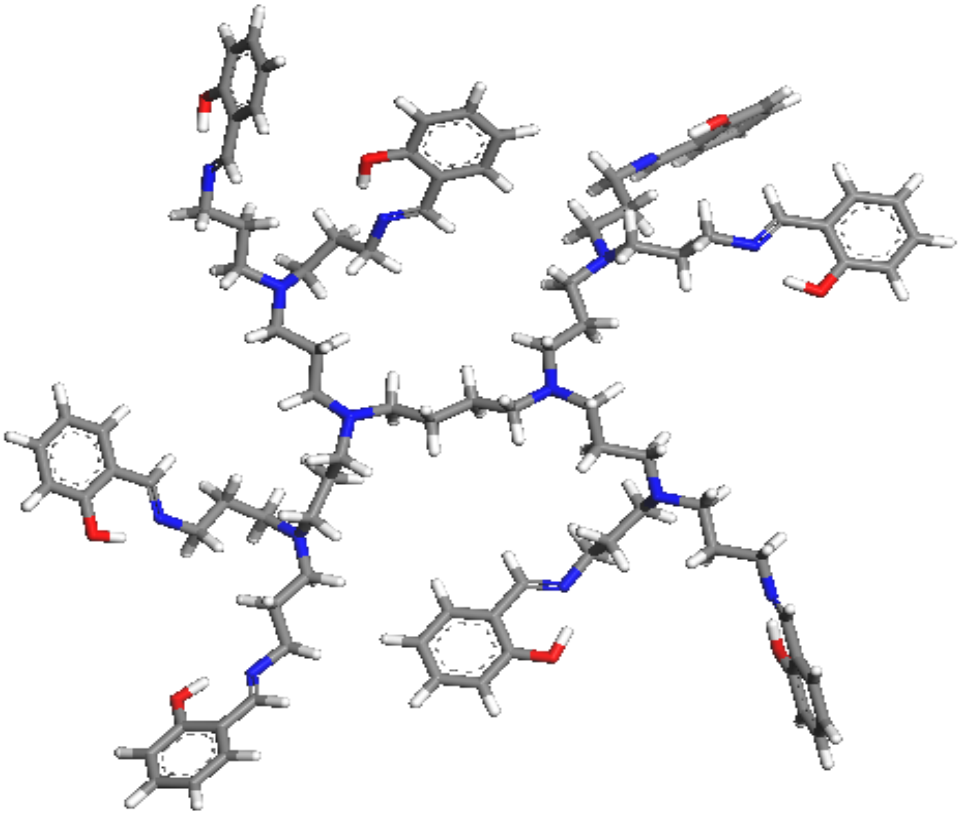

Figure 3.20: DAB G2 salicylaldimine modified dendrimer, **DL2**, optimized.

We can clearly see that the G2 dendrimer ligand is much more out of plane than the G1 dendrimer ligand, also proving that the higher generation dendrimer adopts a more spherical arrangement than the lower generation dendrimer.

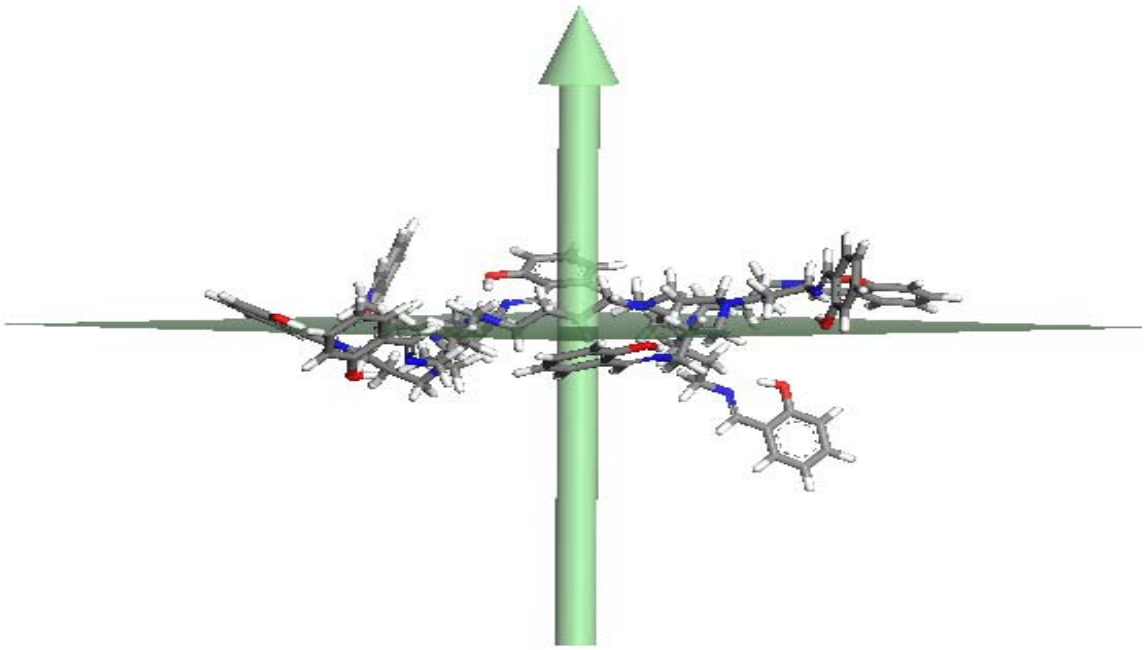

Figure 3.21: Best fit plane of **DL2**.

The bite angles between the OH groups for **DL2** were calculated as 51.1º, 61.6º, 62.5ºand 75.1º as shown in Fig 3.22. These angles are larger than those for the generation 1 ligand, **DL1**. This is possibly because the G2 ligand is more spherical than the G1 ligand, increasing the distances between the functional groups. This could also mean that G1 ligand will more easily coordinate to a metal precursor than the G2 ligand, due to the former's angles being smaller than the latter's. The dihedral angles between the OH groups were calculated as -26.3º, 17.6º, 31.3º and 36.3º as shown in Fig 3.23.

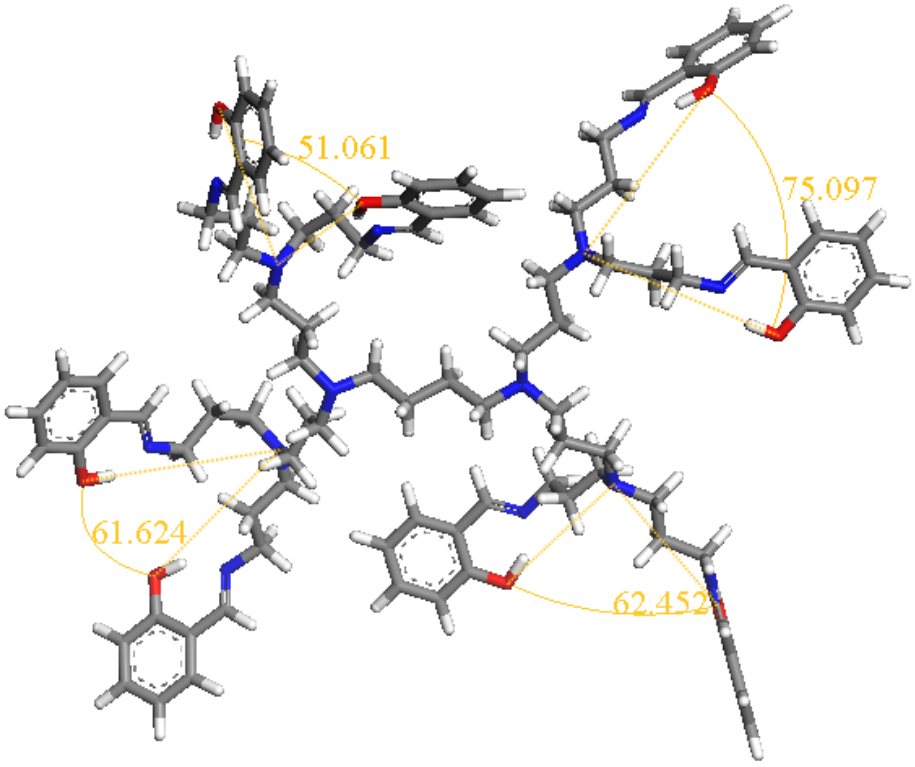

Figure 3.22: Bite angles between the OH groups of **DL2**.

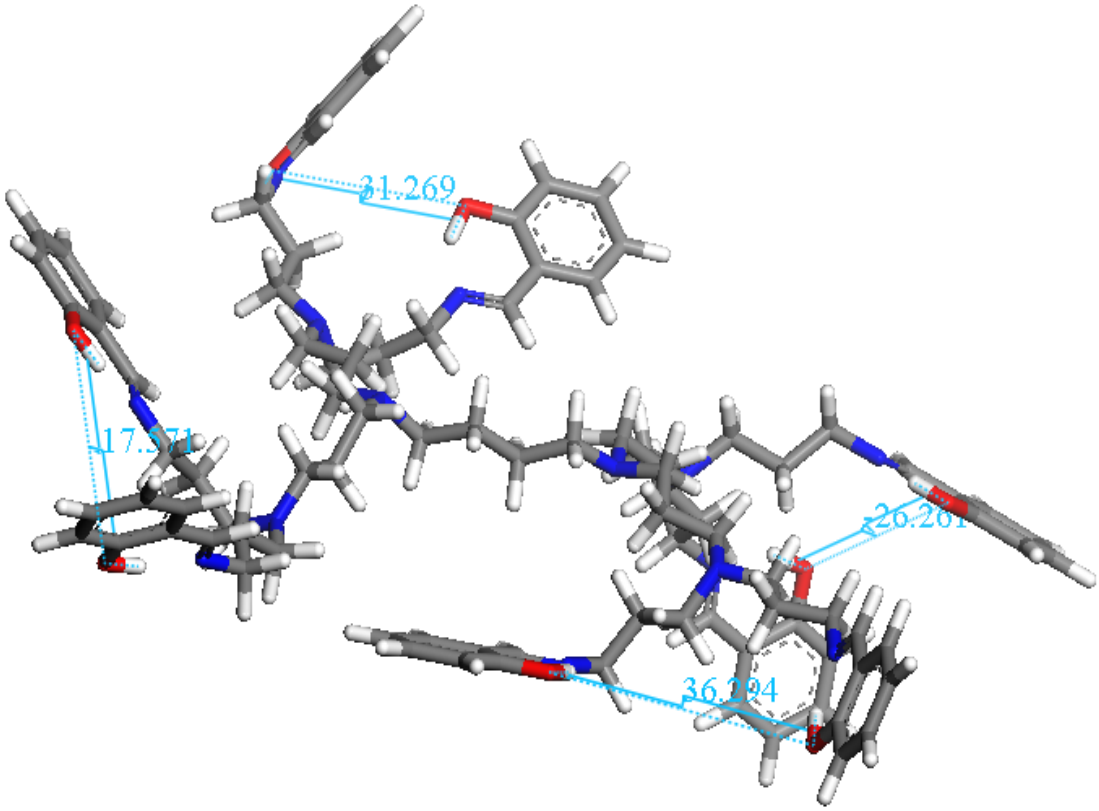

Figure 3.23: Dihedral angles between the OH groups of **DL2**.

The f(-)-Fukui function mapped on the total electron density for ligand, **DL2**, is shown in Fig 3.24. It shows the same electron density as for the generation 1 dendrimer ligand, with the tertiary amine groups having the highest electron density.

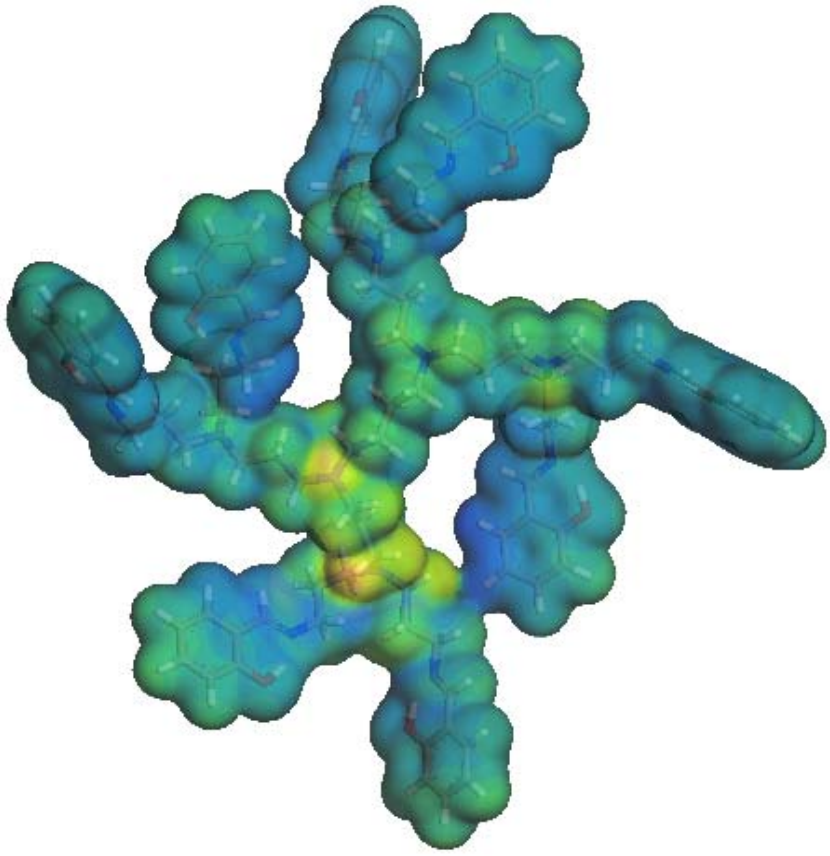

Figure 3.24: The f(-)-Fukui function of **DL2**.

*3.3.3 Optimization of the generation 3 salicylaldimine dendrimer ligand, **DL3.***

The molecule was drawn "flat" in plane, with all the HO-C_6H_4-CHN-groups at ideal orientation. After optimization there was a clear rearrangement in the structure (Fig 3.25). It was found that the more flexible the structure is, the more difficult it became to do the

geometry optimization. So although it was expected that the calculation would take longer than the lower generation dendrimers due to the increase in the number of atoms, it took even longer than anticipated due to the increased flexibility of the G3 dendrimer molecule. This was also observed looking at the change in energy with each optimization step which shows an even fluctuation (Fig 3.26).

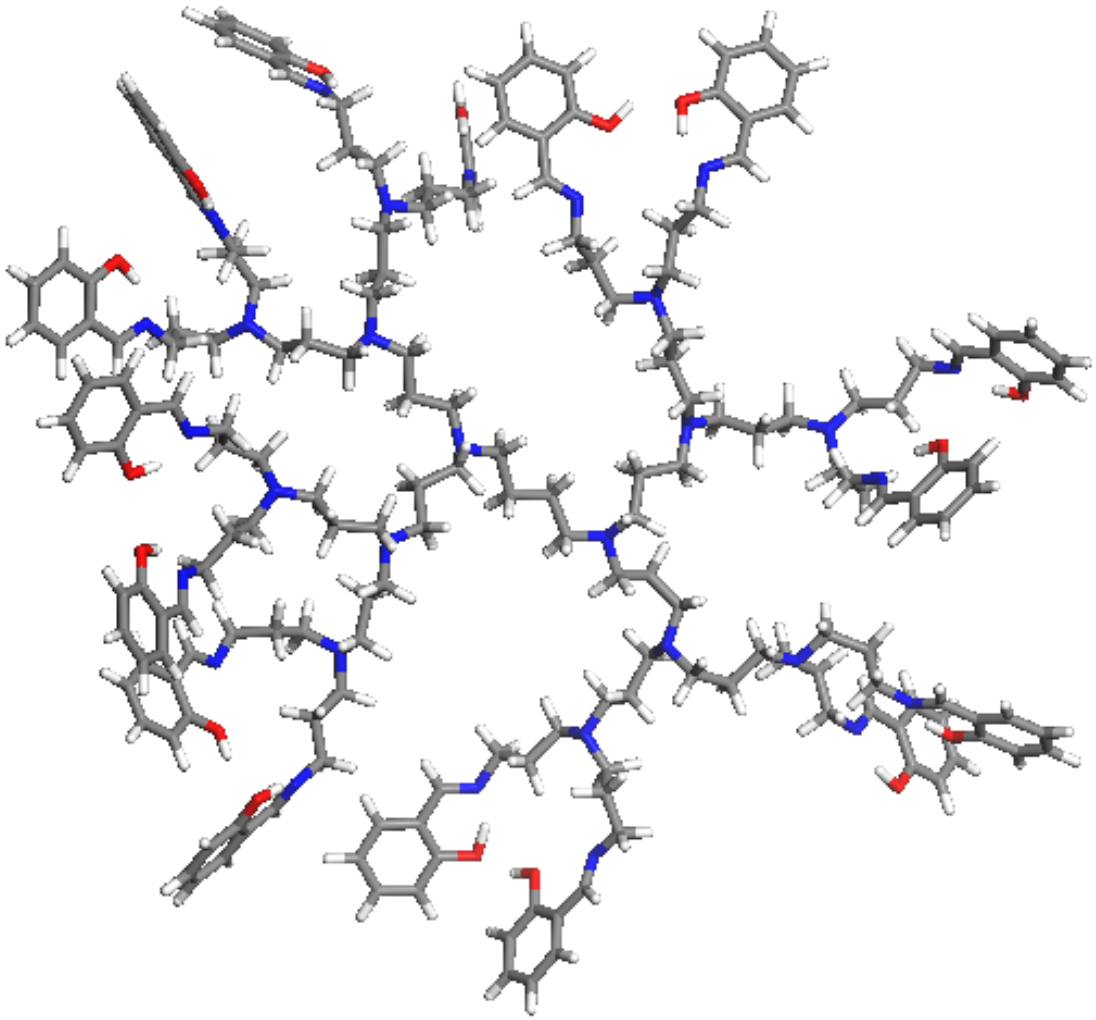

Figure 3.25: DAB G3 salicylaldimine modified dendrimer, **DL3**, optimized.

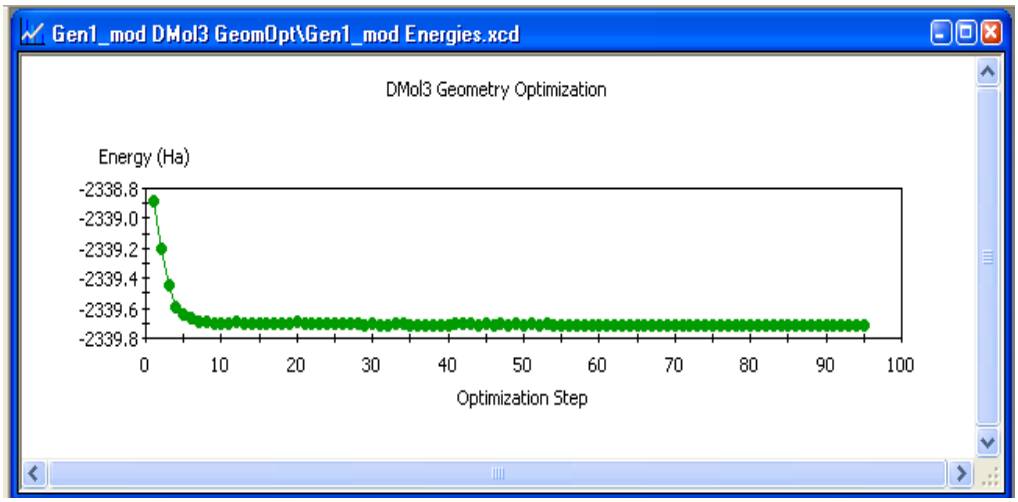

A

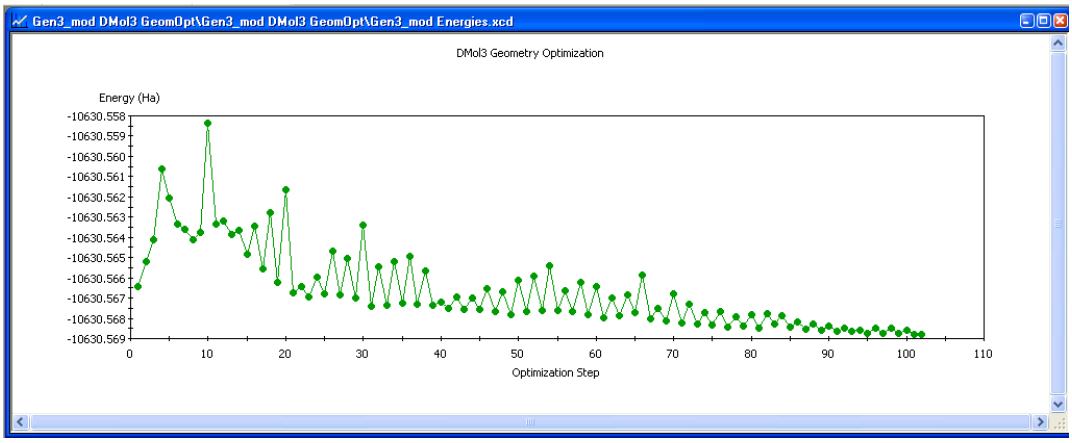

B

Figure 3.26: The change in energy with each optimization step which shows no fluctuation for the G1 ligand (A) and an even fluctuation for the G3 ligand (B).

The best fit plane for the generation 3 salicylaldimine dendrimer ligand is shown in Fig 3.27. It is observed that the G3 dendrimer ligand is even more out of plane than the G1 and G2 dendrimer ligands, again proving that the higher in generation the dendrimer, more spherical the ligand.

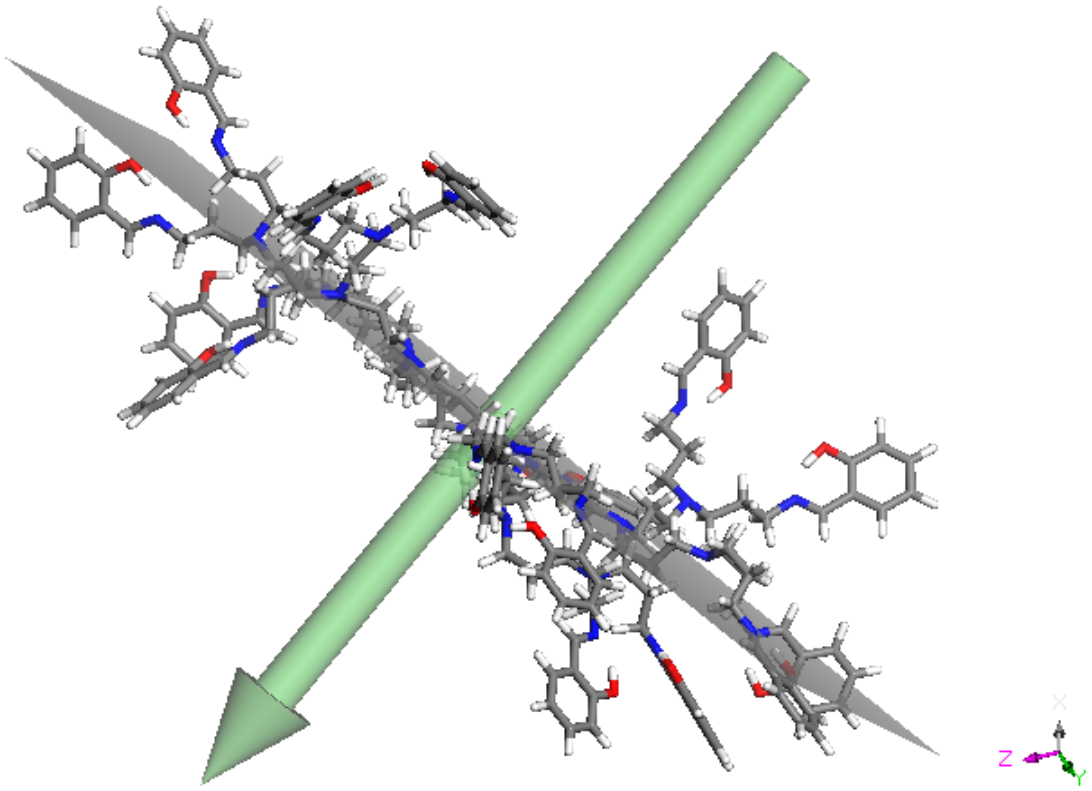

Figure 3.27: Best fit plane of **DL3**.

The bite angles between the OH groups for **DL3** were calculated as 23.3º, 24.3º, 24.8º, 29.1º, 33.8º, 35.8º, 39.7º and 44.3º as shown in Fig 3.28. It is important to note that the bite angles for the G3 ligand are much smaller than the angles for the G1 and G2 ligands. Although the spherical nature of the G2 ligand resulted in larger bite angles than the G1 ligand, it is possible that the very flexible nature as well as the large number of functional groups on the periphery of the G3 ligand result in a very crowded structure, hence the smaller bite angles. The dihedral angles between the OH groups were calculated as 6.6º, 20.4º, 28.8º, 77.6º, -10.1º, -42.9º, -162.9º and -170.6º as shown in Fig 3.29.

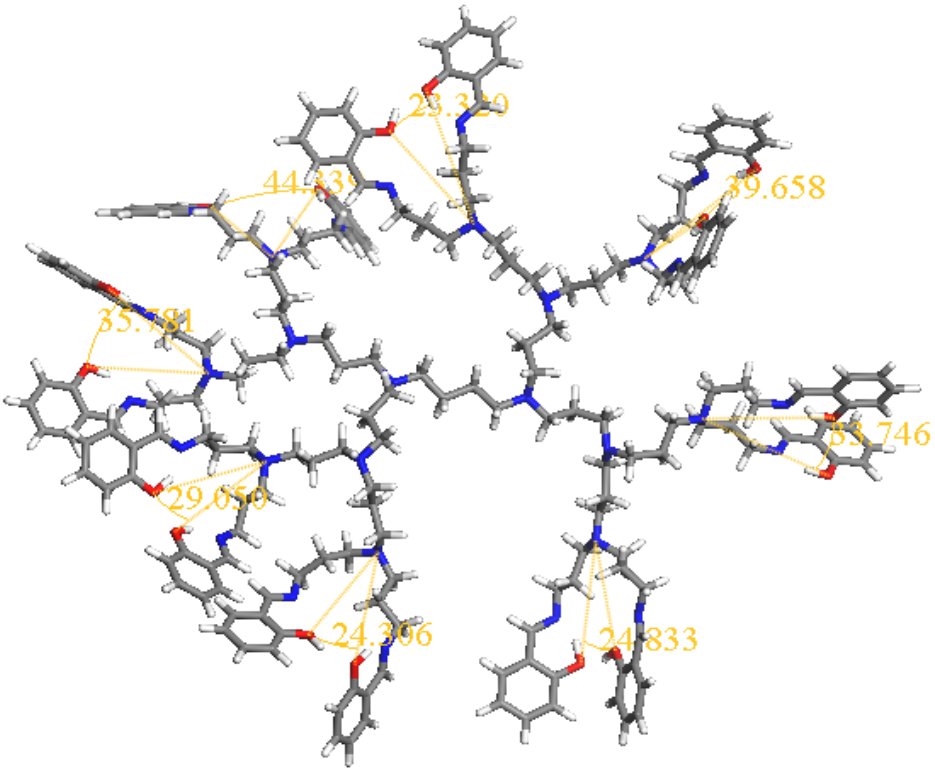

Figure 3.28: Bite angles between the OH groups of **DL3**.

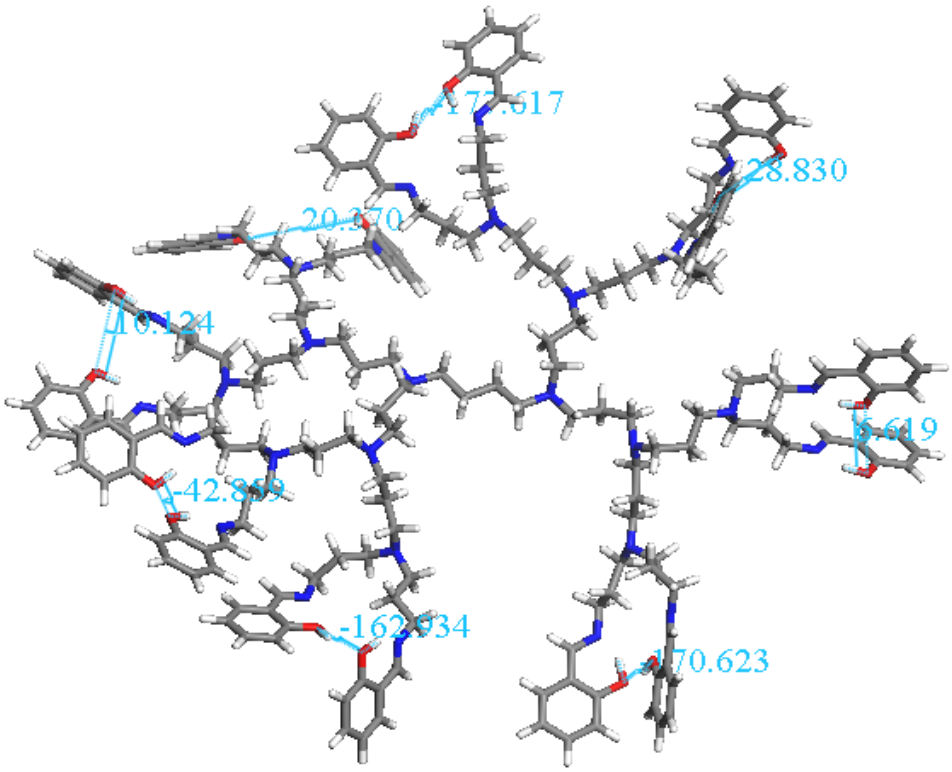

Figure 3.29: Dihedral angles between the OH groups of **DL3**.

The Fukui function of ligand, **DL3**, is shown in Fig 3.30. It confirms that tertiary amine atoms have the highest electron density, as shown by the red and orange regions. The G3 ligand, **DL3**, has more tertiary amine groups than **DL1** and **DL2**.

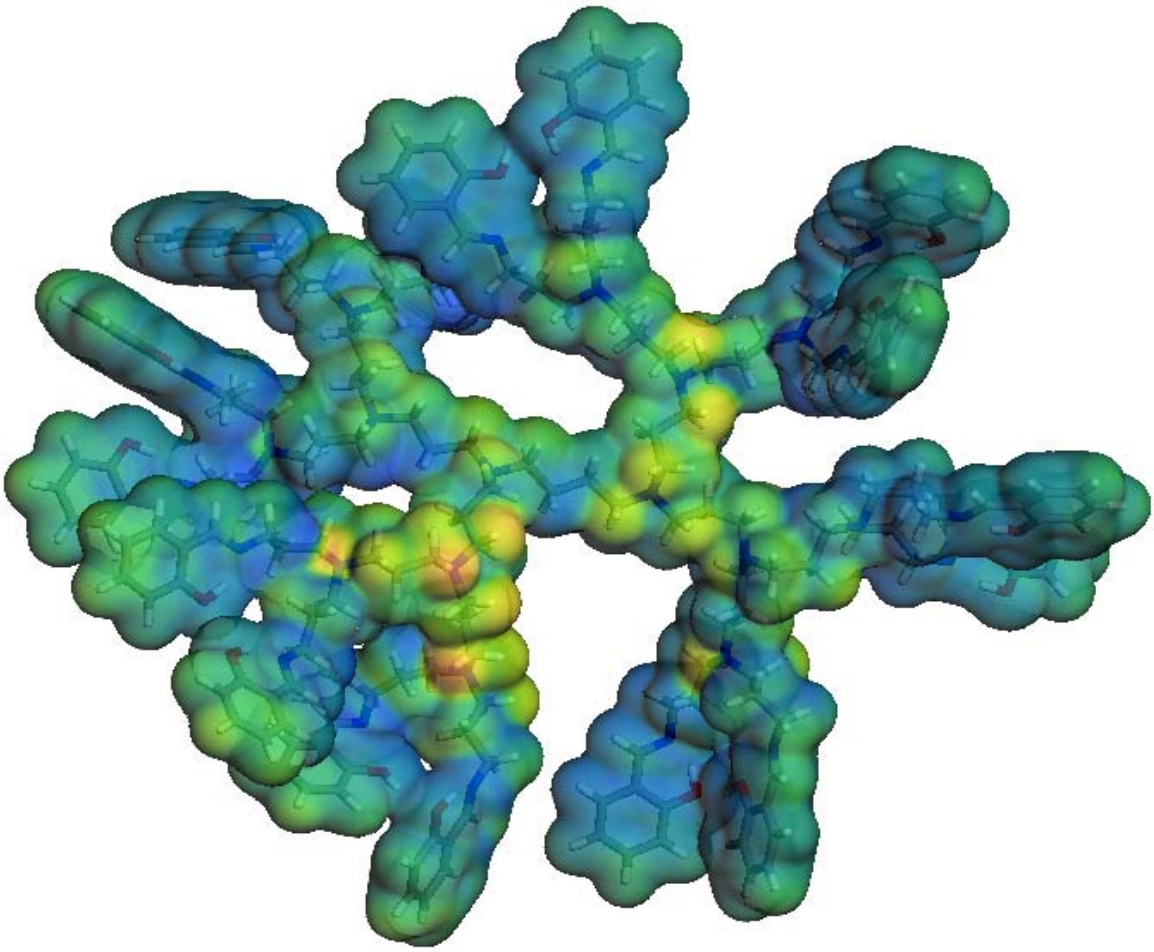

Figure 3.30: The Fukui function of ligand, **DL3**.

The LUMO of **DL2** and **DL3** also show that ligand coordination of the metal will occur at one site at a time. This informs us that synthesis of the G2 and the G3 metal complexes might possibly need longer reaction times than the synthesis of the G1 complex.

3.4 Conclusion.

The DAB G1-G3 dendrimers were successfully modified with salicylaldimine and iminopyridyl functional groups on its outer periphery. Longer reaction time is needed for the synthesis of the higher generation dendrimer ligands than for its lower generation analogues. The unmodified DAB-PPI dendrimer range is highly soluble in water, but after modification with the Schiff bases the dendrimer ligands became water insoluble. This is an example of how dendrimers can be modified to obtain specific properties.

From the molecular modelling studies of the DAB G1-G3 salicylaldimine ligands, it is clear that the lower generation dendrimers have an open structure, but the higher in generation the dendrimer is, the more spherical the structure becomes. This was seen by examining the optimized structure of the generation 3 ligand, **DL3**, which adopts a highly spherical and flexible structure. Based on the modelling results, we predicted that the flexibility of the generation 3 dendrimer ligand could hinder the dendrimer catalyst performance during catalytic reactions. This was confirmed by the results for our catalytic experiments, when the G1-G3 dendrimer catalysts were evaluated in the polymerization of norbornene, which is discussed in Chapter 5.

For this reason, the generation 1 cyclam cored dendrimers were also modified with salicylaldimine and iminopyridyl moieties. It is thought that the cyclam cored dendrimers could be more rigid and spherical than the DAB cored dendrimers, which could subsequently affect the dendrimer's catalytic ability during catalysis.

These modified ligands were subsequently complexed to metal salts, in order to form metallodendrimers (Chapter 4). The metallodendrimers were then evaluated in several catalytic processes which are discussed in Chapter 5 and Chapter 6.

3.5 Experimental.

Toluene was dried by refluxing over sodium/benzophenone. The DAB dendrimer range was obtained from Symochem, Netherlands, and used without any further purification. Salicylaldehyde and 2-pyridine carboxyaldehyde were purchased from Sigma Aldrich, and were used without any further purification. The silica gel used for chromatography was purchased from Merck Chemicals. Infrared spectra were recorded on a Nicolet Avatar 330 FT-IR spectrophotometer, using an ATR accessory with a ZnSe crystal. ^{1}H NMR (300 MHz and 400 MHz) and ^{13}C NMR (75 MHz) spectra were recorded on a Varian VNMRS 300 MHz and a Varian Unity Inova 400 MHz spectrometer, using tetramethylsilane as an internal standard. ESI Mass spectra were obtained using a Waters API Q-TOF Ultima instrument in V-mode. The source temperature was 100 ºC and the desolvation temperature was 350 ºC. The capillary voltage used was 3.5 kV. Microanalyses were done at the University of Cape Town. Density functional theorem (DFT) calculations were done at North-West University.

*Synthesis of **DL1**:*

DAB-G1 dendrimer (0.50 g, 1.6 mmol) was added to dry toluene (10 ml) in a Schlenk tube, under nitrogen. Salicylaldehyde (0.77 ml, 6.3 mmol) was added to the solution. The mixture was allowed to stir for 72 hours at room temperature. The solvent was evaporated on a rotary evaporator and a yellow oil was obtained. Dichloromethane (10 ml) was added to the oil, after which hexane (20 ml) was added. This solution was allowed to stand in the fridge for 72 hours at -4 $^{\circ}$C. The yellow precipitate obtained was filtered off via vacuum filtration to give an air stable yellow solid product. Yield: 90 %. m.p. 66-68 ºC. IR (cm^{-1}): ν(O-H) 2924 (m); ν(C=N) 1632 (s); ν(C-O) 1284 (s); ^{13}C NMR in $CDCl_3$ (δ ppm): 25.1, 28.4,

51.5, 54.0, 57.4, 117.0, 118.4, 118.8, 131.1, 132.1, 161.3, 164.9. MS (MALDI-TOF) Calc. ($C_{44}H_{56}N_6O_4$) $[M]^+$ at m/z = 733.

*Synthesis of Ligand **DL2**:*

The generation 2 ligand was synthesized similarly to **DL1**, using a 1:8 DAB-G2 dendrimer:salicylaldehyde mol ratio under the same reaction conditions. The solvent was evaporated on a rotary evaporator and a yellow oil was obtained. Dichloromethane (20 ml) was added to the oil and the product was extracted five times with 30 ml water. The dichloromethane layer was dried over potassium carbonate after which the latter was filtered off. The filtrate was evaporated to give a yellow oil. Yield: 85 %. IR(cm^{-1}): ν(O-H) 3058 (m); ν(C=N) 1630 (s); ν(C-O) 1279 (s). ^{13}C NMR in $CDCl_3$ (δ ppm): 24.1, 24.8, 30.1, 52.1, 52.2, 116.9, 118.4, 118.7, 131.1, 131.9, 134.5, 161.2, 164.8. MS (MALDI-TOF) Calc. ($C_{96}H_{128}N_{14}O_8$) $[M]^+$ at m/z = 1606.

*Synthesis of Ligand **DL3**:*

DAB-G3 dendrimer (0.53 g, 0.31 mmol) was added to dry toluene (15 ml), in a Schlenk tube, under nitrogen. Salicylaldehyde (0.54 ml, 5 mmol) was added to the solution. The mixture was allowed to stir under reflux, for 96 hours. The solvent was evaporated on a rotary evaporator, and a yellow oil was obtained. Dichloromethane (20 ml) was added to the residue and the product was extracted five times with 30 ml water. The dichloromethane layer was dried over potassium carbonate after which the latter was filtered off. The filtrate was evaporated to produce a yellow oil. Yield: 80 %. IR (cm^{-1}): ν(O-H) 2941 (m); ν(C=N) 1629 (s); ν(C-O) 1277 (s). ^{13}C NMR in $CDCl_3$ (δ ppm): 24.6; 28.7; 31.15; 51.67; 52.48;

57.67; 117.18; 118.63; 131.36; 132.26; 161.48; 165.09. MS (MALDI-TOF) Calc. ($C_{200}H_{272}N_{30}O_{16}$) $[M]^+$ at m/z = 3352 m/z. ESI: $[M]^{2+}$ at m/z = 1676.5.

*Synthesis of **DL4**:*

DAB-G1 dendrimer (1.0 g, 3.2 mmol) was added to dry toluene (15 ml) in a Schlenk tube, under nitrogen. 2-Pyridine carboxyaldehyde (1.2 ml, 12.8 mmol) was added to the solution. The mixture was allowed to stir for 48 hours at room temperature. The solvent was evaporated on a rotary evaporator and a dark brown oil was obtained. Dichloromethane (20ml) was added to the oil and the product was extracted five times with 30 ml water. The dichloromethane layer was dried over potassium carbonate after which the latter was filtered off. The filtrate was evaporated to give a brown oil. Yield: 80 %. IR (cm^{-1}): ν(C=N) *aliphatic* 1647 (s); ν(C=N) pyr 1586 (s); ν(C=C) pyr 1562 (m). ^{13}C NMR in $CDCl_3$ (δ ppm): 24.7; 27.8; 51.2; 53.6; 59.1; 120.7; 124.0; 136.0; 148.9; 161.4; 154.1. MS (MALDI-TOF) Calc. ($C_{40}H_{52}N_{10}$) $[M]^+$ at m/z = 672.80.

*Synthesis of **DL5**:*

DAB-G2 dendrimer (0.523 g, 0.676 mmol) was added to dry toluene (20 ml) in a Schlenk tube, under nitrogen. 2-Pyridine carboxyaldehyde (0.51 ml, 0.541mmol) was added to the solution. The mixture was allowed to stir for 48 hours at room temperature. The solvent was evaporated on a rotary evaporator and a dark brown oil was obtained. Dichloromethane (20 ml) was added to the oil and the product was extracted five times with 30 ml water. The dichloromethane layer was dried over potassium carbonate after which the latter was filtered off. The filtrate was evaporated to give a brown oil. Yield: 85 %. IR (cm^{-1}): ν(C=N) *aliphatic*

1647 (s); ν(C=N) pyr 1586 (s); ν(C=C) pyr 1562 (m). ^{13}C NMR in $CDCl_3$ (δ ppm): 24.63; 28.25; 51.69; 59.52; 121.16; 124.51; 128.96; 136.41; 149.30; 154.54; 161.78. ESI-MS Calc. ($C_{88}H_{120}N_{22}$) $[M+H]^+$ at m/z = 1487.

*Synthesis of **DL6**:*

DAB-G3 dendrimer (0.60 g, 0.64 mmol) was added to dry toluene (20 ml) in a Schlenk tube, under nitrogen. 2-Pyridine carboxyaldehyde (0.60 ml, 5.80 mmol) was added to the solution. The mixture was allowed to stir for 72 hours at room temperature. The solvent was evaporated on a rotary evaporator and a dark brown oil was obtained. Dichloromethane (20 ml) was added to the oil and the product was extracted five times with 30 ml water. The dichloromethane layer was dried over potassium carbonate after which the latter was filtered off. The filtrate was evaporated to give a brown oil. Yield: 80 %. IR (cm^{-1}): ν(C=N) *aliphatic* 1648 (s); ν(C=N) pyr 1587 (s); ν(C=C) pyr 1567 (m). ^{13}C NMR in $CDCl_3$ (δ ppm): 24.34; 28.18; 30.93; 51.67; 59.53; 121.22; 124.56; 136.49; 149.33; 154.55; 161.68. ESI-MS Calc. ($C_{88}H_{120}N_{22}$) $[M]^{5+}$ at m/z = 622.16.

*Synthesis of **DL7**:*

G1 cyclam-propyl dendrimer (0.31 g, 0.72 mmol) was added to dry toluene (10 ml) in a Schlenk tube, under nitrogen. Salicylaldehyde (0.35 ml, 2.9 mmol) was added to the solution. The mixture was allowed to stir for 72 hours at room temperature. The solvent was evaporated on a rotary evaporator and a red oil was obtained. Dichloromethane (20 ml) was added to the oil and the product was extracted five times with 30 ml water. The dichloromethane layer was dried over potassium carbonate after which the latter was filtered

off. The filtrate was evaporated to give a red oil. Yield: 78 %. IR (cm^{-1}): ν(O-H) 3058 (m); ν(C=N) 1662 (s); ν(C-O) 1276 (s). ^{13}C NMR in $CDCl_3$ (δ ppm): 29.91; 31.31; 48.05; 51.68; 117.84; 120.06; 133.94; 137.27; 141.14; 161.85; 169.09. ESI-MS Calc. ($C_{50}H_{68}N_8O_4$) $[M+H]^+$ at m/z = 846.

*Synthesis of **DL8**:*

The G1 cyclam-propyl iminopyridyl dendrimer ligand **DL8** was synthesized similarly to the ligand **DL7**, using 2-pyridine carboxyaldehyde instead of salicylaldehyde under the same reaction conditions. The solvent was evaporated on a rotary evaporator and a dark brown oil was obtained. Dichloromethane (20 ml) was added to the oil and the product was extracted five times with 30ml water. The dichloromethane layer was dried over potassium carbonate after which the latter was filtered off. The filtrate was evaporated to give a brown oil. Yield: 75 %. IR (cm^{-1}): ν(C=N) aliphatic 1648 (s); ν(C=N) pyr 1586 (s); ν(C=C) pyr 1567 (m). ^1H NMR in $CDCl_3$ (δ ppm): 1.61; 1.83; 2.50; 2.55; 3.65; 7.52; 7.70; 7.94; 8.36; 8.80. ^{13}C NMR in $CDCl_3$ (δ ppm): 10.47; 22.66; 46.10; 47.38; 48.98; 51.05; 51.75; 121.92; 125.35; 136.80; 150.43; 162.62. ESI-MS Calc. ($C_{46}H_{64}N_{12}$) $[M+K]^+$ at m/z = 825.

*Synthesis of **DL9**:*

G1 cyclam-benzyl dendrimer (0.44 g, 0.64 mmol) was added to dry toluene (10 ml) in a Schlenk tube, under nitrogen. Salicylaldehyde (0.31 ml, 2.6 mmol) was added to the solution. The mixture was allowed to stir for 72 hours at room temperature. The solvent was evaporated on a rotary evaporator and a red oil was obtained. Dichloromethane (20 ml) was added to the oil and the product was extracted five times with 30 ml water. The

dichloromethane layer was dried over potassium carbonate after which the latter was filtered off. The filtrate was evaporated to give a red oil. Yield: 72 %. IR (cm^{-1}): ν(O-H) 3058 (m); ν(C=N) 1668 (s); ν(C-O) 1294 (s). ^{13}C NMR in $CDCl_3$ (δ ppm): 27.31; 34.94; 54.17; 63.68; 117.76; 119.29; 120.57; 124.87; 128.23; 132.11; 133.02; 137.72; 161.88; 166.18. ESI-MS Calc. ($C_{70}H_{76}N_8O_4$) $[M+\mathbf{18.3}]^+$ at m/z = 1111.3.

*Synthesis of **DL10**:*

The G1 cyclam-benzyl iminopyridyl dendrimer ligand **DL10** was synthesized similarly to the ligand **DL9**, using 2-pyridine carboxyaldehyde instead of salicylaldehyde under the same reaction conditions. The solvent was evaporated on a rotary evaporator and a dark brown oil was obtained. Dichloromethane (20 ml) was added to the oil and the product was extracted five times with 30 ml water. The organic layer was dried over potassium carbonate and then filtered. The filtrate was evaporated to give a brown oil. Yield: 81 %. IR (cm^{-1}): í(C=N) *aliphatic* 1630 (s); í(C=N) *pyr* 1574 (s); í(C=C) *pyr* 1510 (m). ^{13}C NMR in $CDCl_3$ (ä ppm): 27.29; 34.93; 52.02; 65.45; 122.43; 125.50; 128.58; 129.08; 137.26; 137.78; 150.93; 153.53; 163.41. ESI-MS Calc. ($C_{66}H_{72}N_{12}$) $[M+H]^{2+}$ at m/z = 516.4.

3.6 References.

[1] F. Vogtle, S. Gestermann, R. Hesse, H. Schwierz, B. Windisch, *Prog. Polym. Sci.*, 25, **2000**, 987.

[2] J. C. Roberts, M. K. Bhalgat, R.T. Zera, *J. Biomed. Mater. Res.,* 30, **1996**, 53.

[3] R. Jevprasesphant, J. Penny, R. Jalal, D. Attwood, N. B. McKeown, A. D'Emanuele, *Int. J. Pharm*., 252, **2003**, 263.

[4] K. Endo, Y. Ito, T. Higashihara, M. Ueda, *Eur. Pol. J.,* 45, **2009**, 1994.

[5] K. C. Gupta, A. K. Sutar, *Coord. Chem. Rev.,* 252, **2008**, 1420.

[6] J. Cui, M. Zhang, Y. Zhang, *Inorg. Chem. Commun*., 13, **2010**, 81.

[7] B. De Clercq, F. Verpoort, *J. Mol. Cat. A: Chem.,* 180, **2002**, 67.

[8] M. Wang, H. Zhu, K. Jin, D. Dai, L. Sun, *J. Catal.,* 220, **2003**, 392.

[9] C. Bianchini, G. Giambastiani, L. Luconi, A. Meli, *Coord. Chem. Rev.,* 254, **2010**, 431.

[10] B. Berchtold, V. Lozan, P-G. Lassahn, C. Janiak, *J. Polym. Sci., Part A: Polym. Chem.,* 40, **2002**, 3604.

[11] A. S. Abu-Surrah, K. Lappalainen, U. Piironen, P. Lehmus, T. Repo, M. Leskela, *J. Organomet. Chem.,* 648, **2002**, 55.

[12] R. Malgas, S.F. Mapolie, S.O. Ojwach, G.S. Smith, J. Darkwa, *Catal. Commum.,* 9, **2008**, 1612.

[13] S. Y. Cho, H. R. Allcock, *Macromolecules,* 40, **2007,** 3115.

[14] K. Tanaka, K. Inafuku, K. Naka, Y. Chujo, *Org. Biomol. Chem.*, 6, **2008**, 3899.

[15] G. Smith, R. Chen, S.F. Mapolie, *J. Organomet. Chem.,* 673, **2003**, 111.

[16] N. Mketo, MSc Thesis: Palladium and copper complexes based on dendrimeric and monofunctional N,N' chelating ligands as potential catalysts in the oxidative carbonylation of alcohols., University of Stellenbosch, **2010.**

[17] B. Delley, *J. Chem. Phys.*, 92, **1990**, 508.

[18] B. Delley, *J. Phys. Chem.*, 100, **1996**, 6107.

[19] B. Delley, *J. Chem. Phys.*, 113, **2000**, 7756.

[20] http://www.accelrys.com [Date of access: 27/08/2010]

[21] J. P. Perdew, Y. Wang, *Phys. Rev.*, B45, **1992**, 13244.

[22] B. Delley, ***Modern Density Functional Theory: A Tool for Chemistry***, J. M. Seminario, P. Politzer, *Theoretical and Computational Chemistry*, Vol. 2, Elsevier, Amsterdam, The Netherlands, **1995**.

[23] J. Andzelm, R. D. King-Smith, G. Fitzgerald, *Chem. Phys. Lett.*, 335, **2001**, 321.

Chapter 4:

Synthesis and Characterization of Nickel Metallodendrimers.

4.1 Introduction to the metallodendrimer synthesis.

In Chapter 1 we discussed the properties of metallodendrimers and its application in various catalytic and other chemical processes. In this chapter we give a brief overview of metallodendrimer synthesis reported in the literature and describe novel metallodendrimers synthesized as part of this project.

4.1.1 Metallodendrimer overview.

As previously mentioned, metals can be positioned at various points in the dendritic molecule i.e. at terminal units, at branching centres or at the core (Fig 4.1) to form a metallodendrimer. The metals are usually introduced into the dendritic framework after construction and modification of the dendrimer molecule.

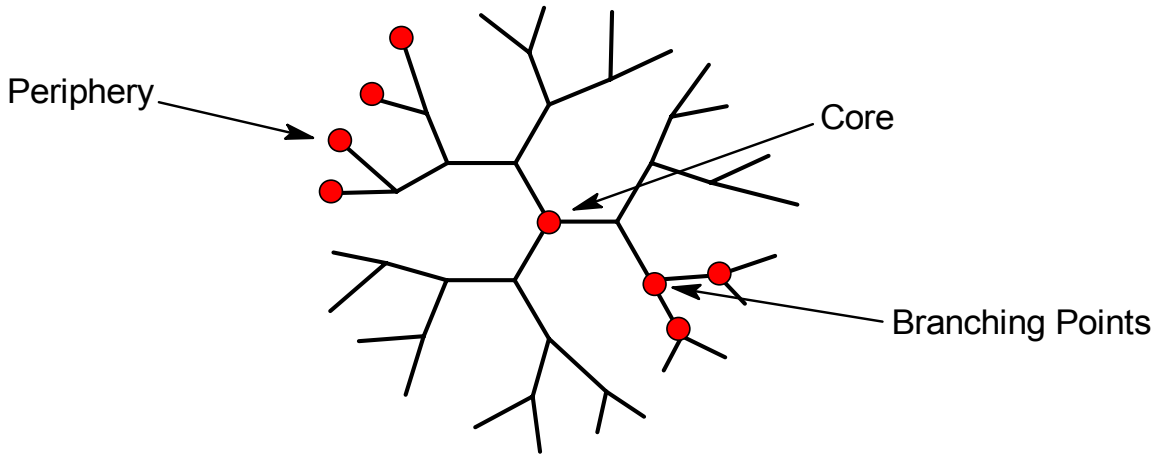

Figure 4.1: Potential positioning of metals within dendrimer frameworks.

4.1.2 Metallodendrimer synthesis.

A few examples of metallodendrimers with metals in various positions are described below.

The synthesis of a modified anionic scorpionate (trispyrazolylborate) ligand with an allyl group attached to boron was reported by Camerano *et al.*[1] The allyl group of the ligand allowed the peripheral attachment of the tris(pyrazolyl)borate ligand to commercial carbosilane dendrimers via a hydrosilylation reaction to give unusual polyanionic dendrimers. Once the carbosilane dendrimers were modified with the anionic tris(pyrazolyl)borate ligand, it was capable of coordinating transition metals on its periphery, as confirmed by the preparation of metallodendrimers that contain up to sixteen rhodium centres (Fig 4.2). These metallodendrimers were characterized by NMR spectroscopy, elemental analysis and MALDI-TOF mass spectrometry.

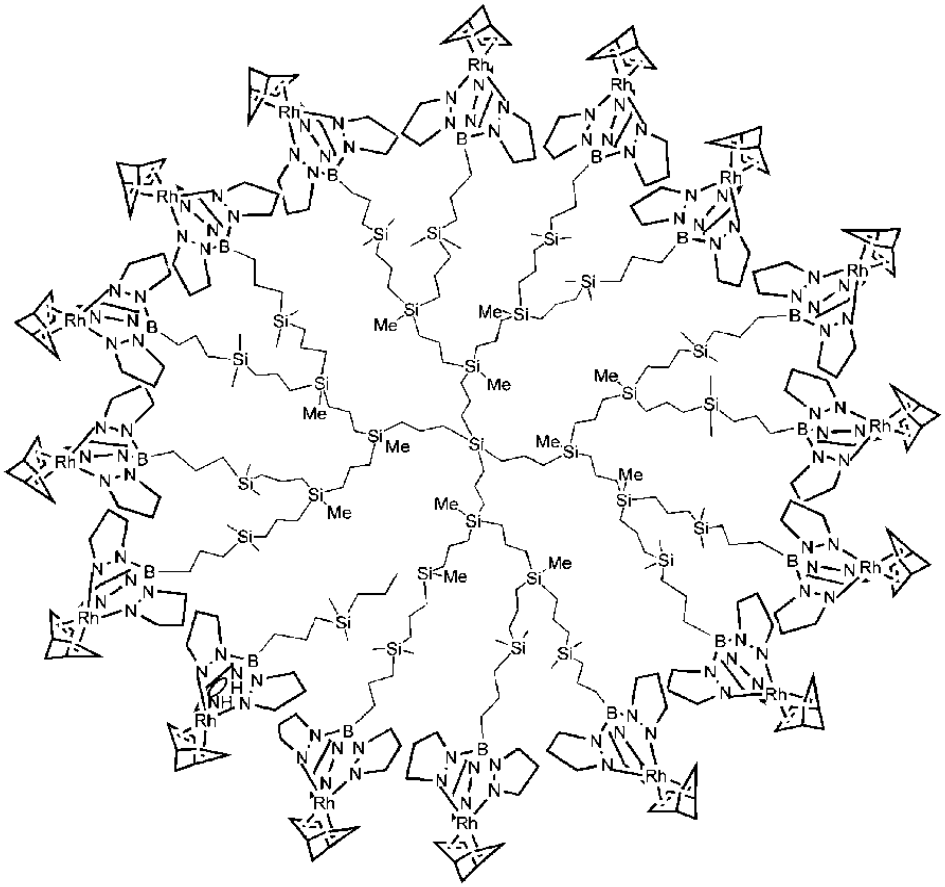

1

Figure 4.2: A generation 2 tris(pyrazolyl)borate rhodium metallodendrimer synthesised by Camerano *et al.*[1]

Angurell *et al* first reported the synthesis of carbosilane metallodendrimers with (Cy)$RuCl_2$ coordinated to the dendrimer periphery through PPh_2 units.[2] They subsequently proposed that these ruthenium dendrimers are capable of addition of a new shell of different metallic fragments onto the surface of the metallodendrimer.[3] For this purpose they synthesised a rhenium complex [Re(bipy)$(CO)_3$(C≡Cpy)] that can coordinate to peripheral ruthenium atoms through a pyridine group (Fig 4.3). This is an interesting example of a bimetallic metallodendrimer with metal atoms within the dendrimer framework as well as on the dendrimer surface.

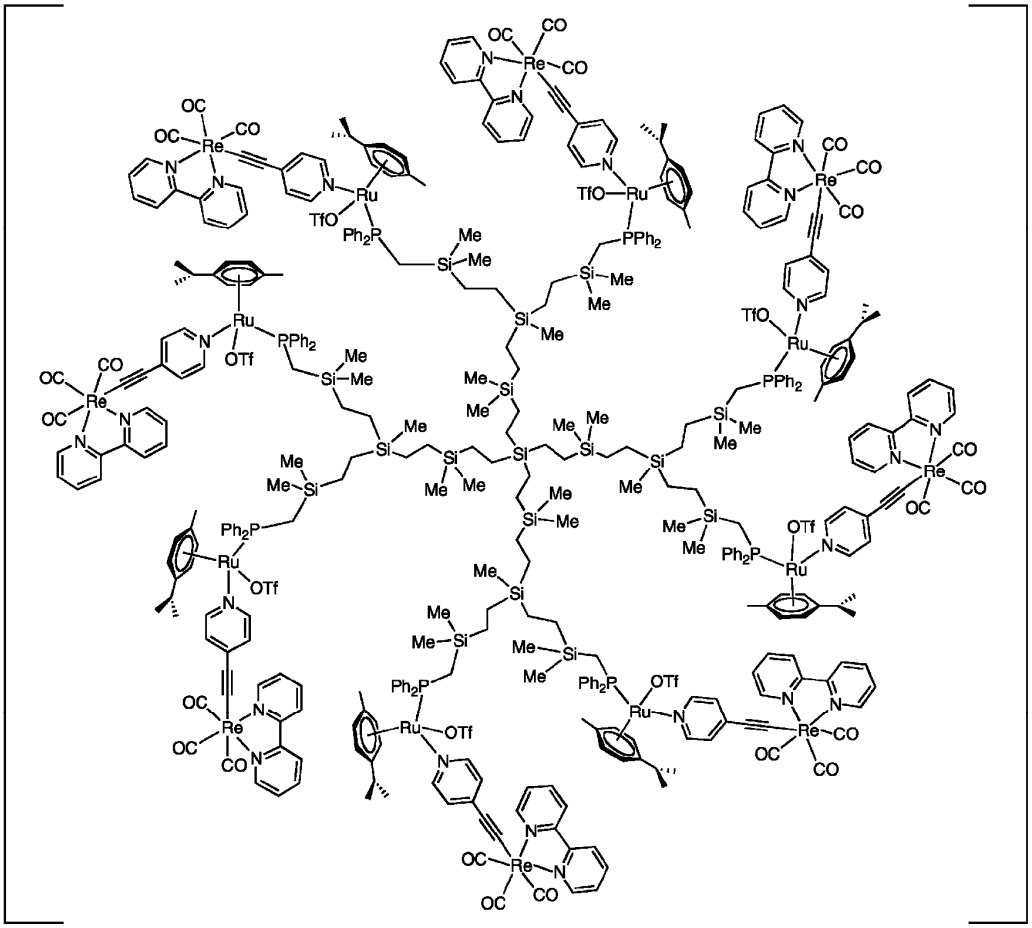

2

Figure 4.3: A generation 2 bimetallic dendrimer functionalised with [{ç^6-(ñ-cymene)} Ru(triflate)(pyC≡C)-Re(bipy)$(CO)_3$] units synthesised by Angurell *et al*.[3]

To synthesize these bimetallic ruthenium–rhenium dendrimers, the chloride ligands attached to the ruthenium atoms first needed to be abstracted with the use of AgOTf. Only then was the rhenium compound coordinated to the ruthenium metallodendrimer.

Leclaire *et al* [4,5] studied the complexation ability of their previously reported octasubstituted metal-free phthalocyanine-cored dendrimer, with phosphorus-containing dendritic branches. They decided to study the complexation of copper(II) and cobalt(II) to the dendritic core (Scheme 4.1) since these metals are very rarely incorporated into the core of phthalocyanine-containing dendrimers. The respective metals were successfully coordinated to the generation 1 dendrimers. Thereafter, coordination of both metals using dendritic ligands up to the 8th generation was carried out successfully.

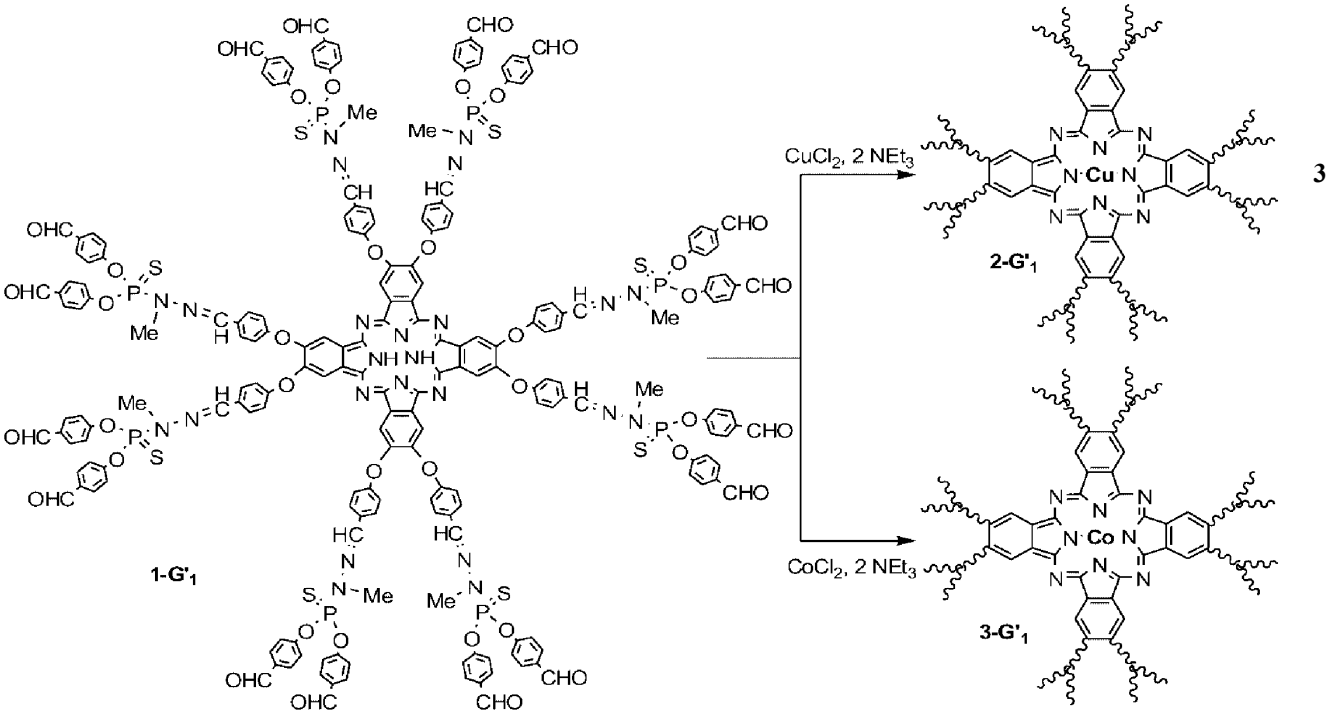

Scheme 4.1: Reaction pathway of phthalocyanine cored metallodendrimers synthesised by Leclaire *et al*.[5]

The complexation reaction is mainly monitored by the disappearance of the pyrrolic N-H band at 3250 cm^{-1} in the infra-red spectra since the absence of the N-H bond is due the complexation of the N-atoms of the phthalocyanine core to metal. These metallodendrimers were further characterized by proton, carbon and phosphorus NMR spectroscopy (only in the copper complexes), UV/Vis spectroscopy as well as elemental analysis. The UV/Vis spectra show that the higher in generation the metallodendrimer is, the more protected the core is. The shielding effect of the branches induces an increase of the intensity of the Q-band in the UV/Vis spectra, specific of phthalocyanines.

The above literature selection shows examples of metallodendrimers with metals positioned at the dendrimer periphery, at the dendrimer branching points, as well as in the dendritic core.

4.1.3 Objectives.

We have modified the synthesized cyclam-based dendrimers and the commercial DAB-based dendrimers **DL1-DL10**, as discussed in Chapter 3, for metal coordination at the dendrimer periphery. Our aim was therefore to synthesize nickel metallodendrimers by reacting the appropriate metal precursor with the periphery modified dendrimer ligands, **DL1-DL10** to form dendritic catalysts **C1-C10**. We chose to coordinate nickel to our modified dendrimers since complexes of nickel are reported to be good catalysts for a variety of catalytic processes, especially for oligomerization and polymerization reactions.[6-9]

4.2 Results and Discussion.

*4.2.1 Synthesis and characterization of the Generation 1-3 DAB salicylaldimine nickel metallodendrimer complexes, **C1-C3**.*

We have recently reported the synthesis of the G1 and G2 nickel salicylaldimine complexes, **C1** and **C2** (Fig 4.4) by reacting the salicylaldimine modified dendrimer ligands **DL1** and **DL2** with $Ni(OAc)_2.4H_2O$.[10]

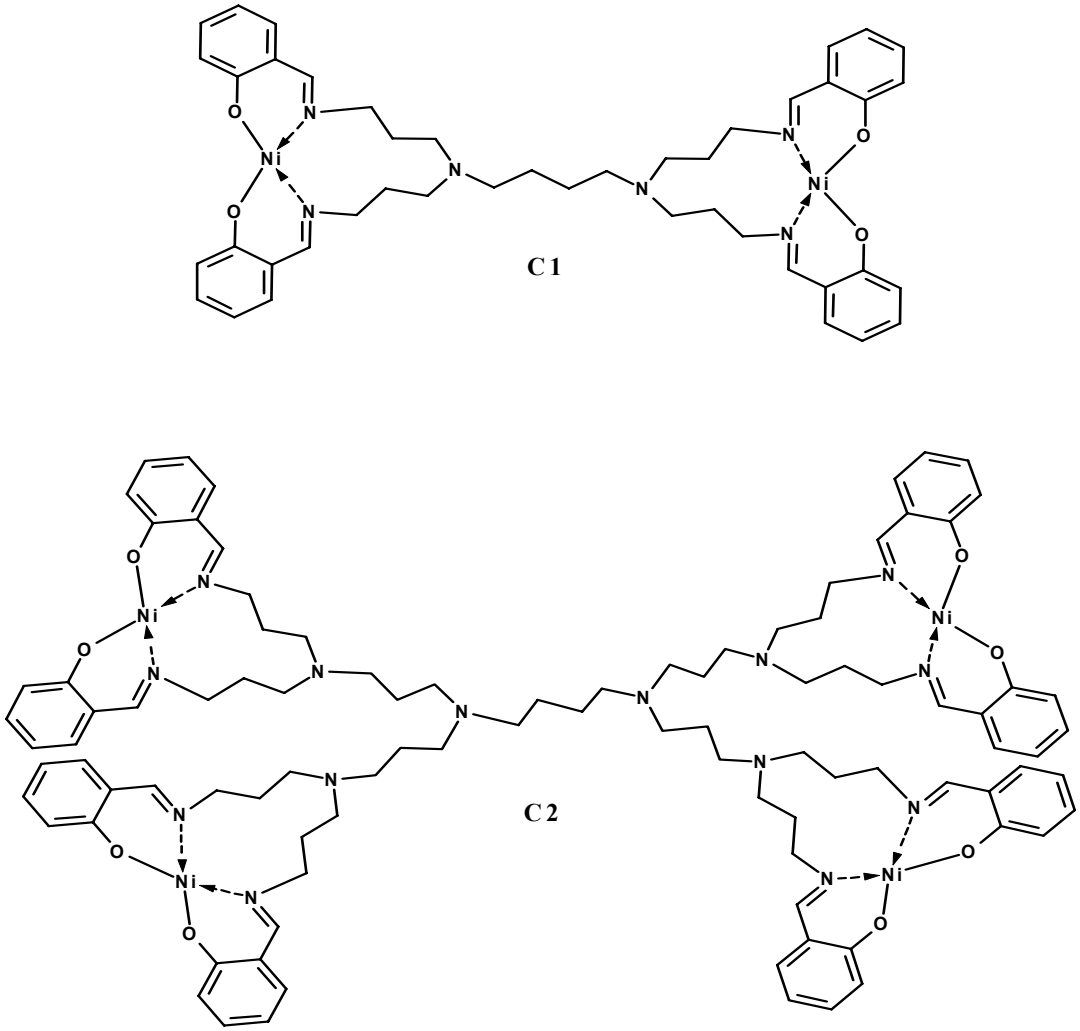

Figure 4.4: Structures of DAB G1 and G2 salicylaldimine nickel metallodendrimers, **C1** and **C2**.[10]

We have subsequently synthesized the generation 3 salicylaldimine nickel complex, **C3**, using the same synthetic procedure employed for **C1** and **C2**, using the generation 3 salicylaldimine ligand, **DL3** (Scheme 4.2).

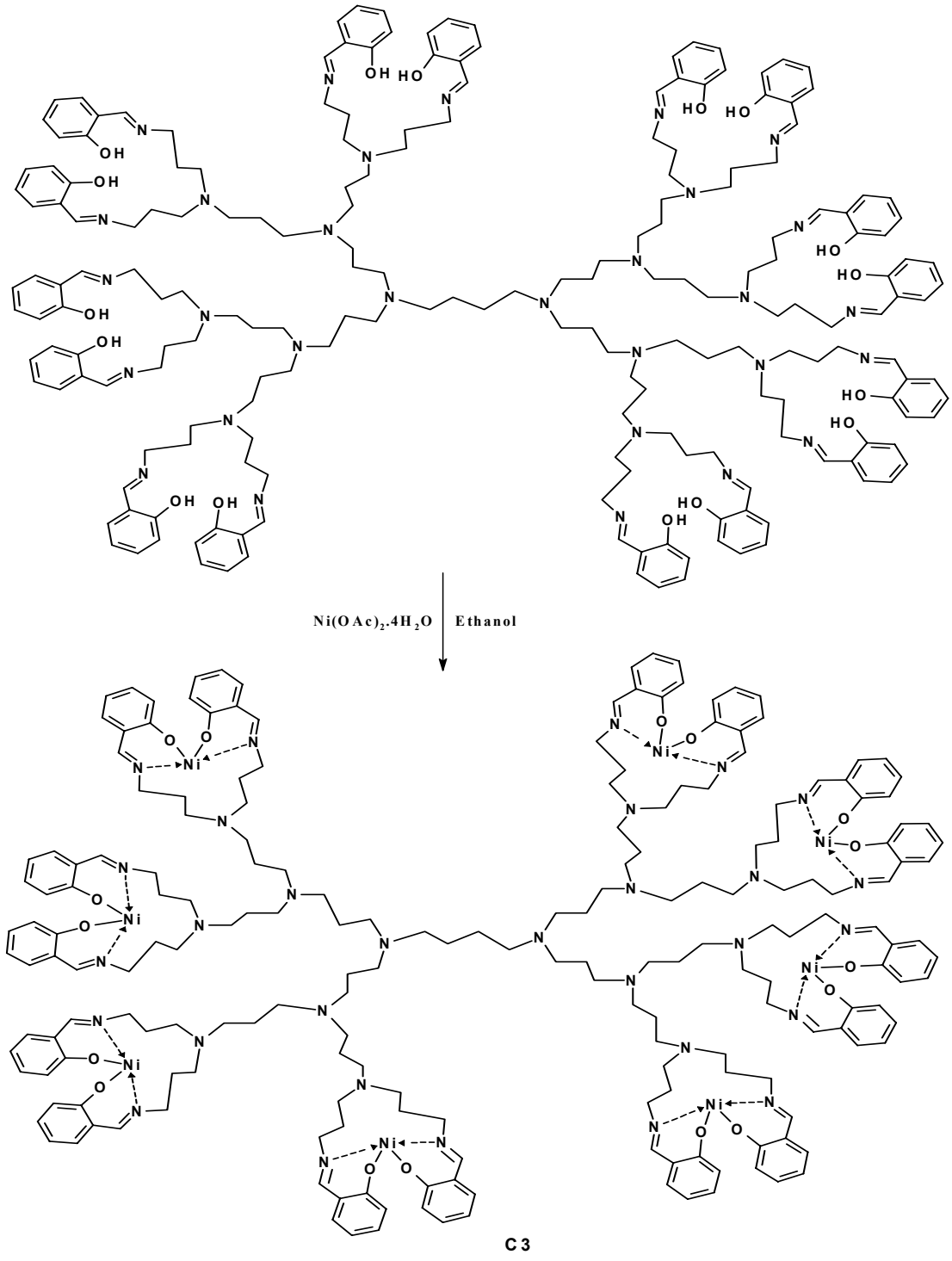

Scheme 4.2: Synthesis of the DAB-G3 salicylaldimine nickel metallodendrimer, **C3**.

The reaction time needed for all three generations was 24 hours and the reactions were conducted at a temperature of 97 ºC. A green precipitate formed in each case and the mixture was filtered to give a green solid. To ensure the removal of unreacted $Ni(OAc)_2$ from the product mixture, the product was extracted with dichloromethane, since $Ni(OAc)_2$ is insoluble in dichloromethane.

All three complexes were isolated as green solids, with yields ranging from 75-85 %. All complexes discussed in this chapter were characterized by FTIR spectroscopy, magnetic susceptibility measurements, mass spectrometry and elemental analysis. A summary of the spectral data for complexes **C1-C3** is shown in Table 4.1. From the IR spectra, we observe a shift in the í(C=N) band from around 1629 cm^{-1} to 1632 cm^{-1} and the í(C-O) stretching frequencies from around 1277 cm^{-1} to 1324 cm^{-1} when comparing the ligand and complex spectra.

Table 4.1: Spectral data for complexes **C1-C3**.

Ligand	**FTIR**[a]		**μ_{eff}**[b]	**[ESI$^+$]**[c]	**Melting Points**[d]
	í(C=N) cm^{-1}	í(C-O) cm^{-1}	(BM)	$[M]^+$	ºC
C1	1628	1324	0.97	848	292
C2	1632	1344	1.41	1833	221
C3	1629	1344	2.01	1269[e]	201

[a] Recorded in solid state on ZnSe crystal using ATR accessory. [b] Magnetic measurements were carried out on a magnetic susceptibility balance according to the Gouy method at 298 K. [c] Recorded in solution using an acetonitrile and water mixture. [d] Melting points recorded on a SMP3 melting point apparatus. [e] $[M+H]^{3+}$ at m/z = 1269.

These shifts are due to the coordination of the nitrogen and the oxygen atoms to the metal ion. These effects are also observed in the FTIR spectra of other salen-type nickel complexes reported in literature.[11-13]

All the complexes are paramagnetic thus no NMR analysis was done. The magnetic moments of these nickel salicylaldimine metallodendrimers range from 0.97 BM for the G1 complex, **C1**, to 2.01 BM for the G3 complex, **C3**. Tetrahedral nickel(II) complexes commonly have a magnetic moment of 3.1 - 4.0 BM as reported in literature.[14-15] This is due to the two unpaired electrons in the d^8 Ni(II) complex. Square planar Ni(II) complexes on the other hand have a magnetic moment of zero because these type of complexes have no unpaired electrons. A possible explanation as to why our Ni(II) complexes have low magnetic moments ranging from 1-2 BM could be due to the fact that: a) the existence of both square planar and tetrahedral geometries are present in our complexes, or b) intermolecular antiferromagnetic interactions between neighboring molecules exist.[16] The most probable reason as to why the BM values are lower than expected, is the antiferromagnetic interaction between the peripheral nickel ions of the complexes. Antiferromagnetic interactions between the nickel ions can align their magnetic moments antiparallel, causing a decrease in the overall magnetic susceptibility value. Ni(II) complexes are also known to exhibit single ion anisotropy, in which the m_s=1 sublevels are split away from the m_s=0 sublevel. This could also lead to a decrease in the magnetic susceptibility value. It has been reported that both antiferromagnetic exchange as well as single-ion effects can occur in the same compound, affecting the μ_{eff}.[17]

The ESI mass spectra for **C1** and **C2** show peaks that correspond to $[M+H]^+$ at m/z = 848 and m/z = 1833 respectively. The mass spectrum for **C3** shows a triply charged peak molecular ion peak at m/z = 1269. It also shows a quadruply charged molecular ion

peak at m/z = 952. In addition peaks at m/z = 761 and m/z = 635 can be assigned to ions carrying a +5 and +6 charge respectively.

The melting points for **C1-C3**, decrease when going from the G1 complex to the G3 complex, indicating that the G3 complex, **C3**, is the least thermally stable and the G1 complex, **C1**, the most thermally stable. This could be due to the high structural flexibility of the G3 compound as compared to the rigid structure of the G1 compound. This was previously noted when discussing the computational results for the dendrimer ligands (Chapter 3).

The TGA plot for complex, **C3** (over the temperature range 25-600 ºC) is shown in Fig 4.5. There's a small weight loss (ca. 5 wt %) below 110 ºC which is due to the loss of 8 molecules of associated waters of hydration.

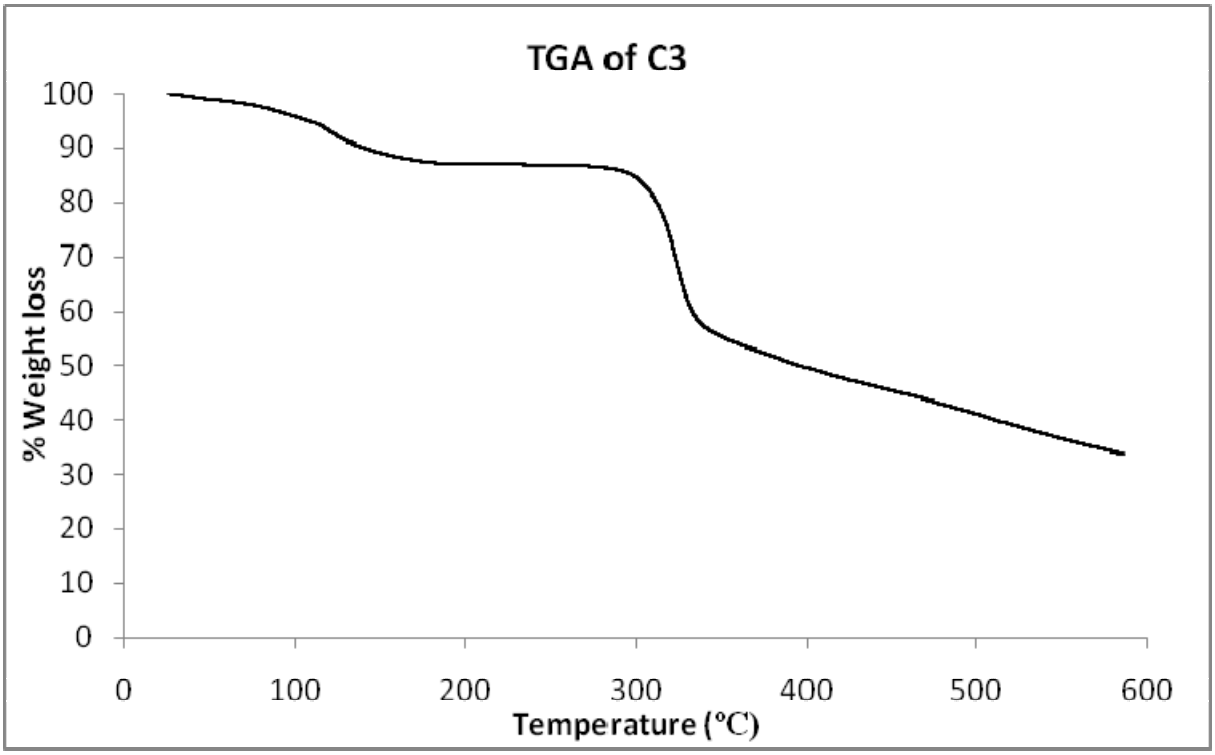

Figure 4.5: Thermal gravimetrical analysis (TGA) of the G1-G3 DAB nickel salicylaldimine metallodendrimer complex, **C3**.

A further weight loss (ca. 9 wt %) is observed up to 200 ºC which is due to 4 molecules of encapsulated dichloromethane. The complex remains stable up to 290 ºC, after which a sudden weight loss (ca. 36 wt %) is observed, and this is due to the loss of the sixteen phenolic rings of the complex. Similar observations were made by Van Wyk.[18] Starting at 320 ºC, a gradual weightloss (due to the DAB dendrimer framework) is observed, ultimately leaving NiO as the remaining residue. The TGA plots for **C1** and **C2** follows a similar decomposition trend as the TGA plot for **C3**, with the exception of **C1** which shows no dichloromethane solvent loss. These TGA plots are consistent with those reported for analogous salen complexes. [19,20]

The microanalysis results for complexes, **C1-C3**, are shown in Table 4.2. The results reported for **C2** and **C3** include dichloromethane molecules, which are trapped within the dendritic cavities. This has been confirmed by TGA analysis.

Table 4.2: Microanalysis data of complexes **C1-C3**.

Ligand	% Calculated			% Found		
	C	H	N	C	H	N
C1	62.18	6.08	9.74	62.18	6.15	9.90
C2	58.77	6.24	9.79	58.24	6.25	9.48[a]
C3	59.10	6.42	10.14	59.84	7.73	9.41[b]

[a]Inclusion of 2 mol CH_2Cl_2. [b]Inclusion of 4 mol CH_2Cl_2.

The UV/Vis spectra of the DAB G1 salicylaldimine ligand, **DL1**, and the DAB G1 salicylaldimine nickel complex, **C1**, in a dichloromethane solution are shown in Fig. 4.6.

The G2 and G3 analogues of these ligands (**DL2** and **DL3**) and complexes (**C2** and **C3**) gave similar UV/Vis spectra, hence only the G1 spectra are discussed.

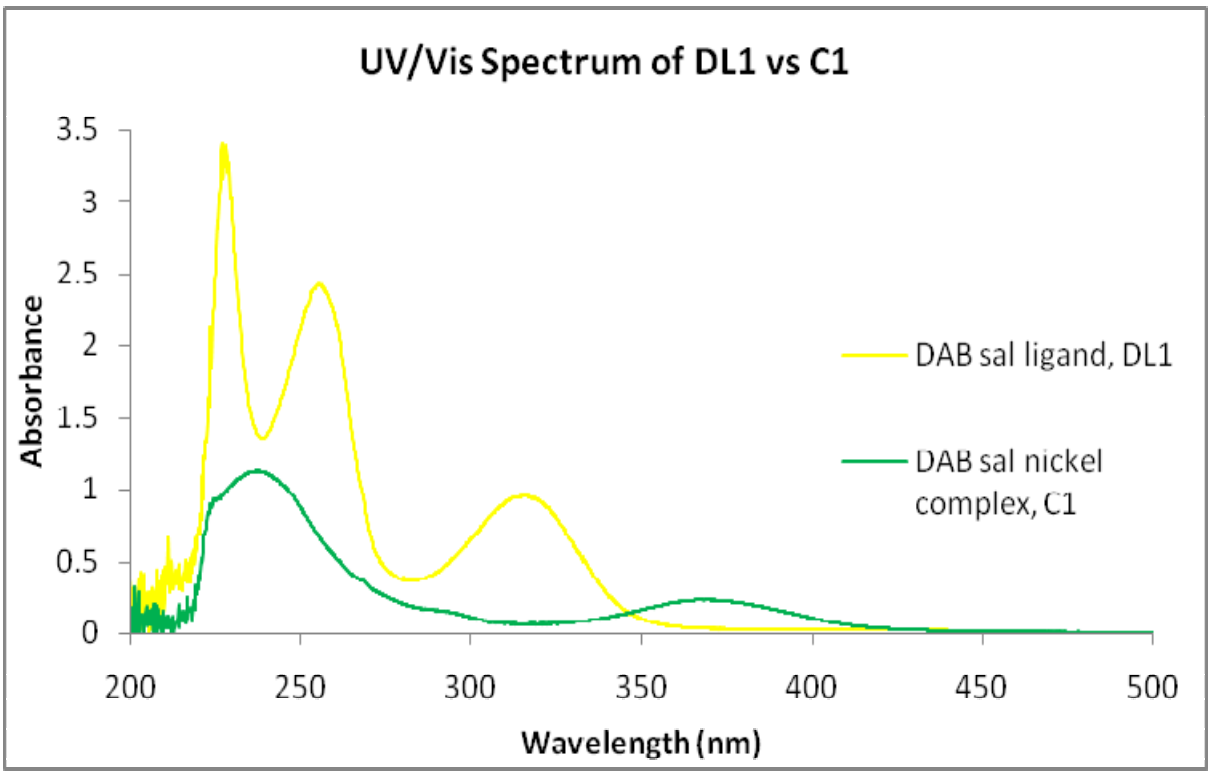

Figure 4.6: UV/Vis spectra of the G1 DAB salicylaldimine ligand, **DL1**, and nickel metallodendrimer complex, **C1**.

The electronic spectra of the salicylaldimine ligands in the solution phase show three absorption bands at 330, 260 and 225 nm, involving ð→ð* transitions. Similar absorption bands were observed by Fan *et al* [21] who reported the synthesis of salen-type Schiff base ligands. The UV–Vis spectra of the salicylaldimine Ni complexes show two bands at 380 nm and 240 nm which is assigned to the transition of n→ð* of the imine group corresponding to the metal complex and the metal-to-ligand charge transfer (MLCT) transition, respectively. The latter is very weak but resembles what is seen for other salen complexes. [11,22]

*4.2.2 Synthesis and characterization of the Generation 1-3 DAB iminopyridyl nickel metallodendrimer complexes, **C4-C6**.*

The G1-G3 DAB iminopyridyl nickel complexes, **C4-C6**, (Fig 4.7) were synthesized by reacting the iminopyridyl modified dendritic ligands, **DL4-DL6**, with Ni(DME)Br_2 as a metal source (Scheme 4.3).

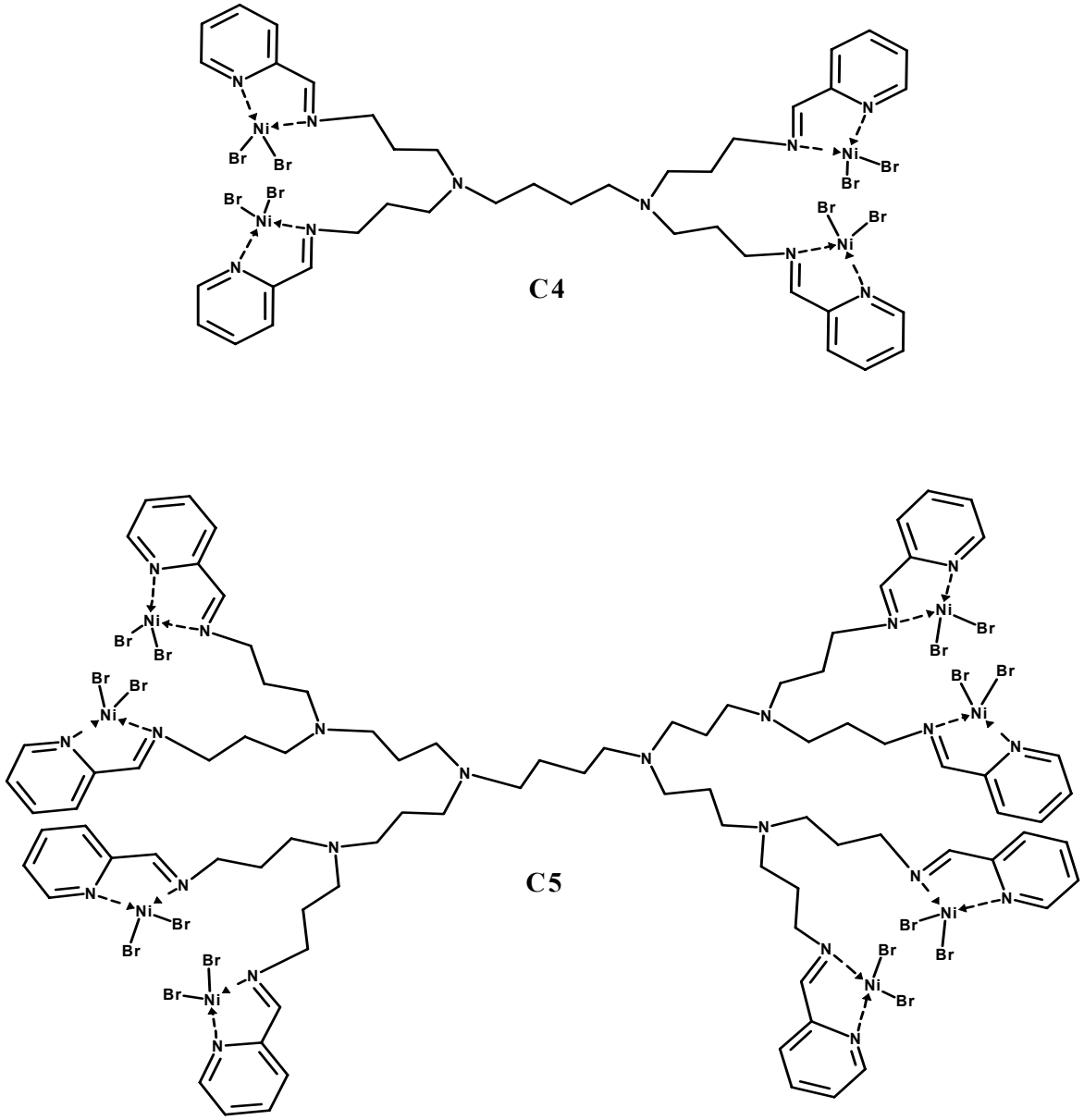

Figure 4.7: Structures of DAB G1 and G2 iminopyridyl nickel metallodendrimers, **C4** and **C5**.

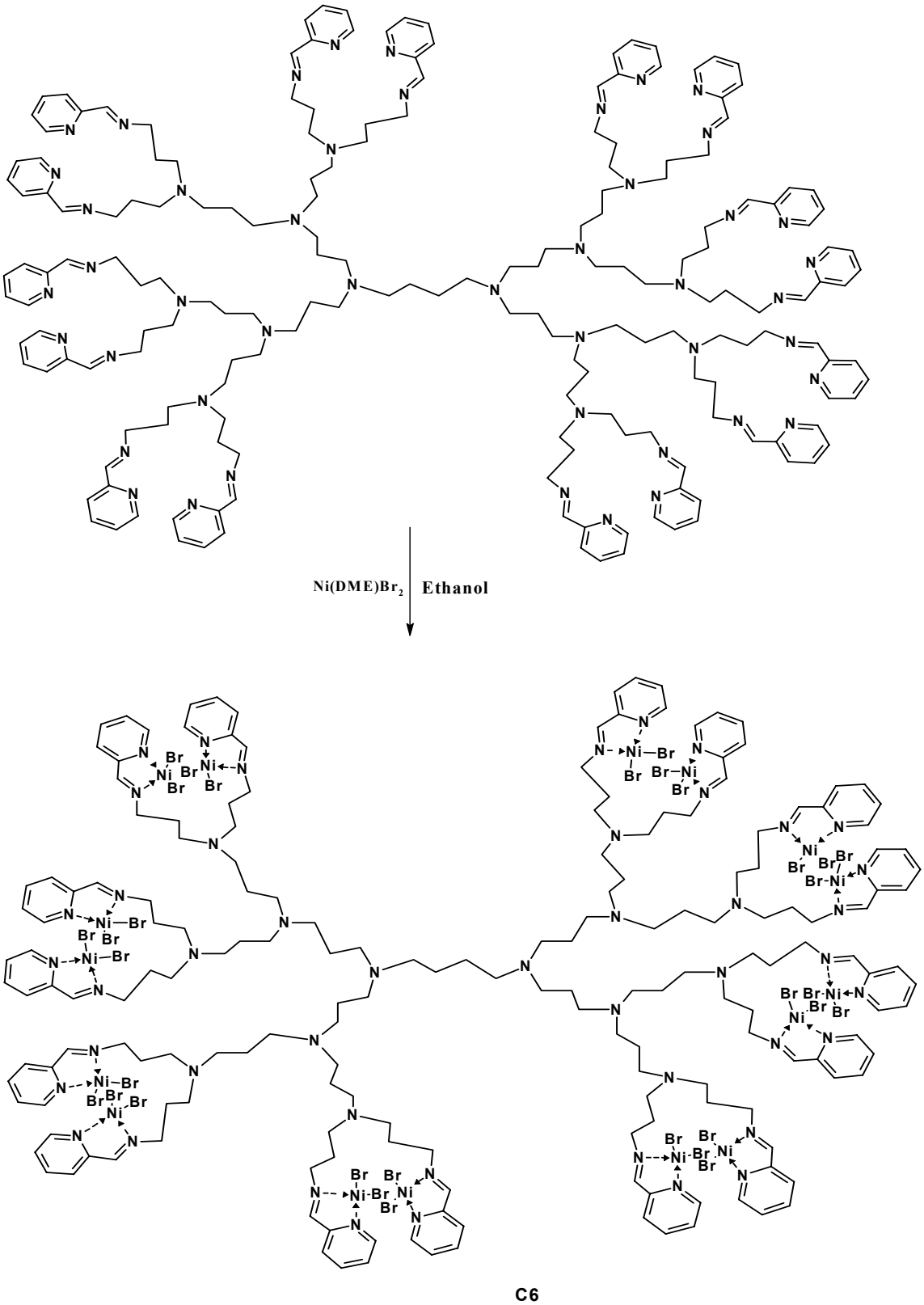

Scheme 4.3: Synthesis of the DAB-G3 iminopyridyl nickel metallodendrimer, **C6.**

These iminopyridyl nickel metallodendrimers are novel complexes. The reaction conditions were similar to those used for synthesis of **C1-C3**, with a reaction time of 24 hours, at a temperature of 97 ºC being the optimal conditions. The reaction of ligands, **DL4-DL6** with $Ni(DME)Br_2$, resulted in brown solids being isolated as products with yields ranging from 78-85 %. Attempts to grow single crystals were unsuccessful which was not unusual since there are very few, if any, reports of crystal structures of metallodendrimers in literature.

The iminopyridyl complexes are all hygroscopic and consequently have to be stored under nitrogen atmosphere. This is in contrast to the salicylaldimine complexes which are quite air stable, as well as stable in solution. Another major difference between the salicylaldimine complexes **C1-C3** and the iminopyridyl complexes **C4-C6**, is that the latter complexes have double the amount of nickel centres than the former for each corresponding dendrimer generation. Thus the G1 iminopyridyl complex, **C4**, has four nickel centres whereas the G1 salicylaldimine complex, **C1**, has only 2 nickel centres.

The characterization data for complexes **C4-C6** are shown in Table 4.3. From the IR spectra, we observe a shift in the í(C=N) stretching frequency from around 1647-1648 cm^{-1} to 1639-1641 cm^{-1} when comparing the ligand and complex spectra. The pyridine ring í(C=N) stretching frequency shifted from around 1586-1587 cm^{-1} to around 1596-1598 cm^{-1} for complexes, **C4-C6**. These shifts are due to the effect of the ligand coordinating to the nickel. Similar observations were reported by Smith *et al* [23] and Massa *et al* [24] who synthesised analogous iminopyridyl complexes.

Since the iminopyridyl complexes were brown in colour, it was expected that these compounds could possibly be square planar in structure. It is known that tetra-coordinate

square planar complexes of Ni^{2+} are normally brown-orange in colour. Square planar d^8 complexes are diamagnetic and usually suitable for NMR analysis. However, NMR analysis proved the complexes to possibly be paramagnetic, since spectra with broad unresolved peaks were observed.

Table 4.3: Characterization data for complexes, **C4-C6**.

Ligand	FTIR[a] (cm^{-1})			μ_{eff} [b] (BM)	[ESI$^+$][c] (m/z)	Melting Points[d] (°C)
	í(C=N)	í(C=N) (*pyr*)	í(C=C) (*pyr*)			
C4	1639	1596	1567	1.20	1592 [e]	249
C5	1640	1597	1568	1.72	814 [f]	231
C6	1642	1598	1571	2.48	1326 [g]	204

[a] Recorded in solid state on ZnSe crystal using ATR accessory. [b] Magnetic measurements were carried out on a magnetic susceptibility balance according to the Gouy method at 298 K.[c] Recorded in solution using an acetonitrile and water mixture. [d] Melting points recorded on a SMP3 melting point apparatus. [e]$[M+2Na]^+$ at m/z = 1592. [f]$[M+Na]^{4+}$ at m/z = 814. [g]$[M+Na]^{5+}$ at m/z = 1326.

The magnetic moments of these nickel iminopyridyl metallodendrimers also gives information regarding the geometry of the complexes. The magnetic moments of the iminopyridyl complexes are in a similar range as that of the salicylaldimine complexes, ranging from 1.20 BM for the G1 complex, **C4**, to 2.48 BM for the G3 complex, **C6**. It is believed that these complexes therefore have a tetrahedral geometry, although the magnetic moments of our complexes are lower than what is expected for conventional tetrahedral

nickel complexes. Tetrahedral iminopyridyl complexes usually have magnetic moments ranging from 3.0-3.2 BM. [25] As previously discussed, the low magnetic moment obtained for these complexes could possibly be attributed to antiferromagnetic interactions of the metal ions.

The melting points for **C4-C6** also decrease when going from the G1 complex to the G3 complex, again indicating that the G3 complex, **C6**, is the least thermally stable and the G1 complex, **C4**, the most thermally stable. However, the iminopyridyl complexes are even less thermally stable than the salicylaldimine complexes, **C1-C3**. The iminopyridyl complexes are more congested at the dendrimer periphery, which could influence the stability of the structure.

The ESI mass spectra for **C4** shows a molecular ion peak at m/z = 1592 which can be assigned to an adduct of the parent ion with two Na ions. The fragmentation pathway for **C1** is shown in Scheme 4.4. One Ni and three bromines are lost to give fragment (**a**) at m/z = 1250. Fragment (**b**) is due to the loss of the second Ni atom and two bromines at m/z = 1030. Fragment (**c**) results from the loss of all the NiBr's as well as the loss of a pyridyl unit and occurs at m/z = 584. This is followed by the sequential loss of the alkyl branches and the remaining pyridyl units. The mass spectra of the G2 and G3 complexes, **C5** and **C6**, show multiply charged ions. This is not unusual since high molecular weight complexes commonly tend to form multiply charged ions. The spectrum for **C5** shows a quadruply charged molecular ion peak as a Na^+ adduct at m/z = 814. The MS for **C6** shows a peak at m/z = 1326 which can be assigned to ions carrying a +5 charge as a Na^+ adduct.

Due to the highly hygroscopic nature of the iminopyridyl complexes, we were unable to obtain satisfactory microanalysis results.

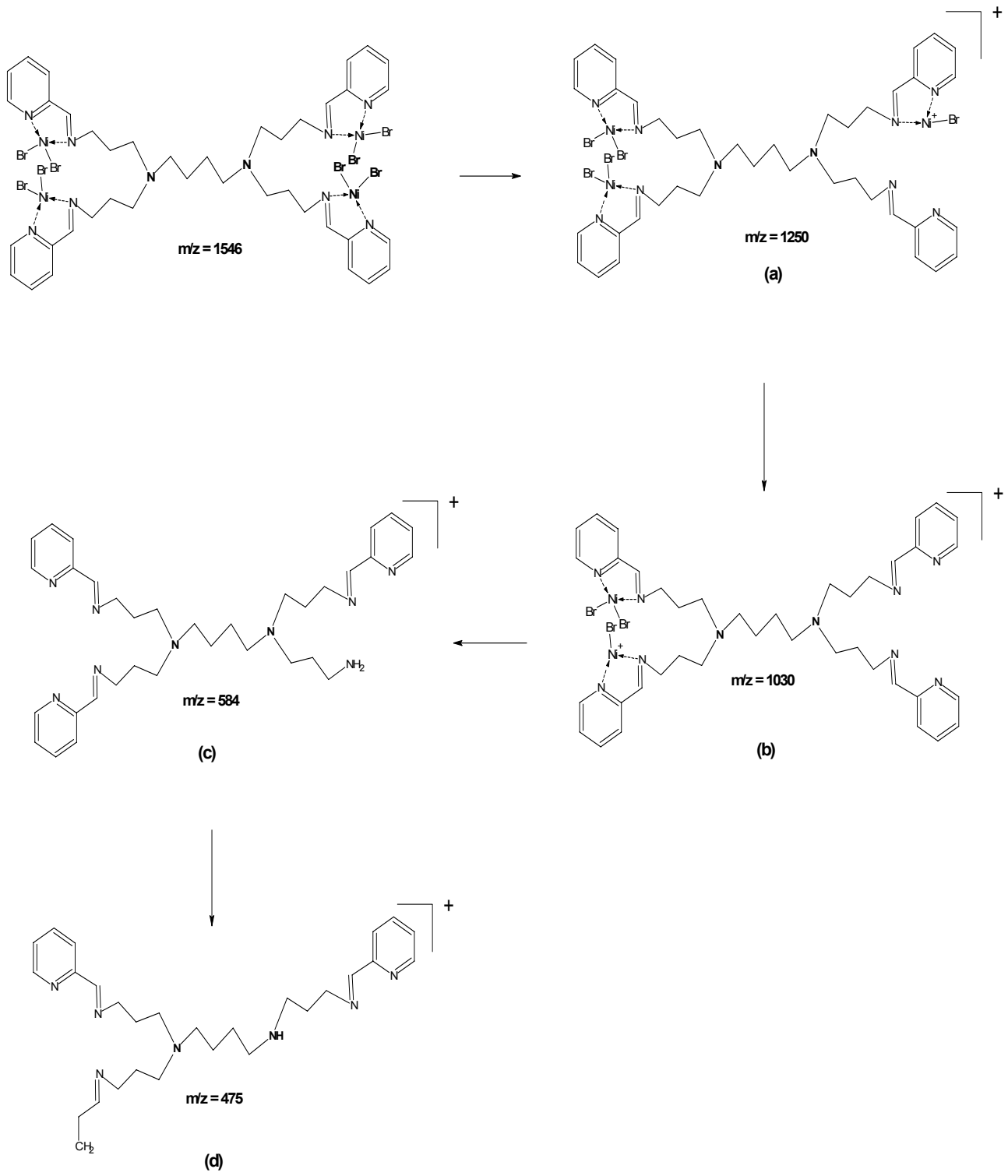

Scheme 4.4: ESI-MS fragmentation pattern for **C4**.

TGA analysis was done on the G1-G3 DAB iminopyridyl nickel complexes. The TGA plots for all three complexes follow a similar decomposition pattern. The TGA plot of **C4** is shown in Fig 4.8. There's an immediate weight loss (ca. 10 wt %) below 110 ºC which is due to the loss of associated waters of hydration. This is not unexpected since these complexes proved to be rather hygroscopic. The complex remains stable up to 300 ºC, after which a steady weight loss (ca. 40 wt %) up to 450 ºC is observed, and this is due to the loss of the eight bromide ions from the nickel centres in the generation 1 complex. Starting at 425 ºC, a very steady weight loss is observed assigned to the loss of the pyridine rings and the rest of the dendrimer framework leaving nickel oxide as the final residue.

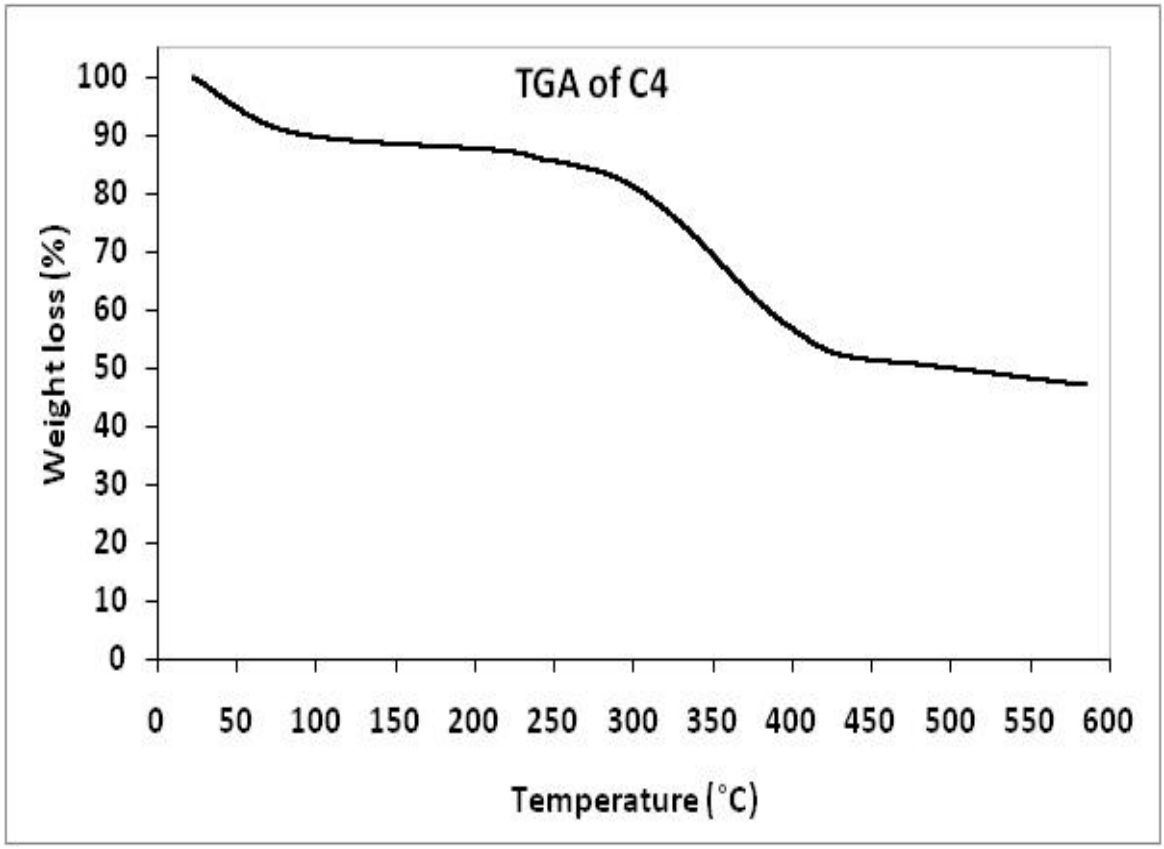

Figure 4.8: Thermal gravimetrical analysis (TGA) of the G1-G3 DAB nickel iminopyridyl metallodendrimer complexes, **C4-C6**.

The UV/Vis spectra of the DAB G1 iminopyridyl ligand, **DL4**, and the DAB G1 iminopyridyl nickelbromide complex, **C4**, are shown in Fig. 4.9. The G2 and G3 analogues of these ligands (**DL5** and **DL6**) and complexes (**C5** and **C6**) gave similar UV/Vis spectra, hence only the G1 spectrum is discussed.

The electronic spectra of the iminopyridyl ligands in DMSO solution show one broad absorption band from 275-250 nm, involving a ð →ð* transition for the C=N chromophore. Roy *et al* [26] and Herrick *et al* [27] reported similar bands for their imine ligands. The UV–Vis spectra of the iminopyridyl nickel complexes show two bands at 300 nm and 250 nm, which are assigned to the metal-to-ligand charge transfer (MLCT) transition of the imine group corresponding to the metal complex and a shift in the ð→ð* transition for the C=N chromophore, respectively.[28]

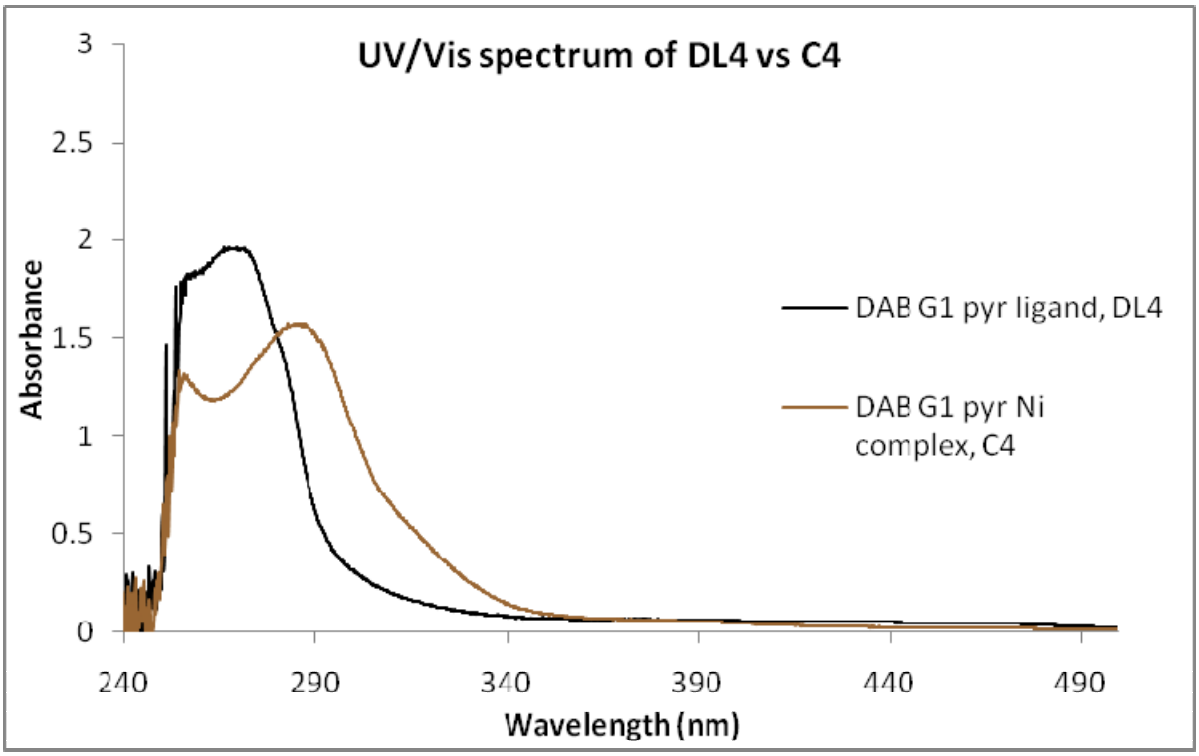

Figure 4.9: UV/Vis spectra of the G1 DAB iminopyridyl ligand, **DL4**, and nickel metallodendrimer complex,**C4**.

*4.2.3 Synthesis and characterization of the Generation 1 cyclam-propyl Schiff base nickel complexes, **C7-C8**.*

The G1 Cyclam-propyl salicylaldimine dendrimer, **DL7**, was reacted with $Ni(OAc)_2.4H_2O$ under the same reaction conditions to those used for the synthesis of **C1-C3**, to give the cyclam-based salicylaldimine nickel complex **C7** as shown in Fig 4.10.

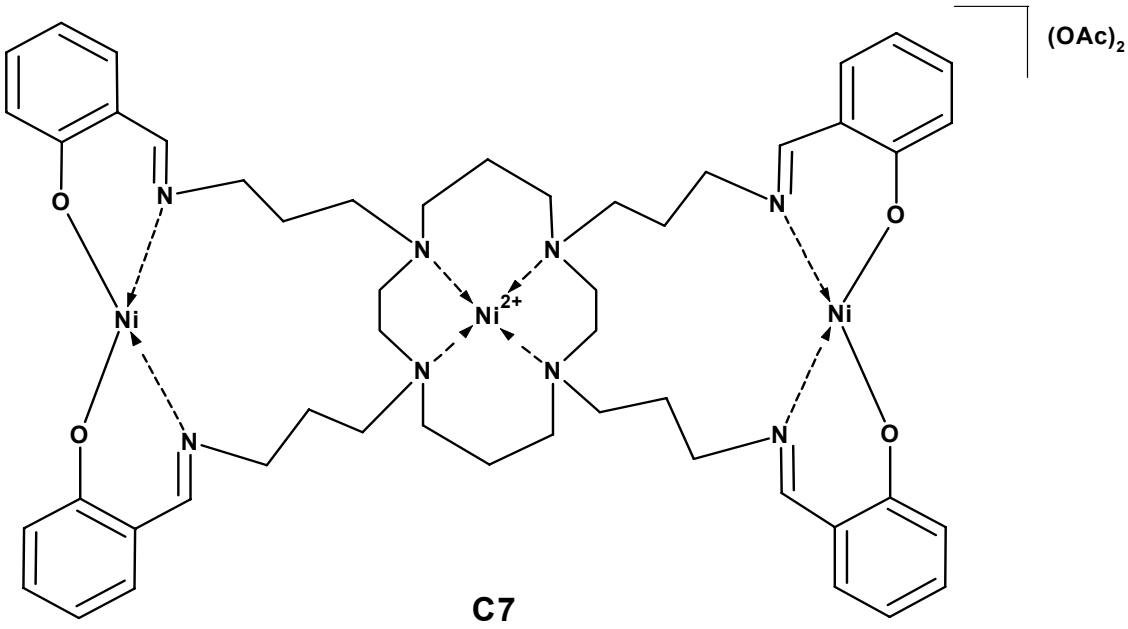

C7

Figure 4.10: The G1 cyclam-based salicylaldimine modified nickel metallodendrimer, **C7**.

The synthesised G1 cyclam-based salicylaldimine metallodendrimer, **C7**, is similar to the G1 DAB-based salicylaldimine metallodendrimer complex, **C1**, with 2 metal centres on the dendrimer periphery. However, the cyclam metallodendrimers also have an extra nickel centre coordinated to the cyclam core. This was confirmed by ICP-OES, which gave a nickel

content corresponding to three nickel centres per mole of ligand. The UV/Vis spectrum also confirms this, as discussed later. The complex was isolated as a lime green solid with a yield of 63 %.

The spectral data for complex **C7** is shown in Table 4.4. The most significant bands monitored by FTIR is the shift in the í(C=N) and the í(C-O) stretching frequencies, which indicates that metal coordination between the nickel and the dendrimer ligand had occurred. The í(C=N) band shifted from 1662 to 1623 cm^{-1} and the í(C-O) band from 1276 to 1319 cm^{-1}.

Table 4.4: Spectral data of the G1 cyclam based dendrimer salicylaldimine complex **C7**.

Ligand	FTIR[a]		μ_{eff}[b]	[ESI$^+$] [c]
	í(C=N) cm^{-1}	í(C-O) cm^{-1}	(B.M.)	$[M+H]^+$
C7	1623	1319	1.05	1057[d]

[a] Recorded in solid state on ZnSe crystal using ATR accessory. [b] Magnetic measurements were carried out on a magnetic susceptibility balance according to the Gouy method at 298 K. [c] Recorded in solution using an acetonitrile and water mixture. [d] $[M+K]^+$ at m/z = 1057.

A magnetic moment measurement was done on a representative cyclam sample, **C7**, and was found to be 1.05 BM. The magnetic moment of **C7** is slightly higher than its G1 DAB analogue, **C1**, which has a magnetic moment of 0.97 BM. A higher magnetic moment is expected for these salicylaldimine nickel(II) complexes, however possible antiferromagnetic interactions between metal ions could lead to a lower magnetic moment.

The ESI mass spectrum for **C7** shows a high mass peak at m/z=1057 which can be assigned to a potassium adduct of the parent ion. The fragmentation pattern for **C7** is shown in Scheme 4.5. Fragment (**a**) at m/z = 845 is due to the loss of the three Ni atoms of the complex. This is followed by the loss of a salicylaldimine unit and a methylene group to give fragment (**b**) at m/z = 712. Fragment (**c**) is due to the loss of the ethyl group as well as the salicylaldimine group of the second branch at m/z = 579. This is followed by the sequential loss of the alkyl chains and the remaining salicylaldimine groups, to ultimately yield fragment (**d**).

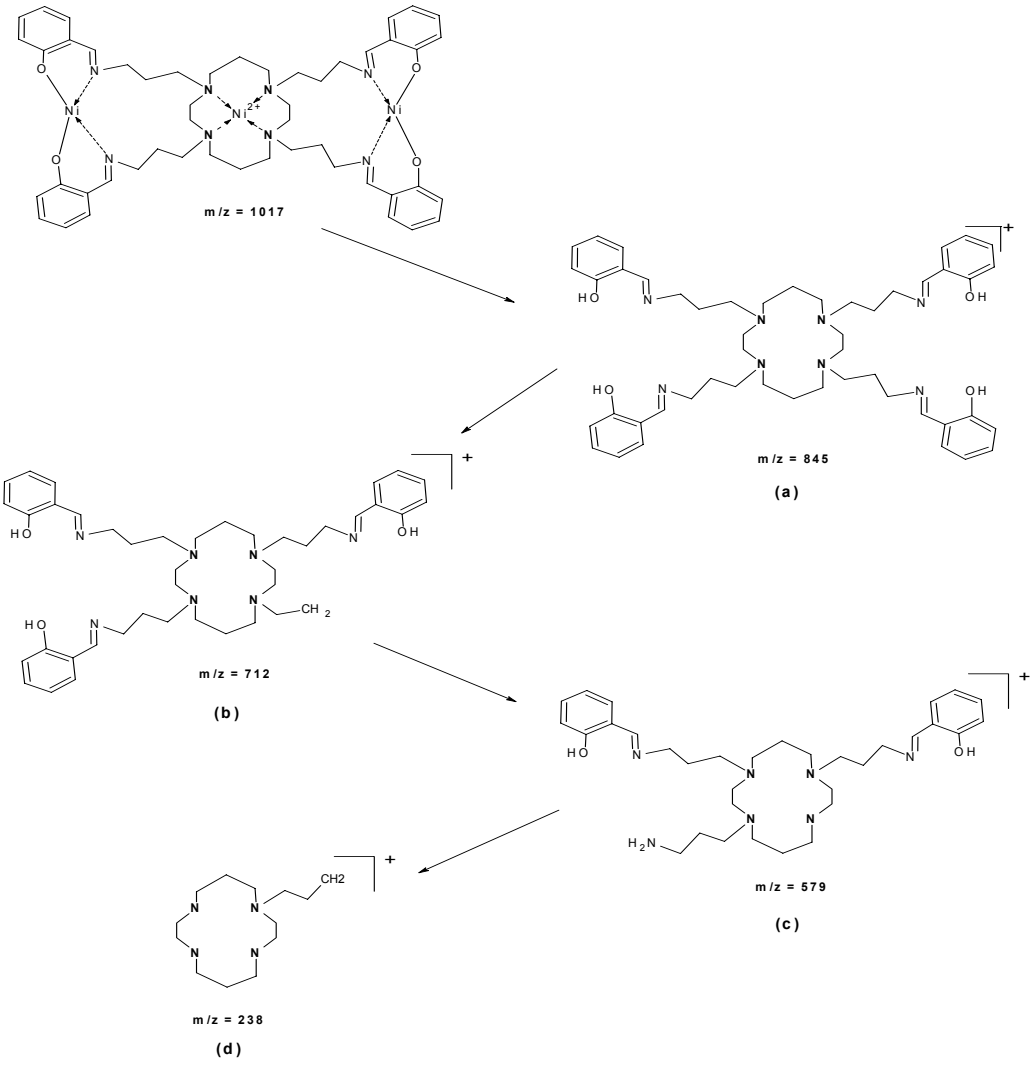

Scheme 4.5: ESI-MS fragmentation pattern for **C7**.

The UV/Vis spectra of ligand **DL7** and complex **C7** are shown in Fig 4.11. The electronic spectrum of the G1 cyclam ligand, **DL7**, in the solution phase is similar to the DAB salicylaldimine ligand spectra, showing three absorption bands. Two of the bands viz at 260 nm and 225 nm are exactly the same for both the DAB salicylaldimine and the cyclam salicylaldimine ligands. The third band however differs and occurs at 330 nm for the DAB ligand spectrum while in the cyclam ligand spectrum it occurs at 320 nm. These bands are assigned to ð→ð* transitions of the aromatic units to the ligands.

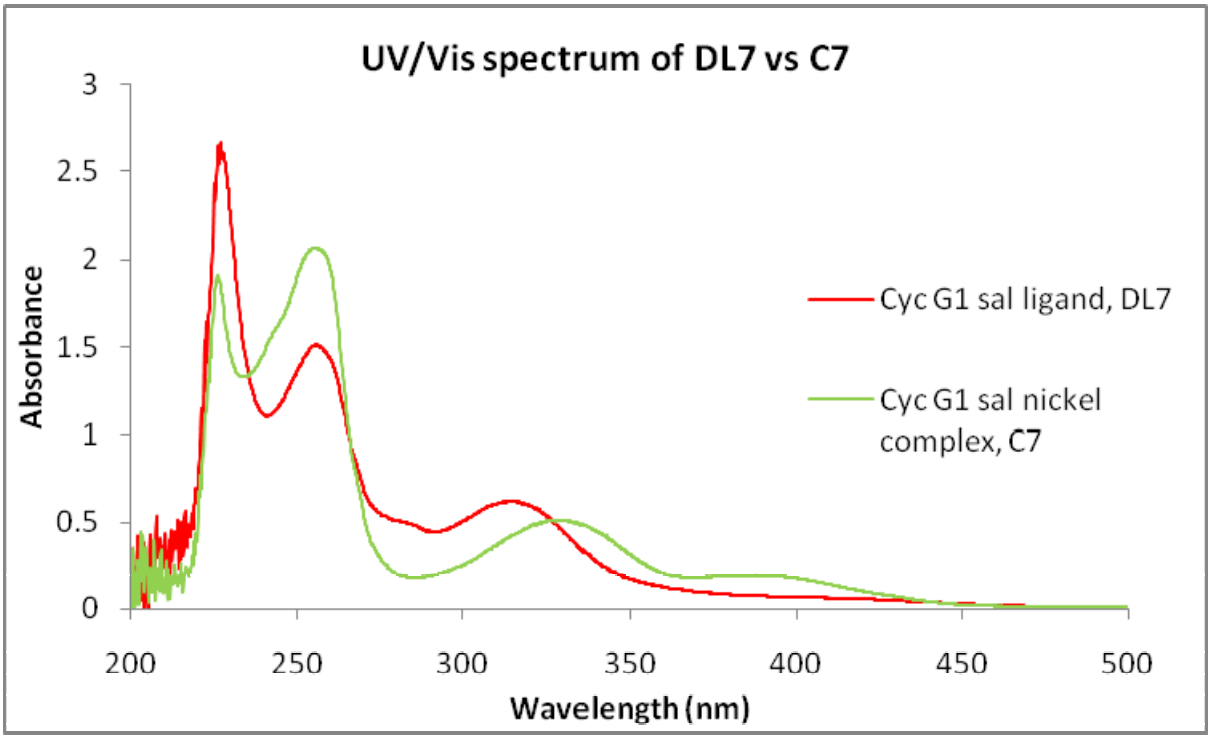

Figure 4.11: UV/Vis spectra of the G1 Cyclam salicylaldimine ligand, **DL7**, and nickel metallodendrimer complex, **C7**.

The electronic spectrum of the G1 cyclam complex, **C7**, in the solution phase shows four absorption bands. Two bands are still observed at 260 nm and 225 nm, assigned to ð→ð* transitions. On complexation of the peripheral oxygen and nitrogen atoms to the metal ion,

the UV–Vis spectrum of the cyclam based salicylaldimine nickel complex shows a shift in the third band from 320 nm (ligand spectrum) to 340 nm (complex spectrum) which is assigned to the metal-to-ligand charge transfer (MLCT) transition. The fourth band at 400 nm is assigned to a n→ð* transition due to the Ni-N bond, confirming the presence of three metal centres, two on the periphery as expected, as well as one Ni atom coordinated to the N-atoms in the cyclam core. Ni coordinated to an unsubstituted cyclam core usually absorbs at around 445 nm as reported by Evers *et al.* [29] When comparing the UV-Vis spectrum of the G1 DAB salicylaldimine nickel complex, **C1**, and the G1 cyclam salicylaldimine nickel complex, **C7**, we observe that the latter has an extra band in its spectrum at 400 nm, and this is thought to be due to the complexation of the nickel to the cyclam core.

The G1 cyclam-propyl iminopyridyl dendrimer, **DL8**, was also reacted with Ni(DME)Br_2 under similar reaction conditions used for the synthesis of **C4-C6**, to give the cyclam-based iminopyridyl nickel complex **C8** as shown in Fig 4.12. This complex was isolated as a brown solid with a yield of 68 %.

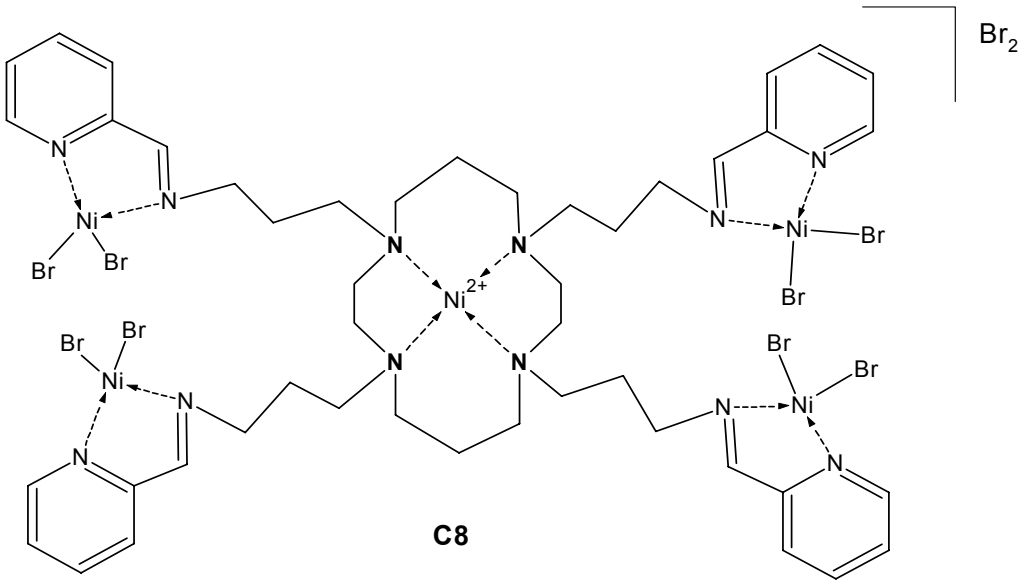

Figure 4.12: The G1 cyclam-based iminopyridyl modified nickel metallodendrimer, **C8**.

The spectral data for complex, **C8** is shown in Table 4.5. The aliphatic í(C=N) band shifted from 1648 to 1618 cm^{-1} and the í(C=N) stretching frequency of the pyridine rings shifted from 1586 to 1593 cm^{-1}. Complex, **C8**, is paramagnetic thus no NMR analysis was performed. The ESI mass spectrum for **C8** shows a quadruply charged ion peak at m/z = 435 which can be assigned to a sodium adduct of the molecular ion.

Table 4.5: Spectral data for the G1 cyclam based dendrimer iminopyridyl complex **C8**.

Ligand	**FTIR[a] (cm^{-1})**			**ESI-MS[b] (m/z)**
	í(C=N)	í(C=N) (*pyr*)	í(C=C) (*pyr*)	$[M]^+$
C8	1618	1593	1569	435[c]

[a] Recorded in solid state on ZnSe crystal using ATR accessory. [b] Recorded in solution using an acetonitrile and water mixture. [c] $[M+Na]^{4+}$ at m/z = 435.

These cyclam-based complexes have similar properties to the DAB based complexes in that the cyclam salicylaldimine complex, **C7**, is air stable which is similar to the DAB salicylaldimine complexes and the cyclam iminopyridyl complex, **C8**, is hygroscopic which is similar to the DAB iminopyridyl complexes.

The microanalysis results for complex **C7** is shown in Table 4.6. However, as mentioned before, we have experienced a common error with the %N (**C7**) throughout our microanalysis characterization. Suitable microanalysis for **C8** could not be obtained due to the hygroscopic nature of the complex, even though precautions were taken with preparing samples for analysis.

Table 4.6: Microanalyses data for complex **C7**.

Ligand	% Calculated			% Found		
	C	H	N	C	H	N
C7	50.05	5.55	8.81	50.19	5.58	6.16[a]

[a]Inclusion of 3 mol CH_2Cl_2.

Attempts to complex the cyclam-based benzyl ligands, **DL9** and **DL10**, to Ni salts proved unsuccessful. Products containing high levels of impurities were obtained and several attempts to purify these complexes were not entirely successful. This was thus abandoned for now.

4.3 Molecular Modelling calculations of metallodendrimer complex, C1.

All computational results in this study were calculated using the DMol^3 DFT (Density Functional Theory) code as discussed in the previous chapter. The energy values that are given in the results are the electronic energies at 0 K.

The following aspects were investigated with the use of molecular modeling:

- The possible coordination site for the Ni to the first generation dendrimer ligand, **DL1**.
- The optimized structure of the first generation salicylaldimine nickel complex, **C1**.

*4.3.1 The possible coordination site for the Ni in the first generation dendrimer ligand, **DL1**.*

It was thought that for the generation 1 salicylaldimine ligand, **DL1**, to interact with a metal salt such as $Ni(OAc)_2$, the H-atom from the OH-group of the salicylaldimine ligand (Fig 4.13) first needs to dissociate. Therefore the energy values for H-dissociation were calculated and the results are shown in Table 4.7.

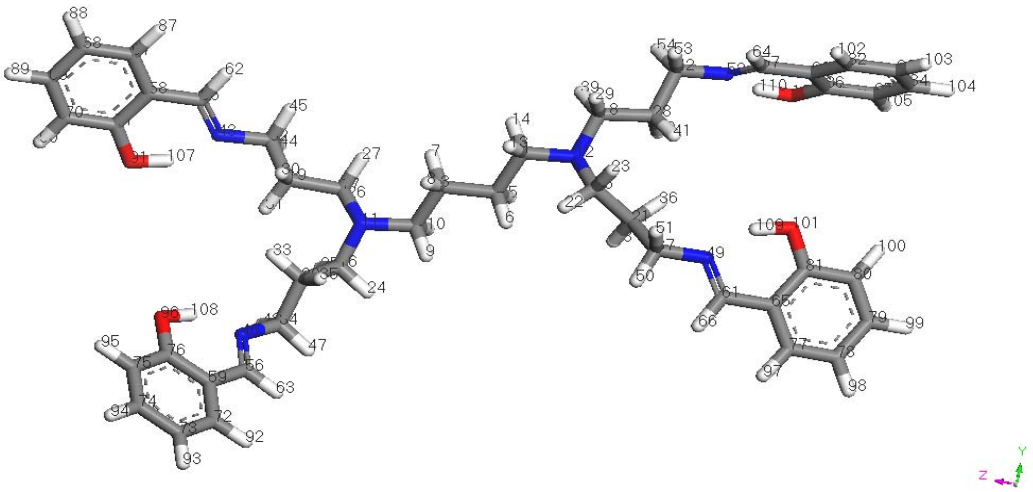

Figure 4.13 Labelled structure for energy calculations.

Table 4.7: Energy calculation for dissociation of H-atom from dendrimer ligand, **DL1**.

H-atom	Dissociation Energy (kJ/mol)
H107	**1497.55**
H108	**1500.60**
H109	**1453.43**
H110	**1501.39**

The positive energy values for the dissociation energy show that the O-H bond is quite stable and therefore it seems that the H-atom will not readily dissociate from the ligand before coordination to the nickel centre of the $Ni(OAc)_2$. Instead, the $Ni(OAc)_2$ first interacts with the OH-group of the salicylaldimine ligand, followed by the expulsion of HOAc as a neutral molecule. The orientation and the placement of the LUMO of the **DL1** (Chapter 3) as well as the HOMO of $Ni(OAc)_2$ (Fig 4.14) supports this.

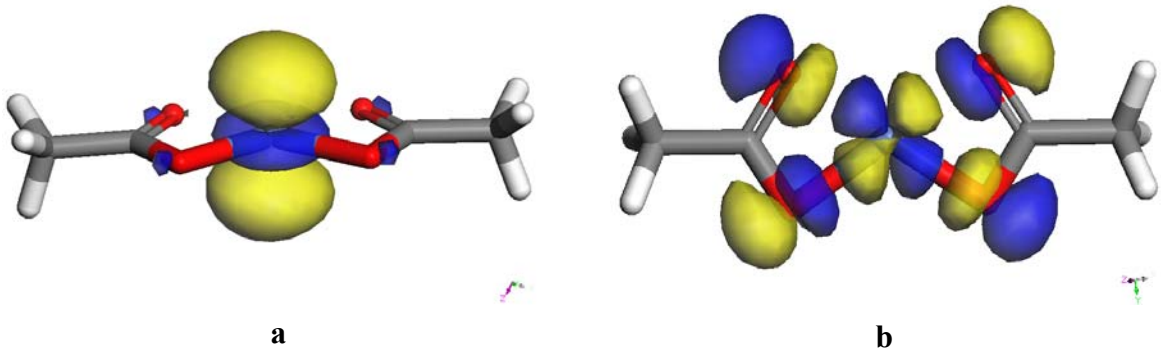

a **b**

Figure 4.14: a) The highest occupied molecular orbitals (HOMO) and b) the lowest unoccupied molecular orbitals (LUMO) of $Ni(OAc)_2$.

Fig 3.19 (Chapter 3) showed that the LUMO of the **DL1** contains a perpendicular p-orbital on the O-atom of the OH group, which is symmetrically compatible with the d_z^2 orbital on the Ni in Fig 4.14a that has the greatest contribution to the HOMO. After overlap of the frontier orbitals of the **DL1** and $Ni(OAc)_2$, **DL1** coordinated to Ni(OAc) and AcOH formed.

These structures were optimized and **DL1** coordinated to Ni(OAc) is shown in (Fig 4.15).

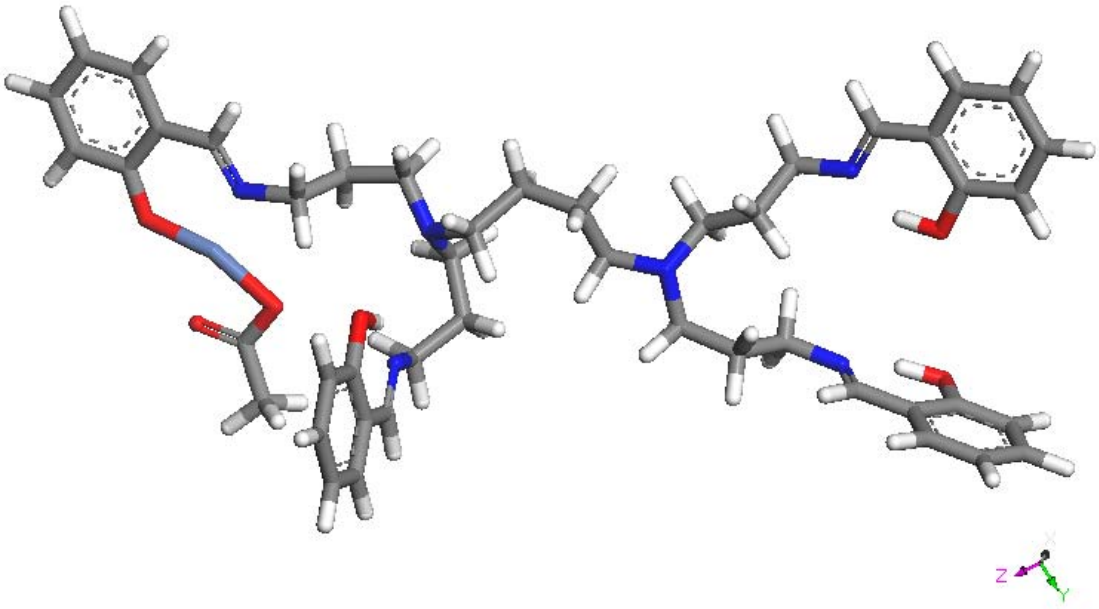

Figure 4.15: Optimized structure of **DL1** coordinated to Ni(OAc).

Proton transfer to the coordinated OAc occurs, followed by subsequent release of acetic acid from the nickel centre. It would thus appear that prior deprotonation of the salicylaldimine ligand is not necessary in this case. These results are supported by our experimental results, where no prior deprotonation of the hydroxyl group was necessary in order for the ligand to successfully coordinate to the metal ion. This is different to what has generally been found in the case of other reactions where similar dendritic ligands have been reacted with other metal precursors. In these cases, coordination of the ligand to the metal centre did not occur before ligand deprotonation took place.[18] Some atom distances of the optimized structure of **DL1** coordinated to Ni(OAc) is shown in Fig 4.16.

The N,N-distance and the O,O-distance on a dendrimer system containing a single $Ni(OAc)_2$ unit on the periphery (Fig 4.16) is smaller than the distances of the optimized

dendrimer ligand on its own (Fig 4.17), possibly indicating that ligand coordination to the second Ni atom is likely.

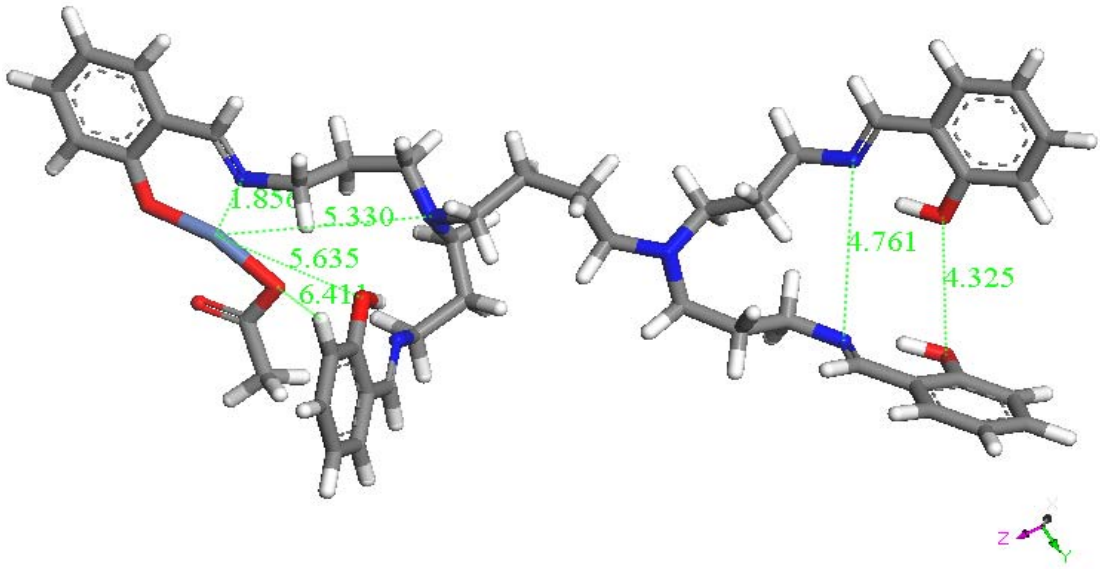

Figure 4.16: Some atom distances of the optimized structure of **DL1** coordinated to Ni(OAc).

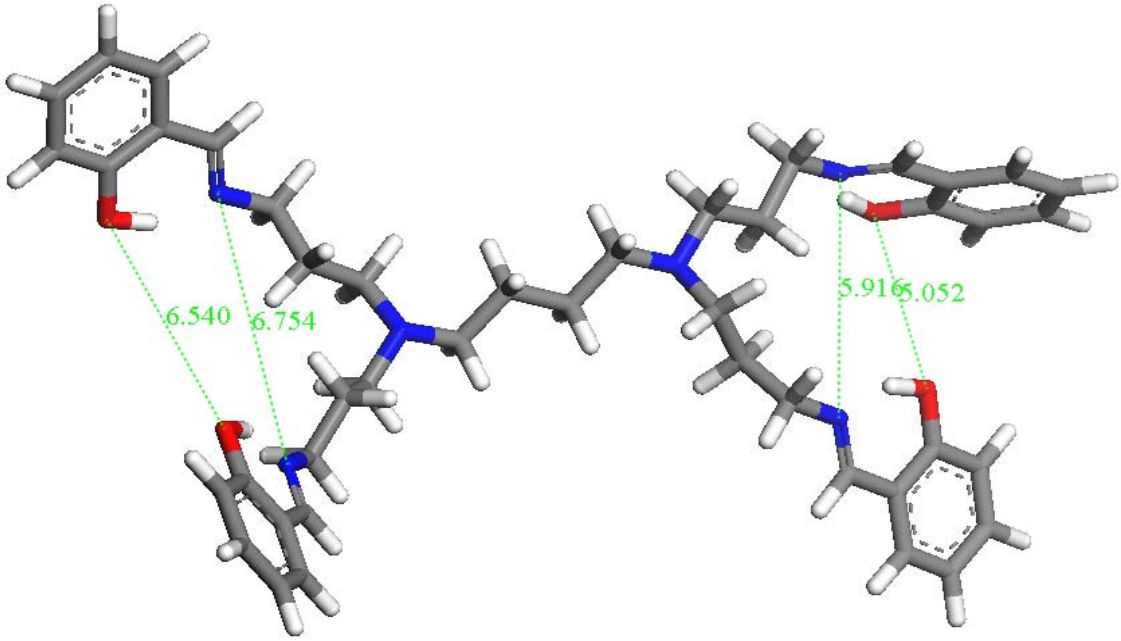

Figure 4.17: The N,N-distance and the O,O- distances of the optimized dendrimer ligand on its own.

Fig 4.18 shows the LUMO of **DL1** coordinated to Ni(II). This supports the interactions of the ligand orbitals with the second $Ni(OAc)_2$'s HOMO. It is assumed that the second nickel centre interact with the ligand in the same way as the first nickel centre, as discussed. This also indicates that the interaction of the ligand with the two metal centres occur sequentially, ie. first coordination occurs to one Ni ion, then followed by the second Ni ion.

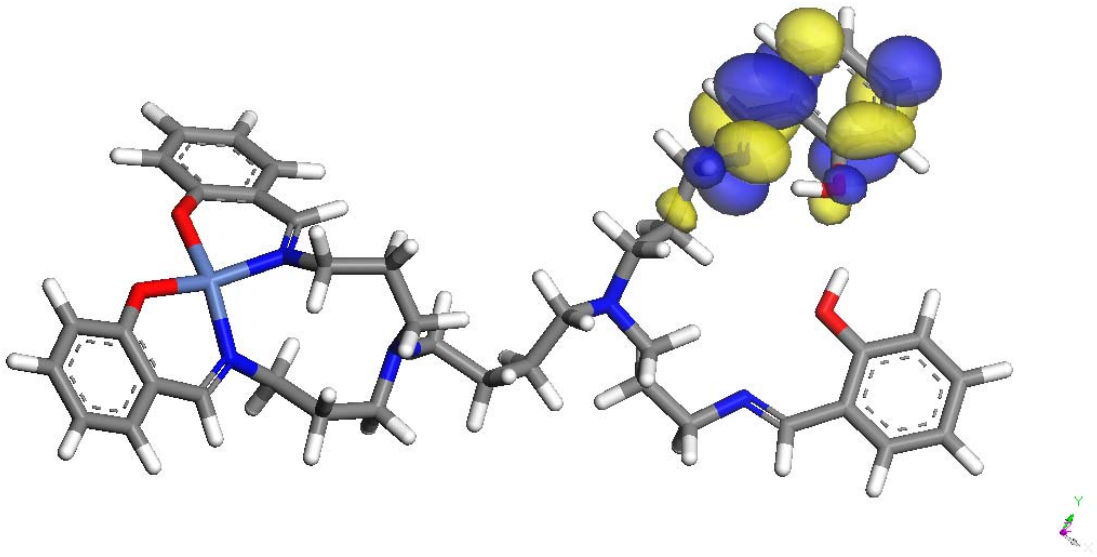

Figure 4.18: The LUMO of **DL1** coordinated to Ni.

*4.3.2 The optimized structure of the first generation salicylaldimine nickel complex, **C1**.*

The computational results also indicates that if we react the dendritic ligand, **DL1**, with $Ni(OAc)_2$, it is possible that a binuclear complex with bridging salicylaldimine ligands will form. This corresponds to our isolated G1 Ni(II) salicylaldimine complex, **C1**. The optimized theoretical structure of **C1** is shown in Fig 4.19. When compared to the optimized ligand structure, **DL1** (in Chapter 3), a fair amount of distortion is observed upon coordination of the metal centre.

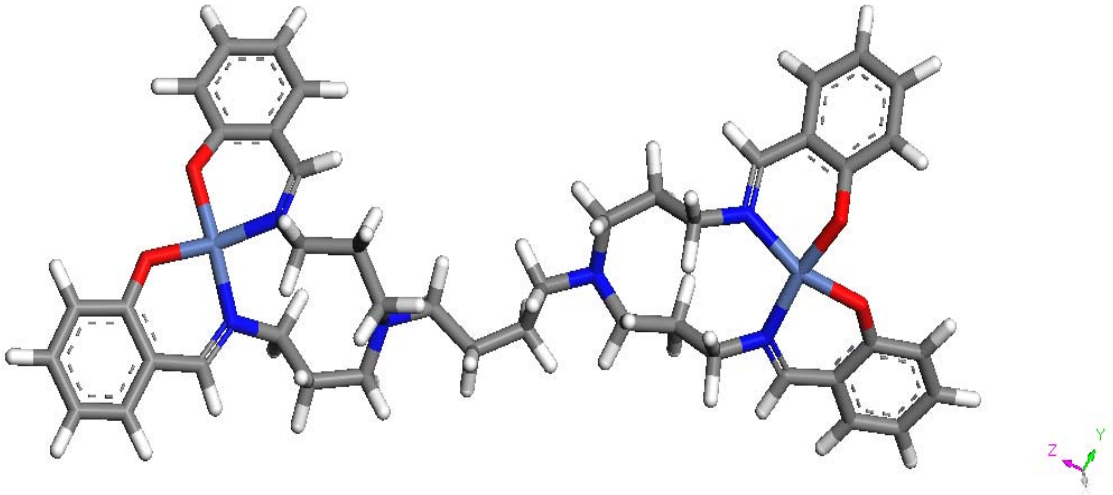

Figure 4.19: The optimized structure of the generation 1 salicylaldimine Ni complex, **C1**.

However, the best fit plane of the G1 ligand and metal complex are similar, with only one branch of the dendrimer out of plane (Fig 4.20).

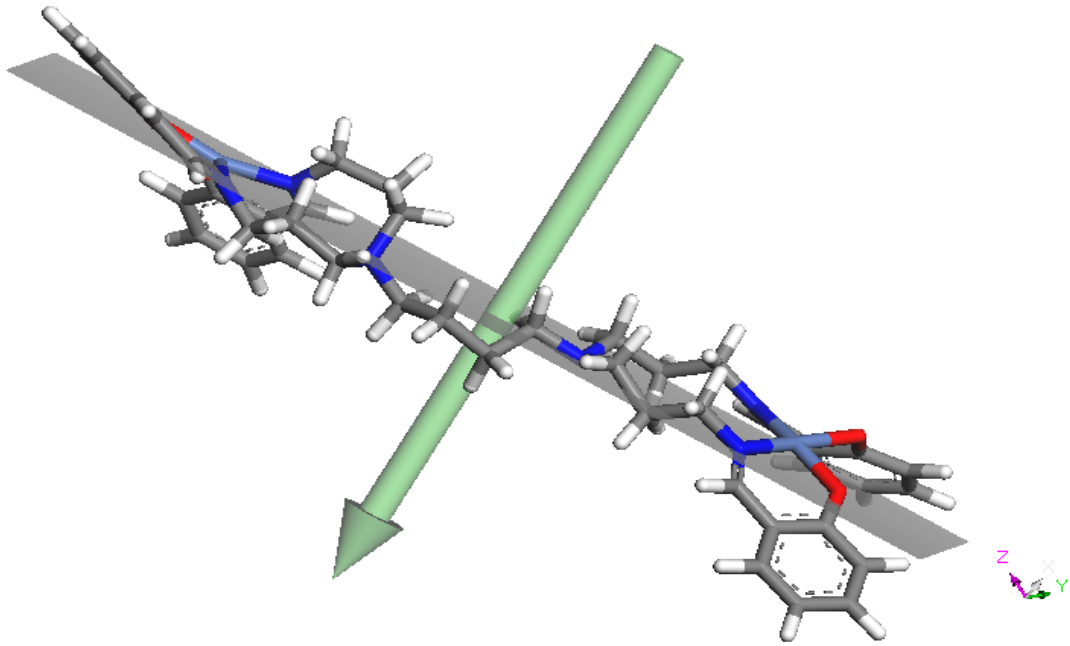

Figure 4.20: The best fit plane for complex, **C1**.

The optimized structure shows that the geometry around the Ni-centre is a distorted tetrahedron. This corresponds well to our spectral studies of complex **C1**.

There is a lack of symmetry surrounding the two metal centres, and this could be due to the distortion of the complex. The bond angles around the metal centre for complex, **C1**, are shown in Fig 4.21 with angles around the metal centre ranging from 81.175 º - 102.666 º for the first Ni-atom, and 83.785 º - 95.391 º for the second Ni-atom.

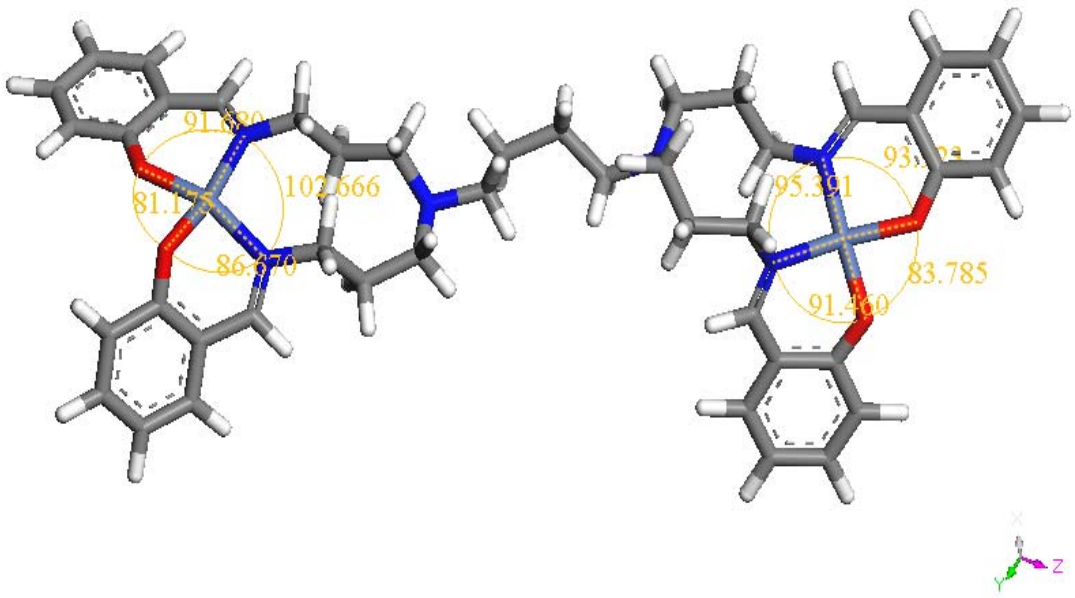

Figure 4.21: The bond angles around the nickel centre for complex, **C1**.

Table 4.8 shows a comparison of the bond angles around the two metal centres. This clearly shows the difference in symmetry between the two metal centres. It can be seen that on one of the Ni centres, the N-Ni-N angle is much larger than the corresponding angle on the other Ni centre. This results in the O-Ni-O and the O-Ni-N angles for the first Ni centre being smaller than those on the second metal centre.

Table 4.8: The difference in the angles between the two metal centres.

Angle	Ni (1)	Ni (2)
	Degrees (º)	Degrees (º)
O-Ni-O	81.175	83.785
O-Ni-N	86.670	91.460
N-Ni-N	102.666	95.391
N-Ni-O	91.820	93.323

The LUMO of **C1** is shown in Fig 4.22 and the HOMO of **C1** is shown in Fig 4.23. The LUMO shows that the complex has the potential to coordinate to an electron rich species such as an alkene at this site (catalytic evaluation).

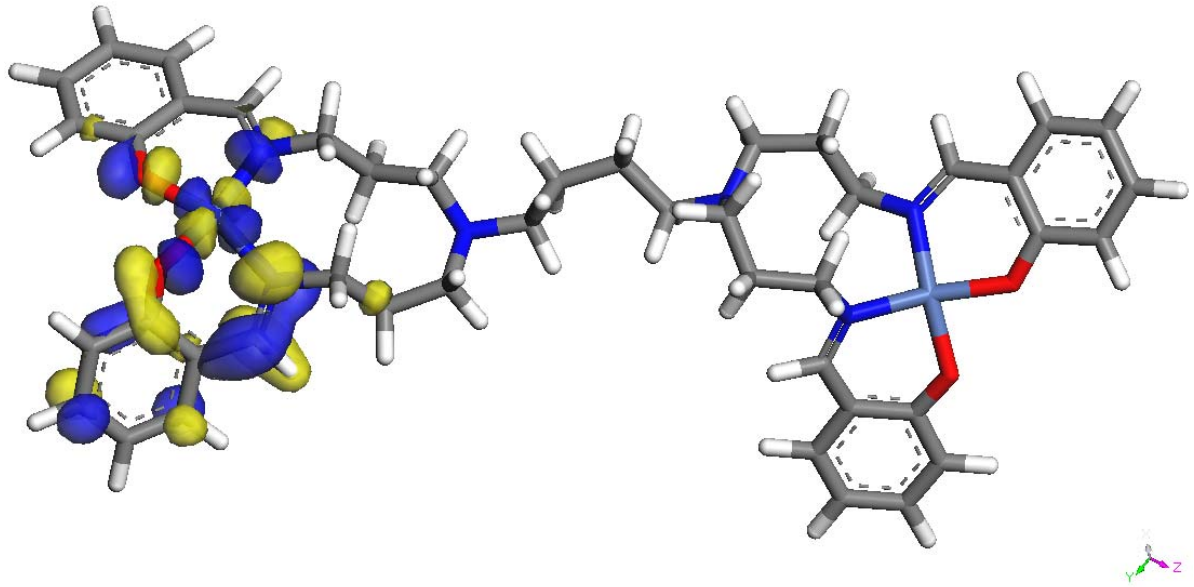

Figure 4.22: The LUMO of complex, **C1**.

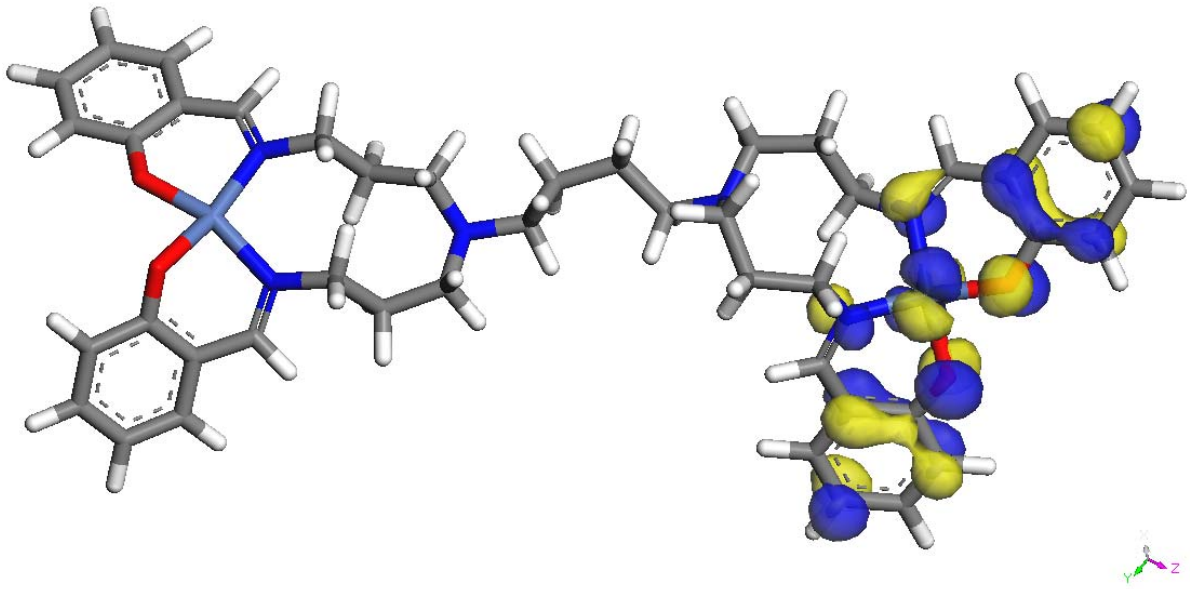

Figure 4.23: The HOMO of complex, **C1**.

It is interesting to see that the HOMO is on one Ni ion and the LUMO on the other Ni ion. This means that at first, only one Ni ion is available for alkene coordination. It is possible that the electron distribution after coordination of the alkene to the first Ni will change and subsequently the second Ni will become available for alkene coordination.

4.4 Conclusion.

Nickel metallodendrimers (**C1-C8**) were successfully synthesized by coordination of metal precursors, $Ni(OAc)_2$ and $Ni(DME)Br_2$, to the periphery of salicylaldimine and iminopyridyl modified dendrimer ligands **DL1-DL8**. The complexes have been successfully characterized by various analytical techniques, such as FTIR and UV/Vis spectroscopy, magnetic susceptibility measurements, ICP, thermal gravimetrical analysis (TGA) and mass spectrometry, and the complex structures have been confirmed. **C1** and **C2** have been previously published by us and **C3-C8** are novel complexes.

DFT calculations on the probability of metal coordination to the modified ligand **DL1** were performed and the results show that coordination to the dendrimer periphery is favourable. Molecular modelling was also done on the G1 nickel salicylaldimine complex, **C1**, to get an idea of the complex structure and symmetry. These results for the optimized structures correspond well to our experimental results. The computational results also show that the metallodendrimer complexes could potentially act as catalysts in olefin oligomerization or polymerization processes.

From the synthesised metallodendrimers, **C1-C7** were chosen for evaluation as potential catalysts. With this catalyst selection, conclusions regarding the effect of dendrimer generation (**C1** vs **C2** vs **C3**), the effect of the cyclam- against the DAB- dendritic core (**C1** vs **C7**) and effect of salicylaldimine vs iminopyridyl ligands (**C1-C3** vs **C4-C6**) on the activity and selectivity of products. These catalysts will be evaluated in the polymerization of norbornene (Chapter 5) and the transformation of á-olefins (Chapter 6).

4.5 Experimental.

Ethanol was dried by refluxing over Mg/I_2. $Ni(OAc)_2$, $NiBr_2$ and dimethoxyethane (DME) were purchased from Sigma Aldrich, and were used without any further purification. Modified dendrimer ligands, **DL1-DL10,** were prepared as described in Chapter 3. Infrared spectra were recorded on a Nicolet Avatar 330 FT-IR spectrophotometer, using an ATR accessory with a ZnSe crystal. Magnetic susceptibility was measured with a Sherwood Scientific MK-1 magnetic susceptibility balance at 298 K. Magnetic data were corrected for the magnetization of diamagnetic contributions, which were estimated from Pascal constants. UV–Vis absorption spectroscopy was measured using a GBC UV/Vis 920 spectrometer at room temperature. TGA data were determined with a Q500 Thermogravimetric analyzer, in which the TGA scans were recorded at 10 ºC/min under a nitrogen atmosphere from 30 to 590 ºC. ESI Mass spectra were obtained using a Waters API Q-TOF Ultima instrument in V-mode. The source temperature was 100 ºC and the desolvation temperature was 350 ºC. The capillary voltage used was 3.5 kV. Microanalyses were done at the University of Cape Town. Melting points were recorded on a Stuart Scientific Melting Point apparatus SMP3, and are uncorrected. Density functional theorem (DFT) calculations were done at North-West University.

*Synthesis of **C1**:*

To the 1st generation DAB-based salicylaldimine dendrimer ligand, **DL1** (0.50 g, 0.68 mmol) in ethanol (10 ml) in a round bottom flask was added nickel acetate tetrahydrate (0.34 g, 1.40 mmol) and the reaction mixture was allowed to stir under reflux for 24 hours forming a green precipitate. The precipitate was filtered by vacuum filtration and washed

extensively with ethanol to afford **C1** as a green solid. Yield = 85 %. m.p.: 290-292 ºC. IR (cm^{-1}): í(C=N) 1628 (s) and í(C–O) 1324 (s). ESI–MS calc for ($C_{54}H_{52}N_6Ni_2O_4$), $[M+H]^+$ at m/z = 848.

*Synthesis of **C2**:*

To a solution of the DAB-G2 salicylaldimine ligand, **DL2** (0.35 g, 2.20 mmol) in ethanol (10 ml) was added nickel acetate tetrahydrate (0.23 g, 9.10 mmol) and the mixture stirred under reflux for 24 hours. After cooling of the reaction mixture, the resulting precipitation was filtered on a Buchner funnel and washed with ethanol to give a green solid. Dichloromethane (10 ml) was added to the solid, and the solution was then filtered. The filtrate was evaporated to give **C2** as a green solid. Yield = 80 %. m.p.: 221-224 ºC. IR (cm^{-1}): í(C=N) 1632 (s) and í(C–O) 1344 (s). MALDI-TOF MS calc for ($C_{96}H_{120}N_{14}Ni_4O_8$), $[M+H]^+$ at m/z = 1833.

*Synthesis of **C3**:*

To a solution of the DAB-G3 salicylaldimine ligand, **DL3** (1.36 g, 0.41 mmol) in ethanol (20 ml) was added nickel acetate tetrahydrate (0.82 g, 3.20 mmol) and the reaction mixture was allowed to stir under reflux for 24 hours, forming a green precipitate. The precipitate was filtered off by vacuum filtration and washed extensively with ethanol to give a green solid. Dichloromethane (15 ml) was added to the solid, and the solution was then filtered. The filtrate was evaporated to give **C3** as a green solid. Yield = 75 %. m.p.:

199-201 ºC. IR (cm^{-1}): í(C=N) 1629 (s) and í(C–O) 1344 (s). MALDI-TOF MS calc for ($C_{200}H_{256}N_{30}Ni_8O_{16}$) $[M+H]^{3+}$ at m/z = 1269.

Synthesis of G1 Ni(DME)Br_2 using triethyl orthoformate as a dehydrating agent.

$NiBr_2$ (0.50 g, 2.30 mmol), a yellow solid, was added to a mixture of ethanol (20 ml) and triethyl orthoformate (1.2 ml) and refluxed for 3 hours to give a clear green solution. The solvent was then concentrated to 1 ml, after which excess Dimethoxyethane (30 ml) was added. The mixture was allowed to crystallize and then filtered to give a bright orange solid. Yield = 84 %. IR (cm^{-1}): í(C-H) *aliphatic* at 2935 (s) and í(C-O) at 1049 (s).

*Synthesis of **C4**:*

Ni(DME)Br_2 (0.18 g, 0.6 mmol) was added to a solution of **DL4** (0.10 g, 0.15 mmol) in dry ethanol (15 ml). There's an immediate colour change from orange to brown, and all reagents dissolved to give a clear brown solution. The reaction mixture was refluxed for 24 hours. The solvent was evaporated to give a brown solid residue. Dichloromethane (5 ml) was added to the residue and then triturated, after which a brown solid precipitates. The precipitate was filtered to give **C4** as a brown solid. Yield = 85 %. m.p.: 249-251 ºC. IR (cm^{-1}): í(C=N) at 1639 (s); í(C=C) *pyr* at 1596 (s) and í(C=N) *pyr* at 1567 (s). ESI–MS calc for ($C_{54}H_{52}N_6Ni_2O_4$), $[M+2Na]^+$ at m/z = 1592.

*Synthesis of **C5**:*

$Ni(DME)Br_2$ (0.33 g, 1.10 mmol) was added to a solution of **DL5** (0.20 g, 0.14 mmol) in dry ethanol (15 ml). There's an immediate colour change from orange to brown, and all reagents dissolved to give a clear brown solution. The reaction mixture was refluxed for 24 hours. The solvent was evaporated to give a brown solid residue. Dichloromethane (10 ml) was added to the residue and then triturated, after which a brown solid precipitates. The precipitate was filtered to give **C5** as a brown solid. Yield = 80 %. m.p.: 225-231 ºC. IR (cm^{-1}): í(C=N) at 1640 (s); í(C=C) *pyr* at 1597 (s) and í(C=N) *pyr* at 1568 (s). ESI–MS calc for ($C_{88}H_{120}Br_{16}N_{22}Ni_8$), $[M+Na]^{4+}$ at m/z = 814, calc 3234 g/mol.

*Synthesis of **C6**:*

$Ni(DME)Br_2$ (0.31 g, 1.0 mmol) was added to a solution of **DL6** (0.20 g, 0.062 mmol) in dry ethanol (20 ml). There's an immediate colour change from orange to brown, and all reagents dissolved to give a clear brown solution. The reaction mixture was refluxed for 24 hours. The solvent was evaporated to give a brown solid residue. Dichloromethane (10 ml) was added to the residue and then triturated, after which a brown solid precipitates. The precipitate was filtered to give **C6** as a brown solid. Yield = 78 %. m.p.: 201-204 ºC. IR (cm^{-1}): í(C=N) 1642 (s); í(C=C) *pyr* at 1598 (s) and í(C=N) *pyr* at 1571 (s). ESI–MS calc for ($C_{184}H_{256}Br_{32}N_{46}Ni_{16}$), $[M+Na]^{5+}$ at m/z = 1326, calc 6608 g/mol.

*Synthesis of **C7**:*

To the 1st generation cyclam-based salicylaldimine dendrimer ligand, **DL7** (0.125 g, 0.15 mmol) in ethanol (10 ml) in a round bottom flask was added nickel acetate tetrahydrate (0.11 g, 0.44 mmol) and the reaction mixture was allowed to stir under reflux for 24 hours forming a lime green solution. The solvent was evaporated to give a lime green oily residue. The solvent was recrystallized from dichloromethane (2 ml) and diethyl ether (10 ml) to afford **C7** as a lime green solid. Yield = 63 %. m.p.: 260-263 ºC. IR (cm^{-1}): í(C=N) 1623 (s) and í(C–O) 1319 (s). ESI–MS calc for ($C_{50}H_{64}N_8Ni_3O_4$), $[M+K]^+$ at m/z = 1057.

*Synthesis of **C8**:*

$Ni(DME)Br_2$ (0.20 g, 0.64 mmol) was added to a solution of **DL8** (0.10 g, 0.13 mmol) in dry ethanol (10 ml). There's an immediate colour change from orange to brown, and all reagents dissolved to give a clear brown solution. The reaction mixture was refluxed for 24 hours. The solvent was evaporated to give a brown solid residue. Dichloromethane (5 ml) was added to the residue which was then triturated, after which a brown solid precipitates. The precipitate was filtered to give **C8** as a brown solid. Yield = 68 %. m.p.: 197-199 ºC. IR (cm^{-1}): í(C=N) at 1618 (s); í(C=C) *pyr* at 1593 (s) and í(C=N) *pyr* at 1569 (s). ESI-MS calc for ($C_{46}H_{64}Br_8N_{12}Ni_5$), $[M+Na]^{4+}$ at m/z = 435.

4.6 References.

[1] J. A. Camerano, M. A. Casado, M. A. Ciriano, L. A. Oro, *Dalton Trans.*, **2006**, 5287.

[2] I. Angurell, O. Rossell, M. Seco and E. Ruiz, *Organometallics*, 24, **2005**, 6365.

[3] I. Angurell, J. C. Lima, L. Rodrýguez, O. Rossell, M. Seco, *New J. Chem.*, 30, **2006**, 1004.

[4] J. Leclaire, R. Dagiral, S. Fery-Forgues, Y. Coppel, B. Donnadieu, A. M. Caminade, J. P. Majoral, *J. Am. Chem. Soc.,*127*,* **2005**,15762.

[5] J. Leclaire, R. Dagiral, A. Pla-Quintana, A. M. Caminade, J. P. Majoral, *Eur. J. Inorg. Chem.,* **2007**, 2890.

[6] X. Tang, D. Zhang, S. Jie, W. Sun, J. Chen, *J. Organomet.Chem.*, 690, **2005**, 3918.

[7] C. Baleizao, B. Ginante, M.J. Sabater, H. Garcia, A. Corma, *Appl. Catal. A: Gen.*, 228, **2002**, 279.

[8] Y. Wang, S. Lin, F. Zhu, H. Gao, Qing Wu, *Eur. Pol. J.*, 44, **2008**, 2308.

[9] Y. Li, M. Gao, Q. Wu, *Appl. Organometal. Chem*., 22*,* **2008**, 659.

[10] R. Malgas, S.F. Mapolie, S.O. Ojwach, G.S. Smith, J. Darkwa, *Catal. Commun.,* 9, **2008**, 1612.

[11] M. Asadi, K. A. Jamshid, A. H. Kyanfar, *Inorg. Chim. Acta,* 360, **2007**, 1725.

[12] B. S. Garg, D. N. Kumar, *Spectrochim. Acta: Part A*, 59, **2003**, 229.

[13] T. Akitsu, Y. Einaga, *Polyhedron*, 24, **2005**, 1869.

[14] A. B. P. Lever, *Inorg. Chem.,* 4, **1965**, 763.

[15] G. G. Mohamed, Z. H. A. El-Wahab, *Spectrochim. Acta: Part A*, 61, **2005**, 1059.

[16] V. T. Kasumov, *Trans. Metal Chem.,* 27, **2002**, 228.

[17] W. Zhang, S. Bruda, C. P. Landee, J. L. Parent, M. M. Turnbull, *Inorg. Chim. Acta,* 342, **2003**, 193.

[18] J. L. Van Wyk, PhD Thesis: Mononuclear and multinuclear salicylaldimine metal complexes as catalyst precursors in the oxidation of phenol and cyclohexene. University of the Western Cape, **2008**.

[19] B. S. Garg, D. Nandan-Kumar, *Spectrochim. Acta: Part A*, 59, **2003**, 229.

[20] K. Nejati, Z. Rezvani, M. Seyedahmadian, *Dyes and Pigments*, 83, **2009**, 304.

[21] Y. Fan, W. You, W. Huang, J-L. Liu, Y-N. Wang, *Polyhedron*, 29, **2010**, 1149.

[22] E. Tas, A. Kilic, N. Konak, I. Yilmaz, *Polyhedron*, 27, **2008**, 1024.

[23] G. Smith, R. Chen, S. Mapolie, *J. Organomet. Chem.*, 673, **2003**, 111.

[24] W. Massa, S. Dehghanpour, K. Jahani, *Inorg. Chim. Acta*, 362, **2009**, 2872.

[25] S. Chattopadhyay, P. Chakraborty, M. G. B. Drew, A. Ghosh, *Inorg. Chim. Acta*, 362, **2009,** 502.

[26] A. S. Roy, M. K. Biswas, T. Weyhermüller, P. Ghosh, *Inorg. Chim. Act*a, **2010**, doi:10.1016/j.ica.2010.03.017.

[27] R. S. Herrick, C. J. Ziegler, M. Precopio, K. Crandall, J. Shaw, R. M. Jarret, *J. Organomet. Chem.*, 693, **2008**, 619.

[28] S. Naskar, R. J. Butcher, S. K. Chattopadhyay, *Inorg. Chim. Acta*, **2010**, doi:10.1016/j.ica.2010.05.009.

[29] A. Evers, R. D. Hancock, *Inorg. Chim. Acta*, 160, **1989**, 245.

Chapter 5:

Metallodendrimers as catalysts in the Vinyl Polymerization of Norbornene.

5.1 Introduction to Norbornene Polymerization.

5.1.1 Types of Norbornene Polymerization.

Bicyclo[2.2.1]hept-2-ene, also known as norbornene, can typically be polymerized *via* three routes leading to different polymer structures. These routes are: (a) ring-opening metathesis polymerization (ROMP), (b) cationic or radical polymerization and (c) vinyl or addition polymerization of norbornene as shown in Fig 5.1.[1]

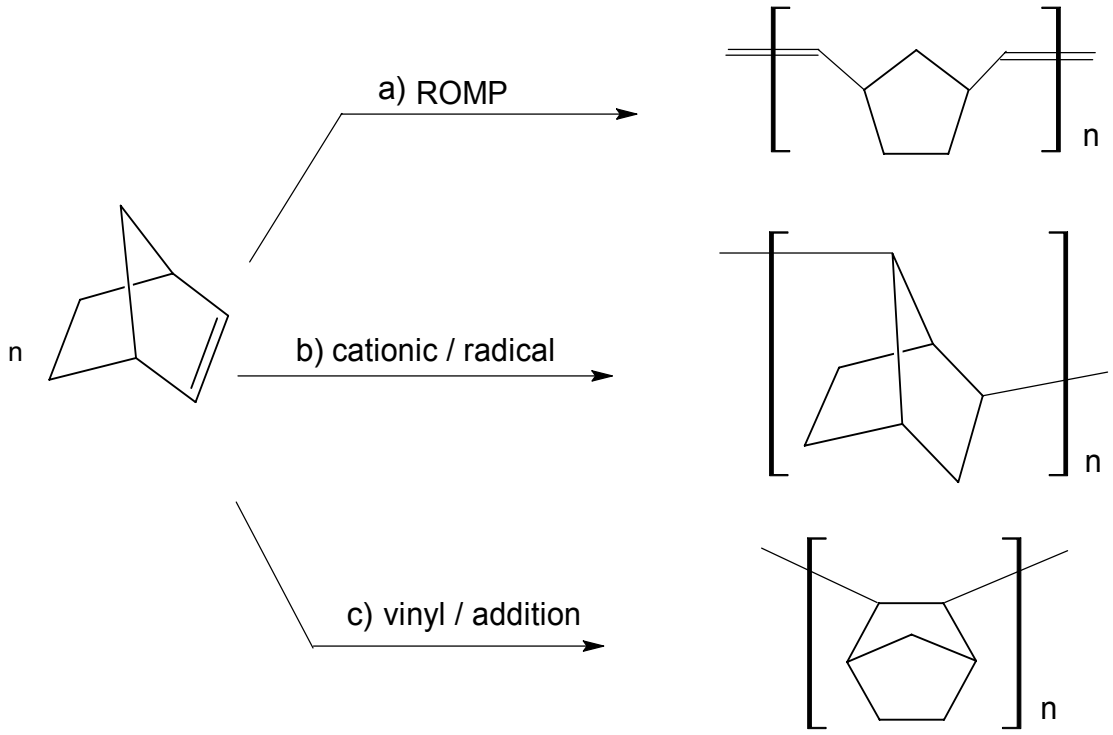

Figure 5.1: Three different routes to polynorbornene formation.[1]

The type of polynorbornene formed depends on the catalyst employed. Ring-opening metathesis polymerization (ROMP) is the most studied route to produce polynorbornene.[2] The unique properties of ROMP polynorbornene are due to the presence of the double bond which links the monomers to form the polymer. This makes crosslinking and vulcanization of

the polymer possible, which can be used as a material for shock-proof bumpers and engine mounts. [3] Polynorbornenes synthesized by ROMP is also used as oil sponges [4], for drug delivery [5] and as highly transparent optical materials amongst others. [6] Catalyst systems based on niobium, molybdenum, ruthenium, iridium, tungsten and tantalum promotes the ROMP of norbornene.[7-12]

In the radical and cationic polymerization of norbornene, the framework is rearranged to produce poly (2,7-bicyclo[2,2,1] hept-2-ene) oligomers.[13] The polymer obtained via this route has low molecular weights (molecular weight <1000 g/mol) at low yields because of rearrangements and chain transfer reactions. The following activators typically initiate radical polymerization; ethylaluminium dichloride ($EtAlCl_2$), azoisobutronitrile (AIBN) and tert butyl perpivilate.[14]

Vinyl or addition polymerization yields a 2,3-connected polymer, which occurs when the bicyclic structural unit remains intact and the double bond of the ð-component is opened. Of the three types of polynorbornene, only the vinyl addition polymerization provides a completely saturated polymer with no rearranged norbornene units.[15] This addition polymer has appealing properties such as high chemical resistance, good UV resistance, low dielectric constant, high glass transition temperature, excellent transparency, large refractive index, and low birefringence.[16-20] As a result of these unique properties, films made from the vinyl polymer are suitable as condensers or insulators and these films are also applied as cover layers for liquid-crystal displays.[21] Vinyl polynorbornene materials are also used in microelectronics and optical applications, as well as in gas separation technologies.[22-25] The vinyl polymerization of norbornene is activated by transition metal complexes such as palladium, chromium, cobalt, titanium, iridium, rhodium, copper, zinc and nickel.[26-31] A brief overview of nickel based catalysts in norbornene polymerization is outlined below.

5.1.2 Nickel complexes as norbornene polymerization catalysts.

Nickel complexes especially display extremely high catalytic activity towards the vinyl polymerization of norbornene. Yang *et al* [32] described the vinyl-polymerization of norbornene using a [2-methyl-8-(diphenylphosphino)quinoline]nickel(II) dichloride/ methylaluminoxane system (Fig 5.2). This catalytic system showed high activity up to 1.70×10^8 g of PNB/mol-Ni/h under optimized reaction conditions.

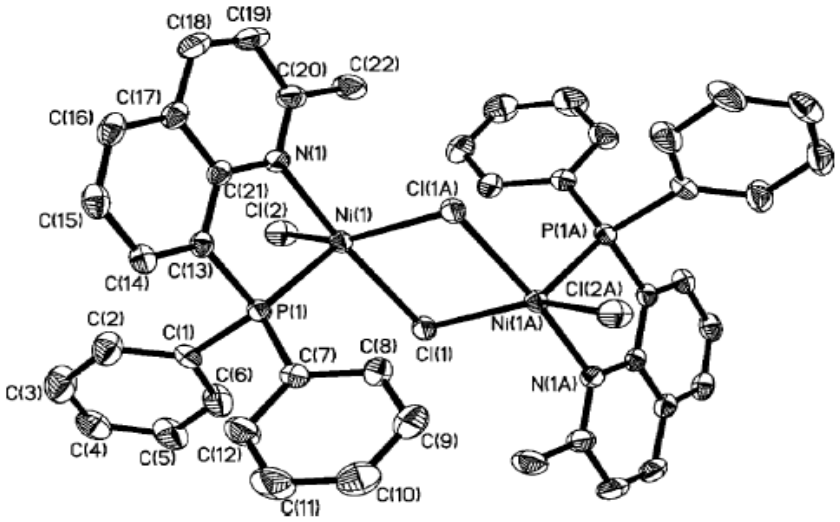

1

Figure 5.2: Crystal structure of the nickel dichloride catalyst synthesised by Yang *et al*.[32]

The catalytic activity is dependent upon the Al/Ni molar ratio which ranged from 250:1-1000:1. The optimized Al/Ni molar ratio for the activity was 600:1, after which the activity decreased with an increase in MAO concentration. GPC analyses showed that the molecular weight (M_w) value increased, with increasing Al/Ni molar ratio, and ranged from 2.30×10^5 - 4.24×10^5 g/mol. The polydispersity index (PDI) values ranged from 2.88 - 3.59 when only the Al/Ni molar ratio was varied.

Bao *et al* [33] reported the synthesis of bis(â-keto-iminato)nickel (II) complexes, and its ability to polymerize norbornene in the presence of methylaluminoxane. Four different nickel complexes with pyrazolone derivatives **2-5** were synthesized and evaluated (Figure 5.3).

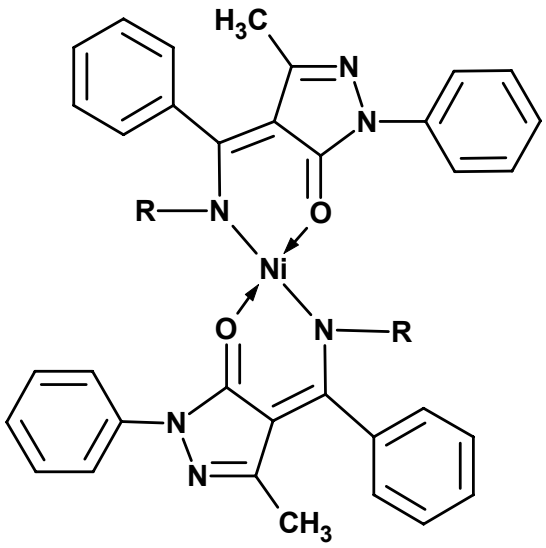

2: R = Phenyl

3: R = o-Tolyl

4: R = Naphthyl

5: R = p-Nitrophenyl

Figure 5.3: The structure of the bis-(â-ketoiminato)nickel (II) complexes synthesised by Bao *et al.*[33]

The Ni/Al ratio was kept constant at 800:1, and the naphthyl derivative gave the highest activity towards the vinyl polymerization of norbornene. The M_w ranged from 7.29×10^5 - 11.2×10^5 g/mol. The PDI values were in a narrow range varying between 2.14-2.34. It was concluded that the catalytic activity and polymer yield could be controlled over a wide range by varying the reaction parameters. Both the steric and conjugating effects of the substituted group played an important role in adjusting the catalytic activity.

Dinuclear nickel(II) complexes bearing two pyrazolylimine ligands were reported by Wang *et al.* [34] These four di-nickel complexes (Fig 5.4) exhibited moderate activity for the vinyl polymerization of norbornene when activated by MAO. Under the optimum polymerization conditions (complex **6**/MAO, Temp = 40 ºC and Al/Ni = 800), a catalytic activity of 6.64 x 10^5 g PNB $mol^{-1}Ni.h^{-1}$ was obtained.

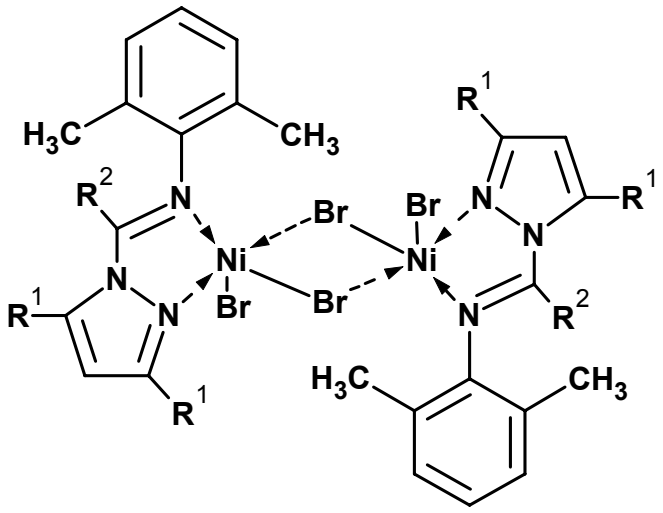

6: R^1=CH3, R^2=Ph

7: R^1=CH3, R^2=2,4,6-Trimethylphenyl

8: R^1=Ph, R^2=Ph

9: R^1=Ph, R^2=2,4,6-Trimethylphenyl

Figure 5.4: Structure of pyrazoylimine dinickel (II) complexes 6–9 synthesised by Wang *et al.*[34]

The PDI values ranged from 2.68 – 6.56 for the four catalysts at different Al/Ni ratio's. The influence of the bulkiness of the substituents on polymerization activity were also investigated, and it was found that the activities of the nickel complexes followed the order **6>7>8>9**, which is the inverse of the sequence of steric bulkiness of the four complexes **(9>8>7>6)**.

Lui *et al* [35] published the results of neutral nickel complexes with chelating monoamidinate ligands as catalysts for norbornene polymerization activated by MAO. Complexes **10–12** (Fig 5.5) showed very high catalytic activities for vinyl-addition polymerization of norbornene. Complex **10** with the most steric hindrance produced the highest molecular-weight polynorbornene, while complex **12** with an electron-withdrawing group exhibited the highest catalytic activity for norbornene polymerization.

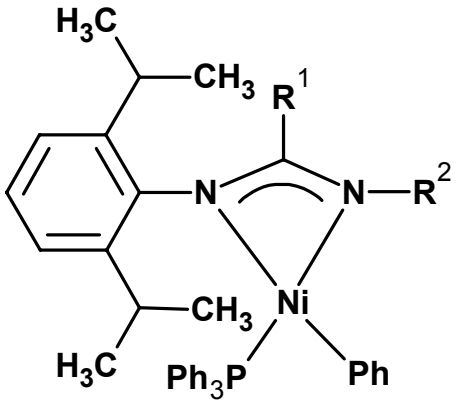

10: R^1 = Phenyl, R^2 = 2,6-diispropylphenyl

11: R^1 = *p*-tolyl, R^2 = 2,6-dimethylphenyl

12: R^1 = *p*-tolyl, R^2 = pentafluorophenyl

Figure 5.5: Neutral nickel complexes synthesised by Lui *et al*. [35]

In this chapter we discuss the use of nickel metallodendrimers (**C1-C7**) as catalysts for the vinyl polymerization of norbornene, and compare our results to those published in literature. The effect of dendrimer generation as well as different ligand systems, is studied. The effect of the more flexible dumbbell-shaped dendrimers (DAB range) versus the rigid cyclic cored dendrimers (cyclam) is also discussed. The reaction conditions were varied to find the optimum conditions for highest catalytic activity.

5.2 Results and Discussion.

5.2.1 Activity of catalysts employed in norbornene polymerization.

*5.2.1.1 Generation 1-3 DAB salicylaldimine nickel complexes, **C1-C3**, as norbornene polymerization catalysts.*

We have recently published the results of using DAB-G1 and DAB-G2 salicylaldimine nickel complexes (Fig 5.6) as catalysts for the vinyl polymerization of norbornene.[36] Methylaluminoxane (MAO) was used as a co-catalyst. The generation 1 nickel catalyst (**C1**) showed optimum activity of 328 kg PNB $mol^{-1}Ni.h^{-1}$ at an Al:Ni ratio of 4000:1 whereas the generation 2 nickel catalyst (**C2**) exhibits optimum activity of 792 kg PNB $mol^{-1}Ni.h^{-1}$ at Al:Ni ratio of 4500:1. The generation 2 catalyst shows enhanced activity compared to the generation 1 catalyst at optimum reaction conditions. This we believe is related to the increased number of active sites in the G2 catalyst as opposed to the G1 catalyst. In addition the generation 2 catalyst, due to its higher degree of branching might also be more effective in stabilizing the catalyst by preventing deactivation via metal agglomeration.

It was also found that the generation 2 catalyst needs more MAO to reach the optimum activity when compared to its generation 1 analogue. It is thought that the tertiary amine groups within the internal framework of the dendrimer complexes can potentially act as Lewis base sites. Thus MAO, which is a Lewis acid, first coordinates to these tertiary N-atoms before activating the metal centres. Only once all the internal tertiary amines have interacted with MAO, does activation of the metal centres take place. It is well known that N-donor molecules form adducts with Lewis acidic aluminium complexes.[37,38]

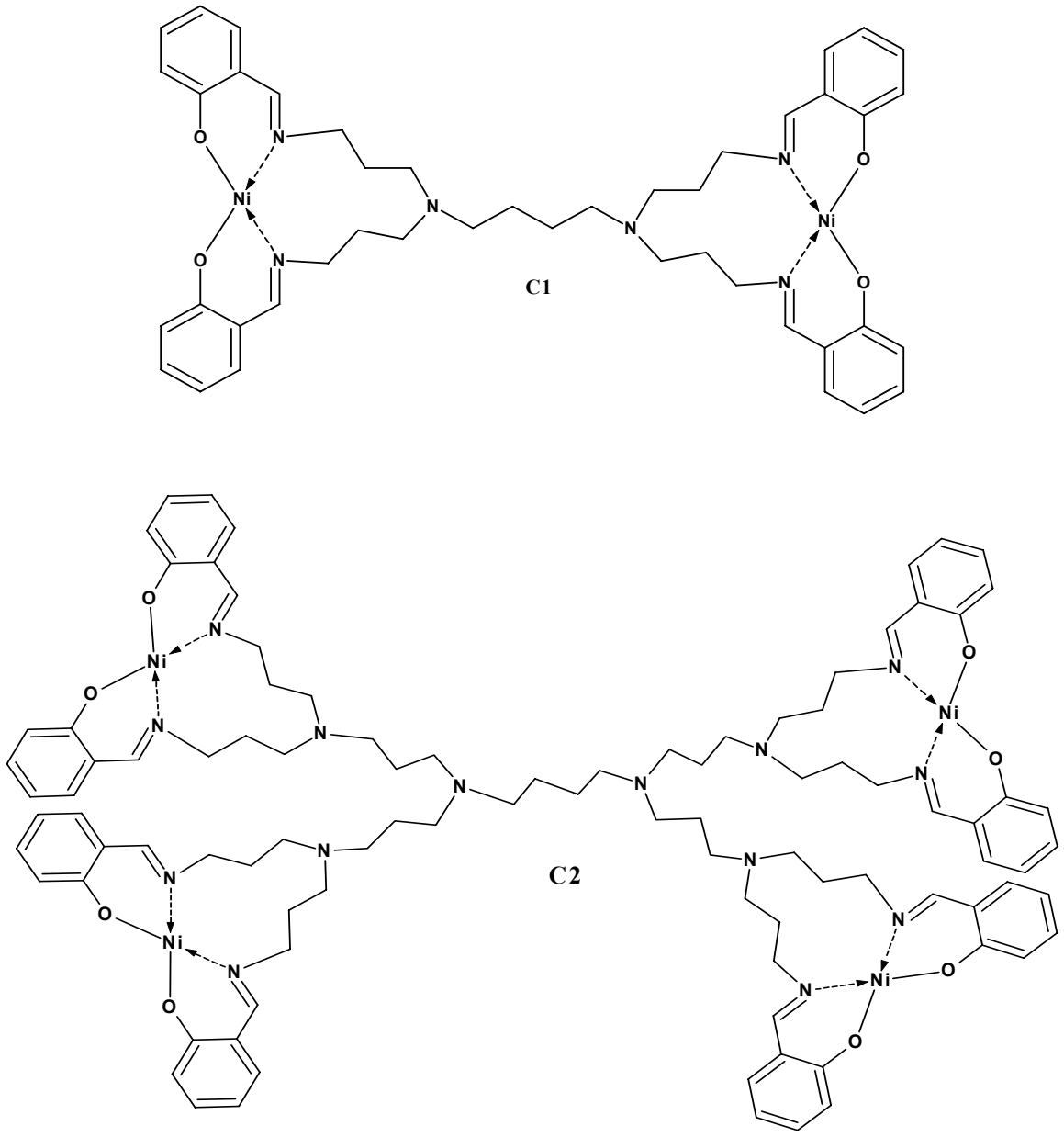

Figure 5.6: Structure of the generation 1 salicylaldimine nickel catalyst **C1** and the generation 2 nickel catalyst **C2**.[36]

The interaction between the tertiary amine centres in the dendrimer and the Al salts is also supported by DFT calculations (Chapter 3). The Fukui function of the dendritic ligands (Fig 3.17) showed the tertiary nitrogen atoms as having a relatively high electron density, thus exhibiting potential electron donating properties.

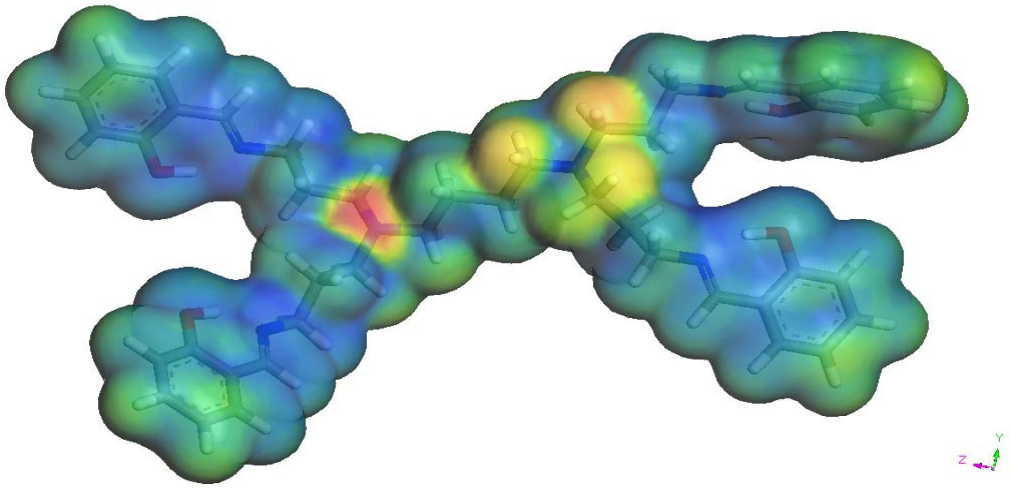

Figure 3.17: Fukui function of **DL1**.

It was therefore in our interest to also evaluate the generation 3 salicylaldimine nickel catalyst **(C3)** (Fig 5.7) in the vinyl polymerization of norbornene, and compare the activity to that of the generation 1 and generation 2 analogues.

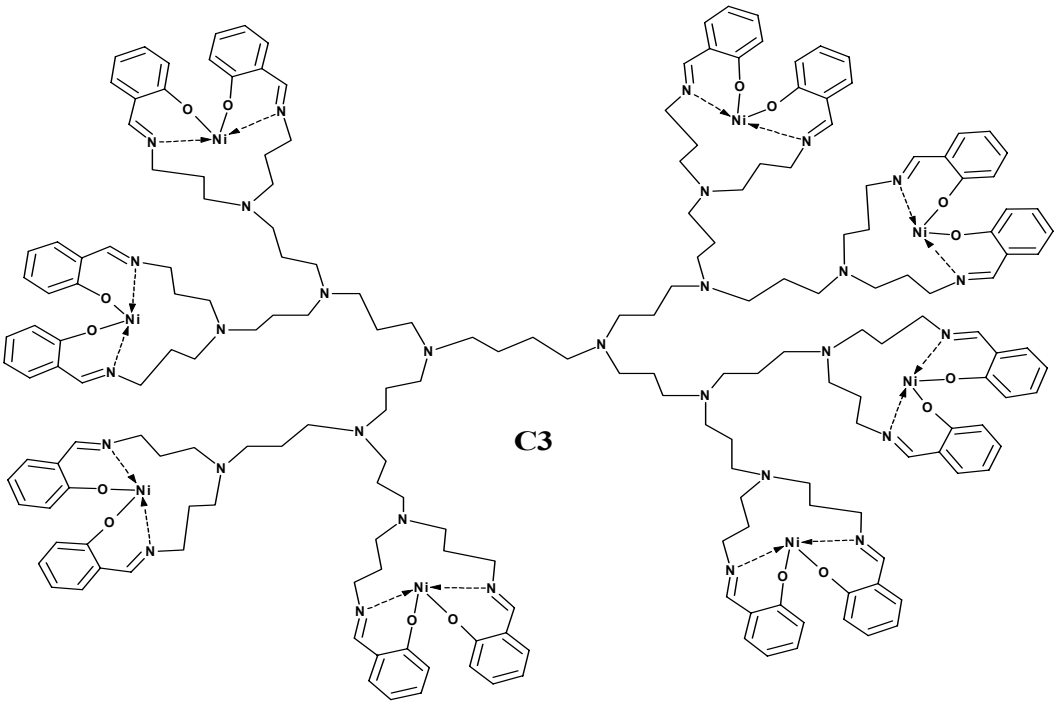

Figure 5.7: Structure of the Generation 3 salicylaldimine nickel catalyst **C3**.

The results of the generation 3 catalyst together with those of the lower generation analogues are tabulated in Table 5.1. The generation 3 catalyst, **C3**, exhibits an optimum activity at an Al/Ni ratio of 5000:1. As expected the generation 3 catalyst needed more MAO to reach its optimum activity, a trend which was observed for the generation 1 and generation 2 catalysts, due to the increased number of Lewis base sites when going from generation 1 to generation 3. The activity however of **C3** peaked at 440 kg PNB $mol^{-1}Ni.h^{-1}$, which is significantly lower than the optimal activity of **C2**, the generation 2 nickel catalyst. Thus of all three generations, the generation 2 catalyst exhibits the highest activity for the vinyl polymerization of norbornene.

Table 5.1: Activity of DAB G1-G3 Salicylaldimine Nickel catalysts for norbornene polymerization.[a]

	TOF[b]		
Al/Ni	DAB-G1 Ni	DAB-G2 Ni	DAB G3-Ni
1000	37.6	72	0
2000	112	96	188
3000	252	440	340
4000	**328**	520	372
4500	292	**792**	-
5000	252	628	**440**
6000	-	-	312
8000	-	-	280

[a] Reaction conditions: catalyst: 5 µmol Ni; time: 30 min, solvent: toluene; total volume: 25 ml; temperature: room temperature; Monomer:Ni = 5000:1. [b] TOF: kg of polymer produced per mol of Ni per hour.

The periphery of the generation 3 catalyst, **C3**, is much denser in comparison to its lower generation analogues. DFT calculations also showed that the G3 dendrimer ligand (**DL3**) is very flexible. This leads to an increased steric interaction between neighbouring arms that could potentially retard the monomer coordination step. The retardation of monomer coordination could possibly lead to a decrease in the overall rate of polymerization. Hence the G3 catalyst is less active than the G2 catalyst. This is known as a negative dendritic effect. The activity of the G1-G3 salicylaldimine nickel complexes is illustrated graphically in Figure 5.8.

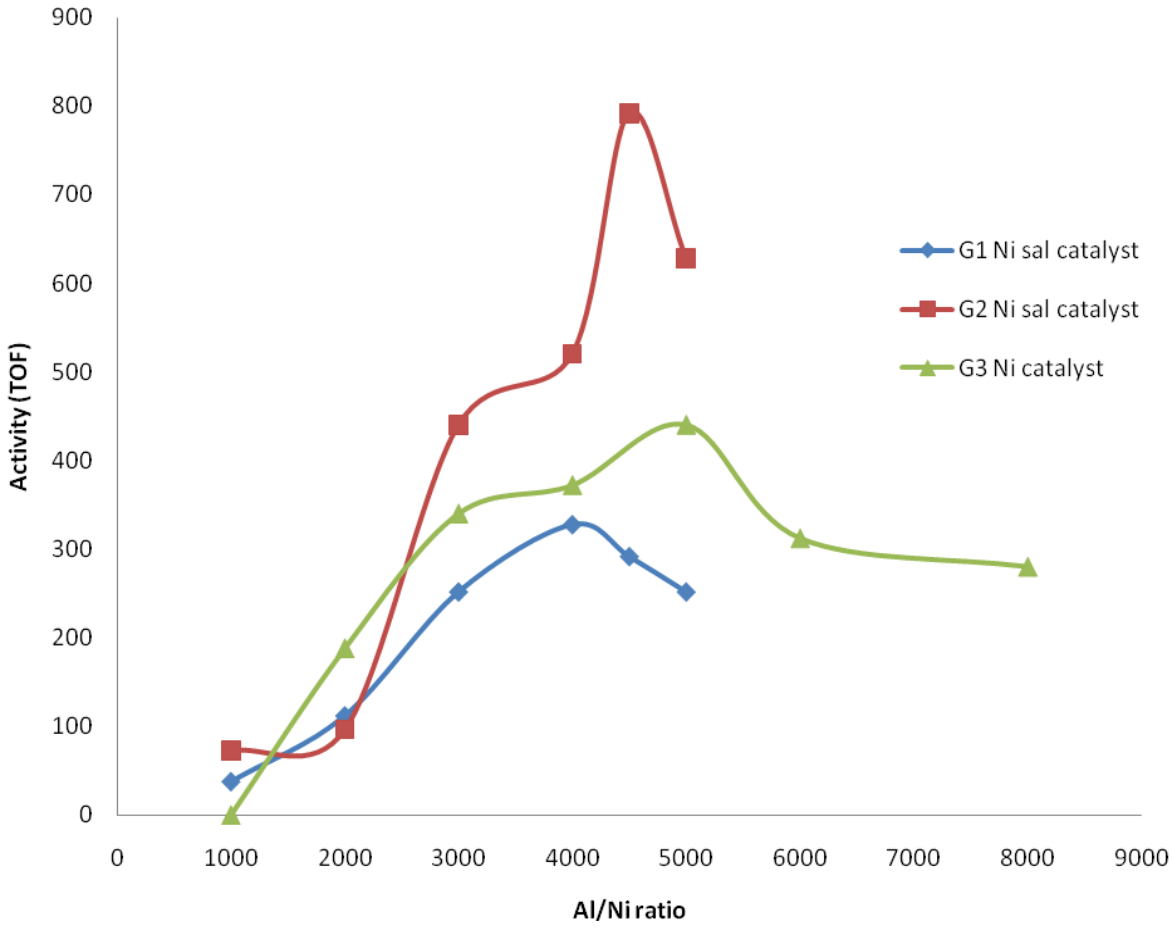

Figure 5.8: The activity of the DAB G1-G3 salicylaldimine nickel catalysts, **C1-C3**.

Yang *et al* [39] reported salicylidene iminato nickel catalysts for the vinyl polymerization of norbornene using MAO as a co-catalyst (Fig 5.9). Each of the four catalysts had different substituents attached to the imine and it was determined that steric hindrance played a major role in the catalyst activity. The catalyst with the highest steric hindrance (**13**) gave the highest catalytic activity. The most active catalyst was further evaluated by varying the catalyst/MAO ratio from 500 :1– 2500:1. The optimal activity for this catalyst was at Al/Ni ratio of 2000:1 with a TOF of 612 kg PNB $mol^{-1}Ni.h^{-1}$, after which the activity decreased on increasing the co-catalyst amount. This mononuclear catalyst is less active when compared to our tetranuclear generation 2 dendrimer salicylaldimine nickel catalyst, **C2**.

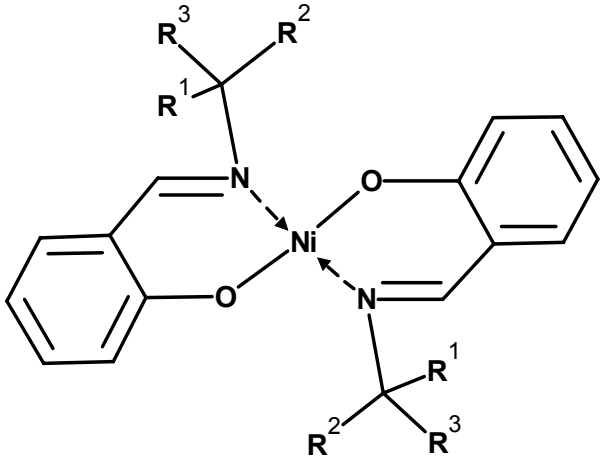

13: $R^1=R^2=Ph$, $R^3=H$;

14: $R^1=CH_3$, $R^2=Ph$, $R^3=H$;

15: $R^1=R^2=R^3=CH_3$;

16: $R^1=R^2=CH_3$, $R^3=H$.

Figure 5.9: Structures of bis-[*N*-(substituted methyl)-salicylideneiminato] nickel complexes synthesized by Yang *et al*. [39]

*5.2.1.2 Generation 1-3 DAB iminopyridyl nickel complexes, **C4-C6**, as norbornene polymerization catalysts.*

The G1-G3 DAB nickel bromide pyridine imine complexes (**C4-C6**) were also evaluated for the vinyl polymerization of norbornene (**C4** is shown in Fig 5.10). The Al/Ni ratio was kept at 2000:1 for all three catalysts and the results are tabulated in Table 5.2, along with the results of the activity of the DAB G1-G3 nickel salicylaldimine catalysts at 2000:1 Al/Ni. For all cases, the amount of nickel was kept the same (5 μmol) irrespective of the catalyst employed.

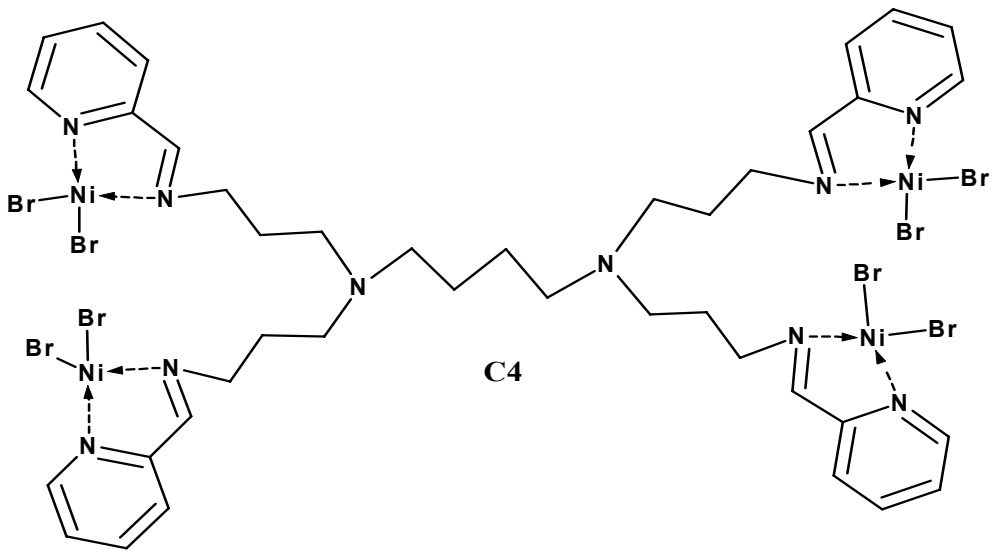

C4

Figure 5.10: Structure of the G1 pyridine imine nickel bromide catalyst, **C4**.

When comparing the activities of the DAB pyridine imine catalysts versus the DAB salicylaldimine nickel catalysts, it is evident that the pyridine imine analogues exhibit higher catalytic activity for the vinyl polymerization of norbornene at the same Al:Ni ratio. This could be due to the fact that for a particular generation of the dendritic catalysts, the iminopyridyl systems have double the amount of active sites than the salicylaldimine

analogues, thus resulting in higher activity. In addition, the nickel centres in the iminopyridyl catalysts are also more accessible than is the case for the salicylaldimine catalysts. This should facilitate the interaction of the substrate with the active centres of the catalyst.

Table 5.2: Activity of DAB G1-G3 Iminopyridyl Nickel and DAB G1-G3 salicylaldimine nickel catalysts at a constant Al/Ni ratio of 2000:1.[a]

Catalyst	Al/Ni	TOF[b]		
		DAB-G1	DAB-G2	DAB G3
DAB-NiBr pyridine imine	2000	300	248	204
DAB-Ni salicylaldimine	2000	112	96	188

[a] Reaction conditions: catalyst: 5 μmol Ni; time: 30 min, solvent: toluene; total volume: 25 ml; temperature: room temperature; Monomer:Ni = 5000:1. [b] TOF: kg of polymer produced per mol of Ni per hour.

In a review by Janiak *et al,*[1] it was reported that catalysts bearing N,O-coordination salicylaldiminato ligands showed activities of at least 10^3 kg PNB $mol^{-1}Ni.h^{-1}$ with a few exceptions. Also from their research, it was concluded that nickel catalysts with N,N-chelating units tend to have a wide range of activities, reaching up to 10^6 kg PNB $mol^{-1}Ni.h^{-1}$, although it can also exhibit rather low activities in some instances.

In Figure 5.11, it can be seen that the activity of the pyridine imine nickel catalysts decreases as the dendrimer generation increases. This is opposite to what is observed for the

salicylaldimine nickel catalysts where the activity increases as the dendrimer generation increases. This occurrence is observed at an Al/Ni ratio of 2000:1. At this stage the overall activity of the pyridine nickel catalysts cannot be compared between various dendrimer generations, because the optimal activities have not yet been established. This can be done by varying the Al/Ni ratio's for the different catalysts. This is proposed as a possible exercise for the future.

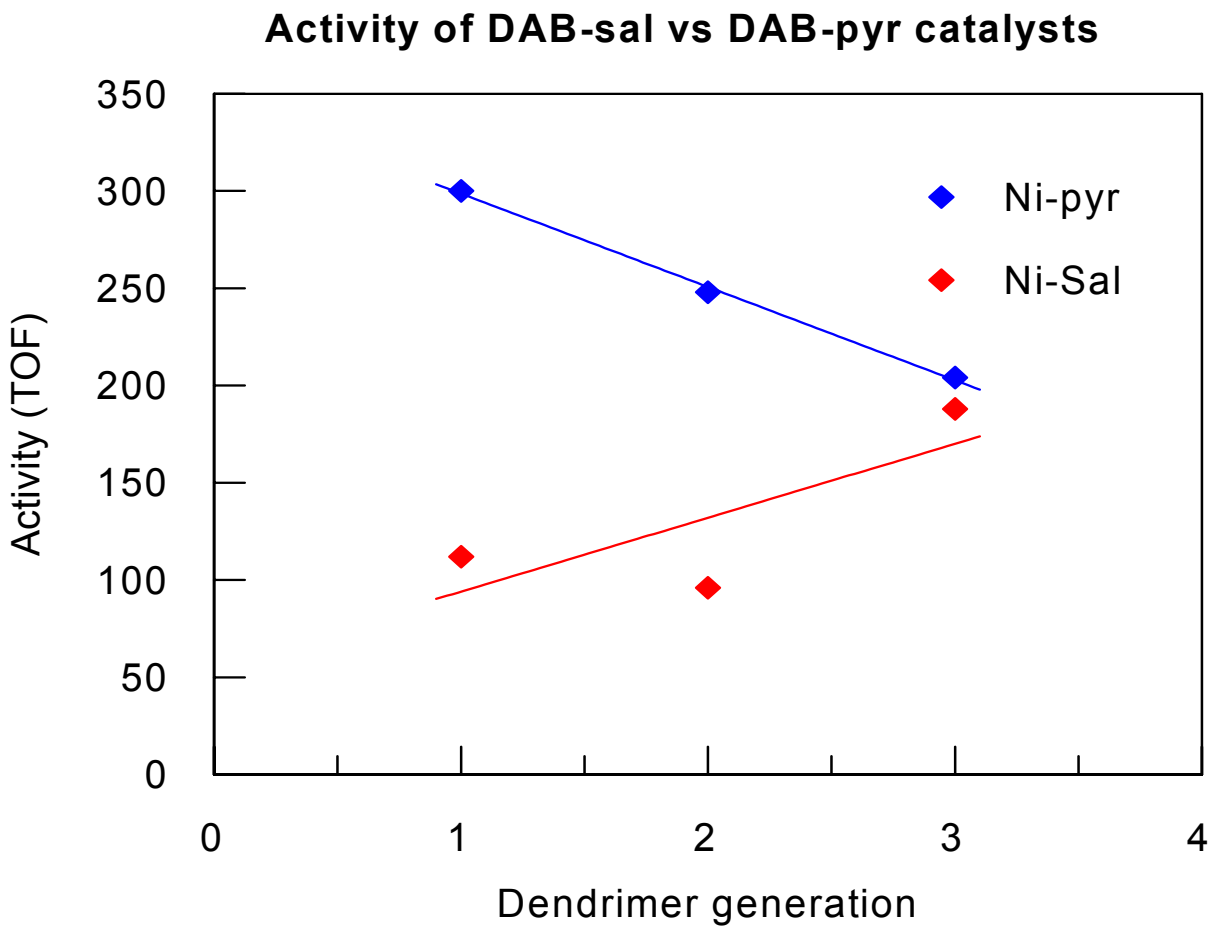

Figure 5.11: The activity of the DAB G1-G3 iminopyridyl vs salicylaldimine nickel catalysts at Al/Ni 2000:1.

5.2.1.3 Generation 1 cyclam-propyl salicylaldimine nickel complex, ***C7****, as a norbornene polymerization catalyst.*

The G1 cyclam-propyl salicylaldimine nickel catalyst, **C7**, was also evaluated in the polymerization of norbornene (Fig 5.12).

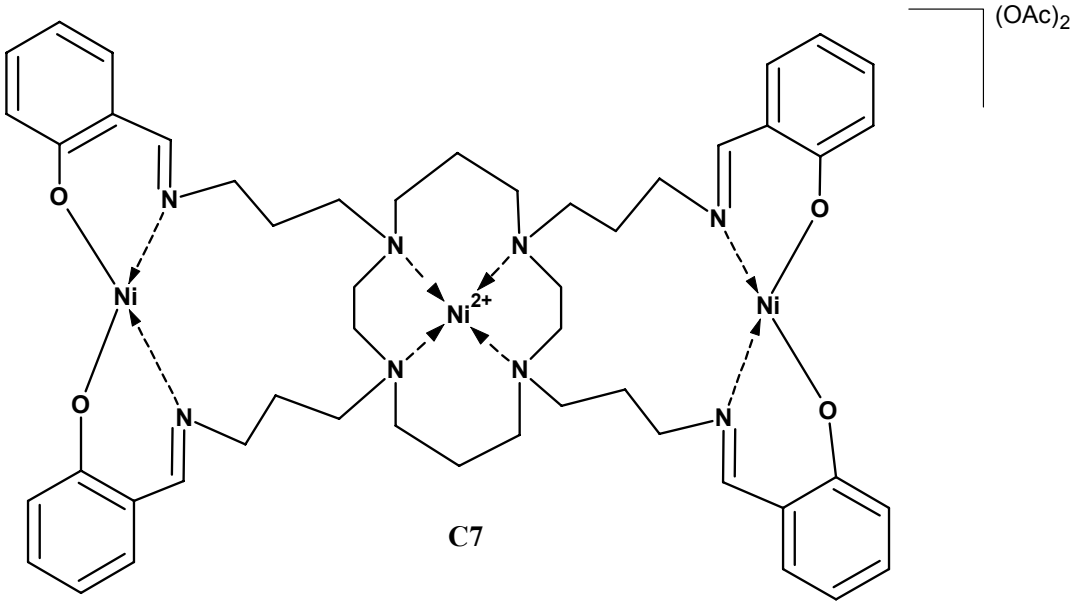

C7

Figure 5.12: Structure of G1 Cyclam salicylaldimine nickel catalyst, **C7**.

The results are tabulated in Table 5.3. The G1 cyclam salicylaldimine nickel catalyst exhibits an optimum activity at Al/Ni ratio of 3000:1 with a TOF of 468 kg PNB $mol^{-1}Ni.h^{-1}$. When compared to the activity of the G1 DAB nickel analogue, the cyclam analogue is the superior catalyst since the optimal activity of the G1 DAB catalyst is only 328 kg PNB $mol^{-1}Ni.h^{-1}$ at Al/Ni 4000:1 (Fig 5.13). The cyclam catalyst has the exact same number of active sites on the periphery as the DAB catalyst, but the former also has an additional nickel centre in the core of the dendrimer.

Table 5.3: Activity of cyclam-propyl G1 salicylaldimine nickel catalyst vs the DAB G1 salicylaldimine nickel analogue for norbornene polymerization.[a]

Al/Ni	Cyclam-G1 Ni TOF[b]	DAB-G1 Ni TOF[b]
1000	0	37.6
2000	198	112
3000	**468**	252
4000	396	**328**
5000	204	252

[a] Reaction conditions: catalyst: 5 µmol Ni; time: 30 min, solvent: toluene; total volume: 25 ml; temperature: room temperature; Monomer:Ni = 5000. [b] TOF: kg of polymer produced per mol of Ni per hour.

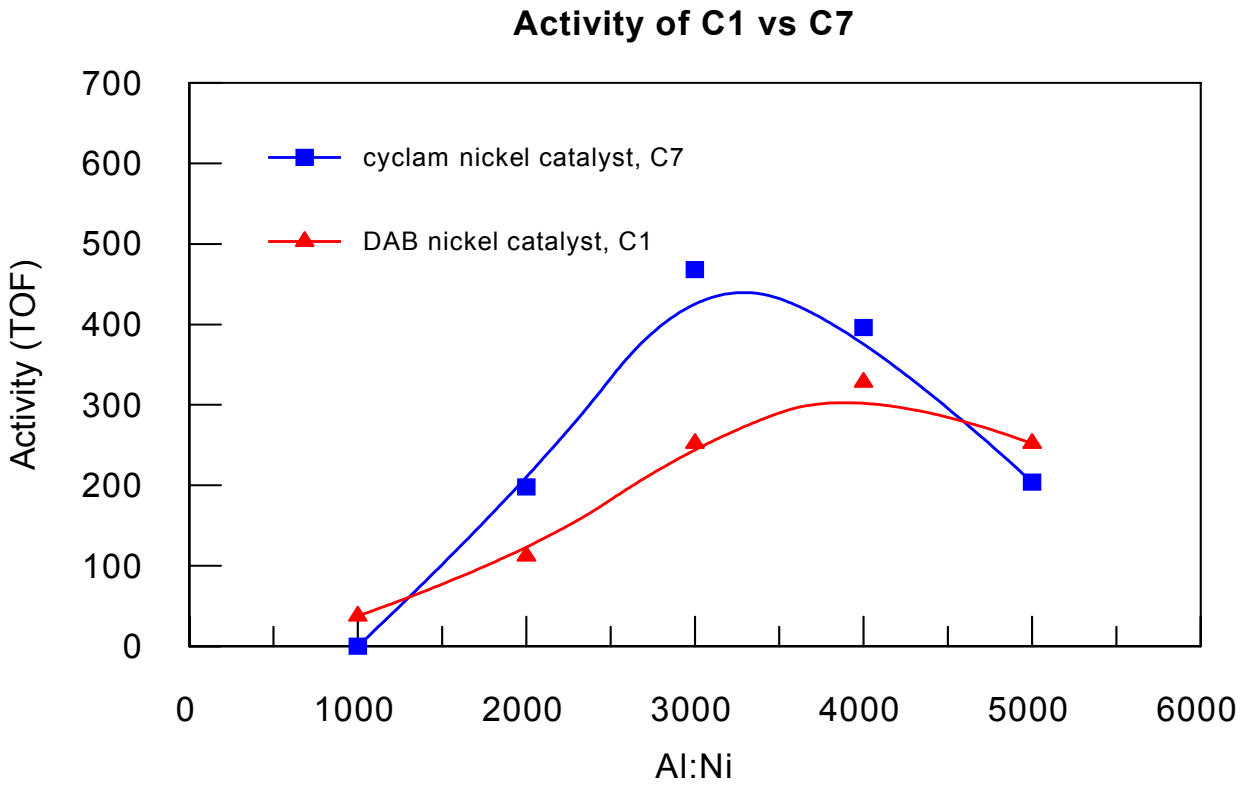

Figure 5.13: The activity of the G1 DAB salicylaldimine nickel **(C1)** vs the G1 Cyclam salicylaldimine nickel dendrimer catalyst **(C7)**.

It should however be noted that when carrying out the comparative study between the DAB and the cyclam nickel precursors, the total nickel concentration was maintained at 5 μmol. An interesting observation is that the cyclam catalyst shows its optimum activity at a lower Al/Ni ratio than the DAB catalyst. As discussed previously, this can be related to the presence of tertiary amine sites in the catalyst molecule. Free tertiary amine sites, being Lewis basic, can potentially interact with the Lewis acidic aluminium co-catalyst. The DAB systems have two free tertiary amine sites available while in the case of the cyclam system, all the tertiary amine sites are already involved in bonding to the central nickel ion. This would lead to the cyclam catalyst requiring a lower amount of the aluminium co-catalyst in order to reach optimum activity, than the DAB catalyst.

Transition metal complexes coordinated to the centre of cyclam-type ligands have been reported as catalysts for various catalytic processes such as oxidation of cycloolefins, [40] atom transfer radical polymerization [41] and the reduction of CO_2.[42]

Ni(II) complexes of cyclam in particular, have been reported as good epoxidation catalysts. Kimura *et al* [43] reported the synthesis of Ni(II) coordinated to a cyclam compound with a triphenylphosphine oxide-unit (Fig 5.14) .

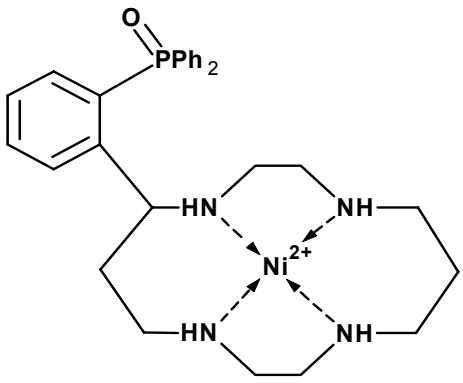

17

Figure 5.14: Ni(II) metal coordinated to a cyclam compound with a triphenylphosphine oxide-pendant.[43]

It was found that this complex was a highly effective catalyst for the epoxidation of trans-stilbene with NaClO as an oxygen source.

Kinnear *et al* [44] reported the results of alkene oxidation using Ni(II) complexes of substituted cyclams (Fig 5.15). Using iodosylbenzene as oxidant, it was found that $Ni(NO_3)_2$ complexes **18-20** catalyzed the epoxidation of various aryl and alkyl substituted alkenes. It was established that the cyclam ligand is crucial to the catalytic process, since it was verified that $Ni(NO_3)_2$ alone does not mediate olefin oxidation under the reaction conditions employed.

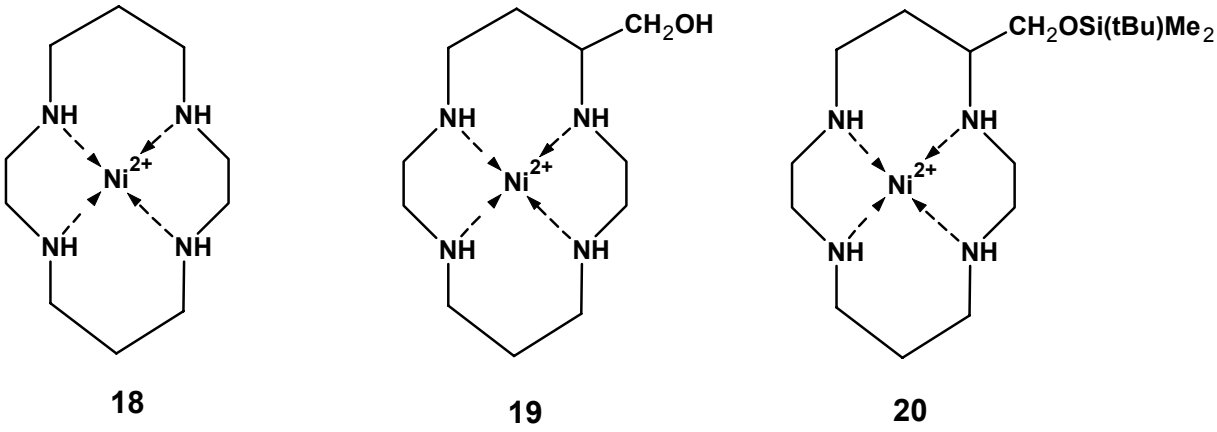

Figure 5.15: Ni(II) complexes of substituted cyclams by Kinnear *et al*.[44]

From the reported literature it is likely that the central metal coordinated to the cyclam core of our dendrimer complex could play a role in the catalytic vinyl polymerization of norbornene.

5.2.2 Characterization of norbornene polymers obtained in the catalytic reactions.

The polymers obtained in the reactions described in the previous section, are not soluble at room temperature in common organic solvents such as dichloromethane, THF,

chloroform and methanol. This is characteristic of vinyl norbornene polymers. These types of polymers are reported in literature to be soluble in cyclohexane, chlorobenzene and in hot trichlorobenzene, and this was also the case for our polymers.

5.2.2.1 FTIR spectroscopy of isolated polymers.

The polymers obtained were characterized by FT-IR (Fig 5.16). The IR spectra revealed no traces of any C=C double bond, which often appear in the region of 1620-1680 cm^{-1}. This eliminates the possibility of ROMP polynorbornene. The ROMP polynorbornene would still have the double bond intact in the backbone of the polymer. As mentioned previously, complexes of nickel tend to polymerize norbornene by the vinyl addition mechanism.

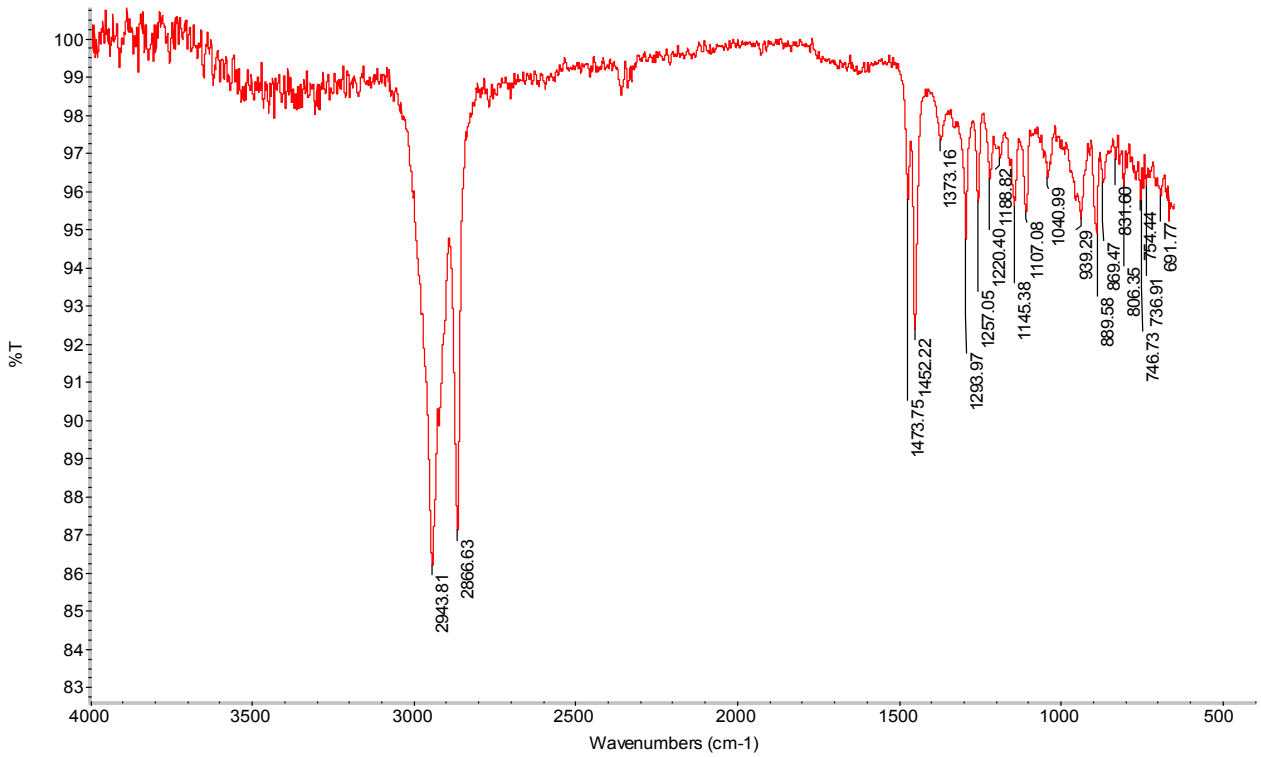

Figure 5.16: FT-IR spectrum of obtained polynorbornene.

5.2.2.2 ^{1}H NMR spectroscopy of isolated polymers.

The polymers obtained are soluble in cyclohexane and hot trichlorobenzene. The ^{1}H NMR was not carried out in cyclohexane since the proton signals of the solvent will mask that of the polymer which is in the same spectral region between 1-3 ppm. Hence the proton NMR was carried out in trichlorobenzene spiked with C_6D_6 at 50 ºC. The sample preparation involves heating the polymer in a 9:1 mixture of trichlorobenzene and deuterated benzene at 110 ºC. After cooling, a viscous liquid was observed, for which a proton NMR spectrum could be obtained at 50 ºC. Figure 5.17 below is an example of a proton NMR spectrum of one of the obtained norbornene polymers obtained. From the ^{1}H NMR spectrum, no trace of the HC=CH protons around 5.1 ppm is present. The presence of the C=C bond usually indicates the formation of polynorbornene by ring opening metathesis polymerization (ROMP).

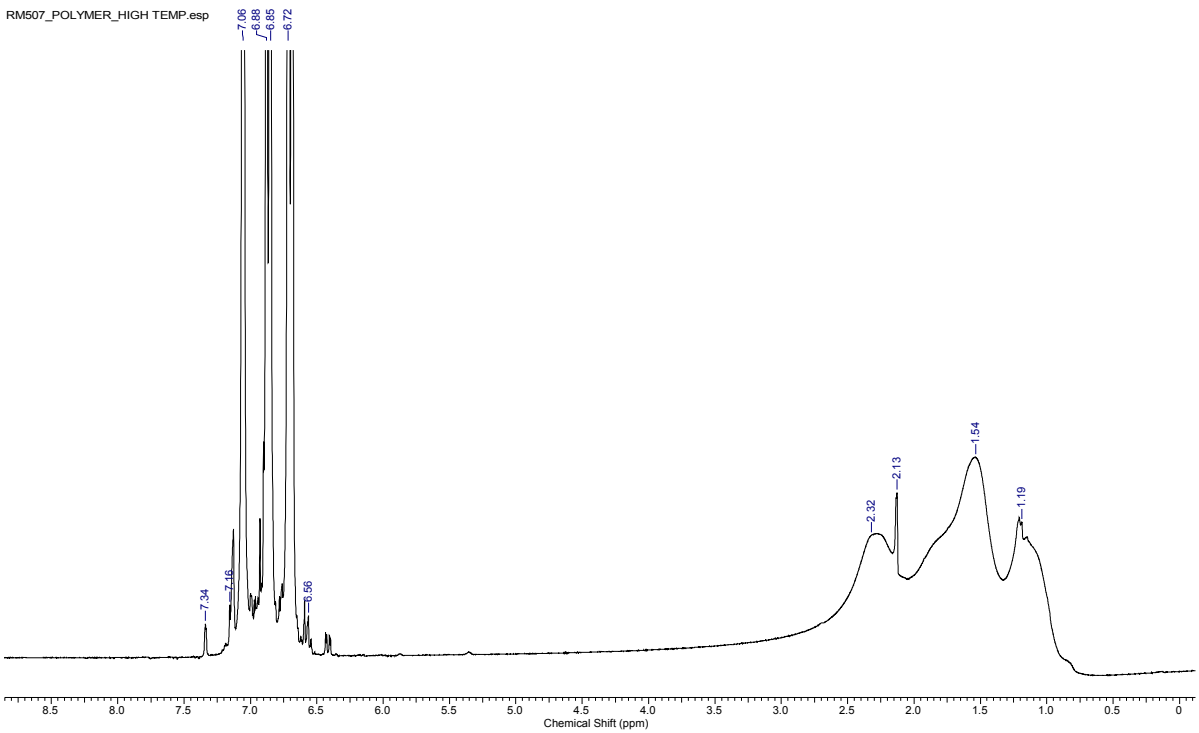

Figure 5.17: ^{1}H NMR spectrum of polynorbornene obtained.

Therefore we can conclude that either vinyl addition polymerization or radical polymerization is occurring. This spectrum also resembles that reported by Yang *et al* [32] who produced polynorbornene via the vinyl polymerization mechanism.

5.2.2.3 TGA and DSC on polymers prepared.

The TGA curve and its derivative shows that the polymers obtained are very stable up to 450 ºC (Fig 5.18). There's an initial weight loss of 5 % from 25-425 ºC, and then a 90 % weight loss from 425-475 ºC. Complete decomposition occurs after 600 ºC. The DTGA curve shows an average decomposition at a temperature of 450 ºC. The TGA curve is similar to that reported by Wang *et al*.[34]

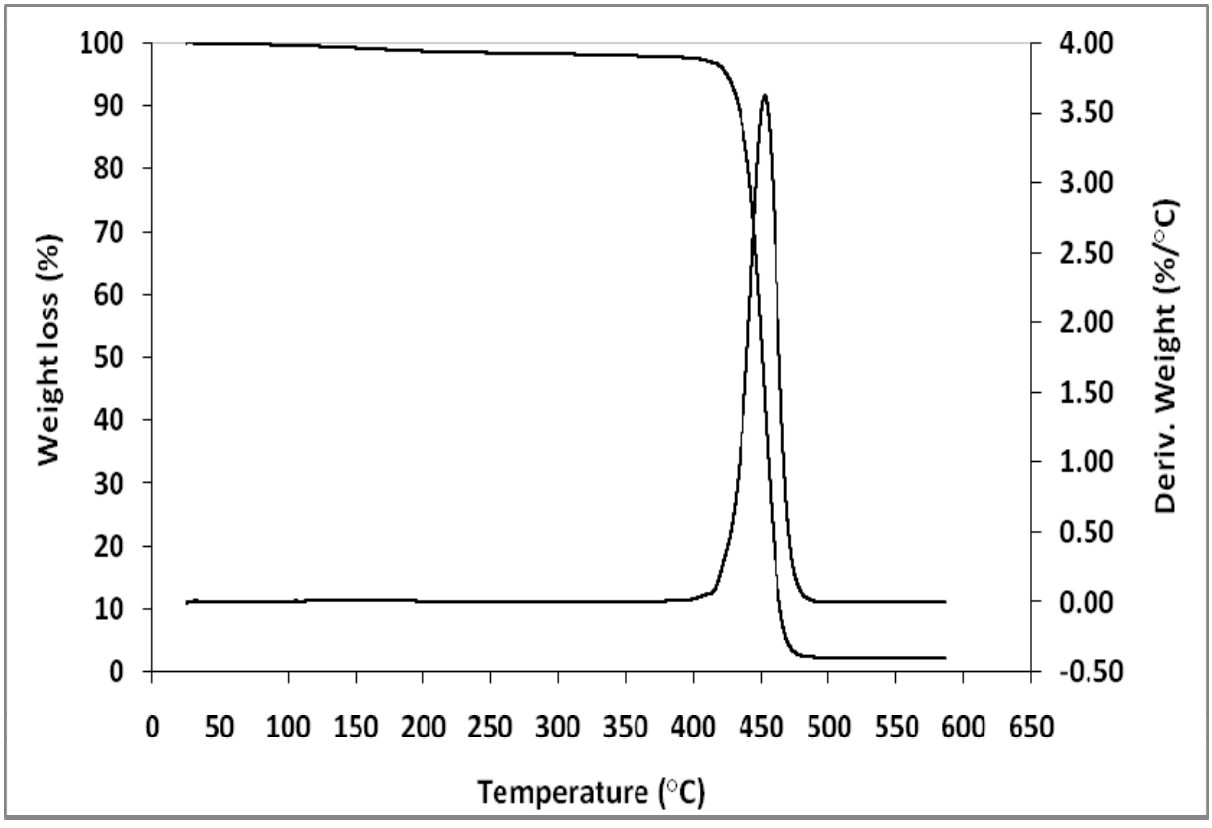

Figure 5.18: TGA/DTGA curves of polynorbornene obtained by catalyst **C3**.

The DSC curve for our polynorbornene does not show an endothermic signal upon heating to 400 ºC. Vinyl norbornene polymers are known to decompose before melting. The polynorbornene obtained from using titanium catalysts, reported by Mi *et al*, [45] exhibited the glass transition temperatures (Tg) in range of 330 – 400 °C, and decomposes without melting.

5.2.2.4 Gel Permeation Chromatography (GPC)

GPC analysis of polynorbornene samples obtained from using catalysts **C1** and **C2** was recently published by us. [36] The molecular weights of the polynorbornene ranged from 5.12 x 10^5 – 7.65 x 10^5 g/mol indicating relatively long polymer chains being present. The polydispersity index (PDI) values ranged from 2.02-2.60 for both **C1** and **C2** at various Al:Ni ratios. The molecular weights and PDI values of the polynorbornene obtained from using **C1-C3** as catalysts are tabulated in Table 5.4.

Table 5.4: GPC analysis results of the polynorbornene obtained using the G1-G3 DAB salicylaldimine nickel catalysts (**C1-C3**) at different Al:Ni ratio's.

Catalyst	Al:Ni = 1500		Al:Ni = 3000		Optimum[a] Al:Ni	
	M_w x 10^5 (g/mol)	PDI	M_w x 10^5 (g/mol)	PDI	M_w x 10^5 (g/mol)	PDI
C1	6.39	2.60	5.12	2.51	7.66	2.02
C2	6.68	2.31	7.38	2.07	7.20	2.31
C3	10.50	2.20	6.27	2.50	8.87	2.0

[a]Al:Ni ratio at which the highest activity was observed. [b] Al:Ni = 2000:1

The polynorbornene molecular weights for polynorbornene obtained from using **C3** as a catalyst range from 6.27×10^5 – 10.50×10^5 g/mol. The PDI values ranged from 2.0-2.5 which compares very well to that of the G1 and G2 Ni salicylaldimine catalysts, **C1** and **C2**. These results indicate that a similar type of polynorbornene is formed irrespective of the catalyst precursor used. However, the G3 Ni salicylaldimine catalyst tends to form slightly longer chain polymers than its lower generation analogues. Since the product obtained is not a low molecular weight oligomer (≤1000 g/mol) which it would have been in the case of cationic or radical polymerization, we can deduce that the product is a vinyl addition norbornene polymer.

The GPC results of the polynorbornene obtained using the G1-G3 nickel bromide iminopyridyl catalysts, **C4-C6**, are shown in Table 5.5. At an Al/Ni ratio of 2000:1, the molecular weights ranged from 10.1×10^5 – 11.1×10^5 g/mol. Also, as the dendrimer generation increases, the molecular weight slightly decreases at Al/Ni ratio 2000:1.

Table 5.5: GPC analysis results of the polynorbornene obtained using the DAB G1-G3 iminopyridyl nickel catalysts (**C4-C6**) at Al:Ni ratio of 2000:1.

Catalyst	Generation	$M_w \times 10^5$ (g/mol)	PDI
C4	1	11.17	2.0
C5	2	10.23	2.1
C6	3	10.11	2.4

The PDI values however increases from 2.0-2.4 with increasing dendrimer generation. When comparing the DAB salicylaldimine to the iminopyridyl catalysts, it can be noted that the pyridine imine analogues, **C4-C6**, forms predominantly higher molecular weight polynorbornenes than the salicylaldimine catalysts, **C1-C3**, under similar conditions.

The GPC results of polynorbornene obtained from the G1-cyclam nickel salicylaldimine catalyst, **C7**, at Al/Ni ratio's ranging from 1000 – 5000:1 is shown in Table 5.6. The G1 cyclam salicylaldimine nickel catalyst yields polynorbornenes with molecular weights ranging from 7.61 x 10^5 – 11.1 x 10^5 g/mol. While the Al/Ni ratio shows no trend with regard to the molecular weights obtained, the PDI is inversely proportional to the Al/Ni ratio, ranging from 2.8-2.0 going from 2000 to 5000:1.

Table 5.6: GPC results of polynorbornene obtained from using the cyclam-propyl G1 salicylaldimine nickel complex (**C7**) as a catalyst.

Al/Ni	**M_w x 10^5 (g/mol)**	**PDI**
1000	- [a]	- [a]
2000	10.30	2.8
3000	7.61	2.3
4000	9.66	2.1
5000	11.07	2.0

[a] No product obtained at Al/Ni ratio of 1000:1.

5.2.3 Proposed catalytic cycle of the Schiff base catalysts in the vinyl polymerization of norbornene.

A proposed catalytic cycle for the polymerization of norbornene using a salicylaldimine nickel catalyst is shown in Fig 5.19. This involves the alkylation of the catalyst by MAO followed by â-hydride elimination, to obtain the active catalytic species.

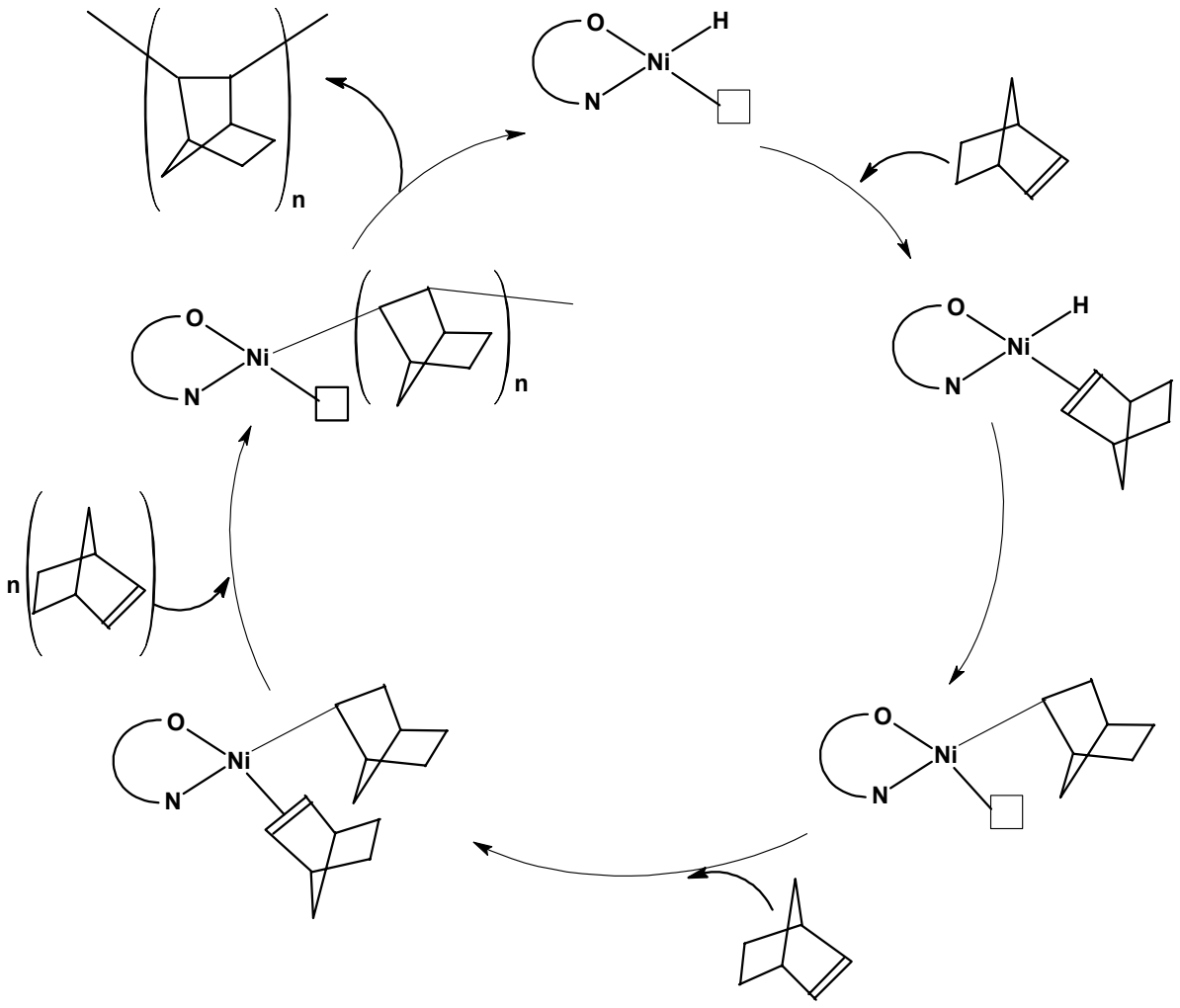

Figure 5.19: Catalytic cycle for the vinyl polymerization of norbornene using the DAB salicylaldimine catalysts.

Monomer insertion follows which initiates the chain propagation step. Chain termination occurs during which the polynorbornene is released.

It is assumed that the cyclam based catalyst follows the same mechanism as the DAB catalysts. Hence, a possible reason why the cyclam catalyst exhibits higher activity than the DAB catalyst could be due to the fact that the former catalyst has a higher concentration of local active sites than the latter.

5.3 Conclusion

NMR and IR spectra of the obtained polynorbornene show that no ROMP occurs in the polymerization processes but that the reaction proceeds via a 2,3-vinyl addition mechanism. The molecular weights of the obtained polynorbornenes are relatively high, ranging from 10^5 to 10^6 g/mol. This means that the polymerization is not a typical cationic or radical polymerization, which usually results in low molecular weights (molecular weight < 1000 g/mol) and low yields because of rearrangements and chain transfer reactions. We can conclude that these types of nickel metallodendrimer catalysts polymerize norbornene through the vinyl-addition coordination mechanism.

Three different types of Ni catalysts were tested, a) the DAB G1-G3 salicylaldimine complexes, b) the DAB G1-G3 iminopyridyl complexes and c) the cyclam G1 salicylaldimine complex. For the DAB salicylaldimine catalysts, a clear dendritic effect was observed. The G2 catalyst, **C2**, proved to have the highest activity of all three generations.

The iminopyridyl complexes exhibit higher activities than the salicylaldimine complexes at an Al/Ni ratio of 2000:1, due to the higher local concentration of metal active

sites for the iminopyridyl catalysts as compared to the salicylaldimine analogues which have half the active sites. The optimum activities for the iminopyridyl catalysts have not yet been established. When the activity of DAB-G1 salicylaldimine dendrimer catalyst, **C1**, was compared to that of its cyclam dendrimer analogue, **C7**, it was found that the cyclam catalyst exhibits higher activity at its optimum Al/Ni ratio of 3000:1. Since the catalytic mechanism for norbornene polymerization using the cyclam catalyst is expected to be similar to that for the DAB catalyst, it is assumed that the higher concentration of active local sites in the cyclam catalyst is the possible reason why higher activity is achieved.

5.4 Experimental

All work involving moisture and air sensitive compounds such as MAO was carried out using standard Schlenk techniques. Infrared spectra were recorded on a Nicolet Avatar 330 FT-IR spectrophotometer, using an ATR accessory with a ZnSe crystal plate. ^{1}H NMR (300 MHz and 400 MHz) and ^{13}C NMR (75 MHz) spectra were recorded on a Varian VNMRS 300 MHz and a Varian Unity Inova 400 MHz spectrometer, using tetramethylsilane as an internal standard. TGA data were determined with a Q500 Thermogravimetric analyzer and DSC analysis was done using a Q100 differential scanning calorimeter. GPC analysis was done at Sasol Polymers Ltd using a WATERS PL GPC 220 instrument with 1,2,4-trichlorobenzene as a solvent at 160 ºC and calibrated against polystyrene standards. Toluene was dried by refluxing over sodium/benzophenone. Norbornene was obtained from Sigma Aldrich and dried over calcium hydride before being distilled. A 5M norbornene stock solution in toluene was prepared and used for the polymerization reactions.

Methylaluminoxane (MAO), a 10 % solution in toluene, was obtained from Sigma Aldrich and used without any further purification.

Typical Polymerization Procedure:

The amount of catalyst corresponding to 5 ìmol of nickel was added to an appropriate amount of dry toluene in a Schlenk tube, under nitrogen. 5 ml (25 mmol) of a 5M norbornene in toluene solution was added to the reaction vessel. The required amount of MAO (1.7 M, 10 %) was then added to the reaction mixture, to initiate the polymerization. The mixture was allowed to stir for 30 minutes at room temperature. The polymerization was stopped by adding the reaction solution to 200 ml of acidic methanol (95:5). A white solid precipitated out of solution. The polymers were filtered and then dried in the oven for 24 hours. The norbornene:nickel ratio was 5000:1 and the total volume of the reaction mixture was 25 ml.

5.5 References

[1] F. Blank, C. Janiak, *Coord. Chem. Rev.,* 253, **2009**, 827.

[2] D. Mery, D. Astruc, *J. Mol. Catal. A: Chem.* 227, **2005**, 1.

[3] C. Janiak, P. G. Lassahn, *J. Mol. Catal. A: Chem.*, 166, **2001**, 193.

[4] J. L. Brumaghim, G. S. Girolami, *Organometallics,* 18, **1999**, 1923.

[5] P. A. Bertin, D. Smith, S. T. Nguyen, *Chem. Commun*., **2005**, 379.

[6] S. Hayano, Y. Takeyama, Y. Tsunogae, I. Igarashi, *Macromolecules,* 39, **2006**, 4663.

[7] A. M. R. Galletti, G. Pampaloni, A. D'Alessio, Y. Patil, F. Renili, S. Giaiacopi, *Macromol. Rapid Commun.,* 30, **2009**, 1762.

[8] B. Duz, C. K. Elbistan, A. Ece, F. Sevin, *Appl. Organomet. Chem., 23*, **2009**, 359.

[9] K. Nomura, Y. Watanabe, S. Fujita, M. Fujiki, H. Otani, *Macromolecules, 42*, **2009**, 899.

[10] Y. Nishihara, S. Izawa, Y. Inque, Y. Nakayama, T. Shiono, K. Takagi, J. *Pol. Sci. A: Pol. Chem.,* 46, **2008**, 3314.

[11] X. Meng, G. Tang, G. Jin, *Chem. Commun.,* **2008**, 3178.

[12] Y. Nakayama, N. Maeda, H. Yasuda, T. Shiono, *Polym. Int.,* 57, **2008**, 950.

[13] H. Liang, J. Liu, X. Li, Y. Li, *Polyhedron*, 23, **2004**, 1619.

[14] J. P. Kennedy, H. S. Makowski, *J. Macromol. Sci. Chem. A1,* **1967**, 345.

[15] Y. Jang, H. Sung, H. Kwag, *Eur. Pol. J.,* 42, **2006**, 1250.

[16] S. Ahmed, S.A. Bidstrup, P.A. Kohl, P.J. Ludovices, *J. Phys. Chem. B*, 102, **1998**, 9783.

[17] C. Janiak, P.G. Lassahn, *Macromol. Rapid Commun.,* 22, **2001**, 479.

[18] T.F.A. Haselwander, W. Heitz, S.A. Krügel, J.H. Wendorff, *Macromol. Chem. Phys.,* 197, **1996**, 3435.

[19] S. Rush, A. Reinmuth, W. Risse, *Macromolecules,* 30, **1997**, 7375.

[20] N. Seehof, C. Mehler, S. Breuning, W. Risse, *J. Mol. Catal.,* 76, **1992**, 219.

[21] N.R. Grove, P.A. Kohl, S.A.B. Allen, S. Jayaraman, R. Shick, *J. Polym. Sci., Part B: Polym. Phys.,* 37, **1999**, 3003.

[22] T.F.A. Haselwander, W. Heitz, S.A. Krügel, J.H. Wendorff, *Macromol. Chem. Phys.,* 197, **1996**, 3435.

[23] T.F.A. Haselwander, W. Heitz, S.A. Krügel, J.H. Wendorff, *Macromolecules,* 30, **1997**, 5345.

[24] K.D. Doorkenoo, P.H. Pfrom, M.E. Rezac, *J. Polym. Sci., Part B: Polym. Phys.,* 36, **1998**, 797.

[25] C. Zhao, M.R. Ribeiro, M.F. Portela, S. Pereira, T. Nunes, *Eur. Polym. J.,* 37, **2001**, 45.

[26] J. A. Olson, T. A. P. Paulose, P Wennek, J.W. Quail, S. R. Foley, *Inorg. Chem. Commun.,* 11, **2008**, 1297.

[27] T. J. Woodman, Y. Sarazin, S. Garratt, G. Fink, M. Bochmann, *J. Mol. Catal. A: Chem.,* 235, **2005**, 88.

[28] Y. Sato, Y. Nakayama, H. Yasuda, *J. Organomet. Chem.,* 689, **2004**, 744.

[29] J. Ni, C. Lu, Y. Zhang, Z. Liu, Y. Mu, *Polymer,* 49, **2008**, 211.

[30] W. Jia, Y. Huang, Y. Lin, G. Jin, *Dalton Trans*, **2008**, 5612.

[31] J. Chen, Y. Huang, Z. Li, Z. Zhang, C. Wei, T. Lan, W. Zhang, *J. Mol. Cat. A: Chem.,* 259, **2006**, 133.

[32] H. Yang, Z. Li, W. Sun, *J. Mol. Cat. A: Chem.,* 206, **2003**, 23.

[33] F. Bao, X. Lu, B. Kang, Q. Wu, *Eur. Pol. J.,* 42, **2006**, 928.

[34] Y. Wang, S. Lin, F. Zhu, H. Gao, Q. Wu, *Eur. Pol. J.,* 44, **2008**, 2308.

[35] F. Liu, H. Gao, K. Song, Y. Zhao, J. Long, L. Zhang, F. Zhu, Q. Wu, *Polyhedron,* 28, **2009**, 673.

[36] R. Malgas-Enus, S. F. Mapolie, G. S. Smith, *J. Organomet. Chem.,* 693, **2008**, 2279.

[37] J.J. Eisch, in: E.W. Abel, F.G.A. Stone, G. Wilkinson (Eds.), *Comprehensive Organometallic Chemistry II*, Pergamon Press, **1995**, 431.

[38] F.A. Cotton, G. Wilkinson, C.A. Murillo, M. Bochmann, in: *Advanced Inorganic Chemistry, 6th ed.*, John Wiley and Sons, New York, **1999,** 196.

[39] H. Yang, W. Sun, F. Chang, Y. Li, *Appl. Catal. A: Gen.,* 252, **2003**, 261.

[40] Sujandi, S. Han, D. Han, M. Jin, S. Park, *J. Catal.,* 243, **2006**, 410.

[41] N. V. Tsarevsky, W. A. Braunecker, W. Tang, S. J. Brooks, K. Matyjaszewski, G. R. Weisman, E. H. Wong, *J. Mol. Catal. A: Chem.,* 257, **2006**, 132.

[42] M. Fujihira, Y. Hirata, K. Suga, *J. Electroanal. Chem.,* 292, **1990**, 199.

[43] E. Kimura, Y. Kodama, M. Shionoya, T. Koike, *Inorg. Chim. Acta,* 246, **1996**, 151.

[44] J. F. Kinneary, T. R. Wagler, C. J. Burrows, *Tetrahedron Lett.,* 29, **1988,** 877.

[45] X. Mi, D. Xu, W. Yan, C. Guo, Y. Ke, Y. Hu, *Polymer Bulletin,* 47, **2002**, 521.

Chapter 6:

Metallodendrimers as catalysts in the transformation of á-olefins.

6.1 Introduction to á-Olefin Transformations.

á-Olefins can undergo many transformations depending on the reagents, the catalyst and the reaction conditions employed. Some of these transformations include hydrogenation, cracking, cyclization, isomerization, oligomerization and polymerization reactions. [1] Below follows a brief overview of olefin oligomerization and isomerization reactions, which is of relevance to this study.

6.1.1 Ethylene Oligomerization.

Ethylene oligomers are the primary source of á-olefins, which find application in the preparation of detergents, synthetic lubricants, plasticizers, alcohols and some copolymers. Therefore this process is of great interest to industry and academic researchers in the field. Major commercial processes for ethylene oligomerization using homogeneous catalysts have been developed by companies like Shell (SHOP) and IFP (Dimersol and Alfabutol).[2-8] Here we discuss a few examples of nickel catalysts employed in the oligomerization of ethylene.

Adewuyi *et al* synthesized nickel(II) complexes chelated by 2-quinoxalinyl-6-iminopyridines (Fig 6.1) and evaluated these complexes in the oligomerization of ethylene.[9] Upon activation with Et_2AlCl, all the complexes showed moderate to good catalytic activity for the dimerization and trimerization of ethylene at low temperature (20-40 ºC) and 10 atm ethylene. Due to the higher solubility of the nickel bromide precursors in toluene, their catalytic performance for ethylene oligomerization is slightly higher than the corresponding nickel chloride precursors.

Phenyl-substituted pyrazolylimine ligands and their nickel(II) complexes (Fig 6.2) were successfully synthesized and characterized by Wang *et al.*[10]

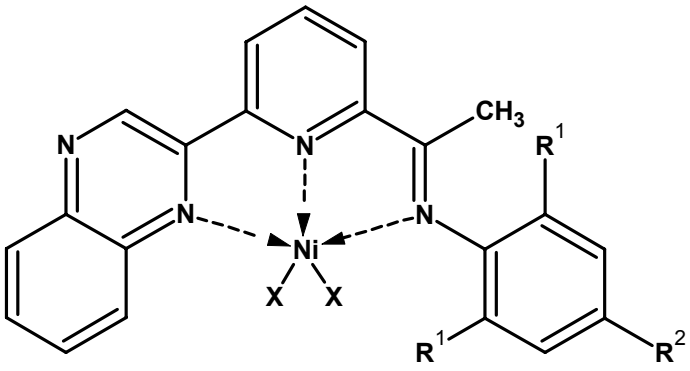

	1	2	3	4	5	6	7	8	9	10	11	12
R^1	Me	Et	i-Pr	Me	F	Cl	Me	Et	i-Pr	Me	F	Cl
R^2	H	H	H	Me	H	H	H	H	H	Me	H	H
X	Cl	Cl	Cl	Cl	Cl	Cl	Br	Br	Br	Br	Br	Br

Figure 6.1: Nickel complexes synthesised by Adewuyi *et al*.[9]

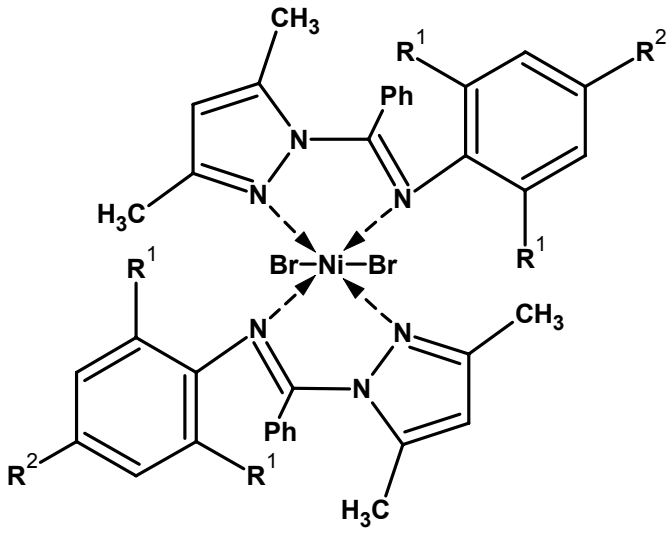

13: R^1=R^2=H

14: R^1=H, R^2=OCH_3

Figure 6.2: Pyrazolyl imine nickel complexes synthesized by Wang *et al*.[10]

Activities of up to 896 kg oligomer.mol $Ni^{-1}.h^{-1}$ were achieved by varying reaction conditions such as temperature and Al/Ni ratio. Catalyst selectivity ranged from C_4-C_{14} oligomers, with the C_4 fraction being the major product in most cases.

Sun *et al* [11] selectively oligomerized ethylene to butene and hexene using N-(2-pyridyl) benzamide-based nickel catalysts (Fig 6.3) and methylaluminoxane (MAO) as a co-catalyst. Most of the complexes showed good activity using an Al/Ni molar ratio in the range of 300:1–1000:1. Complex **16** showed the highest catalytic activity of 494 kg oligomer.mol Ni^{-1}.h at the Al/Ni molar ratio of 1000:1 at 22 ºC.

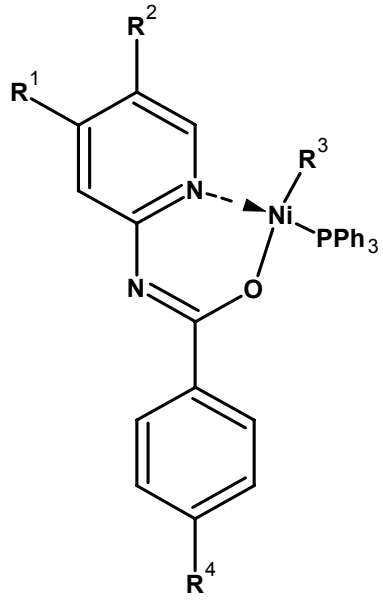

	15	16	17	18	19	20	21	22
R^1	H	Me	H	H	Me	H	H	H
R^2	H	H	NO_2	H	H	NO_2	NO_2	NO_2
R^3	Naph	Naph	Naph	Naph	Naph	Naph	Ph	Ph
R^4	H	H	H	NO_2	NO_2	NO_2	H	NO_2

Figure 6.3: Pyridyl benzamide nickel complexes synthesized by Sun *et al*.[11]

A series of sterically and electronically modulated iminopyridyl Ni(II) bimetallic catalysts synthesized by Bahuleyan *et al* [12] showed high activity for ethylene oligomerization when combined with various co-catalysts (EASC = ethylaluminum sesquichloride ($EtAlCl_2.Et_2AlCl$), MAO = methylaluminoxane, MADC = methylaluminum dichloride). All catalysts (Fig 6.4) showed high selectivity towards C_4, in a range of 72–91 % and yielded small amounts of polyethylene around 1–10 %. Small amounts of C_6-C_{20} oligomers were also observed, and the longer chain oligomers reached a molecular weight of up to 10 000 g/mol. They concluded that catalytic activity was highly influenced by steric and electronic substituents and that the methoxy-substituted catalyst with i-Pr groups in the aryl ring and only hydrogen on the pyridyl ring showed the highest activity.

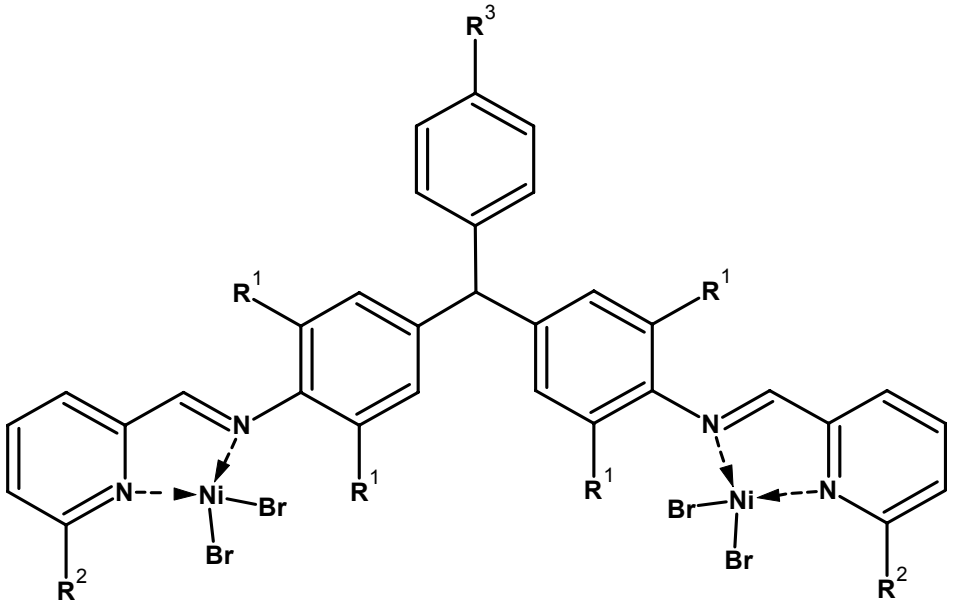

	23	24	25	26	27	28	29	30	31	32	33
R^1	Me	Et	i-Pr	Me	Et	i-Pr	i-Pr	i-Pr	Me	Et	i-Pr
R^2	H	H	H	H	H	H	Me	Ph	H	H	H
R^3	H	H	H	NO_2	NO_2	NO_2	NO_2	NO_2	OCH_3	OCH_3	OCH_3

Figure 6.4: Iminopyridyl Ni(II) bimetallic catalysts synthesized by Bahuleyan *et al.*[12]

Shen *et al* reported a series of novel N^N^N tridentate neutral nickel complexes (Fig 6.5), activated by Et_2AlCl as ethylene oligomerization catalysts with moderate activity.[13] An increase in the steric hindrance in the catalysts, led to a decrease in the catalyst activity. The highest activity obtained was 625 kg oligomer.mol $Ni^{-1}.h^{-1}$ when ethylene pressure was increased from 1 atm to 10 atm. Butenes were the major product with traces of hexenes also formed.

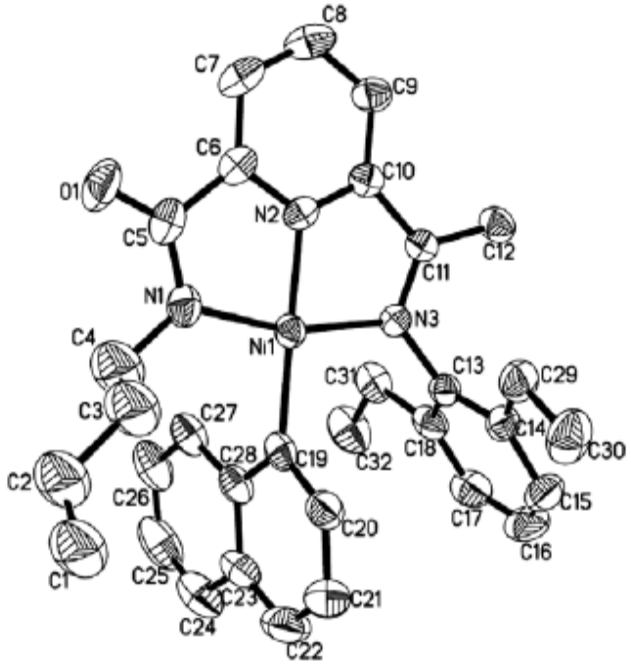

Figure 6.5: Molecular structure of one of the catalysts synthesized by Shen *et al.* [13] Thermal ellipsoids are shown at 30 % probability. Hydrogen atoms have been omitted for clarity.

Another source of á-olefins is the Fischer-Tropsch process. The Fischer-Tropsch reaction converts a mixture of hydrogen and carbon monoxide (derived from coal) to liquid fuels. The product stream from this process contains a mixture of even carbon number olefins (C_4, C_6, C_8 etc) as well as uneven carbon number olefins (C_5, C_7, C_9 etc). Production of such

á-olefins with odd carbon numbers is unique to South Africa, obtained from the Fischer-Tropsch process as operated by SASOL.[14]

6.1.2 Olefin Isomerization.

The isomerization of á-olefins is an important catalytic process to upgrade refinery and petrochemical feedstocks. The olefin content (particularly, pentene and hexene) in most of FCC naphthas is higher than 40 vol. %, with *n*-olefins being more than 30 % (Fig 6.6). As a consequence, different industrial processes have recently attracted great interest for converting C_5 and C_6 olefins to value-added products. The use of branched isomers and internal olefins in fuels usually results in higher octane number and lower Reid vapour pressure (RVP).[1]

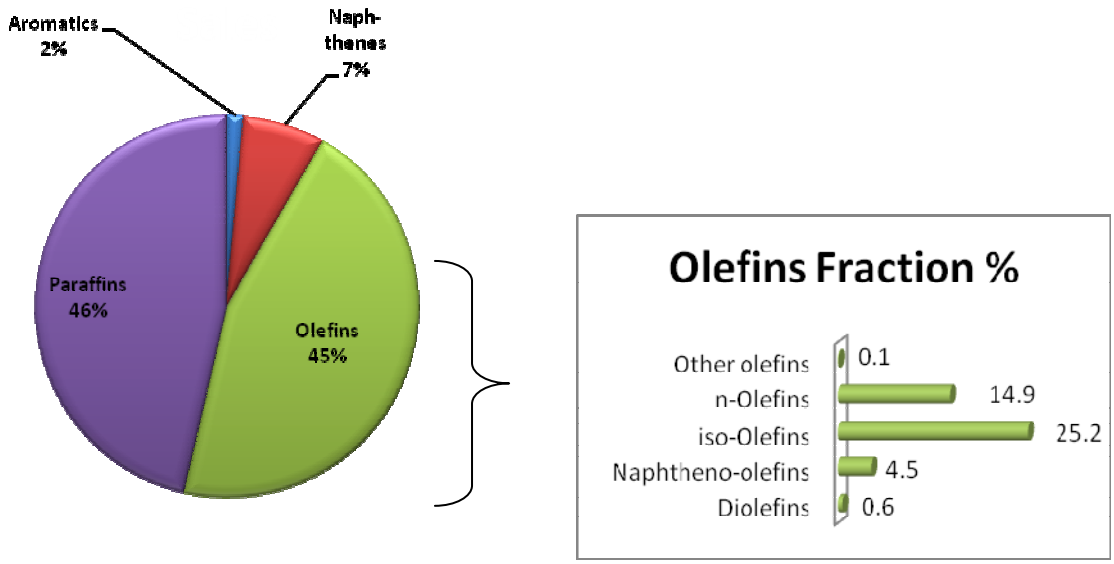

Figure 6.6: Typical composition of a light FCC naphtha (wt.%) showing the content of different olefins. C_5 linear olefins account for ca. 10 % wt.[15]

Alkene isomerization via double bond migration is catalyzed by many complexes of transition metals such as Fe, Co, Pd, Ru, Ni, Rh and Ti.[15]

Kamiguchi *et al* [16] reported the catalytic isomerization of 1-hexene to 2-hexene by halide clusters of Nb, Mo, Ta and W possessing an octahedral metal core. The following clusters were synthesised and tested for olefin isomerization; $[(Nb_6Cl_{12})Cl_2(H_2O)_4]\cdot 4H_2O$ (**34**), $[(Nb_6Br_{12})Br_2(H_2O)_4]\cdot 4H_2O$ (**35**), $(H_3O)_2[(Mo_6Cl_8)Cl_6]\cdot 6H_2O$ (**36**), $[(Ta_6Cl_{12})Cl_2(H_2O)_4]\cdot 4H_2O$ (**37**), $(H_3O)_2[(W_6Cl_8)Cl_6]\cdot 6H_2O$ (**38**), and Re_3Cl_9 (**39**). The results are shown in Fig 6.7. This clearly shows that the Nb cluster (**34**) exhibits the best conversion of 1-hexene to 2-hexene under the same reaction conditions. However, Nb metal on its own, exhibits no catalytic activity towards isomerization of 1-hexene. The activity of the other metal clusters tested is quite low compared to cluster **34**, with the Re cluster also exhibiting no catalytic activity.

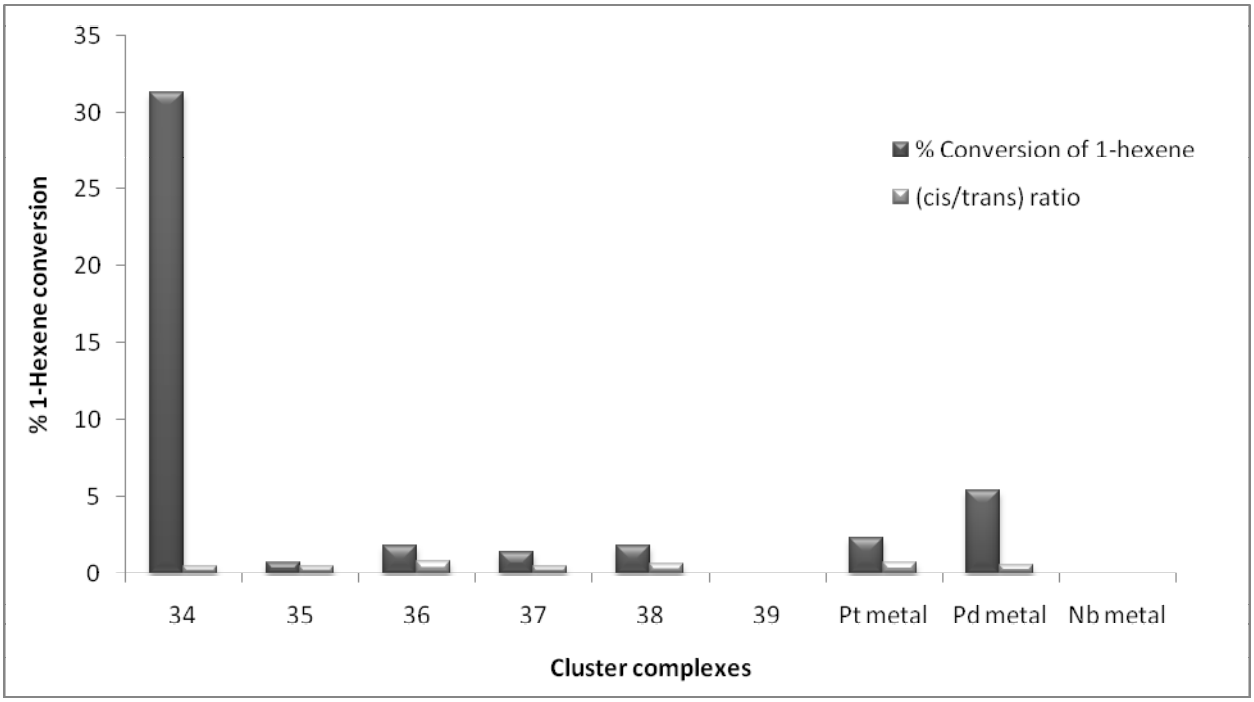

Figure 6.7: Isomerisation of 1-hexene to 2-hexene by halide clusters reported by Kamiguchi *et al*.[16]

The catalytic activity varied with the catalyst employed; however, the *cis/trans* selectivities of 2-hexene remained in a relatively narrow range and the ratios are approximately in agreement with that obtained via the process of thermal equilibrium (0.77 at 250 ºC). [17] They concluded that while molecular halide clusters of Nb, Mo, Ta and W are stable complexes, they showed no catalytic activity until preliminary treatment of the catalysts at 250 ºC for one hour. This resulted in active catalysts for double bond isomerization of the olefin.

Yue *et al* reported the successful isomerization of olefins using hydride-complexes of ruthenium as catalysts.[18] The Ru-H type complexes synthesized were $RuH(NO)(PPh_3)_3$ (**40**), $RuHCl(PPh_3)_3$ (**41**), $RuHCl(CO)(PPh_3)_3$ (**42**), $RuH(CH_3COO)(PPh_3)_3$ (**43**) and $RuH_2(CO)(PPh_3)_3$ (**44**). Only $RuHCl(PPh_3)_3$ (**41**) was further screened for 1-hexene and 1-octadecene isomerization. The influence of temperature, reaction time and catalyst concentration on 1-hexene isomerization was studied and it was found at 120 ºC conversion of 1-hexene to 2- and 3-hexene reached 97.54 %.

The 1-octadecene isomerization by the same catalyst at 180 ºC gave the conversion of 1-octadecene above 94.6 % using a 1:200 ratio of catalyst:substrate. A few differences in the isomerization reaction of 1-hexene and 1-octadecene were observed. Firstly, the reaction temperature for isomerization was higher for 1-octadecene than for 1-hexene while at lower temperatures, 1-octadecene isomerization did not occur. Secondly, solvents such as toluene and benzene were necessary for 1-hexene isomerization to occur, while 1-octadecene isomerization could proceed in the absence of solvent. They concluded that the catalytic activity was closely related to the coordination environment of the central metal, ligand properties and the nature of the substrate.

In this chapter we discuss the activity of some of our synthesised nickel metallodendrimer catalysts (**C1-C7**) in the transformation of á-olefins, namely ethylene oligomerization and 1-pentene isomerization. The effect of dendrimer generation as well as different ligand systems, are reported. The behaviour of the more flexible, dumbbell-shaped dendrimers (DAB range) versus the rigid cyclic cored dendrimers (cyclam) is also discussed. The reaction conditions were varied to find the optimum conditions for the highest catalytic activity.

6.2 Results and Discussion.

6.2.1 Ethylene Oligomerization.

The ethylene oligomerization reactions were carried out in a 300 ml stainless steel autoclave. $EtAlCl_2$ was used as a co-catalyst. The reaction conditions were kept constant except for the Al:Ni ratios which ranged from 1000:1 – 5000:1. The ethylene pressure was kept constant at 5 atm. All reactions were performed at room temperature. The metal concentration was kept constant irrespective of the catalyst precursor employed. These reaction conditions are typical of those reported in the literature for ethylene oligomerization reactions.[9-11]

*6.2.1.1 Catalytic activity and selectivity of nickel metallodendrimer catalysts, **C1-C7**, at a constant Al/Ni ratio of 2000:1.*

Catalysts **C1-C7** were evaluated in the oligomerization of ethylene, keeping the metal loading as well as the co-catalyst:metal ratio constant. The results are shown in Table 6.1.

Table 6.1: TOF[a] of catalysts (**C1-C7**) at 2000:1 Al/Ni ratio.

Dendrimer Generation	TOF values[a]		
	DAB Ni Salicylaldimine catalysts	DAB $NiBr_2$ Iminopyridyl catalysts	Cyclam Ni salicylaldimine catalyst
1	2417.2 (**C1**)	2274.8 (**C4**)	2831.8 (**C7**)
2	2018.0 (**C2**)	629.0 (**C5**)	-
3	2582.0 (**C3**)	971.6 (**C6**)	-

[a] TOF = Kg of oligomer per mol of Ni per hour.

The Turn-Over-Frequency (TOF) values range from 629 - 2881 kg product.mol^{-1}Ni.h^{-1}. Fig 6.8 shows that of the three generation 1 catalysts, the cyclam-cored salicylaldimine catalyst (**C7**) is the most active complex. When comparing the salicylaldimine catalysts (**C1-C3**) to the iminopyridyl catalysts (**C4-C6**), it is evident that the salicylaldimine complexes generally exhibit the highest activity throughout generations 1-3. At this constant Al/Ni ratio of 2000:1, no clear dendritic effect is observed. This is due to the fact that usually each generation of metallodendritic catalyst is expected to have a different optimum Al/Ni ratio. It is not confirmed at this stage that an Al/Ni ratio of 2000:1 represents the optimal ratio for the different generation catalysts tested. As indicated previously (Chapter 5) the higher generation catalysts usually need more co-catalyst to achieve optimum activity. Due to time constraints, the optimum activities for catalysts **C4-C7** were not established.

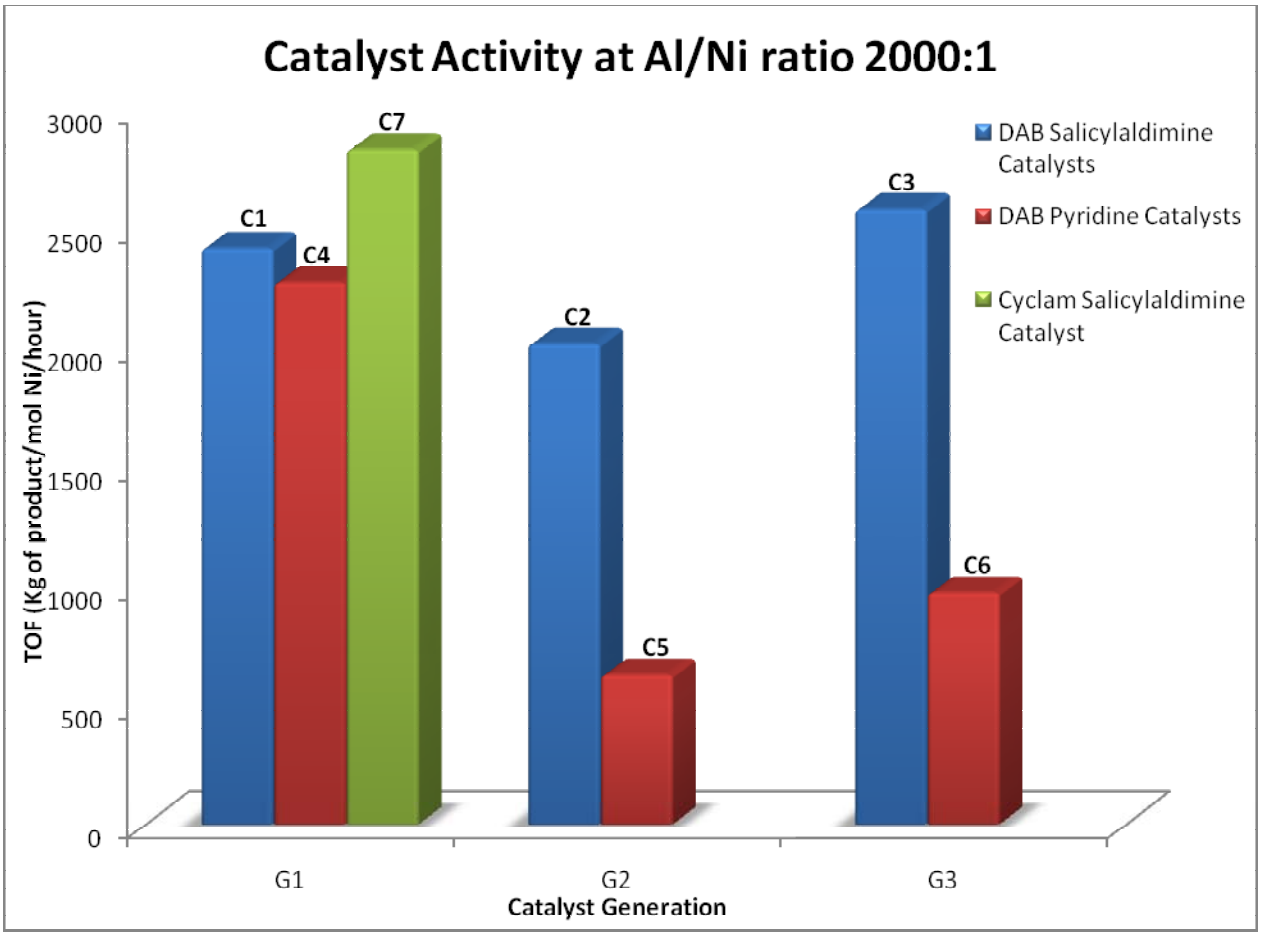

Figure 6.8: Graphical representation of catalyst activity of **C1-C7** at Al/Ni 2000:1.

The selectivity of catalysts **C1-C7** is shown in Table 6.2. All the generation 1 catalysts (**C1**, **C4**, **C7**) tend to form mostly short chain oligomers ($C_4 - C_{16}$) rather than long chain oligomers. Also the G1-G3 Ni salicylaldimine catalysts (**C1-C3**) form mostly short chain oligomers, whereas the higher generation G2 and G3 Ni pyridine catalysts (**C5** and **C6**) form predominantly long chain oligomer (C_{22+}). Thus the latter catalysts seem to be favouring chain propagation over chain termination processes. This could be due to the high degree of congestion on the dendrimer periphery which retards chain termination of **C5** and **C6** via â-hydride transfer, thus leading to longer chain products.

An interesting observation is the presence of uneven carbon number compounds in the product mixture. For all the catalysts evaluated, a C_{11} product is formed in relatively high amounts and in the case of DAB G3 Ni salicylaldimine catalyst (**C3**) a C_{13} product is also formed. An explanation for this is that Friedel-Crafts alkylation of the solvent, toluene, occurs in the presence of the short chain oligomers (C_4 and C_6) to yield alkylated toluenes (C_{11} and C_{13}).

Table 6.2: Selectivity of catalysts, **C1-C7** at 2000:1 Al/Ni ratio.

Catalyst	%C_4	% C_6	% C_8	% C_{11}[a]	% C_{13}[a]	% C_{14}	% C_{16}	% C_{22}^+
C1	24.2	5.1	4.2	31.6	-	11.8	8.4	14.7
C2	16.8	-	-	42.4	-	6.8	7.5	26.5
C3	-	-	-	46.0	3.5	17.8	14.0	18.7
C4	55.6	6.4	0	18.0	-	-	-	20.0
C5	-	-	-	17.3	-	5.2	1.5	76.0
C6	4	-	-	21.5	-	-	-	74.5
C7	11.9	-	-	48.2	-	14.5	8.4	17.0

[a] Friedel-Crafts alkylation products.

The Friedel-Craft reaction was proven independent by carrying out a test reaction in which 1-hexene was reacted with $EtAlCl_2$ in the absence of any metal catalyst. This produced hexyl toluenes as the sole products.

Darkwa *et al*, recently described similar reactions when evaluating their (pyrazol-1-ylmethyl)pyridine nickel catalysts in the oligomerization of ethylene, using

$EtAlCl_2$ as a co-catalyst.[19] However, they report that their catalysts exclusively produce Friedel-Crafts products **A-C** (Scheme 6.1), whereas we observe the formation of even numbered ethylene oligomers in addition to the F/C alkylation products. This indicates that the Ni/$EtAlCl_2$ active species catalyzes the oligomerization of ethylene, while the $EtAlCl_2$ on its own catalyzes the F/C alkylation simultaneously. With our dendritic catalyst systems, the oligomerization reaction appears to proceed faster than the F/C alkylation reaction, hence the presence of ethylene oligomers in the product mix.

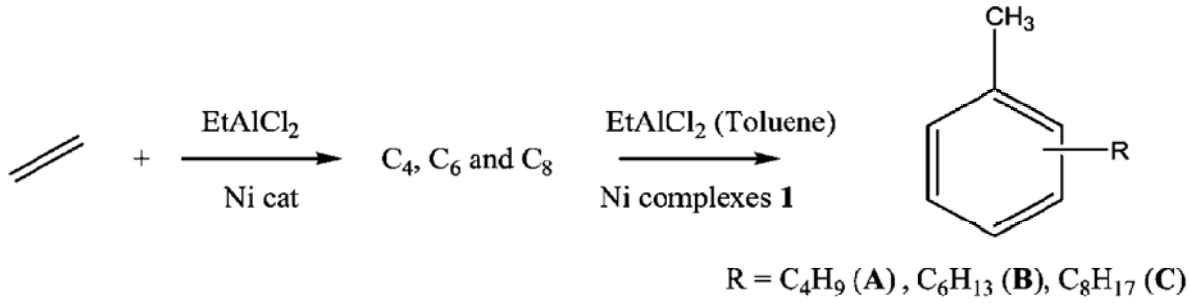

Scheme 6.1: Friedel-Crafts alkylation products reported by Darkwa *et al*.[19]

In the case of Darkwa's catalytic system, it seems the F/C alkylation occurs faster than the oligomerization process, leading to the oligomeric products being consumed as soon as they are produced. Therefore no traces of oligomeric products are observed directly.

It should be noted that in our case, a fair amount of the butene produced initially subsequently becomes consumed in the Friedel-Crafts alkylation reaction to produce the C_{11} product. In fact, in almost all cases more than half of the butene produced reacts with the solvent in a subsequent reaction. In the case of catalysts **C3** and **C5**, all the butene produced is converted, as none is detected in the final product mix. Catalyst **C4** interestingly shows the

lowest % of butene produced being converted to the alkylated toluene product. It also seems that the lower generation catalysts (**C1** and **C4**) tend to undergo Friedel-Crafts alkylation less readily than the higher generation catalysts, as proven by the higher amounts of butene still present in the product mix for the former catalysts.

*6.2.1.2 Catalytic activity and selectivity of the Generation 3 DAB nickel catalyst, **C3**.*

Since we've previously reported the evaluation of **C1** and **C2** in the oligomerization of ethylene [20], at various Al/Ni ratio's, we found it apt to also evaluate **C3** at different Al/Ni ratio's. The results are shown in Table 6.3.

Table 6.3: TOF[a] of Generation 3 DAB nickel catalyst, **C3**.

Al:Ni	DAB G3 Ni Sal
1000	1796.2
2000	2582.0
3000	2568.4
4000	2714.6
5000	**3582.8**
7000	2963.2

[a] TOF = Kg of oligomer per mol of Ni per hour.

As expected, the DAB generation 3 salicylaldimine catalyst (**C3**) needed a much higher Al/Ni ratio than its lower generation counterparts (**C1** and **C2**) to reach optimum activity at 5000:1, reaching up to 3582.8 kg PE.mol^{-1}Ni.h^{-1}. In the reaction using an Al/Ni ratio of 7000:1, the catalyst activity is possibly lower due to catalyst deactivation caused by the high amount of co-catalyst in the reaction mixture.

The optimum Al/Ni ratios for **C1** and **C2** were 500:1 and 2000:1 respectively, as reported by us. [20] These results also support our theory that the tertiary amine units present in our dendritic systems act as Lewis donor sites, and therefore are potential positions for coordinating to the Lewis acidic organoaluminium co-catalyst. The G1 catalyst has two tertiary amine units within its internal structure, while the G2 catalyst has six tertiary amine units and the G3 catalyst has twelve. Thus the co-catalyst, $EtAlCl_2$, first coordinates to these Lewis basic sites before activation of the metal centre occurs. It is well known that N-donor molecules form adducts with Lewis acidic Al complexes.[21-22] Since the G3 catalyst has the most N-donor sites it will need to react with a larger amount of the aluminium alkyl than its lower generation counterparts therefore requiring larger amounts of co-catalyst before the optimum activity is reached. The activity graph for **C3** is shown in (Fig 6.9).

Table 6.4 shows the selectivity obtained at the different Al/Ni ratio's ranging from 1000:1-7000:1. The results indicate that irrespective of the Al/Ni ratio, the major product remains short chain oligomers. C_4 is only present at an Al/Ni ratio of 1000:1. Uneven carbon number products C_{11}, C_{13}, C_{15} and C_{17} are present in the product mixture. This is again due to Friedel/Crafts alkylation of the solvent, toluene, as discussed earlier. In all cases, except at Al/Ni ratio of 1000:1, all the butenes formed is converted to C_{11} Friedel-Crafts alkylation products. Furthermore, all the hexenes formed is converted to C_{13} Friedel-Crafts alkylation products.

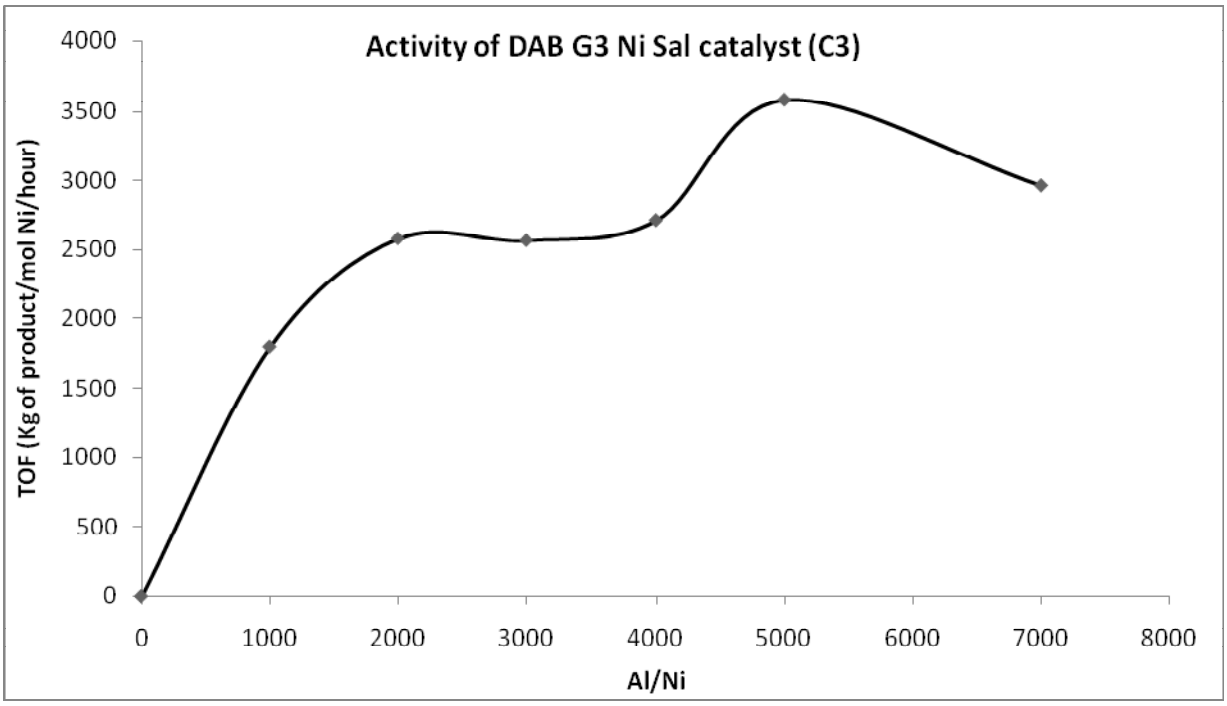

Figure 6.9: Graph of catalyst activity of **C3** at varying Al/Ni ratios.

Table 6.4: Selectivity of **C3** at various Al/Ni ratios.

Al/Ni	**% C_4**	**% C_6**	**% C_{11}[a]**	**% C_{13}[a]**	**% C_{14}**	**% C_{15}[a]**	**% C_{16}**	**% C_{17}[a]**	**% C_{18}**	**% C_{22}^{+}**
1000	10.1	-	49.3	-	14.6	-	12.9	-	-	13.1
2000	-	-	46.0	3.5	17.8	-	14.0	-	-	18.7
3000	-	-	31.5	11.1	19 .6	5.6	8.8	3.9	2.1	17.4
4000	-	-	40.0	4.0	6.8	-	9.6	-	-	39.6
5000	-	-	38.1	10.2	13.0	-	6.5	-	-	32.2
7000	-	-	33.8	30.5	2.5	11.0	2.6	-	-	19.6

[a] Friedel-Crafts Products.

It is also noted that an increase in the Al/Ni ratio leads to a decrease in the production of C_4 and subsequently a decrease in the formation of C_{11} Friedel-Crafts alkylation products.

Since all catalytic reactions formed C_{11} as a product, we thought it best to run a blank reaction, containing no metallodendrimer catalyst, with only $EtAlCl_2$ present under the same reaction conditions. After one hour, the reaction mixture was worked-up as described earlier, and no product was observed. This proves that without our dendritic catalyst systems, neither ethylene oligomerization nor Friedel-Crafts alkylation of toluene to ethylene occurs. It is proposed that the F/C alkylation only occurs after the formation of C_4 and other even carbon number olefins, as a result of ethylene oligomerization by the metallodendritic catalyst systems. Therefore, the two processes occur in tandem. First we have the oligomerization of the ethylene to even numbered olefins, followed by the F/C alkylation of the toluene by the even numbered olefins mediated by $EtAlCl_2$. This is why *even* as well as *uneven* carbon number products are observed in the reaction mixture. We can therefore conclude that no oligomerization will occur if there's no metallodendritic catalyst present. In addition the $EtAlCl_2$ does not mediate the alkylation of toluene in the presence of ethylene to produce ethyl benzene. Hence, the alkylation only occurs when C_4 and longer olefins are present.

We decided to test this theory by using 1-hexene as a substrate instead of ethylene. No metallodendritic catalyst was included in the reaction mixture, only $EtAlCl_2$. Under similar reaction conditions, the $EtAlCl_2$ converted the 1-hexene to products within 10 minutes, with 100 % conversion. From GC analysis, we observed the selective formation of C_{13} and C_{19} compounds, which can possibly be assigned to the Friedel/Crafts single- and di-alkylation of C_6 to toluene respectively. The GC-MS chromatogram is shown in Fig 6.10, where we also observe C_{25} (tri-alkylated) Friedel/Crafts products.

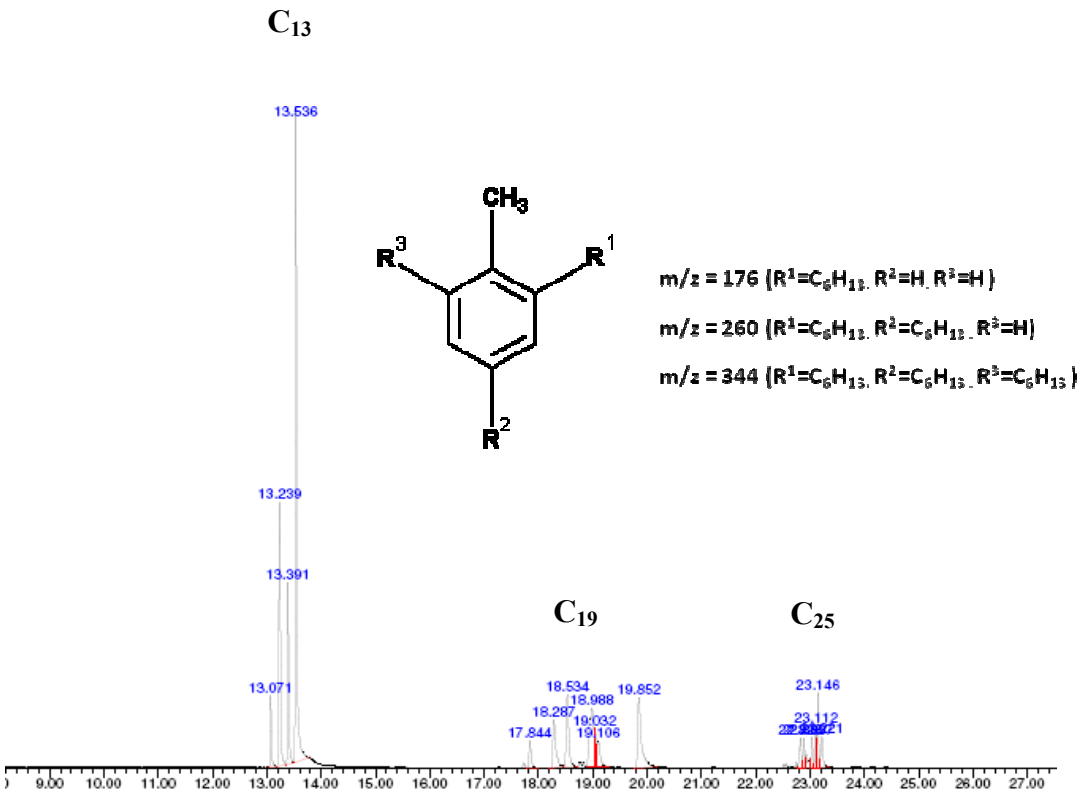

Figure 6.10: The GC-MS chromatogram indicating F/C alkylation with 1-hexene and toluene.

We can conclude that even though $EtAlCl_2$ on its own does not alkylate toluene in the presence of ethylene, it does alkylate toluene with 1-hexene without the presence of any transition metal catalyst system. Reactions with 1-pentene and 1-octene were also evaluated and similar results were obtained where the toluene was alkylated to produce pentyl- and octyl-toluenes respectively. Therefore, using this co-catalyst ($EtAlCl_2$) in toluene for attempts at 1-pentene and 1-hexene oligomerization would prove futile, as the substrates will react with the solvent before oligomerization can take place.

A proposed catalytic cycle for oligomerization of ethylene and tandem Friedel-Crafts alkylation is shown in Fig 6.11. As discussed, the first catalytic process to occur is the oligomerization of ethylene. The first step involves the alkylation of the Ni catalyst with

$EtAlCl_2$, followed by â-hydride elimination to form the Ni-hydride which is thought to be the catalytic active species. Step 2 is the coordination of ethylene at an open site on the metal, after which ethylene insertion into the metal-alkyl bond occurs. Continuous insertion of the ethylene species promotes chain growth. At step 3, either chain propagation continues to give longer chain oligomers or â-hydride elimination can occur as shown in Step 4. After chain termination, 1-butene is eliminated initially as an ethylene dimerization product, **A**, which is one of the products we observe in our catalytic reactions.

After the oligomerization process, the Friedel-Crafts alkylation occurs. Step 5 involves the double bond of the 1-butene attacking free $EtAlCl_2$ to form a secondary carbocation. After a typical Friedel-Crafts mechanism ensues, the Friedel-Crafts alkylation product, **B**, is released. **C** and **D** represent the longer chain products from ethylene oligomerization and also longer chain F/C products.

The Friedel-Craft products is probably singly alkylated instead of di- or tri-alkylated products, since C_{11} (butyl) and C_{13} (hexyl) F/C products is observed rather than C_{15} (di-butyl) and/or C_{19} (tri-butyl) F/C products. Therefore we can conclude that toluene undergoes Friedel-Crafts single-alkylation with oligomers of ethylene.

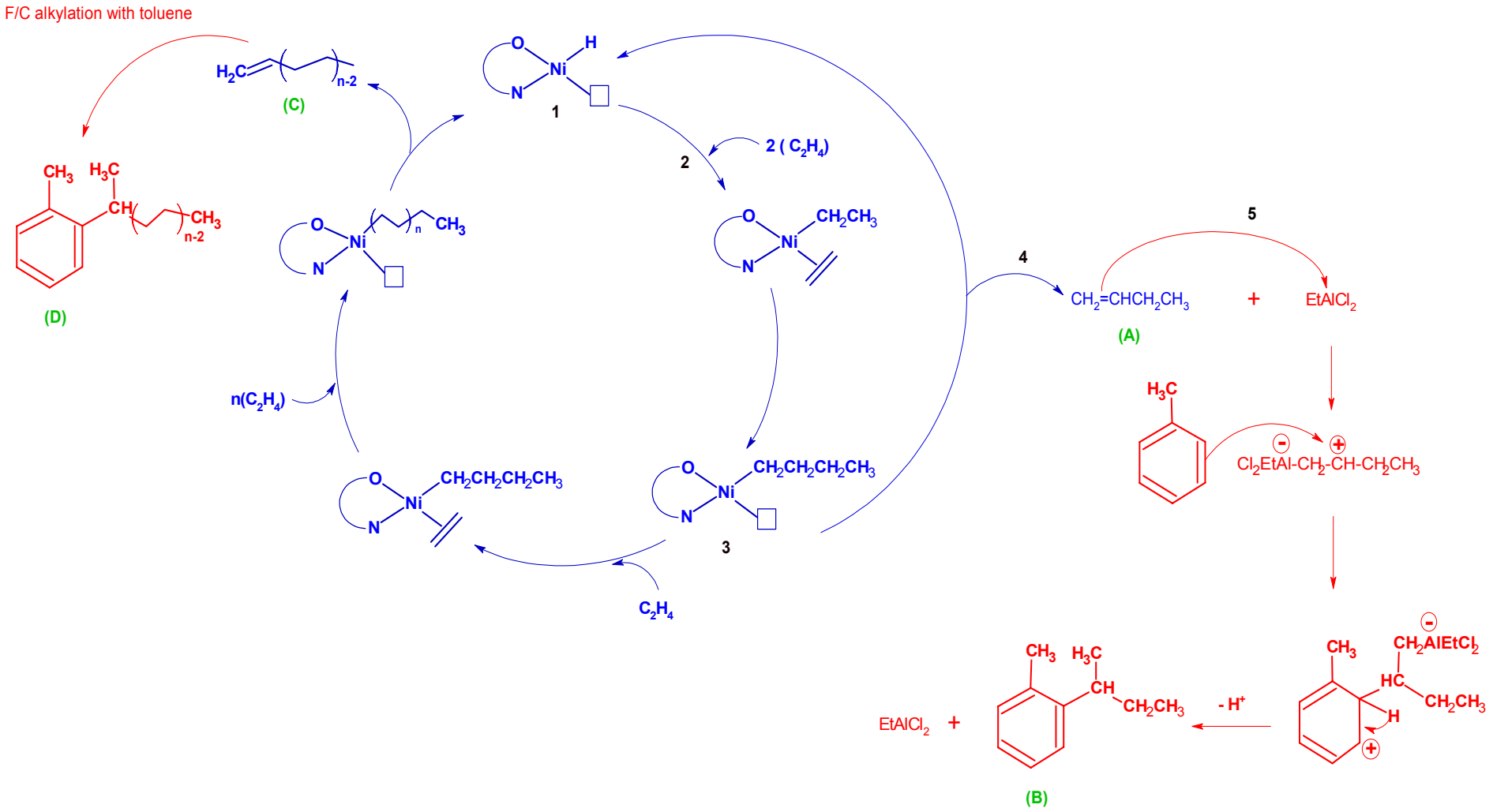

Fig 6.11: Proposed mechanism for tandem ethylene oligomerization (blue) and Friedel-Crafts alkylation (red) using Schiff base catalysts.

6.2.2 1-Pentene Isomerization and Dimerization.

1-Pentene was isomerized and dimerized at room temperature using methylaluminoxane (MAO) as a co-catalyst and toluene as a solvent. The nickel amount (25 μmol) was kept constant irrespective of the catalyst employed. The pentene:metal ratio was 1000:1 and reaction time was 3 hours. These reaction conditions are typical for olefin oligomerization. After the appropriate reaction time, the catalytic process was stopped by quenching with 10 ml of a 2M HCl solution. The two layers were separated after which the organic layer was dried over potassium carbonate. The drying agent was filtered and an aliquot of the reaction mixture was taken for GC analysis. Scheme 6.2 shows the double bond migration products of 1-pentene isomerization.

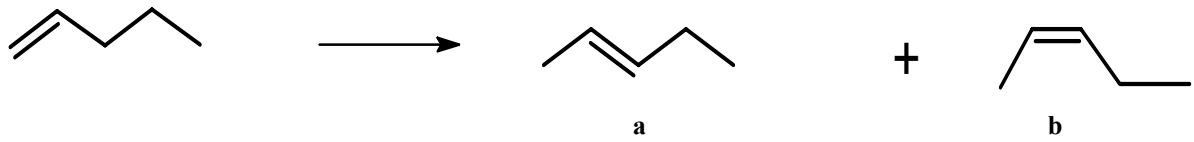

Scheme 6.2: 1-Pentene isomerization to a) trans-2-pentene and b) cis-2-pentene.

*6.2.2.1 Generation 1-3 DAB Salicylaldimine nickel complexes (**C1-C3**) as isomerization and dimerization catalysts.*

The salicylaldimine nickel metallodendrimers were evaluated as catalysts in the isomerization and dimerization of 1-pentene. Methylaluminoxane (MAO) was used as a co-catalyst and the Al:Ni ratio was varied in different reactions. The products obtained were internal pentene isomers as well as decenes (dimerization of 1-pentene). The conversion and selectivity of 1-pentene using **C1** as catalyst is shown in Table 6.5. These results show that **C1** has the highest conversion of 1-pentene at an Al:Ni ratio of 200:1.

Table 6.5: 1-Pentene conversion and product selectivity using DAB G1 Ni salicylaldimine complex **(C1)** as catalyst.

Al :Ni	% Conversion	ISOMERS		DIMERS
		Trans-2-pentene	**Cis-2-pentene**	**C_{10}**
50	78.3	51.3	47.7	1.0
100	82.2	38.7	43.8	17.5
200	87.7	44.5	54.5	1.0
300	80.3	38.3	60.7	1.0
1000	85.5[a]	0	0	0

[a] C_{25}^{+} products formed.

The isomerization products are trans- and cis-2-pentene, with cis-2-pentene being the more dominant of the two isomers in all cases except at Al:Ni ratio of 50:1. This selectivity is unusual since literature reports of pentene isomerization typically confirm trans-2-pentene as the dominant isomer.[23-24]

De Klerk reported the reactivity of 1-octene over solid phosphoric acid (SPA) as a catalyst. [25] They found that at 75 ºC, no reaction took place and at 100 ºC only double bond isomerization was observed. At 120 ºC however, the conversion of 1-octene was mostly due to double bond isomerization, although a small amount of skeletal isomers and dimers (less than 0.5 % yield) were also formed. Similar to our results, they found that the most dominant product was the cis-isomer. It was concluded that the mechanism over SPA involved the

formation of a phosphoric acid ester and that the stability of this ester intermediate determined the reactivity of the olefin. Hence the SPA followed a non-classic carbocation mechanism, which accounts for the cis-favoring double bond isomerization observed.

The highest selectivity towards dimerization occurred at Al:Ni ratio of 100:1 with 17.5 % of the total products being C_{10}. The catalyst, **C1**, was also evaluated at an Al:Ni ratio of 1000:1, to determine whether the selectivity towards isomerisation and dimerization is influenced by Al concentration. It was found that no short chained isomers or oligomers were formed at this high Al:Ni ratio. It is assumed that at this high Al/Ni ratio the catalyst becomes more active, hence the isomers as well as any short chain oligomer products formed will possibly undergo further oligomerization to form longer chain products. The product isolated from this reaction (Al/Ni, 1000:1) was an oily substance, and was found to be an unsaturated hydrocarbon from FTIR analysis.

Zhang *et al* [26] reported similar results when using 1-hexene as a substrate and a â-diketiminato Ni(II) bromide complex/methylaluminoxane catalyst system. Their catalysts also produced selectively 1-hexene isomers and dimers. The coordination wedge of the bulky â-diketiminato Ni(II) catalysts blocked the migration of the Ni atom from a secondary or tertiary carbon to another one along the alkyl chain of the Ni-alkyl intermediates. This is why 3-hexenes, trimers and higher oligomers were not produced. They only achieved 53.4 % conversion of 1-hexene at similar reaction conditions to ours, when using the catalyst **34** shown in Fig 6.12.

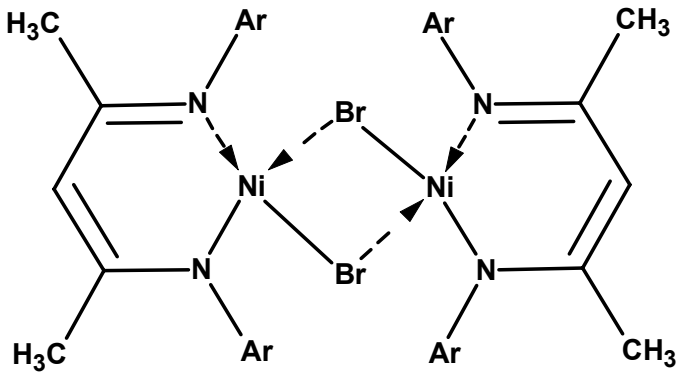

34 **Ar** = 2,6 diisopropylphenyl

35 **Ar** = 2,6 dimethylphenyl

Figure 6.12: The â-diketiminato Ni(II) bromide catalysts synthesised by Zhang *et al*.[26]

The conversion and selectivity of 1-pentene using **C2** as catalyst is shown in Table 6.6. The highest conversion for catalyst **C2** is at an Al:Ni ratio of 200:1 with 83.3 % conversion to isomers and dimers of 1-pentene. The highest selectivity towards dimerization is also at the optimal Al:Ni ratio, with 20.5 % of the product mix being dimers.

Table 6.6: 1-Pentene conversion and product selectivity using DAB G2 Ni salicylaldimine complex **(C2)** as catalyst.

Al:Ni	% Conversion	ISOMERS		DIMERS
		Trans-2-pentene	**Cis-2-pentene**	**C_{10}**
50	65.0	49.7	49.3	1.0
100	76.7	45.5	53.5	1.0
200	83.3	35.6	43.9	20.5
300	78.3	40.2	58.8	1.0

Table 6.7: 1-Pentene conversion and product selectivity using DAB G3 Ni salicylaldimine complex **(C3)** as catalyst.

Al:Ni	% Conversion	ISOMERS		DIMERS
		Trans-2-pentene	**Cis-2-pentene**	**C_{10}**
50	46.1	46.0	53.0	1.0
100	69.4	42.2	56.8	1.0
200	80.1	40.9	58.1	1.0
300	46.1	39.9	59.1	1.0

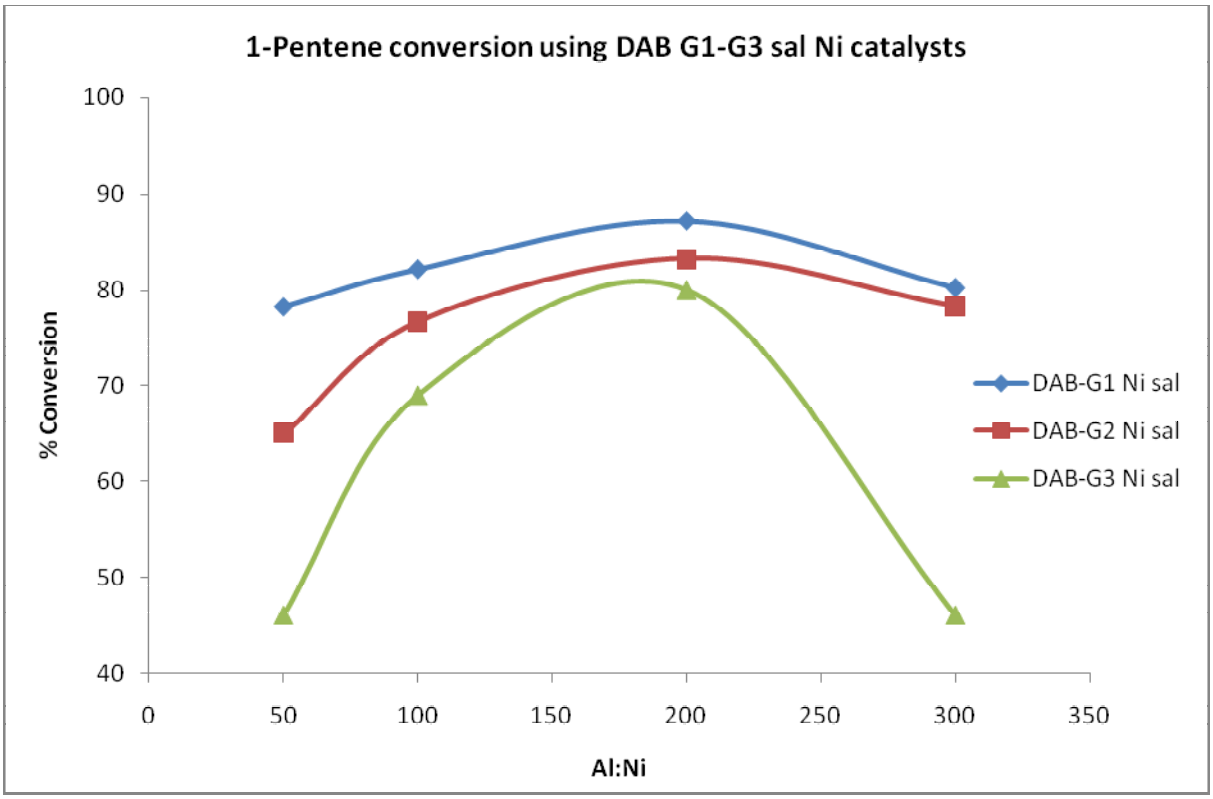

Figure 6.13: The conversion of 1-pentene using the DAB G1-G3 salicylaldimine nickel catalysts, **C1-C3**.

At all Al/Ni ratios, the G1 catalyst exhibits higher conversion than the G2 catalyst, which in turn exhibits higher conversion than the G3 catalyst. Also, for all three catalysts, optimal conversion of 1-pentene is found at an Al/Ni ratio of 200:1.

*6.2.2.2 Generation 1-3 DAB iminopyridyl nickel complexes (**C4-C6**) as isomerization and dimerization catalysts.*

The iminopyridyl nickel metallodendrimers were also evaluated as catalysts in the isomerization and dimerization of 1-pentene using MAO as a co-catalyst. For each generation, the catalysts were evaluated at an Al/Ni ratio of 100:1 and 200:1. The conversion and selectivity using **C4-C6** as catalysts at Al/Ni 100:1 are shown in Table 6.8.

Table 6.8: 1-Pentene conversion and product selectivity using DAB G1-G3 Ni iminopyridyl complexes **(C4-C6)** as catalysts at Al/Ni ratio 100:1.

Catalyst	Dendrimer Generation	Al:Ni	% Conversion	ISOMERS		DIMERS
				Trans-2-pentene	**Cis-2-pentene**	**C_{10}**
C4	1	100	43.3	43.3	56.7	0
C5	2	100	58.3	48.6	51.4	0
C6	3	100	54.8	45.2	54.8	0

Catalysts **C4-C6** at Al/Ni 100:1, selectively isomerizes 1-pentene to trans- and cis-2-pentene. No dimerization or other oligomerization products are observed. The conversions were modest and ranged from 43-58 %. The results for **C4-C6** at 200:1 are shown in Table 6.9. An increase in the Al/Ni ratio led to an increase in the conversion of 1-pentene, ranging from 69-77 %. Also, in each case a small percentage of dimers in addition to the trans- and cis isomers of 1-pentene are also formed.

Table 6.9: 1-Pentene conversion and product selectivity using DAB G1-G3 Ni iminopyridyl complexes **(C4-C6)** as catalysts at Al/Ni ratio 200:1.

Catalyst	Dendrimer Generation	Al:Ni	% Conversion	ISOMERS		DIMERS
				Trans-2-pentene	**Cis-2-pentene**	**C_{10}**
C4	1	200	74.4	42.8	56.2	1.0
C5	2	200	68.7	44.2	54.8	1.0
C6	3	200	77.2	46.5	52.5	1.0

When comparing the salicylaldimine catalysts (**C1-C3**) to the iminopyridyl catalysts (**C4-C6**) it is evident that the salicylaldimine analogues yield higher conversions of 1-pentene to its isomers and dimers. The salicylaldimine catalysts also show higher selectivity towards dimerization under certain reaction conditions than the iminopyridyl catalysts. This difference can possibly be attributed to the electronic effects of the different catalyst systems.

*6.2.2.3 Generation 1 Cyclam salicylaldimine nickel complex (**C7**) as an isomerization and dimerization catalyst.*

The cyclam-cored salicylaldimine nickel catalyst, **C7**, was also evaluated at varying Al/Ni ratios. The results are shown in Table 6.10.

Table 6.10: 1-Pentene conversion and product selectivity using Cyclam G1 Ni salicylaldimine complex **(C7)** as catalyst.

Al:Ni	% Conversion	ISOMERS		DIMERS
		Trans-2-pentene	**Cis-2-pentene**	**C_{10}**
50	82.2	47.3	51.7	1.0
100	80.0	42.6	56.4	1.0
200	89.4	54.3	44.7	1.0

The conversion of 1-pentene ranges from 80-89 %. The major products are once again pentene isomers. We found that generally, the cyclam based catalyst shows higher conversions than the DAB based catalysts, under the same reaction conditions. These results are in agreement with the catalytic performance of the cyclam catalysts for norbornene polymerization activity. The possible reasons for this were previously discussed in Chapter 5.

6.3 Conclusion

A range of metallodendritic catalysts were evaluated in ethylene oligomerization and 1-pentene isomerization and dimerization reactions. The synthesized nickel catalysts produced a range of ethylene oligomers (C_4-C_{18}), as well as some longer chained oligomers when employing $EtAlCl_2$ as a co-catalyst. An interesting observation was the presence of products due to Friedel-Crafts alkylation of the solvent, in addition to the ethylene oligomers. This was due to the reaction of the ethylene oligomers produced with the solvent, toluene. While the more active DAB G1-G3 salicylaldimine catalysts (**C1-C3**) form mainly short chain oligomers, the less active higher generation iminopyridyl catalysts (**C5-C6**) form mainly longer chain oligomers.

Although the attempted ethylene oligomerization reaction using only $EtAlCl_2$ (i.e. in the absence of a metal catalyst) showed no activity, a different situation is observed when using 1-pentene and 1-hexene as a substrate. It was found that the $EtAlCl_2$ catalyzes the Friedel-Crafts alkylation of the substrate and its dimers to the toluene solvent, in the absence of the metallodendritic catalysts. Consequently, 1-pentene isomerization and dimerization were performed using methylaluminoxane (MAO) as a co-catalyst. At low Al/Ni ratios predominantly isomers of 1-pentene are formed, with traces of dimers also present in the reaction mixture. An increase in the Al/Ni ratio led to the formation of longer chained oligomers. Again the salicylaldimine catalysts exhibit higher activity towards isomerization and dimerization than the pyridine imine catalysts. In both catalytic processes, the cyclam-cored dendrimer catalyst showed the highest activity towards olefin transformation.

6.4 Experimental

All work involving moisture and air sensitive compounds such as MAO and $EtAlCl_2$ was carried out using standard Schlenk techniques. Infrared spectra were recorded on a Nicolet Avatar 330 FT-IR spectrophotometer, using an ATR accessory with a ZnSe crystal. ^{1}H NMR (300MHz and 400MHz) and ^{13}C NMR (300MHz) spectra were recorded on a Varian VNMRS 300MHz and a Varian Unity Inova 400MHz spectrometer, using tetramethylsilane as an internal standard. Toluene was dried by refluxing over sodium/benzophenone. $EtAlCl_2$ (25 % solution in toluene) and Methylaluminoxane (MAO), a 10% solution in toluene, were obtained from Sigma Aldrich and used without any further purification. Ethylene (99.9%) was obtained from Afrox. The GC analysis was done using a Varian CP-3800 gas chromatograph equipped with a HP PONA column. The internal standard used for GC analysis was o-Xylene.

6.4.1: Ethylene oligomerization.

The catalyst amounts were varied to ensure a constant amount of Ni in the system at 5μmol. $EtAlCl_2$ was employed as a co-catalyst. Reaction time was one hour at room temperature. The ethylene pressure was maintained at 5 atm and the solvent employed was toluene (50 ml). Acidic ethanol (10 ml) was used to quench the reaction. The Al:Ni ratios ranged from 1000:1 – 5000:1.

Typical Ethylene Oligomerization procedure:

The ethylene oligomerization reactions were carried out in a 300 ml stainless steel autoclave equipped with an overhead stirrer and internal cooling coil. The autoclave was loaded in a nitrogen-purged glove box. The appropriate amount of catalyst corresponding to 5 μmol of nickel was suspended in dry toluene (50 ml) in a stainless steel PARR reactor. The required amount of $EtAlCl_2$ was added to the solution using a glass syringe. The reactor was sealed and removed from the glovebox. The reactor was flushed with ethylene 3 times. The ethylene pressure was set at 5 atm and maintained at this pressure throughout the oligomerization procedure. The reaction was conducted at room temperature for 1 hour. Unreacted ethylene was vented from the reactor at the end of the designated reaction time and the oligomerization was stopped by quenching the reaction mixture with 10 ml of acidic ethanol (ethanol:HCl, 95:5). A GC aliquot was taken after which the solvent from the remaining sample was evaporated via rotary evaporation and dried on the vacuum line for 24 hours. Any remaining non-volatile product were weighed and subjected to GPC analysis.

6.4.2: 1-Pentene isomerization and dimerization.

Reaction conditions:

The amount of Ni used was 25 μmol. MAO (10% in toluene solution) was employed as a co-catalyst. The reaction time was 3 hours at a temperature of 50 ºC. The total volume of the reaction mixture was constant at 10 ml using toluene as a solvent. The pentene:Ni ratio was kept constant at 1000:1. Acidic methanol (5 ml) was used to quench the reaction. The Al:Ni ratios ranged from 50:1 – 300:1.

Typical Pentene Isomerization procedure:

The appropriate amount of catalyst was added to 5ml of dry toluene in a parallel reactor reaction vessel. 2.8 ml of 1-pentene (1000:1, pentene:Ni) was added to the reaction vessel. The required amount of MAO (10 % in toluene) was then injected into the reaction solution to initiate the oligomerization. The reaction was allowed to continue for 3 hours at 50 ºC after which the reaction was stopped by quenching it with 10 ml of a 2M HCl solution. The two layers were separated after which the organic layer was dried with potassium carbonate. The drying agent was filtered and a GC sample of the filtrate was taken.

6.5 References

[1] I. Coleto, R. Roldan, C. Jimenez-Sanchidrian, J. P. Gomez, F. J. Romero-Salguero, *Catalysis Today,* 149, **2010**, 275.

[2] J. Skupinska, *Chem. Rev.* 91, **1991**, 613.

[3] M. Peuckert, W. Keim, *Organometallics,* 2, **1983**, 594.

[4] W. Keim, R.P. Schulz, *J. Mol. Catal.,* 92, **1994**, 21.

[5] W. Keim, *Chem. Eng. Technol.,* 56, **1984**, 850.

[6] Y. Chauvin, J.F. Gaillard, D.V. Quang, J.W. Andrews, *Chem. Ind.*, **1974**, 375.

[7] E.R. Freitas, C.R. Gum, *Chem. Eng. Proc.,* 75, **1979**, 73.

[8] F.A. Alsherehy, *Stud. Surf. Sci. Catal.,* 100, **1996**, 515.

[9] S. Adewuyi, G. Li, S. Zhang, W. Wang, P. Hao, W. Sun, N. Tang, J. Yi, *J. Organomet. Chem.,* 692, **2007**, 3532.

[10] Y. Wang, S. Lin, F. Zhu, H. Gao, Q. Wu, *Inorg. Chim. Acta,* 362, **2009**, 166.

[11] W. Sun, W. Zhang, T. Gao, X. Tang, L. Chen, Y. Li, X. Jin, *J. Organomet. Chem.,* 689, **2004**, 917.

[12] B. K. Bahuleyan, U. Lee, C. Ha, I. Kim, *App. Catal. A: Gen.,* 351, **2008**, 36.

[13] Miao Shen, Peng Hao, Wen-Hua Sun, *J. Organomet. Chem.,* 693, **2008**, 1683.

[14] M. E. Dry, *Appl. Catal. A: Gen.*, 276, **2004**, 1.

[15] C. J. Yue, Y. Liu, R. He, *J. Mol. Catal. A: Chem.,* 259, **2006**, 17.

[16] S. Kamiguchi, M. Noda, Y. Miyagishi, S. Nishida, M. Kodomari, T. Chihara, *J. Mol. Catal. A: Chem.,* 195, **2003**, 159.

[17] R. Maurel, M. Guisnet, L. Bove, *Bull. Sco. Chim. Fr.,* **1969**, 1975.

[18] C. J. Yue, Y. Liu, R. He, *J. Mol. Catal. A: Chem.,* 259, **2006**, 17.

[19] S. O. Ojwach, I. A. Guzei, L. L. Benade, S. F. Mapolie, J. Darkwa, *Organometallics,* 28*,* **2009**, 2127.

[20] R. Malgas, S. F. Mapolie, S. O. Ojwach, G. S. Smith, J. Darkwa, *Catal. Commun.*, 9, **2008**, 1612.

[21] J. J. Eisch, in *Comprehensive Organometallic Chemistry II*, ed. E. W. Abel, F. G. A. Stone, G. Wilkinson, Pergamon, **1995**, 431.

[22] F. A. Cotton, G. Wilkinson, C. A. Murillo, M. Bochmann, in *Advanced Inorganic Chemistry*, John Wiley and Sons, New York, 6th edn.,1**999**, 196.

[23] M. Höchtl, A. Jentys, H. Vinek, *Appl. Catal. A: Gen.,* 207, **2001**, 397.

[24] G. C. Bond, M. Hellier, *J. Catal.,* 7, 1**967**, 217.

[25] A. De Klerk, *Ind. Eng. Chem. Res.,* 45, **2006**, 578.

[26] J. Zhang, H. Gao, Z. Ke, F. Bao, F. Zhu, Q. Wu, *J. Mol. Catal. A: Chem.,* 231, **2005**, 27.

Chapter 7:

Thesis Summary

Thesis Summary

The objective of this research project was to synthesize new metallodendrimers for application as catalysts in oligomerization and polymerization processes. The metallodendrimer framework, generation and ligand environment was varied in order to confirm which dendritic catalyst exhibits optimal catalytic activity.

The first step was to synthesize cyclam-cored dendrimers similar to the commercial diaminobutane-poly(propyleneimine) (DAB-PPI) dendrimer, but with the cyclic core rendering the cyclam dendrimer more spherical than the linear-cored DAB dendrimer range. The divergent synthesis of these cyclam based dendrimers was discussed in Chapter 2. We successfully synthesized and characterized cyclam dendrimers with propyl branches (**L1-L4**) and cyclam dendrimers with benzyl branches (**L5-L8**) up to the second generation. It was found that the higher the dendrimer generation, the more difficult the synthesis, due to increasing number of purification steps as well as longer reaction times required. This prompted us not to proceed with the synthesis beyond the second generation.

After successful synthesis of these new cyclam based dendrimers, we modified the G1 cyclam dendrimers as well as the G1-G3 DAB-PPI dendrimer range with salicylaldimine and iminopyridyl functionalities to obtain the dendrimer ligands, **DL1-DL10**. These Schiff base reactions are discussed in Chapter 3. We found that longer reaction time is needed for the higher generation dendrimer ligand syntheses than is required for its lower generation analogues. We have also shown how dendrimer properties can be tweaked since before modification of the DAB-PPI with the Schiff bases, the dendrimers were water soluble but after modification the dendrimers became water insoluble. The modified dendrimer ligands were successfully characterized by FTIR and NMR spectroscopy, elemental analysis, mass spectrometry and UV/Vis spectroscopy. Attempts to modify the G2 cyclam propyl based dendrimers with Schiff bases proved unsuccessful.

The molecular modelling studies of the DAB G1-G3 salicylaldimine ligands, show that the lower generation dendrimer has an open structure while the higher generations are more spherical in structure. It also confirms that the distances between the dendrimer branches is not equal, proving that the DAB dendrimers are very flexible and it was anticipated this could hinder the dendrimer catalyst performance during catalytic reactions. This was indeed confirmed when the G3 catalyst (**C3**) proved to be less active than the G2 catalyst (**C2**) in the vinyl polymerization of norbornene.

Nickel metallodendrimers (**C1-C10**) were successfully synthesized by coordination of metal precursors, $Ni(OAc)_2$ and $Ni(DME)Br_2$, to the periphery of salicylaldimine and iminopyridyl modified dendrimer ligands, **DL1-DL10**. Complexes **C3-C8** are novel complexes, and attempts to successfully purify **C9** and **C10** were unsuccessful.

DFT calculations on the probability of metal coordination to the modified ligand **DL1** were performed and the results show that coordination to the dendrimer periphery is favourable. Molecular modelling was also done on the G1 nickel salicylaldimine complex, **C1**, to get an idea of the complex structure and possible steric hindrance with increasing dendrimer generation. The results show that after coordination of the nickel to the dendrimer periphery, the complex became very distorted.

Some of the synthesized metallodendrimers, **C1-C7** were chosen for evaluation as potential catalysts. With this catalyst selection, conclusions regarding the effect of dendrimer generation (**C1** vs **C2** vs **C3**) and the effect of the cyclam-core against the DAB-dendritic core (**C1** vs **C7**) could be drawn. We also studied the effect of the salicylaldimine vs iminopyridyl ligands (**C1-C3** vs **C4-C6**) on the activity and selectivity of products. These catalysts were evaluated in the polymerization of norbornene (Chapter 5) and the transformation of á-olefins (Chapter 6).

All metallodendrimer catalysts tested proved to be active for the vinyl polymerization of norbornene. The vinyl polymerization mechanism was confirmed by NMR and IR spectra of the polynorbornene obtained which shows that ROMP does not occur in the polymerization process. Also the molecular weights of the obtained polynorbornenes are high ranging from 10^5 to 10^6 g/mol which is not typical of the cationic or radical polymerization process, but rather of vinyl polymerization. The cationic polymerization mechanism usually results in low molecular weights (molecular weight < 1000) and low yield because of rearrangements and transfer reactions. Therefore we can conclude that these types of nickel metallodendrimer catalysts polymerize norbornene through the vinyl-addition coordination mechanism.

It was found that the iminopyridyl complexes, **C4-C6**, exhibit higher activities than the salicylaldimine complexes, **C1-C3**, at a constant Al/Ni ratio. When the activity of DAB-G1 salicylaldimine dendrimer catalyst, **C1**, was compared to that of its cyclam dendrimer analogue, **C7**, it was found that the cyclam catalyst exhibits higher activity at its optimum Al/Ni ratio.

In Chapter 6, the same selection of metallodendrimer catalysts was evaluated in ethylene oligomerization as well as 1-pentene isomerization and dimerization reactions. The synthesized nickel catalysts produced a range of ethylene oligomers (C_4-C_{18}), as well as longer chained oligomers when employing $EtAlCl_2$ as a co-catalyst. Friedel-Crafts products were also obtained in the product mixture. This was due to the reaction of the ethylene oligomers with the solvent, toluene. While the more active DAB G1-G3 salicylaldimine catalysts (**C1-C3**) forms mainly short chain oligomers, the less active higher generation pyridine imine catalysts (**C5-C6**) form mainly longer chain oligomers.

The ethylene oligomerization reaction with $EtAlCl_2$ in the absence of a transition metal catalyst showed no activity, however when using 1-pentene and 1-hexene as a substrate, Friedel-Crafts products are observed. We thus concluded that the $EtAlCl_2$ /Ni catalytic species first oligomerizes the ethylene, and then subsequent Friedel-Crafts alkylation occurs between the toluene and the oligomeric products. This is mediated by the Al alkyl co-catalyst.

1-Pentene was isomerized and dimerized when using our Schiff base metallodendrimers in conjunction with methylaluminoxane (MAO) as a co-catalyst. An increase in the Al/Ni ratio led to the formation of longer chained oligomers. Again the salicylaldimine catalysts exhibit higher activity towards isomerization and dimerization than the pyridine imine catalysts. In both olefin transformation processes, the cyclam-cored dendrimer catalyst showed the highest activity towards olefin transformation.

The cyclam based catalysts seem to exhibit the highest activity for all catalytic processes evaluated. While the salicylaldimine catalysts proved to be the most active towards oligomerization, the iminopyridyl catalysts were the most active for polymerization. The generation 2 catalyst showed higher activity than the generation 3 catalyst, and this is probably due to the structural flexibility of the higher generation dendrimer, making monomer coordination difficult as a result of steric hindrance.

While most researchers concentrate on either: a) divergent/convergent dendrimer framework synthesis or b) surface modification of commercial dendrimers, we have embarked on both types of processes where we divergently synthesized cyclam-cored dendrimers, with a periphery that's receptive to further modification in order to synthesize metallodendrimers. We've also shown these metallodendrimers to be active as catalysts in a variety of catalytic processes.

Thesis Summary

In conclusion, we managed to synthesize new cyclam-cored dendritic systems via a divergent approach. These cyclam-based dendrimers as well as the G1-G3 DAB dendrimers were then functionalized with Schiff base nickel complexes, to form metallodendrimers. The metallodendrimer systems were active catalysts in oligomerization and polymerization processes with the cyclam-based catalysts proving to be more active than the DAB-based catalysts. Also, dendrimer generation affects the catalyst activity and selectivity, therefore a dendritic effect exists. The salicylaldimine catalysts gave the highest activity towards oligomerization whereas the iminopyridyl catalysts were more active towards polymerization.

Future research will include synthesis of the generation 3 cyclam-cored dendrimers, and subsequent immobilization of the Schiff base nickel catalysts onto the G2 and G3 dendritic scaffolds. These cyclam-cored metallodendrimers would then be evaluated as catalysts to determine whether structural rigidity will result in higher activities than that obtained by the DAB- based metallodendrimer catalysts.